JAERI-Review
2003-033

TIARA Annual Report 2002

November 2003

Advanced Radiation Technology Center

日本原子力研究所
Japan Atomic Energy Research Institute

本レポートは，日本原子力研究所が不定期に公刊している研究報告書です。
入手の問合わせは，日本原子力研究所研究情報部研究情報課（〒319-1195　茨城県那珂郡東海村）あて，お申し越しください。なお，このほかに財団法人原子力弘済会資料センター（〒319-1195　茨城県那珂郡東海村日本原子力研究所内）で複写による実費頒布をおこなっております。

This report is issued irregularly.
Inquiries about availability of the reports should be addressed to Research Information Division, Department of Intellectual Resources, Japan Atomic Energy Research Institute, Tokai-mura, Naka-gun, Ibaraki-ken, 319-1195, Japan.

編集兼発行　　日本原子力研究所

JAERI-Review 2003-033

TIARA Annual Report 2002

Advanced Radiation Technology Center

Takasaki Radiation Chemistry Research Establishment
Japan Atomic Energy Research Institute
Watanuki-cho, Takasaki-shi, Gunma-ken

(Received October 1, 2003)

This annual report describes research and development activities which have been performed with the JAERI TIARA (Takasaki Ion Accelerators for Advanced Radiation Application) facilities from April 1, 2002 to March 31, 2003. Summary reports of 113 papers and brief descriptions on the status of TIARA in the period are contained. A list of publications, the type of research collaborations and organization of TIARA are also given as appendices.

Keywords: JAERI TIARA, Ion Accelerators, Solid State Physics, Radiation Effects in Materials, Materials for Space, Semiconductors, Organic Materials, Inorganic Materials, Nuclear Fusion Reactor, Functional Materials, Radiation Chemistry, Radiation Biology, Nuclear Medicine, Biotechnology, Radioisotope Production, Nuclear Chemistry, Radiation Shielding, Materials Analysis, Microbeam Technology, Accelerator Technology, Safety Control

(Eds.) Masahiro SAIDOH, Yoshihiro OHARA, Shigeru TANAKA, Tamikazu KUME
Hiroshi NARAMOTO, Tomihiro KAMIYA, Masaru YOSHIDA, Masato YOSHIKAWA, Atsushi TANAKA, Yasuhiko KOBAYASHI, Kazuo ARAKAWA, Michiaki OTSUBO, Satoshi TAJIMA and Susumu TANAKA

原研イオン照射研究施設（ＴＩＡＲＡ）平成１４年度年次報告

日本原子力研究所高崎研究所
放射線高度利用センター

（2003年10月 1日受理）

本年次報告は、原研イオン照射研究施設で、2002年4月1日から2003年3月31日までの間に行われた研究活動の概要をまとめたものである。1）宇宙用半導体、2）バイオテクノロジー、3）放射線化学および有機材料、4）無機材料、5）材料解析、6）核科学およびラジオアイソトープ製造、7）マイクロビーム応用、8）加速器施設の放射線遮蔽、9）加速器技術の９部門にわたる１１３編の研究報告に加えて、施設の運転保守・利用状況、公表された文献、企業・大学等との研究協力関係、研究開発・施設運営組織を収録する。

高崎研究所：〒370-1292 群馬県高崎市綿貫町 1233

PREFACE

This report covers research and development activities which have been conducted with TIARA(Takasaki Ion accelerators for Advanced Radiation Application) during the period from April 2002 to March 2003, and also gives an outline of the operation of TIARA in the same period.

All accelerators in TIARA, the AVF cyclotron, the 3MV tandem accelerator, the 3MV single-ended accelerator and 400kV ion implanter, have been operated steadily since the construction were completed in 1993, and have supplied the beam-time to the research programs as had been recognized in advance by the Subcommittee of TIARA of Advisory Council for JAERI's Research Facilities. In the same time, available species and energy ranges of ions have been widened to meet requirements from users, and the quality of ion beams have been improved gradually.

In the semiconductor devices for space, triple-junction space solar cells were examined by irradiation experiments with various energies of protons and optimized for space use from relative damage coefficient curves. Test chips of deep sub-micron CMOS were also examined by high-energy heavy ion irradiation to evaluate sensitivity or immunity for single event latch-up and single event upset. Measurement of transient ion beam induced current was newly applied to silicon carbide pn junction using the heavy ion microbeam system. Charge collection mechanism of single event transient was studied in photonic devices such as InP-InGaAs avalanche photodiodes. Anomalous charge collection in SOI structure devices are also examined by 100 MeV O ions and theoretical analyses were tried to introduce for it.

In the field of biotechnology, human fibroblast cells were hit individually with a predefined exact number of ions of ^{40}Ar or ^{20}Ne using heavy-ion microbeam. A clear bystander response was observed in a confluent cell population independent of these LETs and number of charged particles delivered to the target cells. For the positron emitting tracer imaging system (PETIS), the PETIS was applied to the analysis of photoassimilate transportation in a bean plant using $^{11}CO_2$, and the effect of CO_2 enrichment on the transportation was evaluated quantitatively. For the mutation induction of plants by ion-beam irradiation, many crops were used in order to generate new varieties for the purpose of food resources and promoting new industry. Explants of trees were also irradiated to breed new plants for the conservation of global environment.

In the field of radiation chemistry and organic materials, it was newly found out that the formation of crosslinked polymer nano-wires by single ion hitting is possible for not only polysilane but also a variety of Si-based polymers in relation closely to the efficiency of the crosslinking reaction on the size controllability. The absorption spectroscopy system that was obtained by introducing the single photon counting technique enabled the heavy ion pulse radiolysis in the nanosecond time region.

In the field of nuclear fusion reactors, various materials (ferritic/martensitic steels, Li_2TiO_3 ceramics, SiC/SiC composites, vanadium and austenitic stainless steels) were irradiated with single, dual or triple-ion beams for the simulations of neutron damages and effects of He and H accumulation due to transmutation reactions. Effects of simultaneous irradiation on physical, chemical and thermo-mechanical properties as well as microstructural evolutions are investigated. The fuel cladding materials (austenitic stainless steel, SUS304L, zircaloy-2) for light water reactors were also irradiated at elevated temperatures to examine the generation mechanisms of the radiation-induced corrosion

cracking.

In the field of inorganic materials, highly-mobile defects in Cu and Au disks were found by in-situ TEM observation during ion-irradiation and the defect-impurity interactions were clarified. The irradiation effects of carbon cluster ions (C_4^+, C_8^+) with energies of 0.5 MeV/atom on solid samples were investigated by using the energy spectra of electrons emitted from them compared with C_1^+. The crystalline-to-amorphous transformation due to Ar ion-implantation was investigated for various carbon materials including C_{60} by using X-ray photoelectron and Raman spectroscopies. As for the application of micro-PIXE, the two dimensional distribution for Fe, Ca, Si, Al, Mg and Na atoms in the clay minerals was successfully obtained by the combination of the Ge and newly installed Si(Li) detectors.

In the field of materials analysis, this item contains the studies based on various different motivations, and they are at the leading edge in the relevant fields. The point defect studies with MeV electrons have been extended up to an applicative study such as the radiation-induced precipitation in a model alloy of high pressure vessel in nuclear reactors. Effort on functionalization has been made by employing the processes associated with the introduction of atomic defects and/or impurities, and also the general radiation effect on physical/chemical modification was utilized as a kind of fine-machining. Recent progress in generating the intense C_{60} beams has opened up the new and interdisciplinary studies covering from radiation effects for chemical modification to fundamental collision process of cluster ions with solid matter.

In nuclear science and radioisotope production, the development of positron-emitting radioisotopes to be used in biology was continued. In particular, production of Br isotopes (especially ^{76}Br) was developed using an isotope separator. For the therapy of cancer of bone, synthesis method of endohedral ^{133}Xe-fullerol was developed by addition reaction of hydroxyl groups to endohedral ^{133}Xe-fullerene.

In the field of ion beam engineering, the effect of thin layer (Bonding agent) on fluorine penetration in the teeth were measured by using proton induced gamma-ray emission (PIGE) in the micro beam system. In the in-air micro-PIXE analysis, the accumulation of cisplatin in the nucleus was confirmed for the first time in human gullet cancer cells TE-1. In order to study the particle scavenging properties and the chemical characteristics of snow crystals, in air micro-PIXE analysis was newly applied. The sub-micron ion beam system was successfully achieved to produce the minimum beam width of 0.16±0.02μm in diameter with 46keV H_2^+ beam. The stable generation of fullerene (C_{60}) ions have succeeded by Freeman ion source with grain size sample of C_{60}. To study the interaction between MeV energy cluster ions and matter, secondary charged particles were measured by using TOF mass spectrometer. The 1MeV H^+ and 3MeV Zr^{+4} ion beams were irradiated on silica glasses and phosphosilicate glasses. The result indicated that H^+ density in the glass after doping was no drastically change to effect ion conductivity of the glasses.

In the field of radiation shielding for accelerator facilities, three experiments have been conducted aiming to contribute to the radiation safety of the accelerator facilities. The first one is on the characterization of ^{38}Cl and ^{39}Cl produced by high-energy(40MeV) neutron

irradiation to Ar gas containing aerosol, and these radio nuclides turned out to be formed as aerosol, acidic gas and gases. The second one is on a successful measurement of secondary charged particle spectrum from tens of MeV neutron induced reactions using a newly-developed Bragg Curve Spectrometer (BCS). The third one is on a successful test of a newly-developed phoswitch-type neutron monitor detector applicable to neutrons with energies from the thermal energy up to 100MeV.

In the field of accelerator technology, on development of a flat-top acceleration system for the AVF cyclotron, a preliminary beam of 260MeV $^{20}Ne^{7+}$ was accelerated successfully by flat-top conditions. In order to measure the energy spread of the beams with high resolution using a dispersive magnet system, a new micro-slit system with a minimum gap of 10μm was planned. On measurement of the energy spread for the several MeV proton beams using the nuclear resonance method, an automatic measurement technique was applied so that acquisition time reduced to a third. An emittance value of the Helium beam generated by the RF source was measured using the multi-slit CCD type monitor, which was developed to measure it easily and quickly with low cost.

The AVF cyclotron was operated 3433 hours in 2002 fiscal year. The frequencies of the changes of ion species, beam energy, beam course and harmonics in a year has been gradually increased. This is the result the machine has accepted many requests of the users. In order to avoid from the radiation damages for the electronic components of the cyclotron, an estimation of accumulated dose for the surrounding devices of the cyclotron was carried out.

The reception of the users and the supports on utilizations for the experiments, safety management of the radiation controlled area, and other duties have been practiced smoothly.

The Twelfth TIARA Research Review Meeting was held on June 19 and 20, 2003 in Takasaki, of which subjects were reported in this issue. 13 oral and 87 poster papers, and two invited lectures were presented. 313 persons participated the meeting.

We owe the progress mentioned above to advices of the Consultative Committee for the JAERI-Universities Joint Research Project and Subcommittee of TIARA of Advisory Council for JAERI's Research Facilities.

Masahiro Saidoh, Director
Advanced Radiation Technology Center
Takasaki Radiation Chemistry Research Establishment

This is a blank page.

Contents

1. Semiconductor for Space

This is a blank page.

1.1 Analysis of proton degradation for triple-junction space solar cell

T. Sumita*, S. Kawakita*, M. Imaizumi*, S. Matsuda*,
T. Ohshima**, A. Ohi** and T. Kamiya**
National Space Development Agency of Japan*
Department of Material Development, JAERI**

1.Introduction

Since satellites are mainly powered by solar cells in space, analysis of proton radiation damage on solar cells is extremely important for predicting performance of solar cells on an orbit. Although radiation tolerance of Si and GaAs space solar cells has been investigated by many groups[1-3], multi-junction solar cells consist of various bandgap semiconductors have recently received considerable attention because of their high conversion efficiency. Therefore, analysis of radiation tolerance of the multi-junction solar cells is necessary in order to apply the such cells to space satellite missions.

The Jet Propulsion Laboratory (JPL) has developed much methodology for predicting performance degradation due to trapped protons and electrons in space with certain energy spectra, using ground-based irradiation experiments with mono-energetic particle irradiations. In the prediction methodology, relative damage coefficients (RDC) are derived from the irradiation measurements. The RDC curve indicates the cell output degradation attributed to high energy particle-induced defects as a function of particle energy.

In this paper, we report the results of irradiation experiments with various energies of protons on triple-junction (3J) solar cells optimized for space use and analyze the obtained RDC curves.

2.Experimental

Figure 1 shows a schematic of the InGaP/GaAs/Ge 3J solar cell formed by stacking three different sub-cells with tunnel junctions that was used in this study. Anti-reflection coating (ARC) layer was deposited on the top of the cells. In order to investigate the influence of the specific sub-cell damage in detail, we varied the proton energy from 0.03 to 10MeV by using three types of accelerators (ion-implanter for 0.03 to 0.38MeV, tandem accelerator for 1 to 5MeV and AVF cyclotron accelerator for 10MeV) at JAERI. The implanted proton range was determined by the TRIM simulation[4]. The cell performance under calibrated dual light sources solar simulator adjusted to the AM0 spectrum were measured before and after the irradiations. The spectral response (SR) of each sub-cell was obtained by using monochromatic light source with color bias light illumination on a 3J cell. The lock-in amplifier distinguishes between a specific sub-cell response by the chopped monochromatic light and steady output from other two sub-cells due to the color bias light.

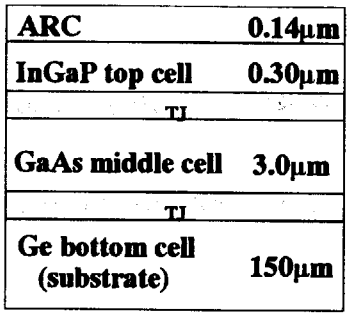

Fig.1 Schematic of the 3J cell for space use. The each sub-cell has connected in series through the tunnel junctions (TJ).

3.Results and Discussion

Figure 2 shows typical degradation trends of the solar cell parameters (short circuit current: Isc, open circuit voltage: Voc, and maximum power: Pmax) as a function of proton fluence for various proton energies. The remaining factor of the vertical axis is defined as the ratio of the value after proton irradiation to the one prior to the irradiation.

The RDCs were derived from fitting both the degradation curve as a function of proton fluence for various proton energies and empirical equation produced by JPL[2]. The RDC values are normalized to the fluence at the degradation level of a certain energy irradiation by that of 10 MeV case. In case of the proton energy range at high RDC values means low radiation tolerance for the proton irradiation. In this study, RDC is chosen at reference

degradation levels of 80% remaining Pmax, 90% remaining Voc and Isc, as shown in Fig.3.

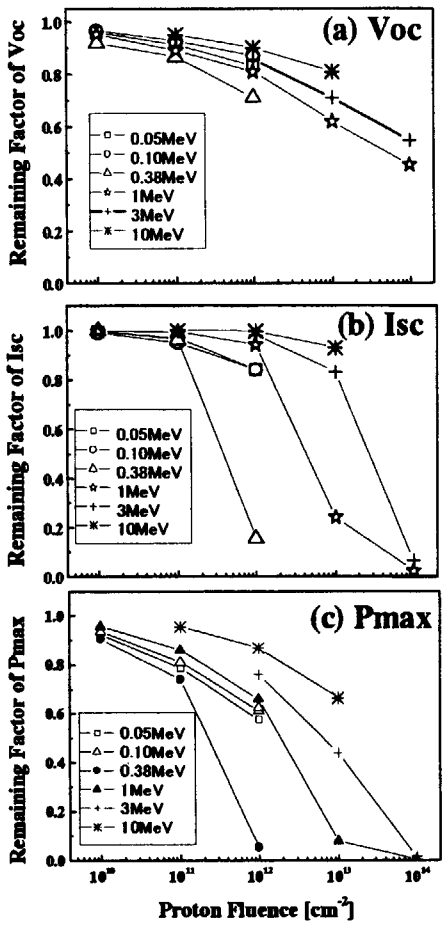

Fig.2 Degradation of (a) Voc , (b) Isc and (c) Pmax as a function of proton fluence for various proton energies.

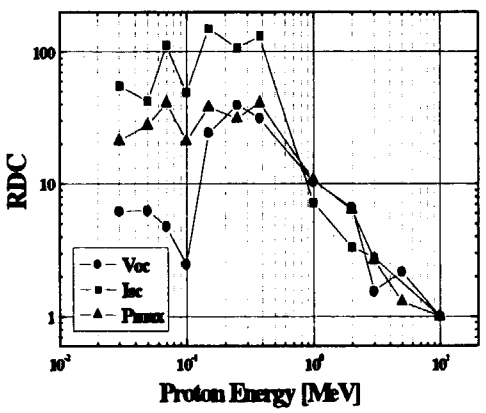

Fig.3 Relative damage coefficients for proton degradation of the 3J cell.

The RDC curve of Voc exhibits three maxima at energies around 0.03, 0.25 and 2.0 MeV. When protons are accelerated with these energies, the proton ranges agree with the depths of p-n junctions for each sub-cell by the TRIM calculation. Because the Voc of the 3J solar cell corresponds to the sum of generated-voltages from each sub-cell, although radiation tolerances for each sub-cell are different, Voc are directly influenced from the damage on each sub-cell due to specific proton energy irradiation. Therefore, proton induced degradation of Voc for 3J cell strongly depends on both the cell structure and the range of the irradiated protons where the density of induced defects is supposed to be maximum.

The RDC curves of Isc and Pmax, however, tend to be scatter for less than 1 MeV irradiation. Isc of the 3J solar cell is determined by a junction that has the lowest current output of all three junctions because the cells are connected in series. For multi-junction solar cells, however, the each sub-cell performance cannot be obtained directly. In order to estimate the current output performance for each sub-cell, spectral response of individual sub-cells was investigated. Numerical convolution of the AM0 solar spectrum with the spectral response provides the relative Isc for the individual sub-cells. Figure 4 shows Isc degradation of InGaP and GaAs sub-cells as functions of proton energy and fluence. For comparison, Isc degradation of 3J cell is also presented in this figure. Since Isc of the Ge bottom cell is much larger than that of the other two sub-cells, the response for the Ge sub-cell was not plotted.

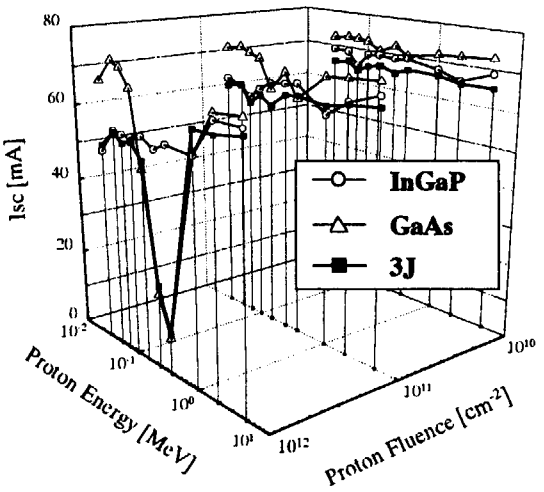

Fig.4 Degradation of Isc for the InGaP, GaAs sub-cells and the triple junction cell 3J as functions of proton energy and fluence.

When proton fluence is less than 10^{11} cm^{-2}, the InGaP top sub-cell is considered to limit the Isc of the 3J cell in the entire energy region. After irradiation with 0.15-0.38MeV at 10^{12} cm^{-2}, however, the performance of GaAs middle cell is significantly decreased and the GaAs cell becomes the current-limiting cell. Therefore, the current-limiting cell changes due to specific proton irradiation conditions. This is the reason that the empirical equation, (which is used to derive the RDC value from the degradation curve), established based on single junction cells cannot accurately express the Isc degradation characteristics for the 3J cells above 10^{12} cm^{-2} fluence.

If the JPL prediction methodology simply applies to the multi-junction cell for satellite mission, we must pay attention the GaAs middle cell damage by irradiated protons that penetrate InGaP top cell on an orbit. Since the protons that cause the most severe damage on the GaAs cell are related to many factors (cover glass thickness, satellite inclination, mission term, cell structure and so on..), the investigation of radiation environment for the certain orbit is also necessary.

4.Summary

The degradation of an InGaP/GaAs/Ge triple-junction space solar cell by proton irradiation was investigated. The relative damage coefficients (RDC) of the cell were derived through measurements of cell performances of Isc, Voc and Pmax. The degradation of Isc is mainly due to damage on the GaAs middle cell, which becomes the current-limiting cell after a certain level of irradiation. On the other hand, the RDC curve of Voc has three maxima for significant proton energies. This is because the Voc degradation for the 3J cell occurs when proton ranges correspond to the junctions of each sub-cell.

References

1) I. Weinberg, S. Mehta and C. K. Swartz, Appl. Phys. Lett. 44 (1984) 1071
2) H. Y. Tada, "*Solar Cell Radiation Handbook, Third Edition*"(JPL Publication, 1982)
3) B. E. Anspaugh, "*GaAs solar Cell Radiation Handbook*" (JPL Publication, 1996)
4) J. F. Ziegler, J. P. Biersack and U. Littmack, in "*The Stopping Range of Ions in Solids*", 1985

1.2 Study about the Hardness-by-design methodology in deep sub-micron CMOS processes

H.Shindo*, Y.Iide*, N.Ikeda*, S.Kuboyama*, S.Matsuda*,
T.Hirao**, T.Ohshima**, M.Yoshikawa** and T.Kamiya**
Office of R&D, National Space Development Agency of Japan*
Department of Material Development, JAERI**

1. Introduction

In recent years, requirements to improve the performance and reduce the cost of the integrated circuits for space use have been increasing. Hardness-by-design methodology utilizing a sub-micron process for commercial ASICs (Application Specific Integrated Circuit) has been extensively investigated over the last several years. Actually, these radiation-hard cells have been developed using up to 0.25μm CMOS commercial processes[1]. In addition, previous works have shown that the total-dose tolerance of integrated circuits manufactured in commercial CMOS processes may satisfy the space mission requirement[2]. There are several advantages and disadvantages in utilizing commercial processes. Because the hardening techniques utilizing the hardness-by-design approach do not require any modification of the fabrication process, we can use state-of-the-art process with the field data including reliability information based on the volume production in commercial markets. However, these hardening techniques impose some penalties on the Si chip size, speed and power for the redundant portion[1]. In addition, the deep sub-micron technologies are generally believed to be more sensitive to Single-Event Effects (SEEs)[3]. So, it is very important to determine whether the deep sub-micron process (<0.2μm) is reasonable for designing the circuits for space use.

The objective of this study is to evaluate SEL (Single event Latch-up) and SEU (Single Event Upset) sensitivities of 0.18μm CMOS process with hardness-by-design methodology.

2. Experimental

2.1 Sample Devices

We designed test chips to evaluate SEE susceptibilities of 0.18μm CMOS commercial processes. The test chips were fabricated at TSMC (Taiwan) and Fujitsu (Japan) with their 0.18μm CMOS processes. The TSMC process uses an epitaxial wafer, a p-substrate, an n-well, six metal layers, one poly-silicon layer, and a drawn poly-silicon gate length of 0.18μm. The Fujitsu process also uses an epitaxial wafer, a p-substrate, a twin-well, six metal layers, two poly-silicon layers, and a drawn poly-silicon gate length of 0.18μm. Figure 1 shows the overview of the test chip. The two test chips contained four types of latch cells with hardness-by-design in addition to the native latch supplied by each foundry. The latches included in the test chips were selected from the published materials. The DICE[4] (Dual Interlocked Storage Cell) has a unique structure in which stored information is retained in two separate nodes. Corrupted information at one node cannot propagate to another node and is recovered automatically by the correct node. The Norly latch[5] also has two separate latch nodes, but it prevents error propagation based on the ratio of the driving capability of the transistors. The Baze inverter[6] also has a unique structure to prevent the transient current signal with an isolated n-well layer.

2.2 Test Setup

Sample devices were controlled by small microprocessor card. The experiments were performed with mono energetic ions obtained from the heavy-ion accelerator at Japan Atomic Energy Research Institute (JAERI) Takasaki. We use N, Ne, Ar, Kr and Xe ion for irradiation test. The test chips fabricated at TSMC and Fujitsu

contain the hardness-by- design latches described above. Each latch was constructed as a 512-bit memory block. Several types of standard SRAM macro were also included in test chip in order to evaluate the SEL susceptibility under more stringent design conditions because the SRAM macro was usually designed with narrower element spacing than the standard cells.

3. Results and Discussion

No SEL was observed during the irradiation up to 64.1MeV/(mg/cm2) of LET with a fluence of $10^7 cm^{-2}$. Both the TSMC and Fujitsu processes utilize an epitaxial wafer, and both of them use Shallow Trench Isolation (STI) technology which effectively reduces the current gain of a parasitic lateral bipolar transistor to prevent SEL[7].

Figures 2 and 3 show the SEU cross-sections as a function of LET for the TSMC and Fujitsu chip. It is said that the most robust latch was the DICE cell. No SEU was observed up to 64.1 [MeV/(mg/cm^2)] of LET in the TSMC chip, and only a few SEUs were observed at a LET of 39.4 [MeV/(mg/cm^2)] in the Fujitsu chip. The Baze latch in Fujitsu chip exhibited an SEU cross-section larger than the native latch in contrast. For the Norly latch, the SEU cross- section was improved about tenfold compared with the native one for the TSMC chip. However, it was not greatly improved for the Fujitsu chip. The fact may indicate that it is difficult to select the ratio of driving capability of the transistors in the cell. A detailed analysis is necessary to explain these phenomena.

4. Conclusion

In this study, we evaluated basic SEL and SEU sensitivities of 0.18μm CMOS technologies with hardness-by-design methodology. The test chips had a strong SEL tolerance with their native standard cells. The result may be attributable to utilization of STI technology. The results suggest that the commercial technologies can be applied to space applications with modification to only several storage cells for SEEs. The results also demonstrated that the DICE cell had a very strong tolerance to SEU and SET effects.

References

1) Joseph M. Bandito, IEEE NSREC Data Workshop Record (2002) 58-61.
2) R. C. Lacoe, V. Osborn, R. Koga, S. Brown, and D. C. Mayer, IEEE Trans. Nucl. Sci., Vol. 47, No. 6 (2000) 2334 -2341.
3) F. Faccio, K. Kloukinas, A. Marchioro, T. Calin, J. Cosculluela, M. Nicolaidis, and R. Velazco, IEEE Trans. Nucl. Sci., Vol. 46, No. 6 (1999) 1434-1439.
4) T. Calin, M. Nicolaidis, and R. Velazco, IEEE Trans. Nucl. Sci., Vol. 43, No. 6 (1996) 2874-2878.
5) M. Norly Lui, and Sterling Whitaker, IEEE Trans. Nucl. Sci., Vol. 39, No. 6 (1992) 1679-1684.
6) M. P. Baze, S. P. Buchner, and D. McMorrow, IEEE Trans. Nucl. Sci., Vol. 47, No. 6 (2000) 2603-2608.
7) A. H. Johnston, IEEE Trans. Nucl. Sci., Vol. 43, No. 2 (1996) 505-521.

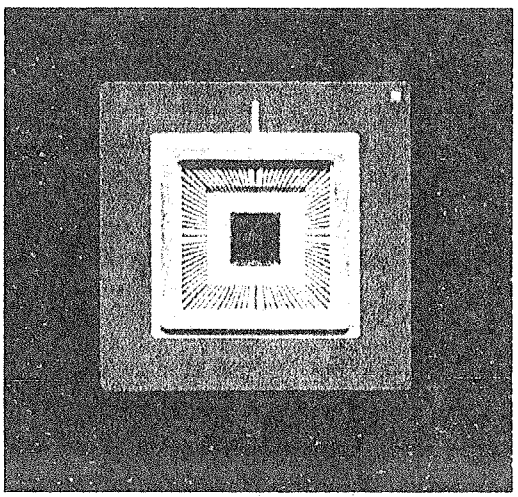

Fig. 1. Test chip (TSMC).

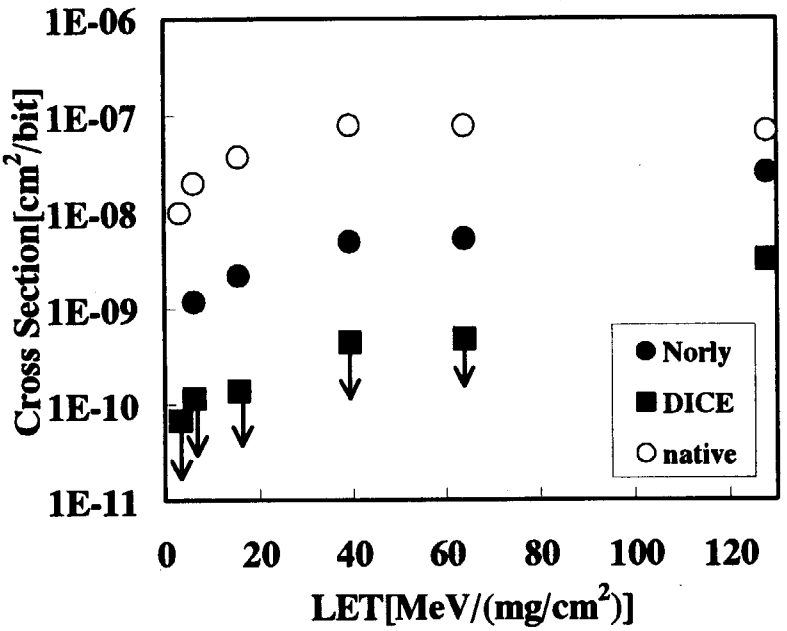

Fig. 2. SEU cross-sections as a function of LET for TSMC chip.

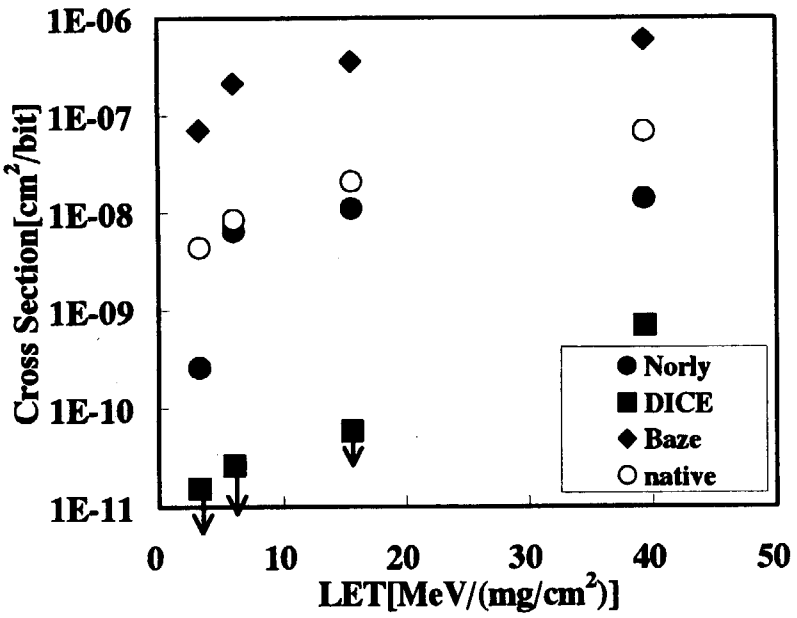

Fig. 3. SEU cross-sections as a function of LET for Fujitsu chip.

1.3 Measurement of Transient Current Induced in Silicon Carbide Diodes using single-ion hit technique

T. Ohshima*, K. K. Lee*, S. Onoda*, T. Kamiya*, M. Oikawa**,
J. S. Laird*, T. Hirao* and H. Itoh*
Department of Material Development, JAERI*
Advanced Radiation Technology Center, JAERI**

1. Introduction

Silicon carbide (SiC) is regarded as a promising candidate for high power and high frequency devices owing to its excellent chemical stability and physical properties[1]. Besides, it is expected that SiC be applied to electronic devices used in high radiation environments like space because SiC has high radiation resistance[2,3]. For the development of radiation resistant devices based on SiC, it is very important to understand their response to ionizing radiation. McLean *et al.*[4] has shown the relationship between bulk damage and electrical characteristics of SiC devices. Furthermore, it was reported that no significant degradation in the electrical characteristics of SiC junction field effect transistors was observed up to the neutron fluence above 10^{15} n/cm^2 at room temperature[5].

Ion Beam Induced Current (IBIC) is a unique technique for the investigation of charge generated by ion irradiation. Furthermore, single-ion hit transient IBIC (TIBIC) is a very useful technique for the study of high-speed current generated in devices without radiation damage[6]. Manfredotti *et al.*[7] reported IBIC induced in 4H-SiC Schottky diodes under different bias voltages. However, in previous studies, only IBIC in SiC Schottky diodes by light ion irradiation were reported. The study of TIBIC in SiC p-n diodes has not yet been reported, especially with heavy ions. However, the study of high-speed transients in devices by heavy-ion irradiation is important because such information is essential to understand the single event phenomena like single event upset. In this article, we report transient current induced in SiC p-n diode by heavy (Nickel) ion irradiation using a single-ion hit system at TIARA.

2. Experimental Details

The p-n diodes used in this study were fabricated on p-type hexagonal (6H)-SiC epitaxial layers grown on 6H-SiC substrates (3.5° off, Si face). The net acceptor concentrations in the epitaxial layers are 5×10^{15} to 1×10^{16} cm^{-3}. The n$^+$-type region with a mean phosphorus (P) concentration of 5×10^{19} /cm^3 was fabricated in the epitaxial layers by a three fold P-implantation (30, 60, 90 keV) at 800 °C, followed by a subsequent annealing at 1650 °C for 3 min. Lift-off technique was used to form Al electrodes on the n$^+$ region. As for electrodes on the backside (p-type) region, Al contacts were alloyed at 850 °C for 5 min, and subsequently Al was re-evaporated on the alloy. Current - voltage (*I* - *V*) characteristics of diodes were measured using Agilent 4156B in a shielded probe station. Leakage currents at a reverse bias of 20V were of the order of several pA. The

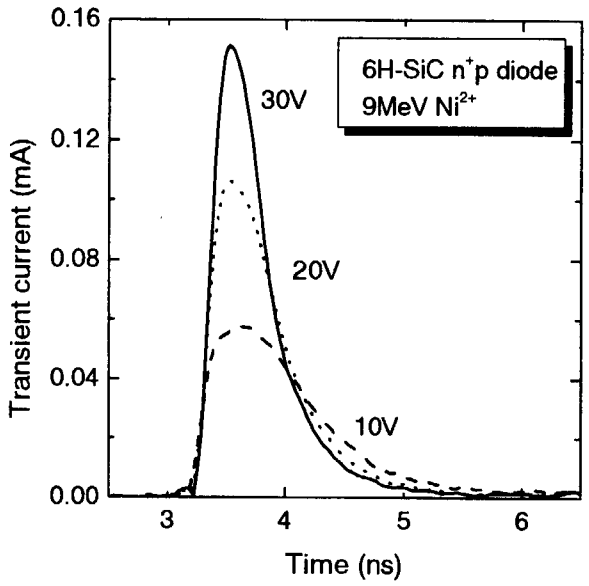

Fig. 1 TIBIC signals for a SiC n^+p diode with a 140 nm thick Al electrode with three different applied biases. The TIBIC signals were obtained using 9 MeV Ni^{2+} particles.

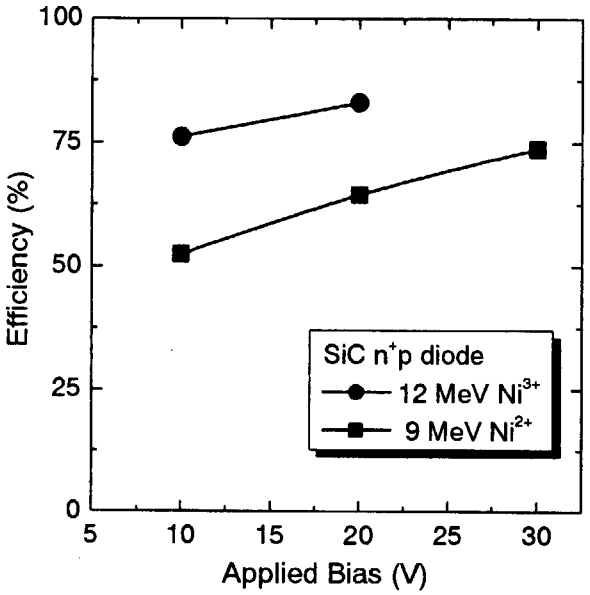

Fig. 2 Applied bias dependence of the charge collection efficiency for n^+p diodes. The circle and square symbols represent results for 12 MeV Ni^{3+} and 9 MeV Ni^{2+} irradiations, respectively.

diodes were irradiated with 9 MeV Ni^{2+} and 12 MeV Ni^{3+} microbeams, and the transient currents were measured using the single-ion hit TIBIC system. The transient current signals were recorded using a 3 GHz Tektronix TDS694C oscilloscope.

3. Results and discussion

Fig. 1 shows the TIBIC signals for a SiC n^+p diode with a 140 nm thick Al electrode with different reverse biases. The TIBIC signals were obtained using 9 MeV Ni^{2+} particles. The amplitude of transients increases with increasing reverse bias. The fall time, which is defined as the time from 90 % to 10 % of the current transients, becomes shorter with increasing reverse bias. This result can be attributed to increasing electric field and depletion width due to increasing applied bias. The depletion width for the diode is approximately 2.5 μm at an applied bias of 30 V. Considering the fact that the end-of-range of 9 MeV Ni^{2+} is about 2.45 μm, therefore, almost all the charges are generated within the depletion layer at an applied bias of 30 V.

The applied bias dependence of the charge collection efficiency is shown in Fig. 2. The circle and square symbols represent the results for 12 MeV Ni^{3+} and 9 MeV Ni^{2+} irradiations, respectively. The charge collection efficiency increases with increasing applied bias. However, the efficiency did not reach 100 % at a reverse bias of 30 V. The ion range of 12 MeV Ni^{3+} is greater than the depletion width (the end-of-range is estimated to be 2.89 μm, and the depletion with is approximately 2.5 μm at an applied bias of 30 V.). This means that both the drift and diffusion components contribute to the TIBIC signal, and some charges generated in the

neutral region did not reach the space-charge region. Thus, a significant portion of the generated electrons recombines with holes in the field-free bulk. On the other hand, as for 9 MeV Ni^{2+} irradiation, the values of efficiency are smaller than those for 12 MeV N^{3+} in spite that the end-of-range for 9MeV Ni^{2+} is shorter than that for 12 MeV Ni^{3+}. In addition, the depletion width at a reverse bias of 30 V is estimated to be longer than the end-of-range of 9 MeV Ni^{2+}, however, the charge collection efficiency is less than 100 %. Manfredotti *et al.*[7] reported that the charge collection efficiency was 100 % when the depletion layer was longer than the ion range. However, their result was obtained using light ions such as He and protons, and the effect of Pulse Height Defect (PHD)[8] is insignificant. On the other hand, in our case, highly ionizing heavy (Ni) particles were used. Therefore, in heavy ion irradiation, it is necessary to consider both nuclear stopping and the recombination of electron-hole pairs within the plasma regions [9]. In addition, Auger and trap-assisted Auger recombination have to be considered for high electron-hole pair generation due to highly ionizing particles. These effects lead to a reduction of the charge collection efficiency. Hence, the result obtained in this study can be interpreted in terms of PHD.

Summary

Transient currents induced in SiC p-n diodes using 9 MeV Ni^{2+} and 12 MeV Ni^{3+} were measured using TIBIC technique. The amplitude of TIBIC signals increases with increasing bias voltage. The fall-time reduces with increasing bias voltage. Complete charge collection efficiency is not obtained even if the depletion width is longer than Ni ion range. This can be interpreted in terms of pulse height defect where the contribution of nuclear stopping and the recombination of electron-hole pairs in initially generated plasma column surrounding the track of the incident ions for highly ionizing particles.

References

1) For example, *"Properties of Silicon Carbide"* Edited by G. L. Harris, EMIS Datareviews Series No. 13, an INSPEC publication, the Institution of Electrical Engineers, London, United Kingdom (1995).

2) T. Ohshima, M. Yoshikawa, H. Itoh, Y. Aoki, I. Nashiyama, Mater. Sci. & Engineer. B **61-62** (1999) 480.

3) K. K. Lee, T. Ohshima, H. Itoh, Mater. Sci. Forum **389-393** (2002) 1097.

4) F. B. McLean, J. M. McGarrity, C. J. Scozzie, C. W. Tipton, W. M. DeLancey, IEEE Trans. Nucl. Sci. **41** (1994) 1884.

5) C. J. Scozzie, J. M. McGarrity, J. Blackburn, W. M. DeLancey, IEEE Trans. Nucl. Sci. **43** (1996) 1642.

6) J. S. Laird, T. Hirao, H. Mori, S. Onoda, T. Kamiya, H. Itoh, Nucl. Instr. and Meth. B **181** (2001) 87.

7) C. Manfredotti, F. Fizzotti, A. L. Giudice, C. Paolini, E. Vittone, F. Nava, Appl. Sur. Sci. **184** (2001) 448.

8) V. Zajic, P. Thieberger, IEEE Trans. Nucl. Sci. **46** (1999) 59.

9) J. Linnros, J. Appl. Phys. **84** (1998) 275.

1.4 Pursuit of Ion Induced Current Collection Process by Multi-Electrodes Structure Diode

- Examination of The Collection Behavior of Ion Induced Current by Adjoined Electrode -

T. Yamakawa [**], T. Hirao[*], S. Onoda [**], J. S. Laird[*], H. Mori [**], T. Wakasa [**], G. Gang[*,***], H. Abe[*], T. Kamiya[*]

Department of Material Development, JAERI [*]
Graduate School of Engineering, Tokai University [**]
Department of Nuclear Physics, China Institute of Atomic Energy [***]

1. Introduction

The highly efficient computer used in the spacecraft contains the mass of memories. SEU (Single Event Upset) and MBU (Multiple Bit Upset), data error in memory cells, are caused by the charge production by due to incident ions. SEU is a memory cell reverses by ion inducing current. MBU is a phenomenon that two or more memory cells reverse by a single ion. The effect of MBU in the space applications is larger than that of SEU. The fundamental processes of MBU have not been fully clarified yet, because MBU is more complicated than SEU. MBU is a phenomenon of reversal of data, which is generated by propagation of a charge in cells that are not irradiated by a single ion. Therefore, the domain where a single ion strikes influences should be investigated.

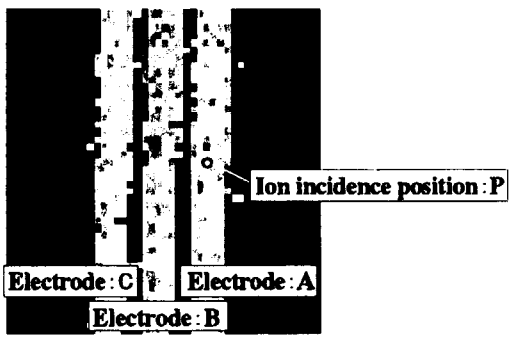

Fig.1 TIBIC image of the line schottky diode.

2. Experiments

In this experiment used the line schottky diode, which has three contacts was used. This device was fabricated on n-type silicon substrate with a doping level of 1.5×10^{15} cm^{-3}. An electrode area and thickness of electrode are 2 μm × 100 μm and about 10 nm, respectively. The each electrode distances of the samples are 4 μm, 6 μm and 8 μm, respectively[1]. During the ion irradiation, bias of −3 V was applied. A microbeam was formed using 15 MeV Carbon ions beam.

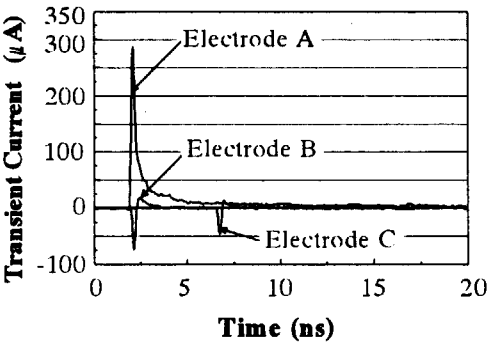

Fig.2 Transient current waveforms collected from each electrode, when 15 MeV C ions hit at position P.

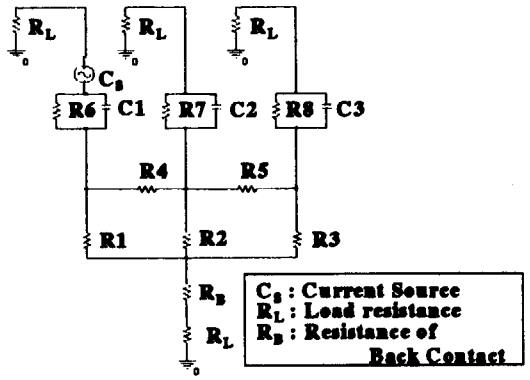

Fig. 3 Equivalent circuit of line schottky diode.

The transient current measurements were made using the Transient Ion Beam Induced Current (TIBIC) system [2, 3]. The microbeam of about 1 μm in diameter was used and the beam was scanned by 1 μm step.

3. Results and Discussion

The obtained TIBIC image was shown in Fig. 1. The width of white portion (~4.5 μm) which means a sensitive area has larger width than the actual electrode (2 μm), because depletion layer extends not only vertically but also horizontally. When a 15 MeV carbon ion hits at position P in Fig.1, a single event transient currents was collected from each electrode as described in Fig. 2. The total collected charges of electrodes A, B and C were 243 fC, 51 fC and 34 fC, respectively. The total collected charge from back contact was 325 fC, which is almost the same as the sum of the charges of there electrodes. Therefore, this fact suggests that Kirchhoff's law is materialized [4]. This seems to be propagation of the charge generation by ion. In order to clarify behavior of the current in the line schottky diode, an equivalent circuit for it was designed as shown in Fig. 3. A regular analysis is performed on a resistance network, which influences a circuit considerably. However, as shown in Fig.2, the different polarity signals were measured. Therefore, it was not able to explain the measured negative signals at electrode B and C by the regular analysis.

Transient analysis was performed with a SPICE code [5]. In order to made the simulation results reproduce the experiment ones, the signal source was decided as follows. The assumed signal source has a pulse current, and a rise time, a fall time, a pulse width (peak hold time), and a peak current of 1.0 ps, 1.2 ns, 0.15 ns and 280 μA, respectively. A signal was introduced from electrode A. This equivalent circuit can be divided into several components; 1) A network of substrate resistances (R_1 – R_5). 2) resistances (R_6 – R_8) and capacitance (C_1 – C_3) for depletion layers. 3) load resistances (R_L). 4) resistance of the back contact (R_B). R_L is the impedance of a measurement system. These parameters are necessary for a SPICE simulation, which are quite difficult to measure, except which the capacitances (C_1, C_2 and C_3) and

Table 1
List and values of the SPICE simulation parameters

R_1	5.00 MΩ
R_2	4.55 MΩ
R_3	5.00 MΩ
R_4	65.8 Ω
R_5	65.8 Ω
R_6	Arbitrary constants
R_7	Arbitrary constants
R_8	Arbitrary constants
C_1	1.46 pf
C_2	1.73 pf
C_3	1.45 pf
R_B	Arbitrary constants
R_L	50.0 Ω
C_s	Signal source

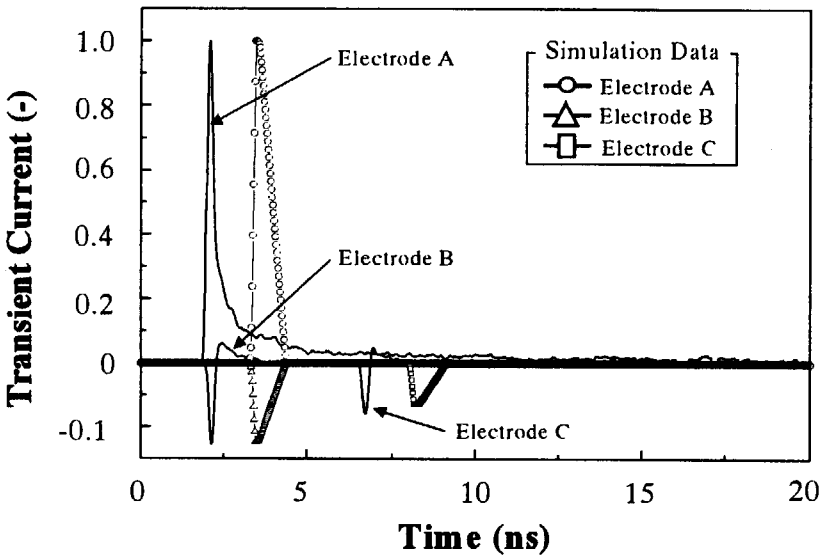

Fig.4 Comparison of the normalized analyzed result with the normalization experimental result.

resistances (R_1, R_2, R_3, R_4 and R_5) which were obtained using C-V meter. The value used for calculation is shown in Table 1.

The result of transient analysis is shown in Fig. 4. Negative signal from electrode B and C, could be explained as a results of charge transformation in the resistance network. The simulation data and the experiment data can be almost the same. However, the same parameters must be arbitrary decided. In order to perform the more accurate simulation, it is necessary to measure these parameters.

5. Conclusion

Transient current waveforms on line schottky diode were measured and simulated. Two negative signals can be explained by the transient analysis on the equivalent circuit using the SPICE simulation code.

Reference

1) H. Mori, T. Hirao, J. S. Laird, S. Onoda, H.Itoh, JAERI-Review 2002-035

2) I. Nashiyama, T. Hirao, T. Kamiya, H. Yutoh, T. Nishizima, H. Sekiguti, IEEE Trans. Nucl. Sci. 40 (6) (1993) 1935

3) J. S. Laird, T. Hirao, H. Mori, S. Onoda, T, Kamiya, H. Itoh, Nucl. Instr. and Meth. B 181 (2001) 87-94

4) *Electrets*, Editor: G. M. Sessler, Publishing Company: Springer-Verlag Berlin Heidelberg New York

5) Gregory J. Fisher, J. A. Connelly, IEEE Transaction Computer-Aided Design. CAD-5 (3) (1986) 429

1.5 Single Event Transients in High-Speed InP/InGaAs Avalanche Photodiodes

J.S.Laird*, T.Hirao*, S.Onoda**, H.Ohyama*** and T.Kamiya*

Department of Severe Environmental Material, JAERI*
Graduate School of Engineering, Tokai University**
Department of Electronic Engineering, Kumamoto National College of Technology***

1. INTRODUCTION

A major source of problems for high-speed communications and optical links are Single Event Transients (SET) induced by MeV ions generated by high-energy proton recoil products and nuclear reactions close to active regions of a device. Since communication systems cannot attenuate these transients without degrading the −3dB bandwidth, they pass directly into photoreceiver encoders generating spurious noise or high Bit Error Rates (BER). Marshall et al. observed that the BER in fiber optic links are primarily dominated by the front-end response of the photodetector, typically a photodiode. They found that BER rates in MHz optical links could be partially mitigated by increasing the optical power[1]. However, modern Gbit optoelectronic links require high sensitivities to maintain negligible BER levels and applying higher power levels can lead to severe non-linearities and a reduction in the receiver bandwidth.

The use of III-V materials such as InGaAsP and InP with higher absorption coefficients results in reduced collection volumes, thereby lowering the sensitivity to vertical strikes. However, high-energy heavy ions impinging within a diffusion length or so of the active volume still pose a problem. Avalanche gain in the multiplication region of an APD enhances charge collection, resulting in a large ultra-fast current transient. Here we discuss charge collection mechanisms responsible for the SET bias and position dependence for an InP-InGaAs APD subjected to focused 18MeV O ions.

2. EXPERIMENTAL

The DUT examined was a 2.5GHz InP-InGaAs Separate Absorption Grading Charge Multiplication (SAGCM) APD. Photons (1.3-1.5μm) pass through the p^+n-n^+ InP region (multiplication) into the InGaAs where absorption and electron hole pair (EHP) formation occurs (~1.5eV per pair). The InGaAsP region increases the bandgap discontinuity reducing the otherwise large dark current from InGaAs (small bandgap of ~0.75eV). The inner region defined by the InP mesa is defined MESA while the device perimeter will be referred to as the EDGE

3. TRANSIENT ION BEAM INDUCED CURRENT

A Transient Ion Beam Induced Current system was used for acquiring the spatial dependence of charge collection across the DUT[2]. An 18MeV O beam focused to ~1μm was scanned over the DUT and transient data

collected in single ion mode on a 3GHz Tektronix DSO.

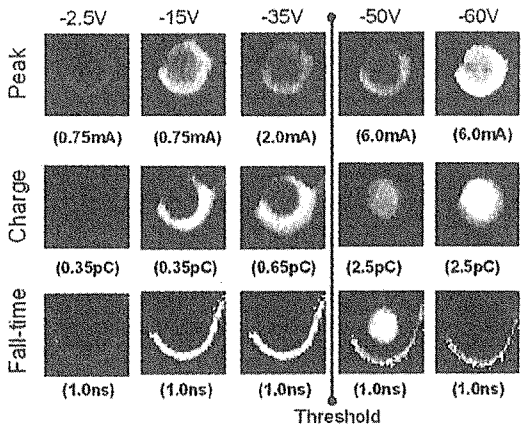

Figure 1: Peak current, charge and transient fall-time images from -2.5V to -60V. At the bottom of each image is the scale used for image generation.

Shown in Figure 1 are 100×100um images generated from the peak current, total charge and transient fall-time for biases ranging from –2.5 to –60V. As seen, the peak current around the EDGE is at all times larger than in the MESA, whereas both the total charge and fall-time undergo a threshold like change between –35V and –50V where the charge in the MESA increases above that of the EDGE while the fall-time decreases. At a threshold bias between –35 and –50V, the MESA charge, peak current and fall-time all increase rapidly due to the onset of multiplication after punch-through.

4. RESULTS AND DISCUSSION

The average MESA SET versus bias dependence shown in Figure 2. Transient characteristics versus bias were extracted for the EDGE and MESA and shown in Fig. 3. The peak current at the EDGE is at all times considerably larger than that of the MESA for all biases. Cho et al. reported enhanced APD currents around the EDGE of guard-less structures using a focused laser and attributed it to higher electric fields[3]. For MESA strikes, the total charge increases in a near-linear manner until a threshold bias of around -35V where it rapidly climbs. Charge at the EDGE undergoes a threshold increase at around -15V, after which it remains flat and again increases. For biases below V_{EDGE}, the InGaAs absorption region in un-depleted and the transient current resulting from the InP field region near the EDGE as well as diffusion in the InGaAs region are small (but non-zero) due to the small potential barrier at the InGaAsP/InP interface.

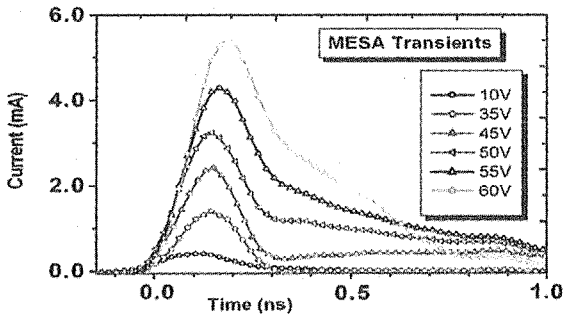

Figure 2: The *magnitude* of the bias dependence for the average SET extracted from the MESA.

A significant fraction of the 18MeV O energy is deposited in the pre-absorption region producing a sharp transient current (<1mA, 0.25pC) due to the large hole mobility of InP. The p^+ diffusion acts as a dead layer resulting in an electron diffusion flow into the field region. At V_{EDGE} (-15V), the InGaAs region near the EDGE begins to deplete and the current increases. Between V_{EDGE} and V_{MESA} (-35V), the InGaAs region near the periphery is depleted and charge is collected

more efficiently (gain mechanisms aside for now). The potential barrier at the interface stops vertical hole transport trapping them in a 2-D well whose shape depends on bias. At this point, they can still diffuse sideways to the EDGE field due to the long carrier lifetimes[4]. As described by Ma et al. the current (and hence total charge) is constant between these two voltages since the diffusion process is independent of bias and the gain is approximately unity. This results in a total charge less than that deposited by 18MeV O (see Figure 3). After V_{MESA}, the potential barrier is surmounted and holes are readily transported to the multiplication region resulting in M>1 and a dramatic increase in the charge.

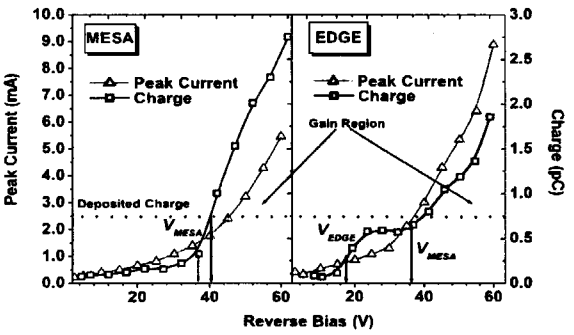

Figure 3: The peak current and total charge as a function of the *magnitude* of the bias for average transients collected from the MESA and EDGE.

5. CONCLUSION

Single Event Transients have been measured in an InP-InGaAs APD for the case of 18MeV O. With the aid of CV and Transient Ion Beam Induced Current Imaging, a simple model explaining the observed bias dependence of the SET has been presented.

REFERENCES

1) C. J. Marshall, P. W. Marshall, C. J. Dale, M. A. Carts and K. A. Label, IEEE Trans. Nucl. Sci NS 45 No 6 pg 2842-2848

2) J.S.Laird, T.Hirao, H.Mori, S.Onoda and H.Itoh," Nuc. Instr. and Meth.B 181 pg 87-94 2001

3) S.R.Cho et al., IEEE Photo. Lett. 12, 5 (May 2000).

4) M.Gallant and A.Zemel, Appl. Phys. Lett. 52 (1988).

1.6 Measurement of Single Event Transient Current using Collimated Heavy Ion Micro Beam (II)

T. Wakasa [**], T. Hirao [*], H. Mori [**], S. Onoda [**], T. Yamakawa [**]
J. S. Laird [*], H. Abe [*], G. Gang [*], T. Kamiya [*]
Department of Material Development, JAERI*
Graduate School of Engineering, Tokai University**

1. Introduction

Semiconductor devises used in the space environments are irradiated with high energy heavy ions. When these ions pass through devices, the dense electron-hole pairs are generated and Single Event Effect (SEE) is induced. Because SEE leads to system failures, it is necessary to clarify the mechanisms of SEE, and raise SEE tolerance to increase the reliability of semiconductor devices used in the space environments. Recently, Silicon on insulator (SOI) structure device is regarded as a high radiation tolerance device, because the buried oxide layer can limit the charge collection. However anomalous charge collection in the SOI structure device was reported [1,2]. In this paper, we discuss the anomalous charge collections in SOI structure devices.

2. Experiments

In this experiment, in order to observe a charge collection we irradiate the heavy ions micro beam to semiconductor devices and measure the single event transient current waveform.

The heavy ions used in this study were 100 MeV O ions accelerated by an AVF cyclotron at JAERI Takasaki TIARA facilities. For 100 MeV O ions, the projection range and LET in Si are 95 μm and 3.1 MeV/ (mg/cm^2), respectively. Details of the method to form the collimated micro beam by using a micro collimator have been described in the previous report [3]. Figure 1 shows the normalized energy spectrum of the collimated micro beam by using 20 μmϕ collimator measured with a Silicon Surface barrier Detector (SSD) and a Multi Channel Analyzer (MCA). In order to decrease the radiation degradation[4] during single event transient current measurement, the beam intensity was reduced by using an attenuator. The beam intensity was several hundred ions/sec.

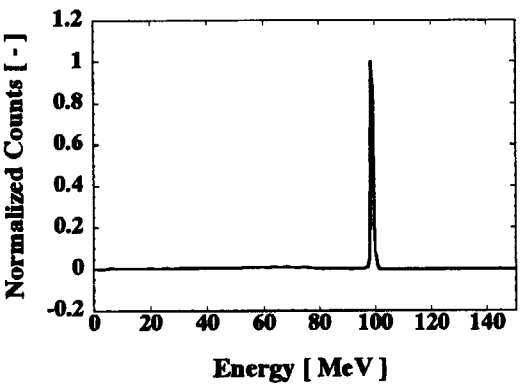

Figure 1. Normalized energy spectrum of 100 MeV O ion beam after passing through collimator (20 μmϕ).

The used samples were silicon SOI p^+n junction diodes with junction diameters of 50 μm, top silicon layer thickness of 3.29 μm and the buried oxide layer thickness of 0.5 μm. We used a digital sampling oscilloscope to measure a single event transient current waveform. In this study, an applied bias was −5 V to −20 V.

3. Results and Discussion

Table 1 lists the dependence of the amount of collected charge on the applied bias. The amount of collected charge Q_{exp} is obtained by integrating the transient current waveform. Q_{top} is the estimated charge in the top silicon layer (width : 3.29 μm). As listed in the table 1, Q_{exp} is about 1.5 times larger than Q_{top}. It was reported that in the case of lower energy, such as 15 MeV C and O ions for the same samples, the amount of collected charge was limited by the buried oxide layer [5]. Recently, similar results were reported, and the various analyses have been done [1, 2]. Vizkelethy et al. suggested that this anomalous charge collection is explained by a displacement current due to perturbation of the electric field at the interface by the ion strike and using the Schockley–Remo-Gun theorem.

However in addition to these analyses, it may be necessary to consider the influence of primary secondary-electron. Figure 2 shows the estimated energy of primary secondary-electron as a function of emission angle at the interface between the top Si layer and the oxide layer. As shown in the figure 2, the maximum energy of primary secondary-electron induced by 100 MeV O ions irradiation is higher than 10 keV and that is one order of magnitude higher than that by 15 MeV C and O ions. For 10 keV electron, the Continuous Slowing Down Approximation range (CSDA range) in Si is about 1.0 μm [6]. It is possible that the secondary-electron reach to the electric field in the top silicon layer, because CSDA range is longer than the oxide layer thickness. According to this effect, the secondary electrons generated within or below the buried oxide layer can contribute to charge collection.

4. Summary

In the case of using high-energy heavy ion, the amount of charge collected in the SOI diodes was found to be larger than collected charge in the top silicon layer. To understand this phenomenon, it is necessary to consider not only the displacement current but also the secondary-electron effect.

In order to clarify this phenomenon, we will simulate the charge transport process in the SOI structure devices by using the ISE-TCAD [7] (3D simulator). In addition to this simulation, we will make an irradiation test using several energy ions to investigate the influence of primary secondary electron.

Reference

1) G. Vizkelethy, et al, Nucl. Inst. and Meth. B (2003) in press.
2) T. Hirao, et al., Nucl. Inst. and Meth. B206 (2003) 457.
3) H. Mori, et al., 9th TIARA Annual Report (1999) 3.
4) T. Hirao, et al., Nucl. Inst. and Meth. B104 (1995) 508.
5) T. Hirao, et al., Nucl. Inst. and Meth. B (1999) 260.
6) J. C. Ashley, et al., IEEE Trans. Nucl. Sci. NS-23 (1976) 1833
7) J. S. Laird, et al., Nucl. Inst. and Meth. B206 (2003) 36

Table 1. Total charge, Q_{exp}, collected in the SOI p^+n junction diode depending on the bias voltage. And estimated charge, Q_{top}, in the top silicon layer is also shown.

	-5 V	-10 V	-15 V	-20 V
Q_{exp}	155 fC	153 fC	152 fC	153 fC
Q_{top}	102 fC			

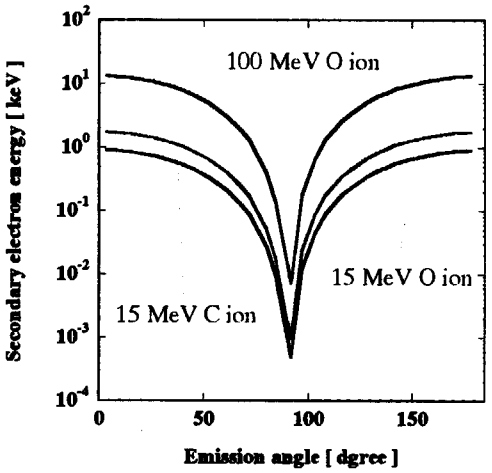

Figure 2. The comparison of primary secondary electron energy generated by the case of 100MeV O ion under the top silicon layer with the case of 15 MeV C and O ion.

1.7 Development of the Measurement System for Quasi-Monoenergetic Neutron Beam Induced Single-Event Effects

H. Abe*, T. Hirao*, H. Hirayama**, T. Sanami**, S. Tanaka***, J. S. Laird*, H. Mori*, S. Onoda*, H. Nakashima****, H. Itoh***** and T. Kamiya*
Department of Material Development, JAERI*
Radiation Science Center, KEK**
Advanced Radiation Technology Center, JAERI***
Center for Proton Accelerator Facilities, JAERI****
Preparations Office for JAERI-JNC Integration*****

1. Introduction

A single event effect (SEE) is caused by the high-density electron hole pairs produced along with the ion track when the charged particle of high energy passes through the activity region in a semiconductor. It is a serious problem when using a semiconductor device in the space environment. It aims at explanation of these effects mechanism. We have already measured the electron charge produced with one ion using the TIBIC (Transient Ion Beam Induced Current) system[1-3], and have obtained the important information for solving the mechanism of SEE.

In recent years, semiconductor devices becomes μm size, therefore the SEE of semiconductor devices for the grounds by the cosmic ray has become a serious problem. It is reported that neutron cause these phenomena[6-8], and the explanation of those mechanisms are pressing need now. It is necessary to clarify the explanation and collection electron charge of the producing processes of a neutron/proton induced SEE.

The final purpose is a synthetic solving and modeling of the mechanism of producing a single event, and is the indicator acquisition to those tolerance semiconductors.

In this research, neutron/proton induced producing the secondary heavy ion charged particles in the semiconductor, when the neutron/proton incidence in it. The transient current measurement system for measuring the amount of collection electron charged currents by the cause of the neutron/proton induced secondary heavy ion charged particles were reconstructed.

2. Experimental

A proton beam from an AVF cyclotron is transported to a ^{7}Li(99.8% purity) target that is a rolled plate of metallic ^{7}Li, 35 mm diameter. A ^{7}Li target with ~5 MeV energy loss was employed for each proton energy as a compromise between the neutron intensity and the energy spread[9]. In this experimental, measurement using neutron energy was 45 and 65 MeV.

A neutron/proton beam measurement system is also make to build the same setup as the TIBIC measurement system performed in the heavy ion beam experiment. As a preliminary experiment, a SSD (Silicon Surface barrier Detector, see the inside of Fig. 1, SSD1) was carried out instead of the semiconductor[10] and a SSD2 was used together with the conventional MCA (Multi-Channel Analyzer). The transient current was measured using the SSD1 which

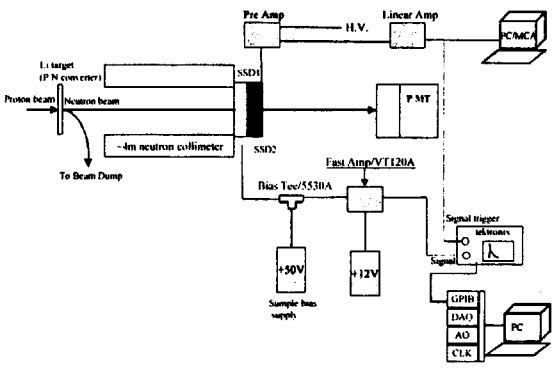

Fig. 1. Outline of reconstructed transient measurement system for neutron/proton beam.

specification is active area: 50 mm^2; sensitive depth: 100 μm; diameter: 10 mmϕ. Since the signal obtained only by SSD1 was small, BiasTee (ORTEC 5530A) and Fast amplifier (ORTEC VT120A) were connected with before DSO (Tektronix model TDS 694C, Fig. 1). Moreover, apart from this measurement system, TOF (Time Of Flight) system was introduced for measurement of neutron beam. Neutron beam energy and incidence beam flux were measured using the TOF method. Irradiation conditions are 45 and 65 MeV neutron/proton beam energy at beam currents ~100 nA/ 300pA.

3. Results and Discussion

The signal was obtained from the SSD1/SSD2 which installed for system reconstruction of a measurement system. A TOF measurement was performed and the quasi-monoenergetic neutron/proton beam measured. A result, the setup for system reconstruction determined Fig. 1. Figure 2 shows TOF measurement checked that was 65 MeV quasi-monoenergetic neutron beam (area inside the solid line in a Fig.). The irradiation condition at this time are beam current: 10 nA, measurement time: 4001.3 sec, an estimation of the amount of neutron irradiation: 6.22 x 10^6 n/cm^2, fluence: 1.6 x 10^4 n/cm^2/sec, yields: 8185 events and 1.32 x 10^{-3} events per neutron 1 n/cm^2.

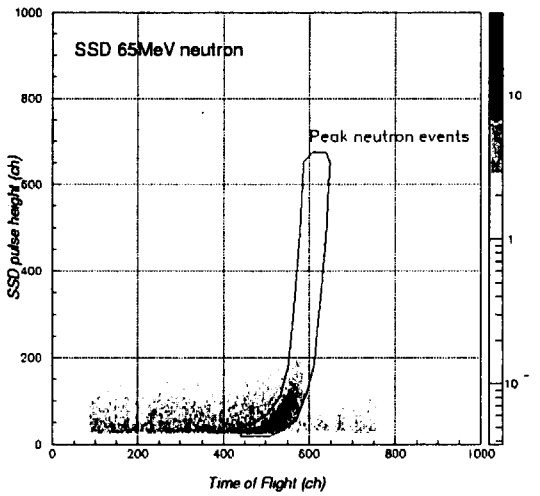

Fig. 2. The 2-dimensional spectrum of 65MeV neutron beam by TOF measurement.

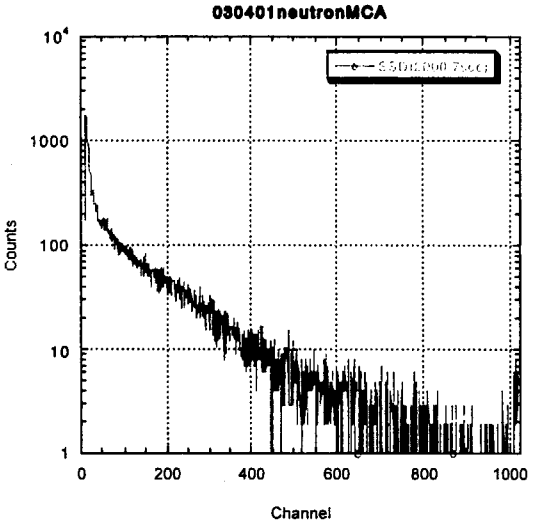

Fig. 3. The spectrum of 65MeV neutron beam by MCA measurement.

Figure 3 shows 65 MeV neutron beam spectrum was obtained by the SSD2. It turns out that the signal is continuously contained to 65 MeV region.

Figure 4 shows the SSD1 obtained the typical transient maximum and minimum peak current waveform at 65 MeV neutron beam. Since it is the amount of collection electron charges that carried out time integration, maximum value -3.556 mA and minimum value -0.145 mA can be estimated as 394.3 fC and 47.2 fC respectively. It turns out that the collection electron charges has occurred within SSD1 between 47 ~ 394 fC.

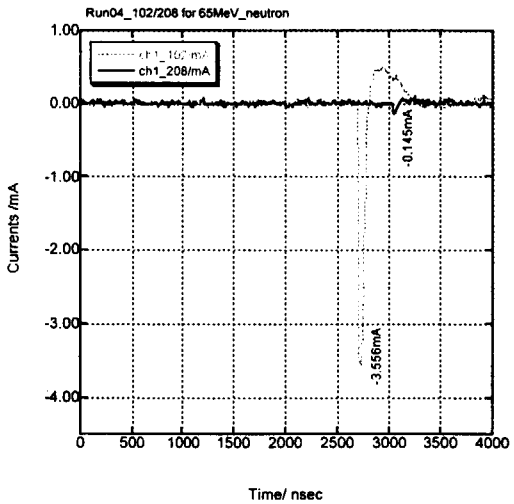

Fig. 4. The transient current waveform were produced within SSD1 (max. and min.)

Similarly, it was set to 13 ~ 573 fC when 45 MeV irradiation was estimated.

Figure 5 shows the same estimate was performed also about 65 and 45 MeV neutron/proton beam. The neutron irradiation shown ● and the proton irradiation shown ■. Neutron/proton irradiation are found that the width of producing of a collection electron charges are narrow range by 65 MeV irradiation, although there is generation of the collection electron charge in a wide range in the case of 45 MeV irradiation. Moreover, it is seen that the neutron induced the collection electron charges range between maximum value and minimum value more widely range than proton induced them. This is considered because the neutron/proton induced particle which generation/reaction probability was carried out inside SSD1.

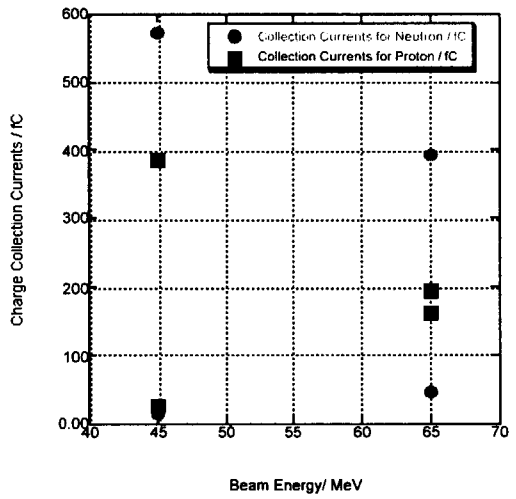

Fig. 5. 45 and 65 MeV neutron/proton beam induced collection electron charge currents (max. value and min. value).

Realizing that ionization produces spurious charge (and current) to cause SEE in sensitive node regions of microcircuits, neutrons can produce such ionization charge through a) neutron collisions that excite nuclei, which de-excite by emitting ionizing gamma rays; b) neutron collisions that produce ionizing recoil atoms or ions from lattice displacements if they are sufficiently energetic; and c) inelastic collisions by which the neutron is absorbed in the nucleus which then emits a charged particle, as in (n, α) and (n, p) reactions where the α and p-product particles can ionize.

As mentioned above, it was completed that the reconstructed measurement system obtained about transient current of quasi-monoenergetic neutron/proton beam induced the secondary heavy ion charged particles.

Although identification of these particles or identification of secondary heavy ion particles' energy has not been performed yet, these charged particles are due to be identified from now on.

A future study, we are going to carry out the irradiation to semiconductor devices using a neutron/proton beam.

References

1) T. Hirao, I. Nashiyama, T. Kamiya, T. Suda, T. Sakai and T. Hamano, Nucl. Inst. and Meth. B 130 (1997), p.486.
2) T. Hirao, T. Hamano, T. Sakai and I. Nashiyama, Nucl. Inst. and Meth. B 158 (1999), p.260.
3) T. Hirao, H. Itoh, S. Okada and I. Nashiyama, Radi. Phy. and Chemi. 60 (2001), p.269.
4) J. S. Laird, T. Hirao, H. Mori, S. Onoda, T. Kamiya and H. Itoh, Nucl. Inst. and Meth. B 181 (2001), p.87.
5) H. Mori, T. Hirao, J. S. Laird, S. Onoda, T. Kamiya, H. Itoh, T. Okamoto, Y. Koizumi, Nucl. Inst. and Meth. B 181 (2001), p.340.
6) C. S. Dyer, J. Farren, A. J. Sims, J. Stephan and C. Underwood, IEEE Trans. Nucl. Sci., NS-39 (3), (1992) p.413.
7) C. S. Guenzer, E. A. Wolicki and R. G. Allas, IEEE Trans. Nucl. Sci., NS-26 (6), (1979) p.5048.
8) C. A. Gossett, B. W. Hughlock, M. Katoozi, G. S. LaRue and S. A. Wender, IEEE Trans. Nucl. Sci., NS-40 (6), (1993) p.1845.
9) M. Baba, Y. Nauch, T. Iwasaki, T. Kiyosumi, M. Yoshioka, S. Matsuyama, N. Hirakawa, T. Nakamura, Su. Tanaka, S. Meigo, H. Nakashima, Sh. Tanaka and N. Nakao, Nucl. Inst. and Meth. in Phys. Res. A 428 (1999) p.454.
10) R. G. Miller and R. W. Kavanagh, Nucl. Inst. and Meth. 48 (1967) p.13.

1.8 Analysis of Failure Caused by Cosmic Rays in High-Voltage High-Power Semiconductor Devices

(3rd Report)

Hideo Matsuda*, Ichiro Omura*, Yoko Sakiyama*,
Satoshi Urano*, Susumu Iesaka*, Hiromichi Ohashi**,
Toshio Hirao***, Hiroyuki Abe***, Tomihiro Kamiya***,
Hideki Mori****, Shinobu Onoda****,
Takeshi Wakasa****, Takeshi Yamakawa****
Toshiba Corporation, Semiconductor Company *
Toshiba Corporation, R&D Center **
Department of Material Development, JAERI***
Graduate School of Engineering, Tokai University****

1. Introduction

High power semiconductor devices have been widely used in key industries, for instance, traction, transmission, etc. A failure of such power devices induced by cosmic rays at the sea level has been observed[1]. It is considered that high power devices fail or breakdown by interaction between Si and cosmic rays, e.g., high energy neutrons and protons.

The aims of this work are to examine the device failure by proton irradiation, to compare and investigate the failure modes and the failure rates obtained by actual cosmic rays to those by proton irradiation test and to estimate the failure rates by cosmic rays by the new method obtained by equivalent proton irradiation. That is quite useful for designing high power devices having high performance as well as high reliability. The other aim is to establish model of failure mechanism and design rule of power devices from the dependence of electric field at failure on heavy ion irradiation energy.

2. Experiments

2.1 Field Test

The test circuit of field test is shown in Fig.1. DC high voltage is applied to DUT (Devices Under Test) during field test. Resistance is inserted between DC high voltage supply and each DUT to restrict the current. Time when DUT failed is monitored to estimate the failure rate.

2.2 Proton irradiation

An AVF-cyclotron at TIARA has been used for proton irradiation. Parameters are proton energy and fluence. The failure rate of high power devices was derived from the number of failures divided by proton fluence. The block diagram of test system is schematically shown in Fig.2.

2.3 Heavy ion irradiation

An AVF-cyclotron at TIARA has also been used for heavy ion irradiation. Ne(75MeV) beam, Ar(150MeV) beam and Kr(322MeV) beam were irradiated on DUT. As increasing voltage during irradiation, voltage was monitored when DUT were failed.

3. Results and discussion

3.1 Field Test

The field test results are shown in Fig.3 indicated by "cosmic ray". Horizontal

axis represents electric field parameter $S^{(2)}$, which relates to maximum electric field in DUT. Vertical axis represents failure rate divided by resistivity of DUT, which is equivalent to cross-section of single event burnout. The failure rates increase exponentially with electric field.

3.2 Proton irradiation

The DUT suddenly failed by proton irradiation during voltage supplied. The phenomenon is very similar to the failure caused by actual cosmic rays. Fig.3 also shows the failure rate by proton irradiation. The failure rate increases as irradiation energy and electric field increases. The slope of the failure rate obtained in this test is similar to that of the failure rate by actual cosmic rays or by neutrons irradiation. These results show that it is possible to carry out an equivalent testing of cosmic ray failure rate by proton irradiation instead of real cosmic ray irradiation.

3.3 Heavy ion irradiation

Fig.4 shows the results of heavy ion irradiation. Horizontal axis represents electric field (E_f) where heavy ion stop. Vertical axis represents irradiation energy. As irradiation energy is higher, electric field at DUT failure is lower. For example, "device type A" failed at E_f=8.0E4 with 75MeV Ne beam and at E_f=7.0E4 with 322MeV Kr beam. Electric field at DUT failure also depends on device structure.

4. Conclusion

The test results obtained by proton irradiation are similar to those by actual cosmic ray. It is shown that it is possible to carry out a new equivalent acceleration testing of cosmic ray failure rate by proton irradiation instead of cosmic ray irradiation. Model of failure mechanism and design rule of power devices would be established from the dependence of electric field at failure on heavy ion irradiation energy.

References

1) H.Matsuda, et al, "Analysis of GTO Failure Mode During DC Voltage Blocking", Proc. of the 6th ISPSD, pp221-225, 1994

2)H.R.Zeller, "Cosmic Ray Induced Failures in High Power Semiconductor Devices", Solid State Electronics, 38, pp2041-2046, 1995

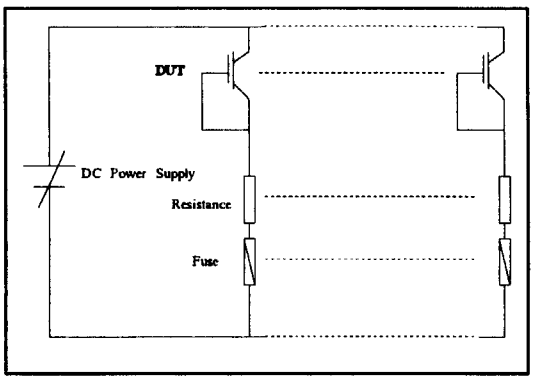

Fig.1 Test Circuit for Field Test

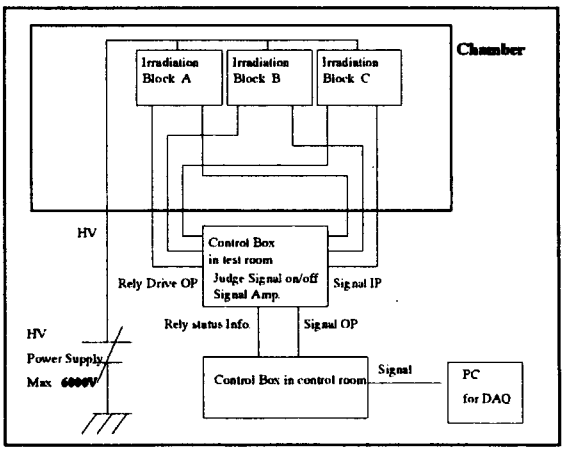

Fig.2 Diagram of Proton Irradiation Test System

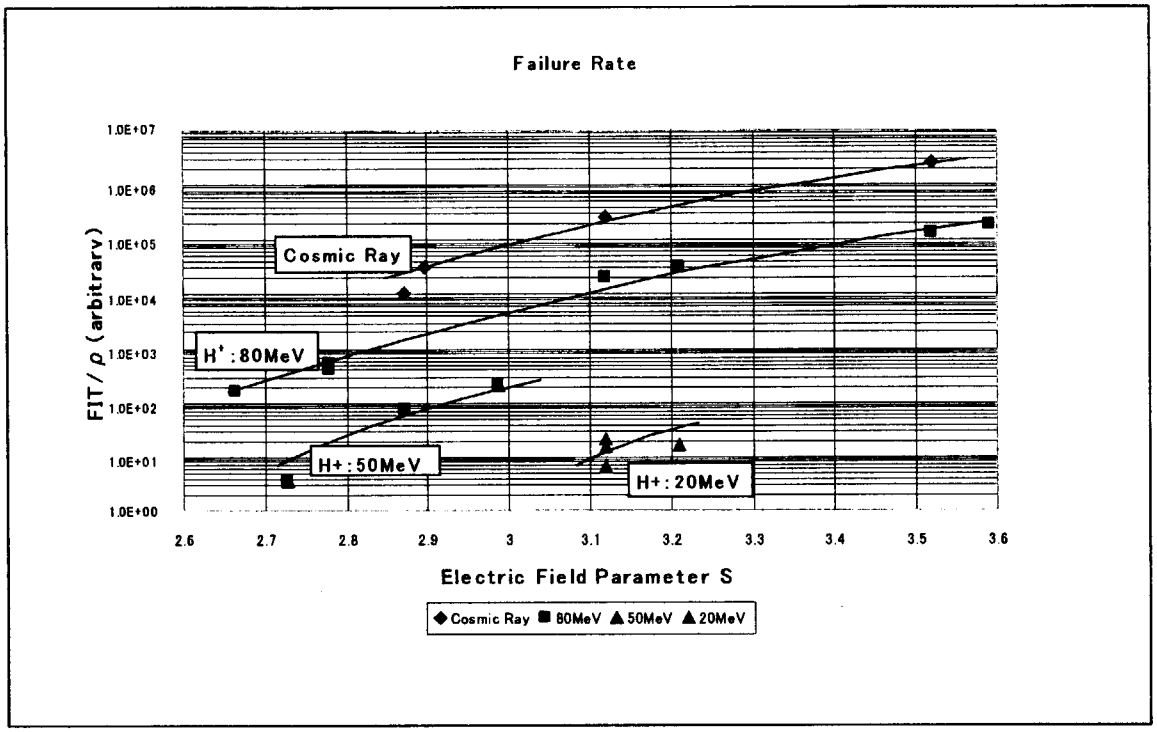

Fig.3 Dependence of Failure Rate on Electric Field

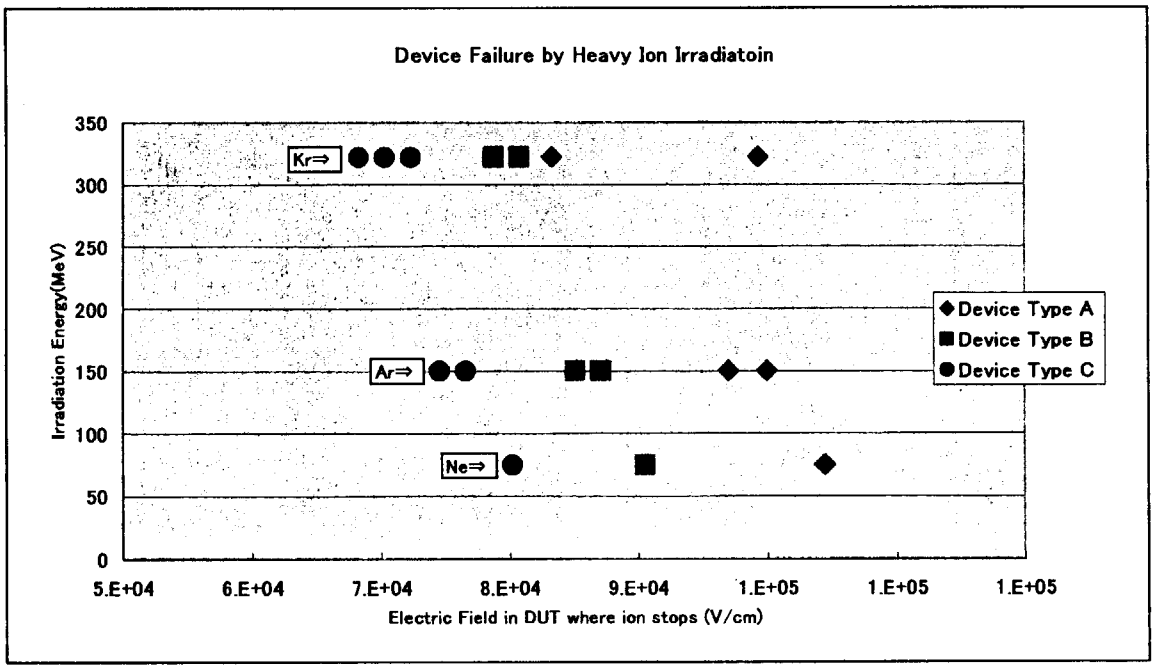

Fig.4 Device Failure by Heavy Ion Irradiation

1.9 Investigation of Irradiation Effects in $CuInSe_2$ Thin Films

A. Yoshida*, A. Wakahara*, H. Okada*, H.-S. Lee*, T. Ohshima**, and T. Kamiya**

Department of Electrical and Electronic Engineering, Toyohashi University of Technology*

Department of Material Development, JAERI**

1. Introduction

$CuInSe_2$ (CIS) is a one of the chalcopyrite semiconductor with a direct band-gap of 1eV. CIS is expected as a base material for realization of thin film solar cells due to its large absorption coefficient. At a present, in CIS-based cell, it was reported that conversion efficiency of 18.8%[1], comparable to that in poly-Si cells. Additionally, recent studies showed that CIS-based cells possess much larger tolerance against high-energy irradiation than Si- or GaAs-based cells.[2)-4)] Thus, CIS-based cell is a strong candidate for space utilization.

For realization of space solar cells, which have larger efficiency and longer lifetime, it is important to clarify the irradiation effects of cell component. Many studies have been reported on irradiation effects of major cell materials of Si or GaAs, however, reports of irradiation effects of CIS itself have not been so much yet[5)-7)]. In this study, we studied fundamental irradiation effects of CIS thin films. Single-crystalline CIS thin films were prepared, and high energy proton and electron irradiation was made. We also observed annealing effect of irradiated CIS films for investigating a recovering behavior of irradiation-induced damages.

2. Results and Discussion

In this study, CIS thin films were prepared by RF-sputtering. For formation of single-crystalline CIS films, semi-insulating GaAs was used as a substrate. For poly-crystalline CIS film, on the other hand, quartz glass substrate was used. Composition of deposited thin films was investigated by electron probe micro analysis (EPMA). From this, Cu/In ratio of 0.91 to 0.94, and Se/(Cu+In) of 1.03 to 1.05 were obtained. Electric properties of prepared films were characterized by Hall effect measurement using van der Pauw configuration. Both single- and poly-crystalline films showed n-type conductivity. As-grown carrier density was in range of $2x10^{16} \sim 2x10^{17}$ cm^{-3} for single-crystals, and about $1x10^{18}cm^{-3}$ for poly-crystalline films.

High energy proton and electron irradiation on CIS thin films were carried out at JAERI. Here, proton energy of 380keV, 1MeV, and 3MeV were selected. For electron irradiation, accelerating energy in 1-3MeV was chosen. During the irradiation, to avoid a sample from heat-up,

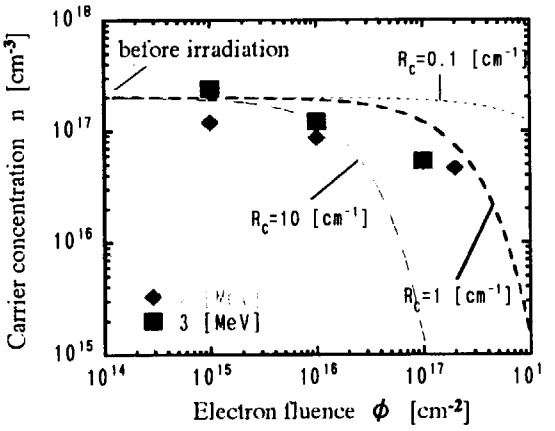

Fig.1: Carrier concentration dependence on the 2MeV and 3MeV electron fluence.

the sample holder was cooled by water circulation, and a sample temperature was kept below 50°C.

Carrier concentration dependence on the electron fluence was characterized by Hall effect measurements. Figure 1 shows carrier concentration dependence on the electron irradiation fluence. It seemed that the decrease of the carrier concentration from the initial value was seen above the electron fluence of $1x10^{17}cm^{-2}$. Similar results were also found in proton irradiation above the proton fluence of $1x10^{13}cm^{-2}$. These results suggest that high-energy irradiation causes introduction of electron traps in CIS films, and density of the trap increased with the increase of irradiation fluence.

Carrier concentration behavior depending on the electron fluence can be empirically expressed as, $n=n_0\exp(-R_c\phi/n_0)$. Here, n is the carrier concentration, n_0 is the carrier density before irradiation, R_c is a carrier removal rate, ϕ is the irradiation fluence. This equation is valid only in the lower fluence region. From the comparison of the equation with experimental results, carrier removal rate, R_c, of about 1 cm^{-1} was obtained for the electron irradiation. For the proton irradiation, carrier removal behavior was also studied, and carrier removal rate was in range from 400 cm^{-1} to 1400 cm^{-1} for single-crystalline CIS. Here, larger carrier removal rate was obtained in lower-energy proton irradiation. These carrier removal rates are comparable to or smaller than those of other compound semiconductor materials for solar cells.

We have studied annealing effects of irradiated CIS films. Recent study demonstrated that annealing of irradiated CIS-based cell is effective to recover its performance [8]. To further investigate this point, we have studied on the annealing effects of irradiated CIS film itself. Annealing of the electron- or proton-irradiated CIS films was performed under the atmospheric environment at 60°C using electric oven. This annealing temperature is chosen as a typical surface

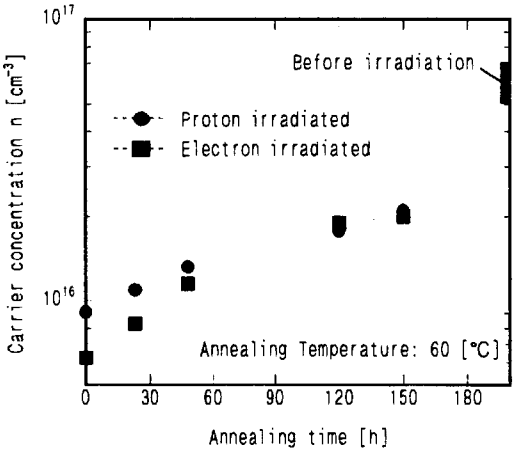

Fig.2: Carrier concentration behavior during the annealing at 60°C.

temperature of the solar cell on the satellite in space. In this study, annealing time dependence of the carrier density of the irradiated CIS films was investigated. As seen in Fig.2, both of the electron- and proton-irradiated CIS films showed increase of carrier concentration that was decreased by the irradiation. These results suggest that annealing possibly makes damaged CIS film recovered.

Change of carrier concentration in irradiated CIS thin film during the annealing was analyzed. In the present analysis, it was assumed that the irradiation-induced damages were recovered by the annealing. We also assumed that carrier concentration behavior obeys a simple rate equation that indicates exponential change of carrier concentration with the annealing time. Experimental results showed reasonable agreement with the proposed rate equation with the time constant τ_T of about 18 days. Obtained time constant of irradiated CIS thin film agrees well with the extrapolated value of similar annealing experiments on CIS-based cells [8]. As stated before, present annealing temperature of 60°C was selected to be close to the temperature of the satellite cell working in space. In space, radiation damage and recover by thermal annealing may occur in cells simultaneously. According to these investigations, we could estimate the performance degradation of the

cell in space radiation environment. A CIS-based cell with 100μm thick cover glass seems to maintain its initial performance in space. This result is well agrees with recent report by NASDA on the MDS-1 satellites.

Reference

1) M. A. Contreras et al., Progress in Photovoltaic, 7-4, pp.311-316 (1999)
2) C. F. Gay et al., Proc. of 17th IEEE Photovoltaic Specialists Conf., pp.151-154 (1984)
3) T. Hisamatsu et al., Proc. of 2nd World Conf. of Photovoltaic Energy Conversion, pp.3568-3571 (1998)
4) H. W. Schock, and K. Bogus, Proc. of 2nd World Conference of Photovoltaic Energy Conversion, pp.3586-3589 (1998)
5) T. Tanaka et al., J. J. Appl. Phys, Vol39, Suppl39-1, pp192-193 (2000)
6) S. Kawakita et al., 17th European Photovoltaic Solar Energy Conf. and Exhibition (2001)
7) Weinberg.I, Swartz.C.K, Brinker.D.J, Wilt.D.M, Conf. Record of the Twenty First IEEE Photovoltaic Specialists Conference, pp1235-40 (1990).
8) S. Kawakita, et al, Jpn. J. Appl. Phys. Vol.41, pp.L797-L799, Part2, No7A (2002)

This is a blank page.

2. Biotechnology

This is a blank page.

2.1 Irradiation of heavy ion microbeam in single tobacco cells

Yuichiro Yokota*, Yasuhiko Kobayashi,** Tomoo Funayama**, Atsushi Tanaka**, Yoshihiro Hase**, Satoshi Kitamura** and Masayoshi Inoue*
Laboratory of Plant Breeding Science, Graduate School of Agriculture, Kyoto Prefectural University*, Department of Ion-beam-applied Biology, JAERI**

Introduction

We showed that tobacco BY-2 cells were 5-10 times more tolerant to ion beams than mammalian cells[1], although the genome size of tobacco was similar to that of mammals. Furthermore, large shoulders were observed in the survival curves of tobacco BY-2 cells. From these results, the tolerance system, probably including DNA repair processes, seems to be different between tobacco BY-2 cells and mammalian cells.

Compared with other radiations, ion beams have differential properties; high LET and the penetration control. Furthermore, microbeam irradiation can control the number of ion particles to be irradiated in a target.

In the present study, we developed the procedures for the microbeam irradiation to tobacco BY-2 cells in order to analyze biological effects of ion beams. Here, the outline was introduced.

Experiments

Irradiation vessel

As shown in Fig. 1, a beam window was opened in the center of a plastic dish, and a sheet of Harzlas TNF-1 (100 μm thickness) was sticked on the beam window. Then, a sheet of sterilized Kapton film (30 μm thickness) was set on the dish, and fixed by a sterilized polycarbonate ring.

Cell culture

Protoplasts were isolated from tobacco BY-2 cell line according to the methods reported by Yokota et al.[1], and mixed with SMLSD medium (LS-salts and -vitamins, 0.2 mg/l 2,4-D, 5 mM MES, 30 g/l sucrose, 0.4 M sorbitol, 0.8 % SeaPlaque agarose and pH 5.8) at a density of 5×10^4 protoplasts/ml. The 48.4 μl of the mixture was poured into the irradiation vessel and covered by a sheet of cover glass (22 × 22 mm, 150 μm thickness). In this procedure, the thickness of the medium containing cells was calculated to be 100 μm.

After the irradiation, 1 ml of the SMLSD medium without agarose was added in the irradiation vessel, and cells were cultured at 27°C under dark condition. After two weeks, colonies having 16 or more cells were counted as survivors. Colony formation rate of the non-irradiated cells was about 20 %.

Irradiation

The cell positions were recorded as a database using an Autoscan system, according to the procedure reported by Kobayashi et al.[2]. Based on the cell-positions database, cells were automatically irradiated with carbon and neon ion microbeams using the MiST-BA (Microbeam System in Takasaki for Biological Application). Properties of ion microbeams used in the present study were shown in Table 1.

Detection of ion tracks

After the irradiation, Harzlas TNF-1 of the irradiation vessel was etched by 13.4 M KOH solution at 27°C for 12 (C ions) and 9 hours (Ne ions), respectively (Fig. 2). After the etching, as shown in Fig. 3, the number and positions of ion tracks passed through a cell could be confirmed based on the superposed

image of the cell and the pits on a surface of Harzlas TNF-1.

In summary, we developed the irradiation vessel and the procedures for ion microbeam irradiation to tobacco BY-2 cells. Using these, we expect to make biological effects of ion beams in single plant cells more clear.

References

1) Y. Yokota, Y. Hase, N. Shikazono, A. Tanaka and M. Inoue (2003) International Journal of Radiation Biology, in press.
2) Y. Kobayashi, T. Funayama, S. Wada, M. Taguchi and H. Watanabe (2002) JAERI-Review 2002-035, 74-76

Table 1 Properties of microbeams used in this study.

Ion	Energy (MeV/u)	Beam size (μm)	Range in water* (mm)	Mean LET in cell position* (keV/μm)
$^{12}C^{5+}$	18.3	ϕ20	1.2	121
$^{20}Ne^{8+}$	17.5	ϕ20	0.6	408

*calculated using E LOSS M computer program.

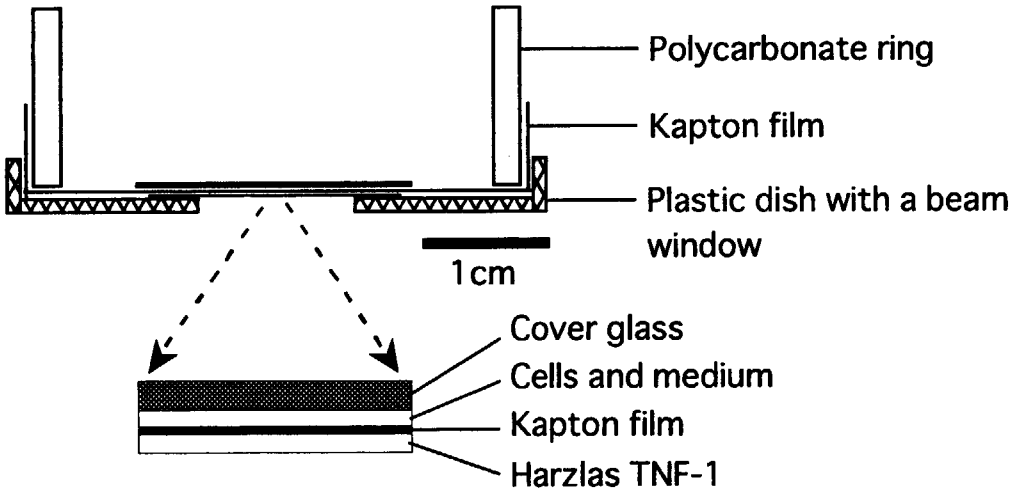

Fig. 1 Vessel for microbeam irradiation to single tobacco cells.

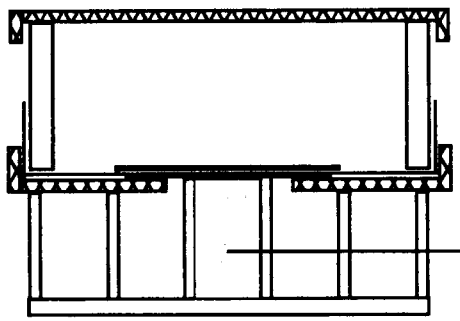

Fig. 2
Alkali etching of Harzlas TNF-1 for detection of ion tracks.

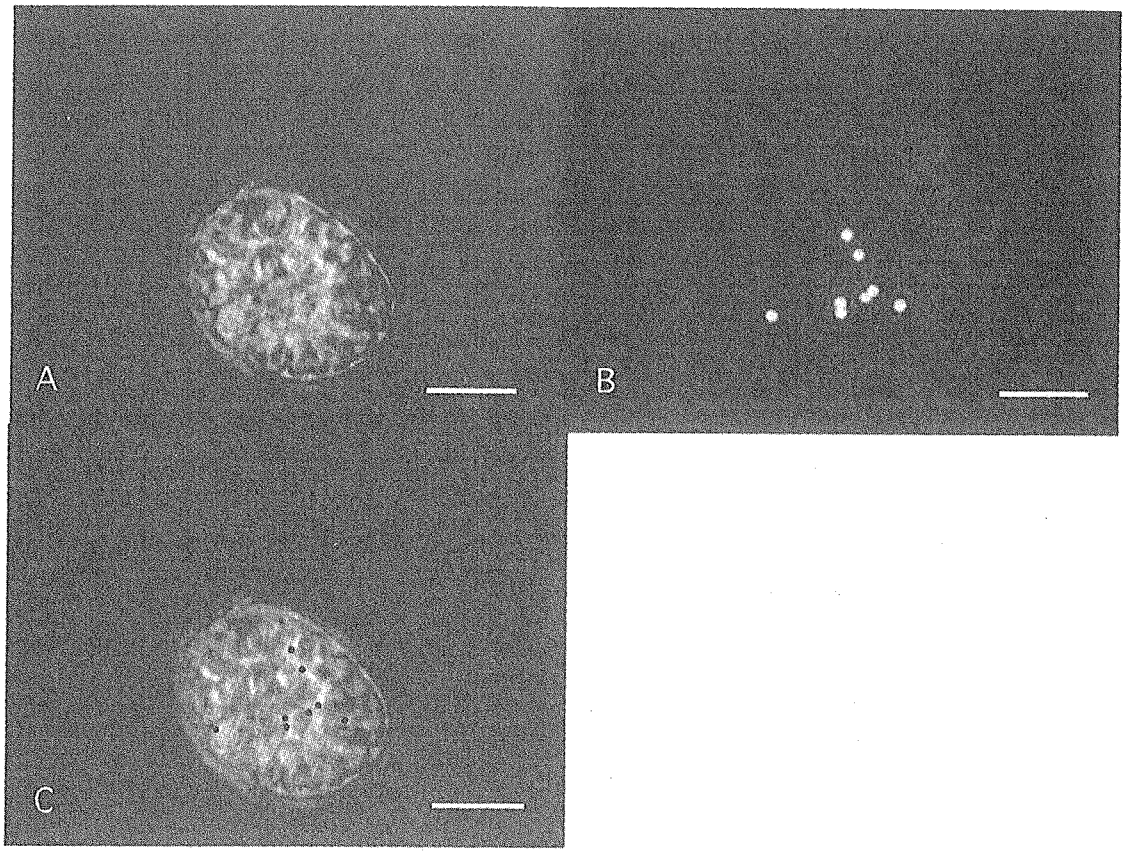

Fig. 3
Images of cell layer (A), Harzlas TNF-1 layer (B) and the superposition (C). Bars are 20 μm.

2.2 Development of gene transfer system using ion beam-irradiated pollen

Masayoshi Inoue*, Yuichiro Yokota*, Satoshi Kitamura**, Yoshihiro Hase** and Atsushi Tanaka**,
Laboratory of Plant Breeding Science, Graduate School of Agriculture, Kyoto Prefectural University*, Department of Ion-beam-applied Biology, JAERI**

We have been analyzing bioeffects of ion beam in *Nicotiana* plants, including pollen and single cells.

In the previous reports, we revealed that ion beam was effective for overcoming cross-incompatibility between distantly related species[1, 2] and for inducing *Potato virus* Y-resistant mutation[3, 4]. We also found a unique phenomenon, "leaky pollen", in which internal substances leaked through an opening in outer wall of pollen grain exposed to He ion[5]. This phenomenon was specific for the ion beam exposure, and seemed to be resulted from physical lesions induced in outer wall of pollen grain. In C ion exposure, the most effective penetration depth for inducing leaky pollen was around 4 μm[6].

Various techniques for gene transfer in plants have been developed and widely used in the plant manipulation; *Agrobacterium*-mediated procedure and direct procedure using electroporation and particle gun. There are, however, problems to be dissolved for efficient application in plant breeding; narrow host range, low yield of plants transformed, and intricate and laborious works for the culture.

Pollen is indispensable to sexual reproduction in wide range of plant species. If exogenous DNA can be incorporated into pollen and transferred to egg cell, pollen can be used as a gene vector in combination with crossing.

We tried to develop the gene transfer system using ion beam-irradiated pollen. In the experiments with 18 MeV C ion from 3MV tandem accelerator, the following results were obtained.

(1) After the irradiation of C ions under different conditions combined with fluence and penetration depth, percentages of pollen stained by trypan blue increased from 24.6% in the unirradiated to 41.4% and over 90% in the 4×10^9 p/cm^2·4 μm and 4×10^{11} p/cm^2·4 μm, respectively. On the other hand, a significant increase was not observed in the irradiation with the depth of 1 μm. These results showed that the irradiation in the depth of 4 μm was available for inducing effective damage on pollen cell membrane[7].

(2) Pollen germination rate on a solid medium was reduced with the increase of dose, resulting in about 60% of the non-irradiated control in the 1000Gy. However, a significant reduction of seed formation following crossing with the 1000Gy-irradiated pollen was not observed.

When the irradiated pollen was suspended in a liquid medium with pBI 221 harboring GUS gene and germinated on a solid medium, GUS expression was observed in the pollen grain and tube. Expression rate in pollen irradiated was 2 ~ 4 times higher than that in non-irradiated control. In the case of 1000 Gy, the rate was about 30%[8]. These results suggested that exogenous DNA could be effectively incorporated into the ion beam-irradiated pollen and transiently

expressed there.

(3) When pollen irradiated with 1000Gy of C ion was suspended in a medium with pCH harboring hygromycin resistance gene, and used for pollination, a number of seeds were obtained. The seeds were germinated and cultured on the medium with hygromycin, and, consequently, several seedlings were survived. However, after PCR amplification specific for the resistance gene, a corresponding band was not detected in survival seedlings, showing that hygromycin resistance was not transferred to the next generation[9].

(4) Also in tobacco pollen, nuclease activity was very high, resulting in the degradation of exogenous plasmid DNA to be incorporated into pollen. This degradation was, to a limited extent, reduced by washing with the medium solution or the EDTA application in the suspension medium. But, simultaneously, pollen germination was greatly reduced. These results showed that preliminary treatment for the reduction and/or the exclusion of nuclease activity was necessary in pollen-mediated gene transfer system[10-12].

As mentioned above, it is conceivable that exogenous DNA can be incorporated into the pollen cell through an opening of pollen grain, specifically induced by ion beam irradiation. However, nuclease released from pollen is an obstacle on the system using pollen as a vector. In order to establish the pollen-mediated gene transfer system, alternative treatment for dealing with nuclease activity should be developed.

References

1) M. Inoue, H. Watanabe, A. Tanaka and A. Nakamura (1993) JAERI TIARA Annual Report, 3, 44-45

2) T. Yamashita, M. Inoue, H. Watanabe, A. Tanaka and S. Tano (1995) JAERI TIARA Annual Report, 5, 44-46

3) K. Hamada, M. Inoue, A. Tanaka and H. Watanabe (1999) Plant Biotechnology, 16, 285-289

4) K. Hamada, M. Inoue, A. Tanaka and H. Watanabe (2000) Plant Biotechnology, 18, 251-257

5) M. Inoue, H. Watanabe, A. Tanaka and A. Nakamura (1992) JAERI TIARA Annual Report, 2, 50-52

6) A. Tanaka, H. Watanabe, S. Shimizu, M. Inoue, M. Kikuchi, Y. Kobayashi and S. Tano (1997) Nuclear Instruments and Methods in Physics Research, B129, 42-48

7) Y. Hase, A. Tanaka, I. Narumi, H. Watanabe and M. Inoue (1998) JAERI-Review 98-016, 81-83

8) M. Inoue, S. Kitamura, Y. Toda, H. Watanabe, A. Tanaka and Y. Hase (1999) JAERI-Review 99-025, 80-81

9) Y. Toda (1998) Thesis of Master degree, Kyoto Pref. Univ.

10) Y. Hase, Y. Toda, A. Tanaka, M. Inoue and H. Watanabe (1999) JAERI-Review 99-025, 82-83

11) S. Kitamura, M. Yamaguchi, M. Inoue, Y. Hase and A. Tanaka (2001) JAERI-Review 2001-039, 88-89

12) S. Kitamura, Y. Yokota, M. Inoue, Y. Hase and A. Tanaka (2002) JAERI-Review 2002-035, 105-107

2.3 Effects of $^{12}C^{6+}$ Ion Beams on Protoplasts, Petals and Leaves of Chrysanthemum (*Dendranthema grandiflorum* R.)

H. Ikegami*, K. Takata*, H. Kai*, K. Hirashima*, T. Nakahara*,
Y. Hase**, N. Shikazono** and A. Tanaka**
Department of Agricultural Biotechnology, Fukuoka Agricultural Research Center*
Department of Ion-Beam-Applied Biology, JAERI**

1. Introduction

Ion beams are widely used to improve many plants and crops. In most cases, materials applied for ion-beam irradiation depend on the aims and situations at which experiments are executed.

In recent work, we grew mutants of chrysanthemum c.v. 'Syuho-no-chikara' derived from protoplasts for two years to demonstrate various types of mutations can be induced by irradiation of ion beams on protoplasts[1)2)]. However, there are still many points that should be solved on the sensitivities and mutation mechanisms when various tissues or cells are irradiated.

To determine the optimum dose of ion beams and to estimate the precise differences of the mutation observed among materials especially between protoplasts and other tissues, we investigated the effects of $^{12}C^{6+}$ ion beams on protoplasts, petals and leaves of chrysanthemum and regenerated plants.

2. Materials and Methods

Chrysanthemum line, 'No.74' (red flower) which was bred by a horticulturist in Fukuoka prefecture was used for the experiment. Isolation and embedding of mesophyll protoplasts derived from leaves were conducted by the modified method[1)]. Petals and leaves were cut into about 2 × 5 mm segments and transferred to solidified medium. Prepared protoplasts and segments were irradiated with 320 MeV $^{12}C^{6+}$ ion beams from the AVF cyclotron in JAERI. Those irradiated protoplasts and segments were cultured for 60 days and we counted the number of emerging callus and shoots.

3. Results and Discussion

The dose response curve of callus and shoot inductions by 320 MeV $^{12}C^{6+}$ ion beams irradiation is shown in Fig.1,2.

In leaf tissues, the callus induction rate was almost 100% between 0Gy and 6Gy(Fig.1).

In protoplasts, the callus induction rate decreased at 2Gy and no callus was observed at 7.5Gy. Median lethal dose(LD50) was between 3Gy and 5Gy(Fig.1).

In petal tissues, the callus induction rate was maintained more than 90% between 0Gy and 4Gy and decreased above 6Gy. On the other hand, shoot induction rate decreased above 2Gy and about 15% was observed at 6Gy. LD50 of callus inductions was estimated about 2Gy. Thus, shoot induction rate is thought to be much lower than callus induction rate(Fig.1,2).

Comparing callus induction rate of these materials, we can suppose that leaf protoplasts are more sensitive to ion beams than petals and leaves. This would be because both petals and leaves are multicellular tissues. In addition, the fact that leaves are less sensitive than petals is interesting (Fig.1).

The regeneration of plant from protoplasts, leaves and petals irradiated with ion beams are in progress.

References

1) T.Nakahara, K.Hirashima, M.Koga, A.Tanaka, N.Shikazono and H.Watanabe, TIARA Annual Report 6:56-57(1998)

2) H.Ikegami, H.Murakami, K.Hirashima, T.Nakahara, Y.Hase and A.Tanaka,TIARA Annual Report 10:28-29(2002)

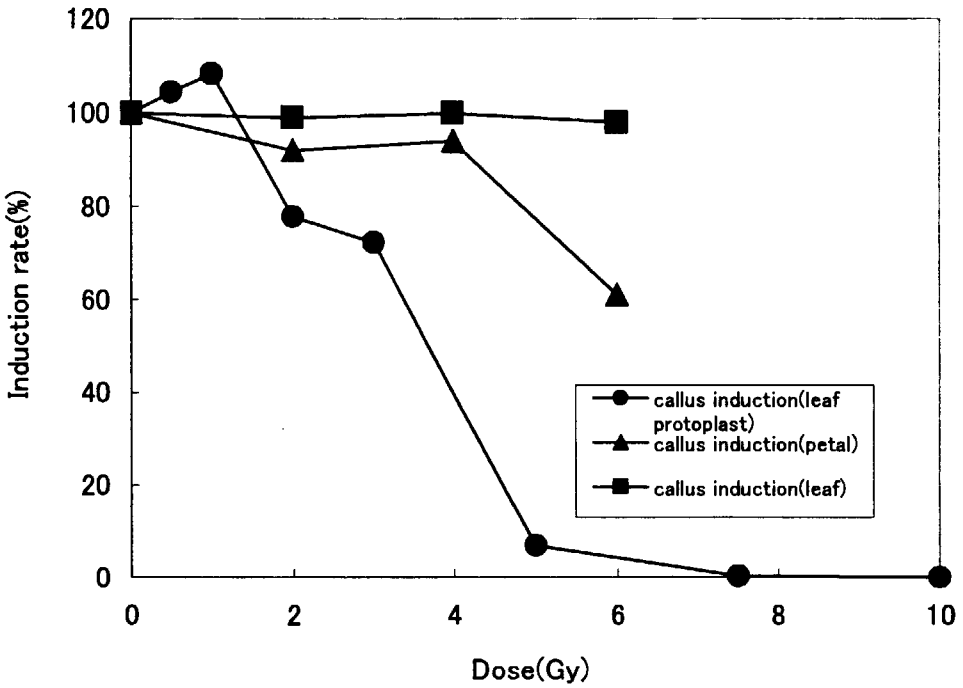

Fig.1 Effects of $^{12}C^{6+}$ ion beams on the inductions of callus derived from protoplast, leaf and petal.

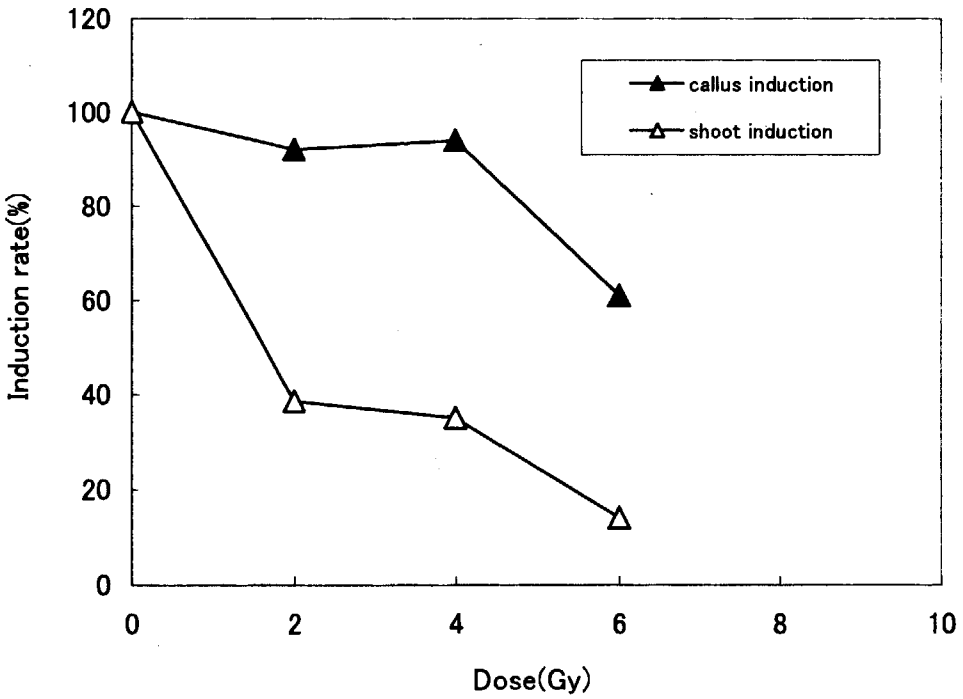

Fig.2 Effects of $^{12}C^{6+}$ ion beams on the inductions of callus and shoot.

2.4 Induction of Mutation in Elatior Begonia (*B. ×hiemalis*) by Ion Beams

Masahide IIZUKA*,Nobuhiro KUDO*, Yasuo KIMURA*,
Yoshihiro HASE** and Atushi TANAKA**
Gumma Horticultural Experiment Station*
Department of Ion-beam-applied Biology, JAERI**

Introduction

Ion beams, which have a higher linear energy transfer (LET) than X and gamma rays, is one of efficient mutagenic agents, applicable to mutation breeding of many horticultural crops. However, there have been few studies on the effects of ion beam irradiation on induction of mutation in vegetables and ornamental crops. The lethal dose of the $^{4}He^{2+}$ and $^{12}C^{5+}$ ion beam irradiation to strawberry, hydrangea and spiraea seed became clear [1),2),3)].

We have the mutation breeding of the Elatior Begonia (*B. ×hiemalis*) that is important pot cultures. An ion beam was used to Elatior Begonia for the purpose of variation of the flower color. We examined effects of ion beam irradiation on regeneration of Elatior Begonia. As a result, less than 5Gy were effective for the irradiation of carbon ion beams. [4)]

Materials and Methods

Elatior Begonia(*B. ×hiemalis*) cv.Line in greenhouse were used as plant materials. Young leaves were excised, and the surface was sterilized by immersing in 70% ethyl alcohol for 1 min, followed in 1%(W/V) sodium hypochlolite solution for 15 mins and then rinsed three times in distilled water. The leaf segments were cultured on modified Murashige and Skoog's (MS) medium supplemented with 0.5 mg/l NAA and 1mg/l BA. The samples covered with Kapton film were irradiated with carbon ion beam (220 MeV $^{12}C^{5+}$ and 320 MeV $^{12}C^{6+}$) at various doses (1 ,2, 5 Gy). After irradiation, the leaf segments were transferred to the fresh medium and cultured at 20 °C with 16 hr-photoperiod. Regenerated shoots were acclimated and transplanted in greenhouse about 2 months later.

Results and Discussion

The regeneration rate was roughly 100% when irradiated with less than 5Gy. The 800 acclimation plants grown from 1200 regeneration shoots and variations are observed.

We are performing cytological studies to investigate horticultural values of the mutants and are screening mutants of flower color variation in the growing plants.

References

1)N. Kudo et al. TIARA Ann. Rep., 16:62-64. (1998)
2)M. Iizuka et al. TIARA Ann. Rep., 2.3:30-31. (1999)
3)M. Iizuka et al. TIARA Ann. Rep., 2.7:45-46. (2001)
4)M. Iizuka et al. TIARA Ann. Rep., 2.3:31-32. (2002)

Table 1. Regeneration and plantlets from Elatior Begonia leaves irradiated by C ion beam.

Cultivar	Radiation	Dose(Gy)	No. of regeneration shoots	No. of plantlets
rine	$^{12}C^{5+}$	1	69	42
		2	64	37
		5	58	26
	$^{12}C^{6+}$	1	81	41
		2	74	45
		5	60	38
anabel	$^{12}C^{5+}$	1	57	34
		2	74	52
		5	66	41
	$^{12}C^{6+}$	1	68	53
		2	51	37
		5	76	53
netia	$^{12}C^{5+}$	1	75	44
		2	62	37
		5	71	50
	$^{12}C^{6+}$	1	69	46
		2	75	49
		5	65	47

Fig.1. Plantlets of Elatior Begonia from regeneration shoots irradiated by $^{12}C^{6+}$ ion beam.

2.5 Molecular and Physiological Analysis of *tt19* in Arabidopsis

Satoshi Kitamura, Naoya Shikazono and Atsushi Tanaka
Department of Ion-Beam-Applied Biology, JAERI.

Flavonoids are secondary metabolites that are unique to the plant kingdom, with a multitude of functions such as acting as pigments and UV-B protectants. Some plant flavonoids are also known to have beneficial effects on human health by their strong antioxidant activities and to prevent bloat in ruminants. Two flavonoids, anthocyanins and proanthocyanidins (PAs; so-called condensed tannins) are exclusively accumulated in the vacuole although they are synthesized in the cytosol. Until vacuolar compartmentalization is completed, these compounds are not stabilized, so they do not exhibit their functions in plant cells.

Although much is known about flavonoid synthesis, the steps involved in their sequestration are poorly understood. Three models have been proposed for sequestering anthocyanins in vacuoles: direct transport of non-modified anthocyanins, transport after their modification, and transport mediated by a carrier protein of glutathione *S*-transferase (GST)[1]. In the latter case, GST activity does not seem to be necessary for the transport itself. On the other hand, little is known about the vacuolar sequestration mechanisms for PAs. All that is known is that a putative membrane-localized transporter protein has been isolated in Arabidopsis[2].

Two *transparent testa* (*tt*) mutant loci (*tt18* and *tt19*) were induced by ion beams in Arabidopsis[3]. Although *tt18* was found to be a putative leucoanthocyanidin dioxygenase (LDOX) gene, the nature of *tt19* has not been elucidated. Purple pigmentation due to anthocyanins was not visible in the basal region of the stem in two independent *tt19* mutants (*tt19-1* and *tt19-2*). The seed coat of *tt19* was pale-brown at the ripening stage, in contrast to brown in the wild type Columbia (Col). However, the seed coat of *tt19* became browner with increasing length of the desiccation period, eventually darkening as much as that of Col after long-term desiccation.

Molecular mapping seems to indicate that a large inversion, which co-segregates with the mutated *tt19* locus, has occurred in the *tt19-1* mutant. TAIL-PCR and sequence analysis demonstrate that a large inversion was generated in *tt19-1*, and that one of the breakpoints in the inversion coincides with a GST-like gene. The other mutant, *tt19-2*, was analyzed by the same strategy, and found to have a 16.7 kb deletion in the promoter region of the GST-like gene. Such large DNA alteration is preferentially induced by ion beams, and this characteristic allowed us to identify the mutated gene. Because both *tt19* mutants have mutations in the GST-like gene, molecular complementation of the *tt19* was carried out using the wild-type GST-like gene with its authentic promoter. In each of five independent T1 plants (named *tt19/AU:TT19* line), anthocyanin in the seedlings (Fig. 1A) and brown pigmentation in the testa at the ripening stage (Fig. 1B) were both restored to the wild-type level. This is conclusive evidence that disruption of the GST-like gene is responsible for the flavonoid-deficient phenotype of the *tt19* mutants. In the following, this gene is referred to as *TT19*.

To date, two kinds of GSTs have been reported to be involved in the flavonoid pathway. The first type is the parsley GST gene, which appears to act in the early steps of a UV light-dependent signal transduction pathway leading to the expression of chalcone synthase[4]. Another class of GST, which includes maize BZ2 and petunia AN9, participates in the last step of anthocyanin accumulation[5]. TT19 is about 70% identical to Arabidopsis EST clone H36860 protein and about 50% identical to petunia AN9. These identities are quite high when compared with the typically low identities of Arabidopsis GST family proteins (as low as 30%). A phylogenetic analysis indicated that TT19 primarily clustered with H36860, and secondarily clustered with AN9, with complete robustness. This result, coupled with the results of the feeding experiment using flavonoid intermediate naringenin and with the RT-PCR results for the flavonoid structural genes, suggests that *TT19* is a better candidate for an *AN9* ortholog. To determine this possibility, the *AN9* gene, driven under the cauliflower mosaic virus (CaMV) 35S promoter, was introduced into the *tt19* mutants. All surviving T1 seedlings (*tt19/35S:AN9* line) exhibited anthocyanin pigmentation (Fig. 1C). Therefore, it is concluded that the function of *TT19* in the Arabidopsis anthocyanin pathway, like that of *AN9* in petunia[1], is to take up anthocyanidin 3-glucosides into the vacuolar membrane.

However, in contrast to complementation of the anthocyanin-less phenotype in *tt19*, the seed color at the ripening stage remained the same as that of *tt19* in all *tt19/35S:AN9* plants (Fig. 1D). The

expression of *AN9* mRNA was shown by RT-PCR even in developing siliques from the *tt19/35S:AN9* line. A control construct of the CaMV 35S promoter with *TT19* cDNA confirmed the ability of *TT19* to complement seed color of *tt19* even under the CaMV 35S promoter (*tt19/35S:TT19* line) (Fig. 1D). Although three plants with pale-brown seeds were found in this control transgenic line, co-suppression might have occurred in a tissue-specific manner. These results indicate that the inability of *AN9* to complement the seed color of *tt19* reflects a difference in gene function between *TT19* and *AN9*.

Complementation of the anthocyanin pigmentation by *AN9* did not restore brown seed color in *tt19*. This suggests that the brown pigments of the wild-type seeds rely mainly on PA derivatives and that *TT19* participates in the PA pathway in Arabidopsis. To determine the distribution of PA precursors, seeds were stained with vanillin, which reacts with PA precursors to give a red color. About three days after flowering (DAF), Col and *tt19* seeds had clearly different patterns of red pigments: in the Col testa, red pigments appeared to accumulate in large vacuoles in cells of the endothelium layer, while in *tt19*, they were restricted to a few smaller vacuoles. At DAF5, the vacuole of Col was fully expanded within each constitutive cell (Fig. 1E), whereas such an expanded vacuole was not detected in *tt19* (Fig. 1F). This indicates that the mechanism by which PA precursors are accumulated in the central vacuoles is affected by the *tt19* mutation, while the precursors would be normally synthesized.

A recent biochemical analysis revealed that BANYULS (BAN) is involved in the synthesis of 2,3-*cis*-flavan 3-ols, which are specific to the PA pathway[6]. To obtain further knowledge of the PA pathway, a double mutant with *tt19* and *ban* was constructed and its phenotype was characterized. The seed color of the double mutant at the ripening stage was about the same shade of brown as *tt19*, although it was a little grayer than the color of *tt19*. The gray coloration of the double mutant seems to be due to leakage of some of the anthocyanins during the immature stage. One of the characteristics of *tt19* is a darkening of seed color during long-term desiccation. In contrast, no change in seed color was observed in the double mutant after an additional desiccation period. If the Arabidopsis *BAN* gene has no other function in planta, it is conceivable that 2,3-*cis*-flavan 3-ols such as (-)-epicatechins are essential for the browning of *tt19* testa during long-term desiccation. Therefore, it is reasonable that the pale-brown color at the ripening stage in *tt19* testa is due to a lack of participation of 2,3-*cis*-flavan 3-ols in PA synthesis until the ripening stage. These genetic results are consistent with the histochemical data using vanillin (Fig. 1F).

Concerning anthocyanin accumulation, the petunia *an9* mutation was complemented by the maize BZ2 and the maize *bz2* mutation was complemented by the petunia AN9[5]. However, the maize *bz2* mutation was not complemented by Arabidopsis H36860, which has about 50% amino acid identity to AN9[5]. This suggested that different plants might use different transport mechanisms without using GST[1]. Examples of such transport mechanisms are direct transport and the transport after modification of anthocyanins, both of which were suggested by in vitro analyses[1]. However, our mutant analysis demonstrates that the GST-like protein clearly participates in anthocyanin transport of Arabidopsis. It is expected that this in vivo role of GST is relatively conserved in many plant species.

Based on our results, we have developed a new model for the flavonoid accumulation pathway (Fig. 2). Our findings clearly show that *TT19* encodes a GST-like protein, and is functionally implicated in vacuolar transport and/or accumulation of PAs. GST has not previously been reported to be involved in the PA pathway. Such an involvement was considered unlikely because of the structural features of TT12 protein, which belongs to the MATE-type transporter family and is the only constituent of the PA sequestration machinery that has been suggested so far[2]. In view of the fact that transport mechanisms for anthocyanins are conserved[1], GST appears to be involved in the PA pathway in many species. The finding that TT19 is part of the sequestration machinery for PAs should help to resolve the puzzle of their transport and accumulation. An understanding of the mechanisms by which PAs are sequestered could lead to the development of new strains of vegetables, fruits, and forage crops with manipulated tannin level. Such crops could have health benefits for both humans and ruminants.

How TT19 is involved in PA accumulation remains unclear, but our results may provide some clues. The vanillin assay clearly showed that PA precursors in *tt19* were wrapped with a membrane-like structure (Fig. 1F). Some flavonoids have been proposed to be transported to the vacuole using small membrane-like structures (so-called vesicles) containing flavonoids[7]. It is thus tempting to speculate that TT19 functions after PA precursors are taken up into the membrane by

TT12 (Fig. 2), for example at the stage of the intracellular vesicle trafficking of flavonoids.

References

(1) L. A. Mueller, V. Walbot, *Recent Adv. Phytochem.* **35**, 297 (2001).
(2) I. Debeaujon *et al.*, *Plant Cell* **13**, 853 (2001).
(3) N. Shikazono *et al.*, *Genetics* **163**, 1449 (2003).
(4) L. Loyall *et al.*, *Plant Cell* **12**, 1939 (2000).
(5) M. R. Alfenito *et al.*, *Plant Cell* **10**, 1135 (1998).
(6) D.-Y. Xie *et al.*, *Science* **299**, 396 (2003).
(7) E. Grotewold, *Recent Res. Devel. Plant Physiol.* **2**, 31 (2001).

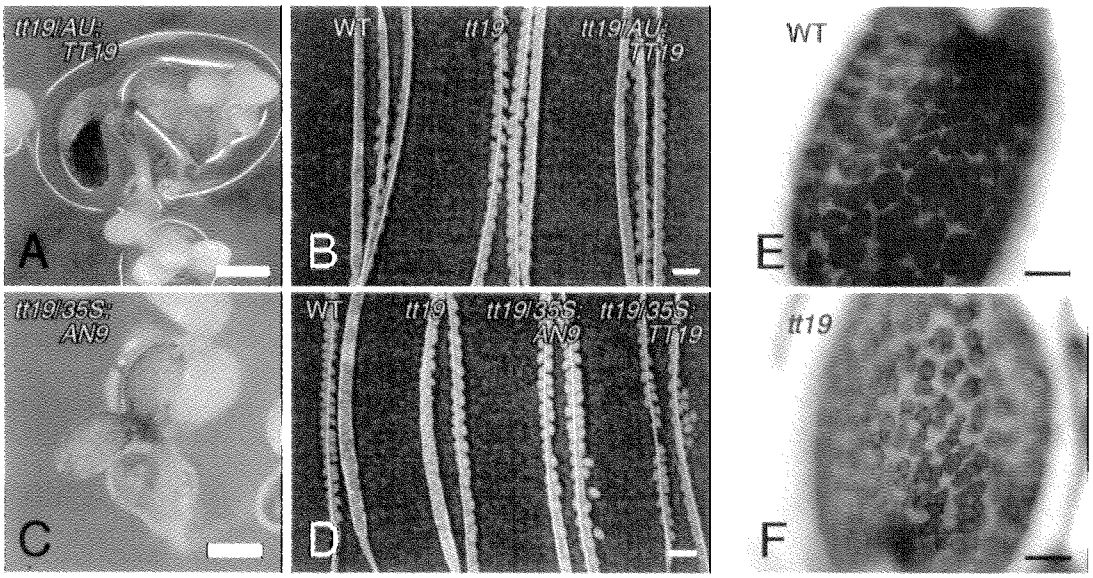

Fig. 1 Characterization of gene function of *TT19*.
(A, B) Phenotype in the seedling (A) and the testa at the ripening stage (B) of the *tt19/AU:TT19* line.
(C, D) Phenotype in the seedling (C) and the testa at the ripening stage (D) of the *tt19/35S:AN9* line.
(E, F) Depositional patterns of PA precursors in seed coat of immature seeds DAF5.
Scale bars in (A, B, C, D) indicate 1 mm, and those in (E, F) indicate 50 μm.

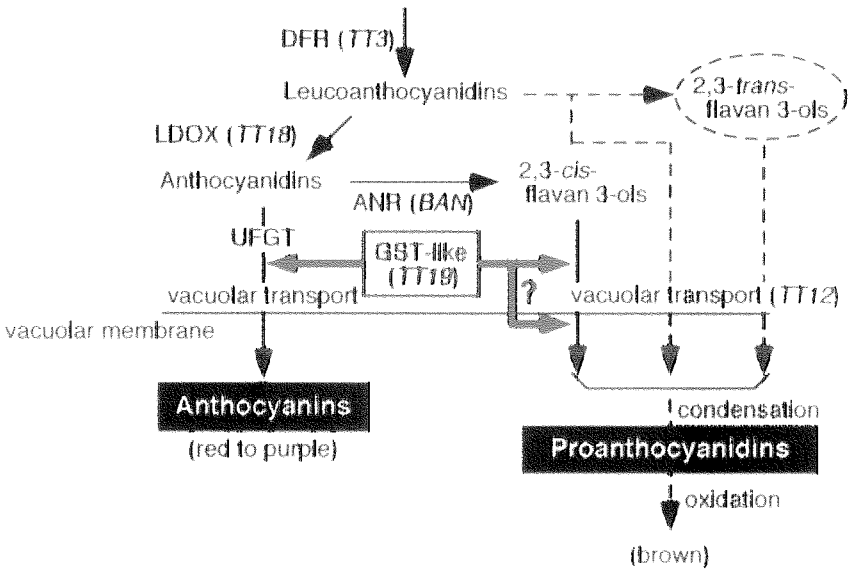

Fig. 2 Model of the flavonoid accumulation pathway.
Putative steps are shown as dotted lines.

2.6 Development of the efficient mutation breeding method using ion beam irradiation

T. Morishita*, H. Yamaguchi*, K. Degi*,
Y. Hase**, N. Shikazono** and A. Tanaka**
Institute of Radiation Breeding, NIAS*
Department of Ion-beam-applied Biology, JAERI**

1. Introduction

Most mutagens used for registered crop mutant varieties in the world were gamma rays. Recently, heavy-ion beams have been regarded as a new mutagen because such high-LET (linear energy transfer) irradiation provides higher RBE (relative biological effectiveness) for various endpoints, compared with gamma rays. In this study, to develop the method for ion beam breeding in buckwheat, which is noticed as a healthy food ingredient, the biological effects of ion beams were investigated. We reported the results about these experiments.

2. Material and Method

Intact and hulled dry seeds of common buckwheat (var: Botansoba) and tartary buckwheat (var: Rotundatiem) were irradiated with helium ion ($^{4}He^{2+}$, 50 MeV, penetrating depth 1.7 mm and 100 MeV, 6.2 mm), carbon ion ($^{12}C^{5+}$, 220 MeV, 1.1 mm and $^{12}C^{6+}$, 320 MeV, 2.2 mm) and neon ion ($^{20}Ne^{8+}$, 350 MeV, 0.6 mm). $^{4}He^{2+}$, $^{12}C^{5+}$, $^{12}C^{6+}$, and $^{20}Ne^{8+}$ ion beams were generated by an AVF cyclotron (JAERI, Takasaki, Japan). A gamma ray from 44 TBq ^{60}Co (IRB, Ohmiya, Japan) was used as the low LET ionizing radiation control. Irradiated seeds were sown in nursing soil. After 7-10 days, the capacity for germination was investigated. After 3 weeks, the survival capacity was investigated.

Irradiated seeds (M_1) of the tartary buckwheat (self fertilizing) were sown in an upland field. After 3 months, the mature buckwheat was harvested, and the individual plants were threshed. The seeds (M_2) obtained were sown in an upland field by plant-to-row lines. Visible traits, chlorophyll, and morphological mutations were investigated.

3. Result and Discussion

The relationship between the dose of various ion beams and survival rates are shown in Fig. 1. In both of intact and hulled seeds of tartary buckwheat, lethal dose 50 (LD_{50}) of $^{4}He^{2+}$ (100 MeV) ions are about 350 Gy. Those of $^{4}He^{2+}$ (50 MeV) ions are about 350 Gy and 200 Gy, respectively. Those of $^{12}C^{5+}$ (220 MeV) ions are about 70 Gy and 30 Gy, respectively, but flattened over 100 Gy, and the 100% lethal dose of $^{12}C^{5+}$ (220 MeV) was not observed. While in $^{12}C^{6+}$ (320 MeV) ions, 100% lethal dose was

observed at 200 Gy in both common and tartary buckwheat. That of $^{20}Ne^{8+}$ did not exhibit the decreasing rates until 1,000 Gy. In $^{12}C^{5+}$ (220 MeV), $^{12}C^{6+}$ (320 MeV), and $^{4}He^{2+}$ (50 MeV), the irradiation effect of hulled seeds was higher than that of intact seeds. From these results, it defined that the penetrating depth of 1.7 mm was necessary to reach the target cells in hulled seeds, and in the case of the penetrating depth less than 2.2 mm, the effect of the hulls is remarkable.

Table 1 and Fig. 2 show the mutation rates under 100 Gy in the M_2 generation of tartary buckwheat. The total mutation rates increased as the dose rose in $^{4}He^{2+}$ (100 MeV) ions and $^{12}C^{5+}$ (220 MeV) ions. Compared with the relationship between dose, mutation rate and survival rate about these ions, the mutation rates of $^{4}He^{2+}$ (100 MeV) ions and $^{12}C^{5+}$ (220 MeV) ions at 100 Gy were about 15%, while survival rates were different in these ions. The chlorophyll mutation rate of $^{20}Ne^{8+}$ ions was lower than those of any other ion beams. Further study will be necessary to define the mutagen effect of ion beams.

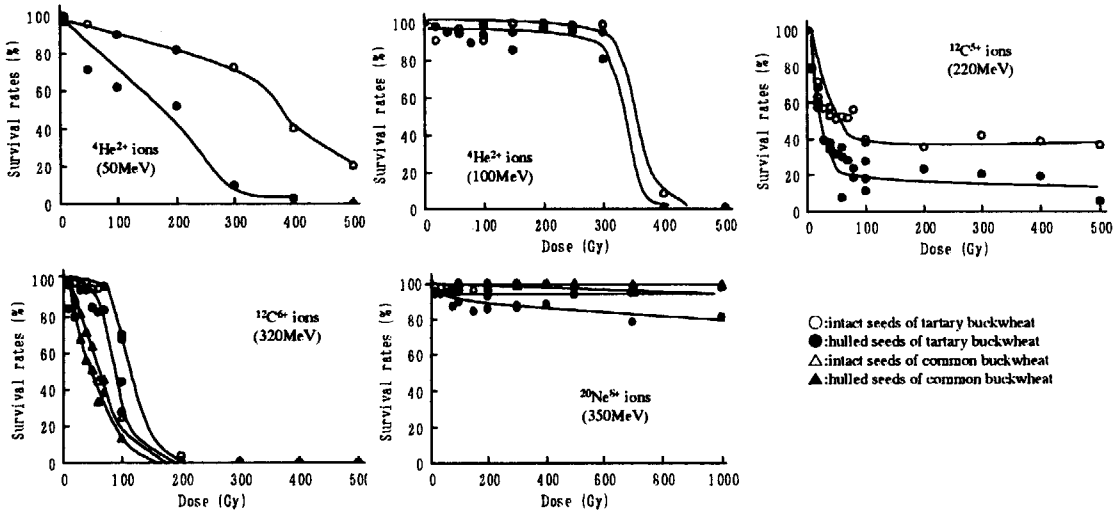

Fig. 1. Dose responses of ion beams irradiated buckwheat seeds.

Table 1. Mutants observed on ion beams irradiated M_2 generation of tartary buckwheat.

Ion	Dose (Gy)	No. of lines	Chlorophyll mutation No.	Chlorophyll mutation (%)	Morphological mutation No.	Morphological mutation (%)	Total mutation No.	Total mutation (%)
He 100MeV Hulled seeds	20	165	3	1.8	8	4.8	10	6.1
	40	144	3	2.1	12	8.3	14	9.7
	60	162	12	7.4	12	7.4	20	12.3
	80	71	3	4.2	9	12.7	10	14.1
	100	99	5	5.1	9	9.1	14	14.1
He 100MeV Intact seeds	20	145	4	2.8	7	4.8	10	6.9
	60	167	5	3.0	11	6.6	14	8.4
	100	150	4	2.7	14	9.3	16	10.7
Ne 350MeV Hulled seeds	20	164	1	0.6	8	4.9	8	4.9
	40	162	1	0.6	8	4.9	8	4.9
	60	184	1	0.5	17	9.2	18	9.8
	80	98	0	0.0	7	7.1	7	7.1
	100	137	1	0.7	6	4.4	7	5.1
Ne 350MeV Intact seeds	20	130	0	0.0	5	3.8	5	3.8
	60	120	2	1.7	6	5.0	8	6.7
	100	126	2	1.6	7	5.6	9	7.1
C 220MeV Hulled seeds	20	61	1	1.6	4	6.6	4	6.6
	40	22	1	4.5	2	9.1	3	13.6
	100	7	0	0.0	1	14.3	1	14.3

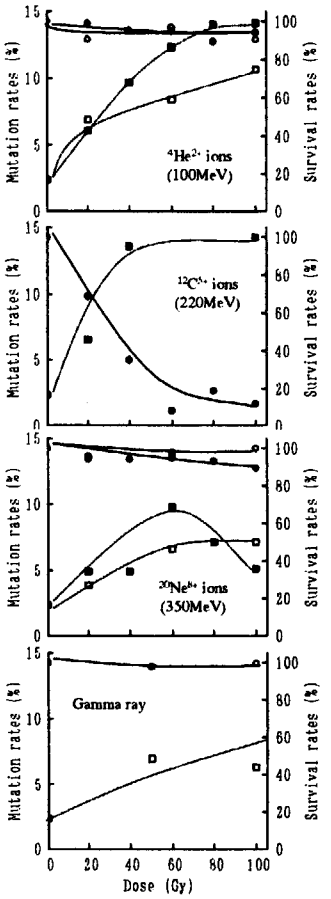

Fig. 2 The relationship between mutation rates, survival rates and irradiation dose in tartary buckwheat.

□: mutation rates of intact seeds, ■: mutation rates of hulled seeds, ○: survival rates of intact seeds, ●: survival rates of hulled seeds.

2.7 Mutation Generation in Pot & Garden Carnations Regenerated from Tissue Cultures Irradiated with Ion Beams

M.Okamura*, N.Yasuno*, M.Takano*, A.Tanaka**, N.Shikazono** and Y.Hase**
Plant Laboratory, Agribio business company, Kirin Brewery Co., Ltd.*
Department of Ion-Beam-Applied Biology, JAERI**

1. Introduction

Most mutagens used for mutation breeding of crops in the world are gamma rays and X-rays. Ion beams are expected to be utilized widely as new mutagens, because they have much higher linear energy transfer (LET) and relative biological effectiveness (RBE) than those of gamma rays and X-rays[1]. By ion beam irradiation, specific flower color mutants were obtained in chrysanthemum[2]. By the combined method of ion beam irradiation with in vitro leaf culture, we succeeded in the development of new carnation varieties "Vital Ion series" in 2002 [3].

In this study, we investigate the efficiency of mutation generation by a combined method of ion beam in pot and gardening carnations, Gardencarna®, and characterize the feature of mutation breeding using ion beam irradiation.

2. Materials and Methods

Pot carnation variety 'Pinky' (pink flower), a long seller cv in Europe and America, and Gardencarna®, line OD55, were used for the experiment. In 'Pinky', small stem segments with node were placed in petri dish containing Murashige and Skoog medium supplemented with 0.1mg/l NAA and 0.1mg/l BA, 30g/l sucrose and 7g/l agar. In gardening carnation, micro leaf segments were placed in petri dish containing MS medium supplemented with 0.1mg/l NAA and 2mg/l Zeatin, 30g/l sucrose and 7g/l agar. The samples covered with Kapton film were irradiated with 320 MeV carbon, 220 MeV carbon and 50 MeV helium ion beams from the TIARA AVF cyclotron (JAERI, Takasaki). After irradiation, the tissues were transferred onto fresh medium and cultured in the growth room. The frequency of shoot regeneration was examined 1.5 months after irradiation. The regenerated plants were acclimatized in the greenhouse and their flower color and shape were investigated.

3. Results and Discussion

The dose response curves of the shoot regeneration by ion beam irradiation in 'Pinky' were shown in Fig.1A, and that in Gardencarna® in Fig.1B. In 220MeV carbon ion beams, the median regeneration dose (RD50) was estimated at 13-14Gy and that in 320 MeV carbon and in 50 MeV helium ion were estimated at 17-19Gy and 34-36Gy, respectively. The RBE of 220 MeV and 320 MeV carbon ion beams relative to 50 MeV helium ions were estimated to be about 2.5 and 2, respectively.

The mutants of flower color and shape in plants regenerated from tissues irradiated with ion beams are shown in Table 1. The mutation rates of 'Pinky' are 6.1 % and 4.2% in 50 MeV helium and 220 MeV carbon ion beams, respectively. Flower color mutants such as light pink, salmon pink, bi-colored and flower shape mutants such as smaller petals, cup-shaped flowers were obtained (Fig.2). It is notable that color mutants were obtained at high frequency by ion beams, for 'Pinky' has no color variation yet despite its long history of cultivation in Europe and America. The mutation rates of Gardencarna®, line OD55, are 5.2%, 11.3 % and 6.5% in 50 MeV helium, 220 MeV carbon and 320 MeV carbon ion beams, respectively. Flower color mutants such as light pink, salmon pink, red and flower shape mutants such as Dianthus-type petals were obtained (Fig.3).

In this study the wide spectrum in flower-color and -shape was observed in the mutants derived from ion beam irradiated pot and gardening carnations. The results correspond with the reports in chrysanthemum[2] and carnation.[3] Ion beams have different effect

from that of electron beams on mutation generation of crops and have great impact on plant seed and seedling business.

References

1) A. Tanaka et. al., Int. J. Radiat. Biol 72 (1997), 121-127
2) S. Nagatomi, et. al., JAERI-Review 97-015 (1998), 50-52
3) M. Okamura et. al., Nucl. Inst. and Meth. in Phys. Res. B 206 (2003), 574-578

Table 1. Mutants in pot and gardening carnations obtained by the irradiation of 50 MeV helium and 220MeV, 320 MeV carbon ion beams.

Ion beams	Irradiation dose	Mutants in flower color and/or shape (No.)	Mutation rate (%)
Pot carnation variety 'Pinky' (Pink)			
50 MeV He	10-30Gy	Light pink (4), Small flower (2), Dianthus-type (1)	6.1
220 MeV C	5-15Gy	Salmon pink (2), Light pink (5), Small flower (2), Bi-colored: Pink and pearl (2), Cup shaped (1)	4.2
Gardening carnatio 'Gardencarna®' OD55 (Dark pink)			
50 MeV He	15-40Gy	Light pink (3), Salmon pink (1), Small flower (1), Dianthus-type (1)	5.2
220 MeV C	10-15Gy	Minute striped (3), Light pink (4), Salmon pink (2), Red (1), Small flower (1), Dianthus-type (1)	11.3
320 MeV C	10-15Gy	Minute striped (3), Light pink (2), Salmon pink (1), Small flower (1), Dianthus-type (2)	6.5

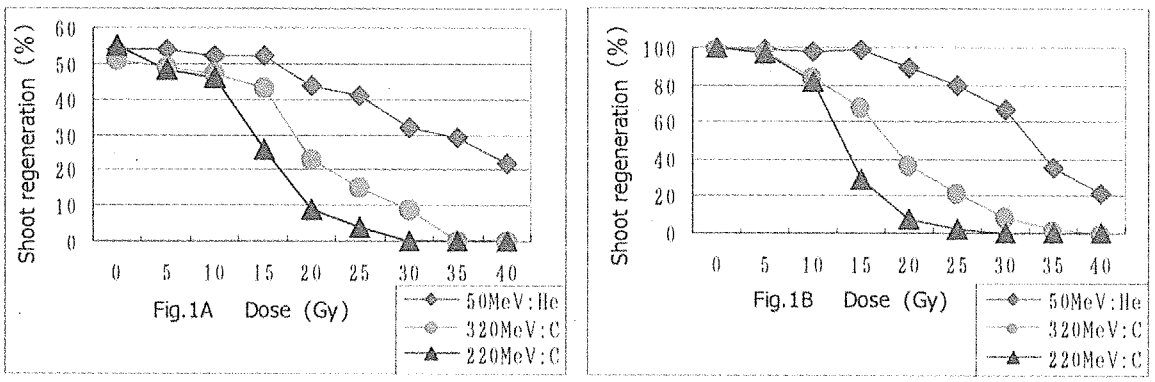

Fig.1 Dose response curves for regeneration frequency in pot (A) and gardening (B) carnations irradiated by 220 MeV, 320 MeV carbon and 50MeV helium ion beams.

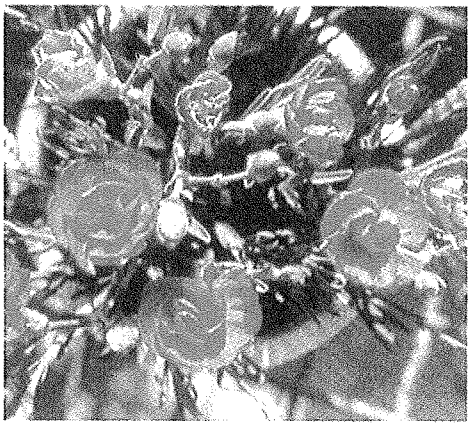

Fig.2 Mutant of pot carnation cv. 'Pinky.'

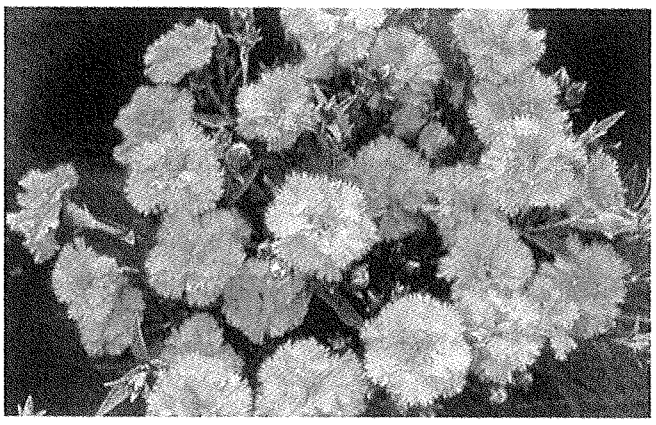

Fig.3 Mutant of gardening carnation, Gardencarna® OD55.

2.8 Effects of Ion Beam Irradiation on the Mutation Induction from Chrysanthemum Leaf Disc Culture

K. Ueno*, S. Nagayoshi*, Y. Hase**, N. Shikazono** and A. Tanaka**
Kagoshima Biotechnology Institute*, Department of Ion-Beam-Applied Biology, JAERI**

1. Introduction

Chrysanthemums have some agronomical traits to be improved such as reducing axillary buds to save farmer's labor and lower temperature flowering to save the cost of heating.

New type plant mutants such as UV-resistant *Arabidopsis* and chrysanthemum with novel flower colors have been obtained using ion beams as a mutagen[1), 2)]. The objectives of our research are to develop an effective method for mutation of chrysanthemums using ion beams and to obtain desirable variations. In this paper, we describe effects of ion beam irradiation on the mutation induction from cultures of chrysanthemum.

2. Materials and Methods

2.1 Plant materials

Chrysanthemum (cv. *Jimba*) leaves were cut into appropriately 4 mm × 2 mm disc and cultured on MS medium with 5 mg/l IAA and 1 mg/l BA prior to 3-6 days of irradiation. After 1 month of irradiation, leaf discs were subcultured on MS medium with 0.01 mg/l NAA and 0.05 mg/l BA for adventitious shoot development. Then after 1 month, adventitious shoots were subcultured on MS hormone free medium for plant regeneration.

2.2 Ion beam irradiation

Leaf discs were irradiated with 220 MeV or 320 MeV carbon ions, accelerated by AVF cyclotron at JAERI at doses of 0.5-5 Gy for chrysanthemum.

2.3 Analysis of DNA contents

DNA contents were estimated by the Proidy Analyzer (PARTEC PA)[3)]. Sugar cane was used as genome size control, then, DNA contents were determined by comparing sugar cane with chrysanthemum.

3. Results and Discussions

In 220MeV $^{12}C^{5+}$ and 320MeV $^{12}C^{6+}$ ion beams, regeneration frequency decreased rapidly with increasing dose and the 90% re-generation dose (RD90) was estimated at 2 Gy and 3 to 4 Gy, respectively[4)]. Therefore, specimens were irradiated at nearly RD90. In this study, approximately 18,000 regenerated plants were obtained and cultured during three years; for selection fewer axillary buds or lower temperature flowering type. From the screening of 13,077 M1 plants derived from the ion beam irradiated leaf discs 66 visible mutants were selected (Table 1).

Under low temperature, flowering period of "*Jimba*" is greatly delayed. Thus, in winter season, this cultivar is forced to culture under high temperature controlled at 15 to 20℃. Therefore, we tried to select early flowering type to behave safely even under low temperature of 10 to 12℃ (Fig. 1, 2).

In 220MeV $^{12}C^{5+}$ ion beams, early flowering type (until 9 weeks flowering after lighting stop) frequency gradually increased with increasing dose (except 5Gy), and late flowering type (more than 14 weeks) frequency also increased (Fig. 2).

A lot of mutants with different flowering period were obtained by ion beam irradiation (Fig. 1).

The mutants of early or late flowering type were selected and analyzed about DNA contents. The chromosome number of chrysanthemum is 54 (hexaploid). So, 2% of total DNA contents are just about same value of one chromosome. Almost normal plants derived from non-irradiated leaf discs did not decrease in any amount DNA (data is not shown). However, 10% of mutants that decreased more than 2% of the total DNA were included in the selected plants derived from non-irradiated leaf discs. Furthermore, the mutants in which the DNA contents were less than 98%, were included in 30 to 70% of mutants irradiated with 220MeV $^{12}C^{5+}$ ion beams of 0.5 to 5 Gy (Fig. 3). These results show that the chromosomes are cut easily by the ion beam irradiation, because the energy is higher than other radiation[5].

We are breeding the improvement of one point; few axillary buds or early flowering type that maintained characteristic of the original cv. "*Jimba*". Therefore, the high irradiation dose of ion beam is not desirable.

In the original cv. "*Jimba*", the number of axillary flower buds is almost more than 30. However, the number of axillary buds of the mutants were less than half to quarter, and these were obtained from leaf cultures irradiated with 320MeV $^{12}C^{6+}$ ion beams at 3 and 1 Gy (Fig. 4)[6]. These two selected plants were proliferated by vegetative propagation and these clonal lines were selected by the line breeding system. These two lines are keeping each character of few axillary buds, no difference in the line. We also obtained the few axillary bud mutants from cv. "*Jimba*" irradiated with 220MeV $^{12}C^{5+}$ (Fig. 4).

These selected plants or lines were analyzed DNA contents. DNA contents of B01-2-15 were approximately 98% of original "*Jimba*". However, other selected line or plants did not decrease any amount of DNA (Fig. 5).

Now, we are going to prepare for selection of mutants which have both few axillary buds and low temperature flowering trait. Therefore, re-irradiation becomes needed for that, and selection of the mutant in which DNA contents are not decreasing may be necessary.

References

1) A. Tanaka *et al.*, TIARA Ann. Rep. 1995, (1996) 32-34.
2) S. Nagatomi *et al.*, TIARA Ann. Rep. 1997, (1998) 41-43.
3) K. Mishiba and M. Mii, Cell Tech., (1988) Vol.17, No. 4: 609-615.
4) K. Ueno *et al.*, Ikushugaku Kenkyu 3 (2001) (Suppl. 2): 62.
5) N. Shikazono *et al.*, Genetics 157, 379-387 (2001).
6) K. Ueno *et al.*, TIARA Ann. Rep. 2001, (2002) 44-46.

Table 1. The number of tested and selected plants in three years, which regenerated from leaf cultures irradiated by ion beam or X-ray.

Cultiver	Radiation	Energy MeV	Dose Gy	Number of tested and (selected) plants for three years. 2000		2001		2002		Total	
Jimba	He	50	1-3	111	(2)	44	(1)			155	(3)
		100	1-10			2,032	(2)			2,032	(2)
	C	220	1-5	35		3,633	(24)	1,794	(12)	5,462	(36)
		320	0.5-10			2,800	(7)	2,628	(18)	5,428	(25)
	X-ray		5	891	(10)	1,086	(3)	445		2,422	(13)
	non-radiated control		0	1,060	(9)			1,420	(6)	2,480	(15)
Total				2,097	(21)	9,595	(37)	6,287	(36)	17,979	(94)

( )= No. of selected plants. Selected by a few axillary buds or early flowering.

Fig. 1 Individual selection in green house for early flowering under low temperature.

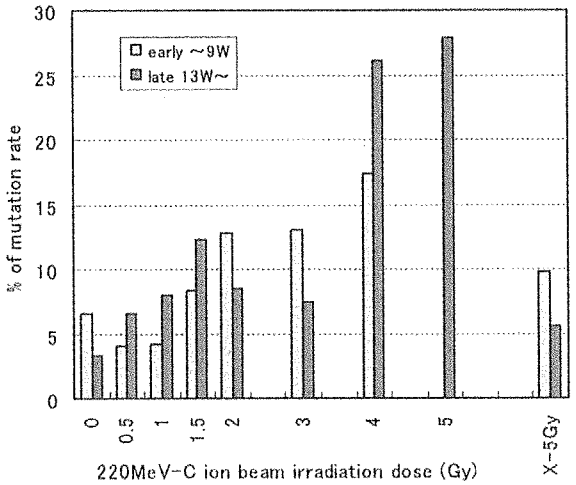

Fig. 2 Mutation rate of early or late flowering.

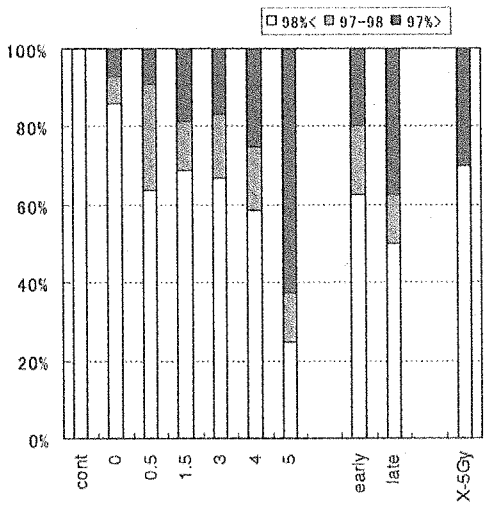

Fig. 3 Percentages of DNA amount of early or late flowering mutants.

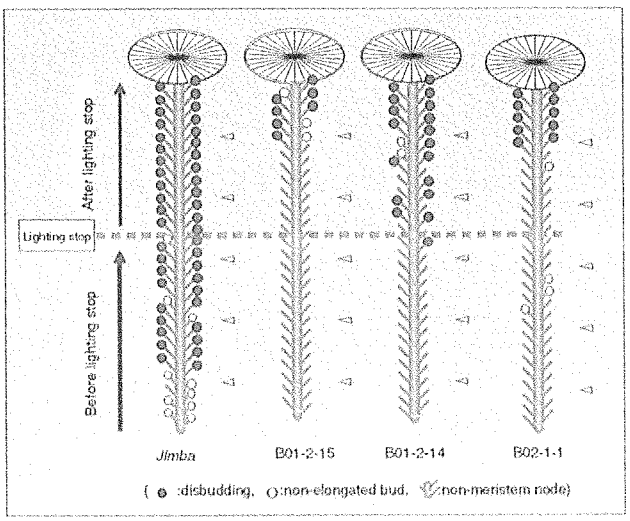

Fig. 4 The characteristics of axillary buds in each lines. (Flowering in December.)

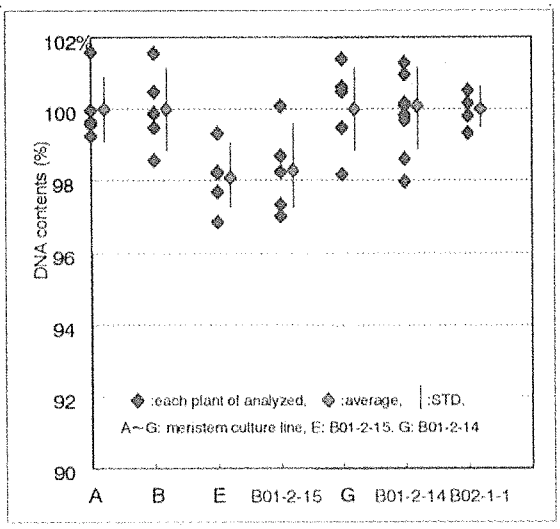

Fig. 5 DNA contents of few axillary buds selected lines.

2.9 Mutation Induction to Sweetpotato with Ion Beam Irradiation

M.Ooe*, J.Nagai*, K.Shimonishi**, Y.Hase***, N.Shikazono*** and A.Tanaka***
Kagoshima Biotechnology Institute*
Agricultural Enviroment Promotion Office, Kagoshima Prefecture**
Department of Ion-beam-applied Biology, JAERI***

1. Introduction

In the breeding of sweetpotato which is high polyploidy, mutation breeding is suitable for minor improvement of some specific trait remaining most of its superior characteristics. Currently, novel type of plant mutants such as UV-resistant *Arabidopsis*[1] have been obtained using ion beams as a mutagen. Therefore, ion beams are considered to be the most suitable tool for the mutation breeding of crops.

The main objective of this study is to modify starch composition of sweetpotato by ion beam irradiation. In this report, effects of ion beam irradiation on morphologic properties and starch composition were examined.

2. Materials and Methods

2.1 Plant materials

Embryogenic calli of sweetpotato (cv. Shirosatsuma) were induced from meristematic tissue and subcultured on MS medium with 0.05 mg/l 2,4-D. Calli were prepared to 2 mm (for $^{12}C^{6+}$) or 6 mm (for $^{4}He^{2+}$) in height prior to irradiation. After irradiation, somatic embryos were induced from calli using 4 mg/l ABA and 1 mg/l GA_3 followed by transfer to hormone-free MS medium for plantlet development.

2.2 Ion beam irradiation

Sweetpotato calli were irradiated with 100 MeV helium ions at doses of 25-750 Gy or 320 MeV carbon ions at doses of 20-300 Gy accelerated by AVF cyclotoron at JAERI.

2.3 Analysis of starch composition and content

Starch content of tuberous roots were determined by iodine binding using spectrophotometer. To calculate Amylose content, 10 mg of extracted starch was dissolved in 0.5 ml of DMSO, and 9.5 ml of distilled water was added. 200 μl of this starch solution was diluted with 4.4 ml of distilled water, and reacted with 400 μl of 0.1% I_2 solution. The amylose contents were calculated by the following equation:

Amylose content % = $(OD_{680} - 0.17)/(1.48 - 0.17) \cdot 100$

3. Results and Discussions

The number of regenerated M1 plants after ion beam irradiation were listed in Table 1 and 2. When sweetpotato calli were irradiated with 100 MeV helium ions, and 320 MeV carbon ions, regenerated M1 plants were obtained at doses of 25-200 Gy and 20-50 Gy, respectively. Almost these plants were obtained at 100 Gy or below in helium ions and 40 Gy or below in carbon ions.

Young leaves of the original cv. Shirosatsuma are reddish, and its tuberous roots are yellowish white. In this experiment, appearances of these organs were mutated in their colors. The color of new leaves and tuberous roots in some M1 plant were altered to pale green and pale purple, respectively. Out of total 965 M1 plants irradiated with helium ions, 13 independent M1 plants had pale green leaves, and the incidence

of this mutation was 1.3% (Table 1) and this mutation was observed in carbon ions as well (Table 2). The frequency of this mutation increased with augmentation of the irradiation dose in helium ions. On the other hand, the mutation of root color had a tendency to incease with the amount of irradiation, but it was also observed in unirradiated plants. It is possible that some of root-color-changed mutants is induced in the process of tissue culture.

When the dosage of irradiation increased, the weight of tuberous roots and measurements of starch (OD_{680}) tended to decrease as shown in Table 3. The decline of OD_{680} was probably caused by decrease of starch content. Amylose contents were calculated based on the measured values of OD_{680}. As a result, the highest amylose content was 16.3% (data not shown).

From above results, it is assumed that the appropriate dose of irradiation for regeneration of sweetpotato is 100 Gy or below in helium ions and 40 Gy or below in carbon ions. These estimates are in accord with the results of previous reports[2), 3)], but it is necessary to consider the tendency for weight of tuberous roots and starch content to decrease with increasing dose of irradiation. This study was chiefly undertaken to alter starch composition of sweetpotato, but the high amylose plant whose amylose content is more than 20% was not obtained. Visible mutations of the leaf and root colors, however, were induced. These results suggest that morphologic mutants, particularly chromatic mutants, of sweetpotato will be obtained with ion beam irradiation. It is expected that color and shape of the sweetpotato tuberous root will be modified more effectively using ion beams.

References

1) A. Tanaka *et al.*, TIARA Ann. Rep. 1995 (1996) 32-24.
2) K. Shimonishi *et al.*, TIARA Ann. Rep. 2000 (2001) 82-84.
3) K. Ueno *et al.*, TIARA Ann. Rep. 2001 (2002) 44-46.

Table 1. Effects of helium ion beam irradiation on sweetpotato plants

dose (Gy)	No. of irradiated petri dish	No. of cultivated plants	No. of green * leaves	% of green leaves	No. of purple ** roots	% of purple roots
250-750	9	0	-	-	-	-
200	6	10	0	0	0	0
150	4	29	2	6.9	1	3.4
100	6	415	9	2.2	13	3.1
75	2	79	1	1.3	1	1.3
50	4	83	0	0	2	2.4
25	2	105	1	1.0	0	0
0	-	244	0	0	5	2.0
total	33	965	13	1.3	22	2.3

*: young leaves altered to pale green
**: tuberous roots altered to pale purple

Table 2. Effects of carbon ion beam irradiation on sweetpotato plants

dose (Gy)	No. of irradiated petri dish	No. of cultivated plants	No. of green * leaves	% of green leaves	No. of purple ** roots	% of purple roots
60-300	19	0	-	-	-	-
50	2	4	0	0	1	25.0
40	2	142	7	4.9	9	6.3
25	2	56	0	0	0	0
20	2	10	0	0	1	10.0
0	-	40	0	0	1	2.5
total	27	252	7	2.8	12	4.8

Table 3. Averages of the tuberous roots and measurements of starch

helium ion beam

dose (Gy)	weight of root tubers (g)	measurements of starch (OD_{680})
200	63.8	0.656 **
150	187.6	0.716
100	290.7	0.705 **
75	314.3	0.787
50	333.4	0.754
25	417.4	0.825 **
0 (control)	411.6	0.763

carbon ion beam

dose (Gy)	weight of root tubers (g)	measurements of starch (OD_{680})
50	-	-
40	309.6	0.682 **
25	334.5	0.709 *
20	513.3	0.627 **
0 (control)	455.9	0.794

*: significantly different from the control at 5% level
**: significantly different from the control at 1% level

2.10 Comparison between Ion Beam Irradiation and Particle Bombardment in the Transformation of Hinoki Cypress *(Chamaecyparis obtusa)*

K. Ishii*, Y. Hase**, and A. Tanaka**

Department of Molecular and Cell Biology, Forestry and Forest Products Research Institute*, Department of Ion-beam-applied Biology, JAERI**

1. Introduction

Hinoki cypress (*Chamaecyparis obtusa* Sieb. et Zucc.) covers 24 % of the plantation area in Japan and is the most important domestic forest conifer. It produces the highest quality wood and can be grown throughout Japan, excluding Hokkaido and the Ryukyu Island. In forest tree species with long life cycle, genetic transformation is very promising in shortening the breeding time.

Ion beam is expected to increase the mutation frequency and wide spectrum, since it has a high LET (linear energy transfer). The combination of ion beams irradiation and tissue culture was sometimes beneficial for high frequent mutation induction[1)2)3)]. In the previous report, we have obtained the xanta and wax rich mutants by ion beam irradiation[4)].

In this study, we tried to create herbicide resistant mutants by irradiation of the shoot primordia of Hinoki cypress with $^{4}He^{2+}$ and $^{12}C^{6+}$ heavy ion beams. Then, we compare the transformation methods of ion beam irradiation and particle bombardment in the introduction of herbicide resistant trait to Hinoki cypress.

2. Experimental procedure

Shoot primordia of Hinoki cypress was used for the experiments. They are cultured on CD medium[5)6)] supplemented with 10 μ M 6-benzylaminopurine and 0.03 μ M naphthalene acetic acid (NAA). Fresh shoot primordia were subcultured on the same medium in petri dish (35 x 10 mm) which was covered with Kapton film. They were irradiated with 50 MeV $^{4}He^{2+}$ or 320 MeV $^{12}C^{6+}$ ion beam from AVF cyclotron in JAERI. After irradiation the shoot primordia were subcultured to the new CD media containing 0.03 μ M NAA and 0.002% basta or 10 μM bispyribac-sodium for herbicide resistant selection and shoot differentiation.

In another experiment, shoot primordia were targeted by a particle bombardment. The introduction of a useful herbicide resistance gene (bar) into the shoot primordia with the promoter of 35S of cauliflower mosaic virus (pSLJ2011)[7)] or maize ubiquitin promoter (pAHC20)[8)] was tried. The plasmid pSLJ2011 is a binary vector plasmid which was cloned into the site of plasmid pRK290 from *E. coli*. The plasmid pAHC20 has Ubi-1 promoter from maize, herbicide phosphinothricin registance gene (bar), nopaline synthase 3' untranslated sequence and sequence from vector pUC8 of *E. coli*. The Ubi-1 promoter has been shown to be highly active in monocots.

PCR analysis was done according Takumi and Shimada[9]. Southern blotting analysis was done using the genome DNA extracted.

To the regenerated plantlets from the selection medium, 50 times diluted Basta herbicide (This dilution means 0.37 % of glufosinate in the spray liquid) was sprayed and the response of the transgenic and non-transgenic plants was checked just after regeneration. Three resistant lines were also checked with 50 times diluted Basta spray after one growing season in the containment greenhouse. In a preliminary test, untransformed juvenile Hinoki cypress were killed with 100 times diluted Basta spray treatment.

3. Results and Discussion

Shoot primordia irradiated with 5 to 80 Gy $^{4}He^{2+}$ ion beam were all dead after 4 months in the 0.002 % basta or 10 μM bispyribac containing medium. There were totally 7 surviving shoot primordium clusters out of 1350 in the CD selection medium containing 10 μM bisbyribac 40 days after irradiation with $^{4}He^{2+}$ ion beam from 5 to 20 Gy (Table 1.). However, they died after 4 months in the same medium. There were 1 surviving shoot primordium cluster out of 750 in the CD selection medium containing 0.002 % basta and 7 surviving shoot primordia out of 750 in the CD selection medium containing 10 μM bisbyribac 1 month after irradiation with 5 to 80 Gy $^{12}C^{6+}$ ion beam (Fig. 1). However they died later. There were no surviving shoot primordium clusters out of 2250 in the CD selection medium containing 10 μM bisbyribac 2 months after irradiation with 5 to 20 Gy $^{12}C^{6+}$ ion beam. So far, we observed no herbicide resistant mutants in Hinoki cypress shoot primordia after irradiation of $^{4}He^{2+}$ or $^{12}C^{6+}$ ion beam.

According to the bar herbicide selection after particle bombardment, it is appeared that 35S promoter was better than ubiquitine promoter for bar gene expression. The best condition for transformation was with 5 days' preculture using 35S promoter. Nine out of 30 regenerated plantlets showed the positive band (402 bp) of the bar gene. Southern blotting analysis showed the existence of 2 copies of bar genes in two transformed plantlets examined. Surviving plantlets were observed among the regenerated plantlets (Fig. 2) from the selection medium after Basta spray treatment.

In this experiment where the functional genes were already detected, the particle bombardment is much manipulative than ion beam irradiation for creating transformation. However, recent negative public attitude to recombinant DNA technology forces us to develop much acceptable transformation approach like that using ion beam irradiation.

Table 1. Effect of ion beam irradiation on number of surviving shoot primordium clusters on the selection meadium containing herbicide (bispyribac)

Dose	$^{4}He^{2+}$			$^{12}C^{6+}$	
Gy	irradiated	surviving		irradiated	surviving
		40	120days		60days
5	450	3	0	750	0
10	450	3	0	750	0
20	450	1	0	750	0

Fig. 1 Surviving shoot primordium clusters (arrows) of Hinoki cypress on the herbicide selection medium containing 10 μ M bispyribac one month after irradiation of $^{12}C^{6+}$ ion beam.

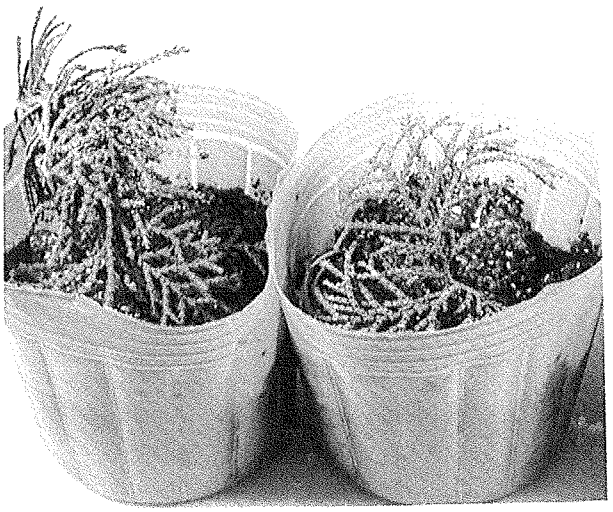

Fig. 2 Genetic transformed Hinoki cypress which was introduced with bar gene by particle bombardment

References

1)S. Nagatomi, A. Tanaka, A. Kato, H. Watanabe and S. Tano, TIARA Annual Report 5(1996)50-52.

2)S. Nagatomi, A. Tanaka, H. Watanabe and S. Tano, TIARA Annual Report 6(1997) 48-50.

3)T. Nakahara, K.Hirashima, M. Koga, A. Tanaka, N. Shikazono and H. Watanabe, TIARA Annual Report 1998(1999)28-29.

.4)K. Ishii, Y.Hase, N. Shikazono and A.Tanaka, TIARA Annual Report 2000(2001)55-56.

5)R.A. Campbell and D.J. Durzan, Can J. Bot. 53(1975)1652-1657.

6)K. Ishii, Plant Cell Tissue and Organ Culture 7(1986)247-255.

7)J. Jones, D.G. Jones, L. Shulumukov, F. Carland, J. English, S.R. Scofield, G.J. Bishop and K. Harrison, Transgen. Res. 1(1992)285-297.

8)A.H. Christensen and P.H. Quail, Transgen. Res. 5(1996) 213-218.

9)S. Takumi and T. Shimada, J. Plant Physiol. 149(1996)418-423.

2.11 Mutation Induction with Ion Beam Irradiation in Garlic (*Allium Sativum* L.) - Morphological Character of Plantlets -

T.Tashiro*, Y. Yamamoto*, A.Tanaka**, N.Shikazono** and Y.Hase**
Farm Station of FSC, Faculty of Bioresources, Mie University*
Department of Ion-beam-applied Biology, JAERI**

1.Introduction

Recently, there is a great demand for garlic because garlic is one of the remarkable health foods. Garlic belongs to a group of the Allium family. Since garlic is sexually sterile and propagated by bulbs, the positive plant breeding is difficult. Therefore, the consumer and the producer could not satisfy the breeding in garlic. We established a novel system of practical micropropagation in garlic, which produced effective bulblets *in vitro*, because it is a wise method to proliferate, to select, and to plant in field[1].

The ion beam is expected to increase the mutation frequency and wide spectrum, since it has the high liner energy transfer (LET) and relative biological effectiveness (RBE) [2]. A combined method of ion beams irradiation with tissue culture was beneficial for high frequent mutation. We supposed that ion beam induced specific mutation not only on morphological character but also on chemical composition in garlic.

The purpose of this study is to investigate the effects of ion beam on the mutant of volatile sulfur compounds of garlic. In this paper, we report the effects of ion beam on callus proliferation and shoot regeneration from the irradiated callus induced from basal plate of garlic bulb, and bulblet induction from explants of basal plate bulb.

2.Materials and Methods

Garlic cultivars, 'Fukuchi-white' treated sterilely were used for the experiments. One of irradiated materials was thin sections of bulb basal plates. Another one was compact and granular callus like embryogenic callus.

2.1 Basal plate

Multiple shoots are induced directly from basal plates in very short culture period (two months), but it is difficult to produce many regenerated plantlets. The basal plate was cut off 1~1.5mm thickness as ion beam could irradiate through them perfectly and trimmed 5x5mm in length, and then divided into 4 equal segments. 8~12 segments were placed on a 60mm diameter plastic petri dish containing 5ml LS medium supplemented with 30g/l sucrose and 3g/l gelrite for shoot differentiation[3]. The dishes were covered with Kapton film, and then irradiated with 320MeV $^{12}C^{6+}$ or 50MeV $^{4}He^{2+}$ ion beams from the TIARA AVF cyclotron in JAERI. The irradiation dosage ranged from 0.05Gy to 10Gy at 6 levels in carbon ion beam and from 0.05Gy to 1KGy at 7 levels in helium ion beam. After irradiations the both samples were transferred to the fresh medium for shoot differentiation. Fresh shoots were subcultured on medium for bulblets formation.

2.2 Callus

It takes over four months to produce

bulblets, but the regenerated plantlets can be produced enough numbers to select mutants. The calluses in liquid-shaking culture were placed on 1mm thickness in 60mm diameter plastic petri dish containing MS medium supplemented with plant growth regulator (2,4-dichlorophenoxy acetic acid). The dishes were covered with Kapton film, and then irradiated with 320MeV $^{12}C^{6+}$ or 50MeV $^{4}He^{2+}$ ion beams same as basal plates. The irradiation dosage ranged from 0.05Gy to 1Gy at 6 levels in carbon ion beam and from 0.05Gy to 10Gy at 7 levels in helium ion beam. After irradiations the both samples were transferred to the medium for shoot differentiation after one month. Fresh shoots were subcultured on medium for bulblets formation.

The experiments were performed under 3000lux (day /night of 16/8hrs.) at 25°C. Proliferation rate of callus and formation rate of callus colony that had the regenerated ability to produce shoot, and survival rate of basal plate segment and bulblet formation rate from basal plate segment were investigated. And the general appearances of the plantlets were observed, comparing the morphological differences among those plantlets induced by irradiating carbon and helium ion beams.

3.Results and Discussions

1) Establishment of micropropagation system of garlic bulblets *in vitro*

The effective micropropagation system of garlic bulblets is established, which can produce plantlets derived from the irradiated basal plates and the irradiated compact yellowish callus like embryogenic callus (data not shown) [4].

2) Effect of basal plate irradiation on plantlet growth and its morphological character

The basal plates were irradiated with 0.2Gy and 0.5Gy carbon or helium ion beams for the effective dosage to produce plantlets as a result of preliminary experiment (Table 1). There was no significant difference among the number of plantlets per segment in each treatment. These results suggest that ionizing radiation almost did not affect the plantlet formation. Various types of plantlets were observed and divided according to their general appearance. The normal plantlets were defined green and over 5cm leaf length like the normal garlic in appearance. Abnormal plantlets were divided into vitrification induced by culture and the variation induced by irradiating ion beam. The vitrification rate was 11.9% in unirradiated treatment. In helium ion beam, vitrification rate was 10.9% at 0.2Gy and was 9.2% at 0.5Gy, respectively. In carbon ion beam, vitrification rate was 17.0% at 0.2Gy and was 8.2% at 0.5Gy, respectively. These results suggest that vitrification occurred equally regardless of radiation. The irradiated variation rate was depended on carbon and helium ion beams. In helium ion beam, irradiated variation rate was 21.7% at 0.2Gy and was 8.0% at 0.5Gy, respectively. In carbon ion beam, irradiated variation rate is 21.0% at 0.2Gy and is 23.4% at 0.5Gy, respectively. Irradiated variation rate was 0% in unirradiated treatment. These data indicated that plantlets derived from irradiated segments had the higher variation rate apparently, and variation rate was higher in carbon ion beams than in helium ion beams. These results suggest that carbon ion beams can induce mutation at low dosage of

irradiation, resulting in the effective induction of the mutants with one or a few point mutations that have no or very few undesired mutations. The plantlets having different morphological character such as multiple shooting, variegated leaves, albino and dwarf were produced by carbon ion beams irradiation.

3) Effect of callus irradiation on plantlet growth

The segments of callus were irradiated with 0.1Gy and 0.2Gy of carbon or helium ion beams for the effective dosage to produce plantlets as a result of preliminary experiment. Because the irradiated callus is cultivated *in vitro*, it is not yet investigated in detail about the appearances of plantlets. We didn't find any mutant for the show in plantlets induced in preliminary experiment for the adequate dosage.

The regenerated bulblets were placed on soil for sprouting, and now they are well grown in experimental field of Farm Station in Mie University. They will be harvested in June 2003 and estimated agricultural traits in details. The differences among ion beams in the effect of mutant and in the spectrum of induced mutants are investigated in detail.

References

1) Y.Yamamoto and T.Tashiro, International Plant Propagatorrs'Society 7:17-18(2000).

2) A.Tanaka, N.Shikazono, Y.Yokota, H.Watanabe and S.Tano, Int. J. Radiat. Biol. 72:121-127 (1997).

3) M.Maybe and S.Sumi, Plant Cell Reports 17:773-779(1998)

4) T.Tashiro, Y.Yamamoto, A.Tanaka, N.Shikazono, and Y.Hase, TIARA Annual Report 2001, JAERI- Review 2001-035:49-51 (2002).

Table 1 Effects of carbon and helium ion beam irradiations on induction of shoot from basal plate of garlic bulb

	$^{4}He^{2+}$(Gy)		$^{12}C^{6+}$(Gy)		control
	0.2	0.5	0.2	0.5	
No. of irradiated basal plates(A)	27	46	180	181	30
No. of total shoots(B)	46	87	305	415	84
No. of normal shoots(C)	31	72	189	284	74
No. of vitrified shoots(D)	5	8	52	34	10
No. of abnormal shoots induced by irrdiation(E)	10	7	64	97	0
No. of multiple shoots(F)	0	0	15	53	0
No. of shoots with variegated leaves(G)	0	0	21	23	0
No. of shoots less than 5mm leaf length(H)	10	0	0	0	0
No. of abortive shoot(I)	0	7	28	21	0
B/A(No. of shoots)	1.7	1.9	1.7	2.3	2.8
C/B(%)	67.4	82.8	62.0	68.4	88.1
D/B(%)	10.9	9.2	17.0	8.2	11.9
E/B(%)	21.7	8.0	21.0	23.4	0.0
F/E(%)	0.0	0.0	23.4	54.6	—
G/E(%)	0.0	0.0	32.8	23.7	—
H/E(%)	100.0	0.0	0.0	0.0	—
I/E(%)	0.0	100.0	43.8	21.6	—

2.12 Characters and Inheritance of Short Internode Induced by the Irradiation of $^{12}C^{5+}$ Ion Beam in Tomato

M. Masuda*, K. Murakami*, T. Yuasa*, A. Tanaka** and Y. Hase**
Department of Applied Plant Science, Faculty of Agriculture, Okayama University*
Department of Ion-Beam-Applied Biology, JAERI**

1. Introduction

Ion beam, a recently innovated technique has been shown to produce a new type of mutant in *Arabidopsis thaliana*[1]. Since biological effects of ion beam is different from that of gamma-rays, we expect that ion beam irradiation will be new technique for obtaining novel mutants. In tomato, 50 Gy of $^{12}C^{5+}$ and 150 Gy of $^{4}He^{2+}$ were the optimum dosages for irradiating seeds with the possibility of generating tomato mutants without causing excessive injury to the embryo[2, 3]. Masuda et al. (2002) reported that tomato cv. First mutant with short internode (Fig. 1) was induced by the irradiation of $^{12}C^{5+}$ ion beam to the seeds [4]. Short internode would be useful for production of indeterminate tomato cultivars with long harvesting period, because it can save training/harvesting labor, especially in protected culture. In this paper, we report that characters and inheritance of short internode tomato.

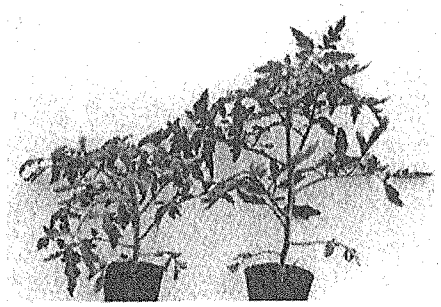

Fig. 1. The mutant with short internode (left), Wild-type First (right).

2. Experimental procedure

2.1 Plant material

A mutant with short internode was induced from tomato cv. First irradiated with 50 Gy of 220 MeV $^{12}C^{5+}$ ion beam to their seeds[2]. Material seeds (M_3) were derived from self-pollination of the M_2 plant.

2.2 Fruit quality of mutant

Seeds of mutant and wild-type First were sown on 27 March. Fruits were harvested from 1st cluster and the concentration of sugars and organic acids were measured with HPLC.

2.3 Effect of GA_3 treatment on shoot growth

Mutant and wild-type First plants at 1st leaf-stage were used. Plants were cultured in the nutrient solution containing GA_3 at the concentration of 0, 0.1, 1 mg·liter^{-1}. Epicotyl length was measured after 12 days culture.

2.4 Segregation in F_2 population

For inheritance studies, the mutant and wild type First were reciprocally crossed. The segregation of short internode in the F_2 population was examined. F_2 seeds were sown in vermiculite on 1 Sep. Phenotype was determined on 26 Sep.

3. Results and Discussion

3.1 Fruit quality of mutant

The sugar levels were lower and the acid levels were higher in the mutant than those in wild-type first, but there were no significant differences between them (Table 1).

Table 1. Sugar and acid contents in fruits of wild-type 'First' and a mutant with short internode.

Line	Sugar (g/100g)		Acid (g/100g)	
	Glucose	Fructose	Citric	Malic
Wild-type	1.26	1.42	0.225	0.023
Short internode	1.09	1.28	0.296	0.027
Significance	NS	NS	NS	NS

3.2 Effect of GA_3 treatment on shoot growth

Application of 1 mg·liter^{-1} GA_3 was effective on the stem elongation in the two lines (Fig. 2). GA_3 at 0.1 mg·liter^{-1} was also effective on wild-type First but not effective on the mutant. The mutant show lower sensitivity to GA_3 application than wild-type. This result suggests that the short internode character is not related to low endogenous GA_3 level.

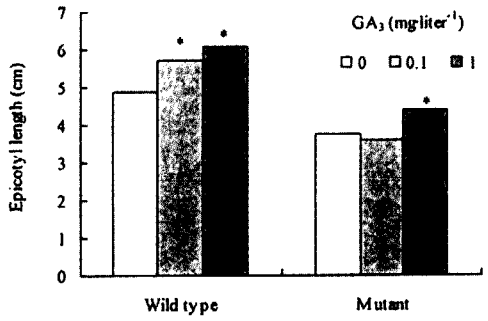

Fig. 2. Effect of GA_3 on the elongation of epicotyl in wild-type 'First' and a mutant with short internode.
* Indicates significant difference (α = 0.05) between each treatment and control.

3.3 Segregation in F_2 population

Both of F_1 derived from reciprocal crossing showed normal growth. F_2 population segregated into two phenotypes ; normal and short internode-type (Table 2). Segregation ratio fitted well to 3 : 1 (normal: short internode). These results indicate that the short internode character is controlled by a single recessive nuclear gene.

Table 2. Segragation of the mutant phenotype in the F_1 and F_2 generation.

Crosses	F_1	Phenotype in F_2 (No)		χ^2	
		Normal	SI-type	(3 : 1)	*P*
SI × WT	Normal	147	43	0.667	0.414
WT × SI	Normal	118	42	0.133	0.715

SI : mutant with short internode
WT : wild-type First

Symbol marks, *br* (brachytic) and *bu* (bushy), are known as the genes of short internode character in tomato[5]. Further studies are required to confirm whether the mutant gene induced by ion beam is different from *br* or *bu*.

References

1) A. Tanaka, N. Shikazono, Y. Yokota, H. Watanabe and S. Tano. Int. J. Radiat. Biol. 72 (1997) 121-127.
2) M. Masuda, S. G. Agong, A. Tanaka, N. Shikazono and Y. Hase. JAERI-Review 2001-039 (2001) 42-44 .
3) M. Masuda, S. G. Agong, A. Tanaka, N. Shikazono. Acta Hort. (2003) (in press).
4) M. Masuda, K. Murakami, T. Yuasa, A. Tanaka and Y. Hase. JAERI-Review 2002-035 (2002) 52-53.
5) Rick, C. M. and L. Butler : Advances in Genetics 8 (1956) 267-382.

2.13 Mutation Breeding of Rice, Eggplant and Gloriosa by Ion Beam Irradiation

M. Mizobuchi*, M. Okada*, M. Matsumoto*, A. Iwasaki*, A. Tanaka** and Y. Hase**
Kochi Prefectual Agricultural Research Center*,
Department of Ion-beam-applied Biology, JAERI**

1. Introduction

In Kochi prefecture, we are carrying out mutation breeding of rice, eggplant and gloriosa. Though we have used γ-rays and MNU as mutagens, we attempt to use ion beams in this study. Because the linear energy transfer and relative biological effectiveness of ion beams are extremely higher than those of γ-rays. Thus, seeds of rice, eggplant, and gloriosa were irradiated with ion beams and several biological effects were examined. Moreover, we selected individuals that have excellent mutant characters. We used helium(He) and carbon(C) ions that were accelerated by using the AVF cyclotron in Takasaki, JAERI.

2. Materials and Methods

In rice, dry seeds of the variety 'Tosapika' were irradiated in 2000, and the seeds of the M_2 generation were sown. In 2001 about 1600 plants from 19 treatments and in 2002 about 2700 plants from 28 treatments were grown in the field. The primary selection was done by the plant forms and the quality of brown rice. Then we investigated the amylose content of the selected 488 lines of brown rice in 2001 and 461 lines in 2002.

In eggplant, the seeds of the variety 'Waseshinnkuro' were irradiated with C 220MeV ion and their anthers were cultured. Then the pollen fertility of the DH(doubled haploid)lines were compared with that of the M_1 generation plants.

In gloriosa, the seeds of two self-pollinated lines and five F_1 hybrid lines were irradiated with He(100MeV) at a dose of 80Gy, C(220MeV) at 10Gy , or C(320MeV) at 5-20Gy. M_1 plants of the 98PM(s) line irradiated with C(220MeV) in 1998 and those of No.2(the Misato-pink line) and No.13(the Kakamega line) irradiated with C(220MeV) or He(100MeV) were grown in a green house. The influence of irradiation on the germination rate of the seeds and the induction of mutation of M_1 plants were evaluated.

3. Results and Discussions

In rice, the mutants those amylose contents were lower than 14% could be obtained from 10 treatments. There were Twenty three mutants of low amylose content were obtained. The irradiation of carbon ion induced low amylose content mutants more than that of helium ion. Though the higher dosage irradiation tended to induce mutations of low amylose content, the proper dosage could not be clarified (Table 1, 2).

In eggplant, the higher dosage of irradiation was done, the fewer numbers of self-pollinated seeds of DH lines could be obtained. No self-pollinated seeds were obtained from DH lines with 50Gy irradiation(Table 3). S1 generations of the irradiated DH lines were the same extent as that of non-irradiated plants and DHlines from non-irradiated plants except for 2 lines of DH lines from the 30Gy irradiated plants

and 1 line from the 40Gy irradiated plant(Fig 1). The pollen fertility of irradiated plants was much lower than that of non-irradiated plants. These results suggest that the pollen fertility was recovered via anther culture.

In gloriosa, the germination rates of the seeds were 12-60%. The irradiation of He with 80Gy and C (220MeV) with 10Gy decreased the germination rates of seeds to 20-60% and 30-80% of the control, respectively. Among 379 M_1 plants of 98PM(s), 12 plants of No.2 and No.13 with brilliant flower were selected primarily. However, no mutant plants in terms of flower color and leaf shape were observed (Table 4) .

4. Reference

1) A. Tanaka et al., TIARA Ann Rep., 1998,p39
2) H. Yamaguchi et al., TIARA Ann Rep., 1998,p42

Table 1 Low amylose content mutants 'Tosapika'

ion	dose (Gy)	No. of analyzed plants	No. of low amylose content plants	rate of low amylose content plants(%)	lowest amylose content(%)
He50MeV	25	54	1	1.9	13.1
He50MeV	200	26	3	11.5	13.8
He50MeV	250	3	1	33.3	10.7
He100MeV	25	72	5	6.9	13.5
C220MeV	10	107	1	0.9	13.7
C220MeV	20	64	3	4.7	11.8
C220MeV	50	1	1	100	13.6
C320MeV	15	22	1	4.5	10.1
C320MeV	20	56	1	1.8	13.9
C320MeV	30	18	6	33.3	13.4

Amylose content less than 14% were selected.
Irradiation were done in 2000-2002.

Table 2 Rate of low amylose content plants irradiated by each ion

ion	No. of analyzed plants	No. of low amylose content plants	rate of low amylose content plants(%)	lowest amylose content(%)
He50MeV	273	5	1.8	10.7
He100MeV	275	5	1.8	13.5
C220MeV	203	5	2.5	11.8
C320MeV	198	8	4.0	10.1

All treatments of each ion are summed up.

Table 3 Self-pollinated seeds of DH lines of eggplant

dose (Gy)	No. of acclimatized lines(A)	No. of lines obtained seeds (B)	A/B
0	22	13	0.59
30	28	11	0.39
40	26	3	0.12
50	6	0	0.00

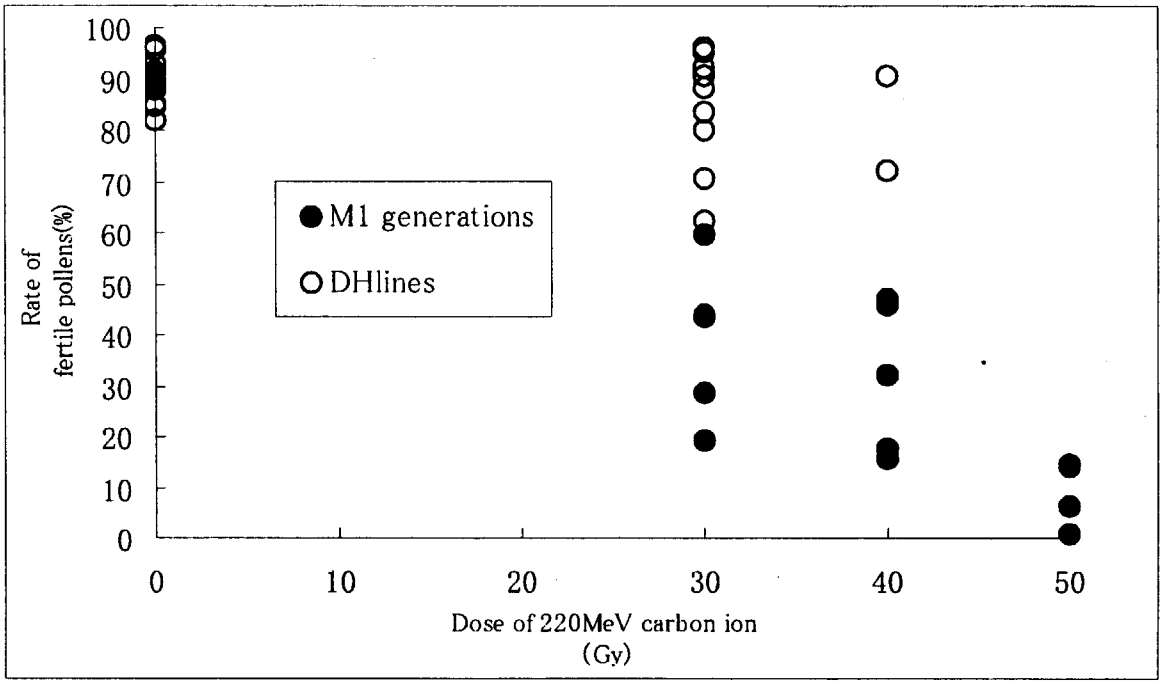

Fig. 1 Variance of the rates of fertile pollens in eggplant

Table 4 Results of the primal selection of gloriosa and traits of the selected plants

name of line[Z]	No. of tested plants	No. of selected plants	name of the selected line	traits of the selected line[Y]				
				shoot length	diameter of flower	petal lenth	petal width	main color of petal
98MP(s)10Gy～40Gy	128	0						
IB12-1-1(No.2)40Gy	30	1	IB1211-02-1	middle	middle	middle	middle	bright red
IB12-1-1(No.2)80Gy	28	1	IB1211-02-2	middle	middle	middle	narrow	deep yellowish pink
IB12-1-1(No.2)160Gy	30	3	IB1211-02-3	short	middle	middle	narrow	vivd reddish orang
			IB1211-02-4	middle	middle	middle	narrow	yellowish pink
			IB1211-02-5	middle	middle	somewhat long	narrow	bright red
IB12-1-1(No.13)40Gy	32	3	IB1211-02-6	short	middle	middle	narrow	dark red
			IB1211-02-7	short	middle	middle	narrow	dark red
			IB1211-02-8	long	middle	somewhat short	narrow	dark red
IB12-1-1(No.13)80Gy	21	1	IB1211-02-9	long	middle	middle	middle	dark red
IB12-1-1(No.13)160Gy	16	0						
IB12-1-2(No.2)40Gy	54	1	IB1212-02-1	middle	somewhat small	middle	narrow	vivd reddish orang
IB12-1-2(No.2)80Gy	40	2	IB1212-02-2	short	middle	middle	middle	strong yellowish pink
			IB1212-02-3	middle	middle	middle	middle	strong pink
total	379	12						

[Z] (No.2),MP(s):self-pollinated line of Misato pink strain, (No.13):self-pollinated line of Kakamega strain.

[Y] shoot length:short less than 1m・middle 1-2m・long more than 2m, diameter of flower:small less than 5cm・middle 7-9cm・large more than 11cm
petal lenth:short less than 6cm・middle 8-10cm・long more than 12cm, petal width:narrow 10-20mm・middle 20-30mm・wide 30-40mm

2.14 Regeneration of Variegated Plants from Ion-Beam Irradiated Explants of *Ficus thunbergii* Maxim.

M. Takahashi*, S. Kohama*, K. Kondo*, M. Hakata*, Y. Hase**, N. Shikazono**, A. Tanaka** and H. Morikawa***

Department of Mathematical and Life Sciences, Graduate School of Science, Hiroshima University*, Department of Ion-beam-applied Biology, JAERI**, Core Research for Evolutional Science and Technology (CREST), Japan Science and Technology Corporation (JST)***

Abstract

The 4-mm-long explants of apical shoots and the 1-mm-long explants of stem with node cut from *Ficus thunbergii*were irradiated with $^{12}C^{5+}$ (220 MeV), $^{12}C^{6+}$ (320 MeV) and $^{4}He^{2+}$ (50 MeV) ion beams using the AVF cyclotron (JAERI). The frequency of regeneration of plants from the irradiated shoots and phenotypic variations were studied. A distinct suppression was observed at 20, 30 and 70 Gray (Gy) with $^{12}C^{5+}$, $^{12}C^{6+}$ and $^{4}He^{2+}$, respectively. Some of regenerated shoots from the irradiated explants had variegated leaves. At most 15%, 20% and 20% of the plants regenerated from explants irradiated with $^{12}C^{5+}$, $^{12}C^{6+}$ and $^{4}He^{2+}$, respectively, had variegated leaves. These results indicate that the ion beam irradiation provides a pivotal method to induce mutation in the genome of *Ficus thunbergii*.

Introduction

Ficus thunbergii Maxim., or "hime-itabi" in Japanese is an evergreen, climber that belongs to Moraceae, the mulberry family. This tree will be useful to cover highway corridors and vertical surfaces of building to decontaminate various pollutants, including nitrogen dioxide derived from vehicles, in urban areas. Plants take up nitrogen dioxide[1] and assimilate its nitrogen through a primary nitrate assimilation pathway[2]. We discovered that among naturally occurring 217 taxa of the higher plants, there is more than a 600-fold variation in the ability to assimilate nitrogen dioxide[3]. We also reported that the overexpression of a chimeric nitrite reductase gene resulted in a 1.4-fold increase in the capability to assimilate nitrogen dioxide as compared with the wild type[4]. Since the irradiation of plants with ion beams may cause modification of the plant genome[5), 6), 7), 8), 9)], we have been studying the production of novel *Ficus thunbergii* plants that have high capability to assimilate atmospheric nitrogen dioxide[10]. In this study we investigated the conditions for irradiation with ion beams.

Materials and Methods

Aseptically grown *Ficus thunbergii* Maxim. plants were propagated and cultured in tubes containing fluorialite with MS[11] medium, supplemented with 2% sucrose and 100 μg/l indole-3-butyric acid (IBA) as reported previsouly[10]. Plants were cultured for up to two months at 25°C in the light (30 to 40 μmol/s/m^2). About 4-mm-long explants with apical shoots (cut longitudinally in the middle) and

1-mm-long stems bearing nodes were cut with a surgical blade, and placed in petri dishes with shoot formation medium, which was consisted of woody plant medium (WPM)[12] supplemented with 2% sucrose, 0.3% Gellan Gum, 1.78 μM benzyl adenine (BA) and 46.7 nM thidiazuron (TDZ), pH 5.8. Twenty explants were placed on each petri dish. Two days after, the samples were irradiated with $^{12}C^{5+}$ (220 MeV), $^{12}C^{6+}$ (320 MeV) and $^{4}He^{2+}$ (50 MeV) ion beams by the AVF cyclotron at Japan Atomic Research Institute (JAERI, Takasaki). The irradiation dose average ranged from 10 to 200 Gray (Gy). During irradiation, the lid was removed and the petri dish was covered with a thin film to avoid the energy loss of the ion beam[13]. After irradiation, the explants were transferred to fresh shoot formation media, and cultured for up to three months. When regenerated shoots became about 1 cm long, they were transferred into glass tubes containing Florialite (Nisshinbo, Japan) with MS medium, and the culture was continued.

Results and Discussion

As reported previously[10], the frequency of regeneration of plants from irradiated explants changed in a dosage-dependent manner for $^{12}C^{5+}$, $^{12}C^{6+}$ and $^{4}He^{2+}$ ion beams throughout the range of 10 to 200 Gy. At more than 20 Gy with $^{12}C^{5+}$, the frequency of regeneration of shoots (RF), or percent shoot-regenerating explants of total explants irradiated, was less than 30%. At the same time, the frequency of the appearance of plants with variegated leaves was increased, at most 15% of regenerated plants had variegated leaves (Fig. 1). These variegated plants showed slow growth and less aerial roots (Fig.1 A and B). Similar results were obtained with $^{12}C^{6+}$ and $^{4}He^{2+}$. RF values were 30% and 20% respectively at 30 Gy with $^{12}C^{6+}$ and 70 Gy with $^{4}He^{2+}$. The appearance of variegated plants were at most about 20% of regenerated plants at 20 Gy with $^{12}C^{6+}$ and 40 Gy with $^{4}He^{2+}$.

Taken together, the present data strongly suggest that ion beam irradiation is a pivotal method to induce mutations in the genome of *Ficcus stipulate*. We are currently studying the capability of these mutated *Ficus thunbergii* plants to assimilate atmospheric nitrogen dioxide.

References

1) A.C. Hill. J. Air Pollut. Contr. Ass. 21 (1971) 341-346.

2) T. Yoneyama, H. Sasakawa. Plant and Cell Physiol. 20 (1979) 263-266.

3) H. Morikawa, A. Higaki, M. Nohno, M. Takahashi, M. Kamada, M. Nakata, G. Toyohara, Y. Okamura, K. Matsui, S. Kitani, K Fujita, K. Irifune, N. Goshima. plant taxa. Plant, Cell Environ. 21 (1998) 180-190.

4) M. Takahashi, Y. Sasaki, S. Ida, H. Morikawa. Plant Phsiol. 126 (2001) 731-741.

5) A. Tanaka, S. Tano, T. Chantes, Y. Yokota, N. Shikazono, H. Watanabe. Genes Genet. Syst. 72 (1997) 141 – 148.

6) A. Tanaka, N. Shikazono, Y. Yokota, H. Watanabe, S. Tano. Int. J. Rad. Biol. 1 (1997) 121 – 127.

7) A. Tanaka, H. Watanabe, T. Shimizu, M. Inoue, M. Kikuchi, Y. Kobayashi, S. Tano. Research B. 129 (1998) 42 – 48.

8) N. Shikazono, Y. Yokota, A. Tanaka, H. Watanabe, S. Tano. Genes Genet. Syst. 73 (1998) 173 – 179.

9) Y. Hase, K. Shimono, M. Inoue, A. Tanaka, H Watanabe. Radiat. Environ. Biophys. 38 (1999) 111 – 115.

10) M. Takahashi, S. Kohama, M. Hakata, Y.

Hase, N. Shikazono, A. Tanaka, and H. Morikawa. Annual Reports of TIARA, 39 (2001) 62-63.
11) T. Musashighe, F. Skoog. Physiol. Plant. 15 (1962) 473 – 489.
12) G. Lloyd, B. McCown. Combined proceedings of the international plant propagators society. 30 (1980) 421 – 427.
13) A. Tanaka, H. Watanabe, T. Shimizu, M. Inoue, M. Kikuchi, Y. Kobayashi, S. Tano. Nucl. Instr. And Meth. B 129 (1997) 42-48.

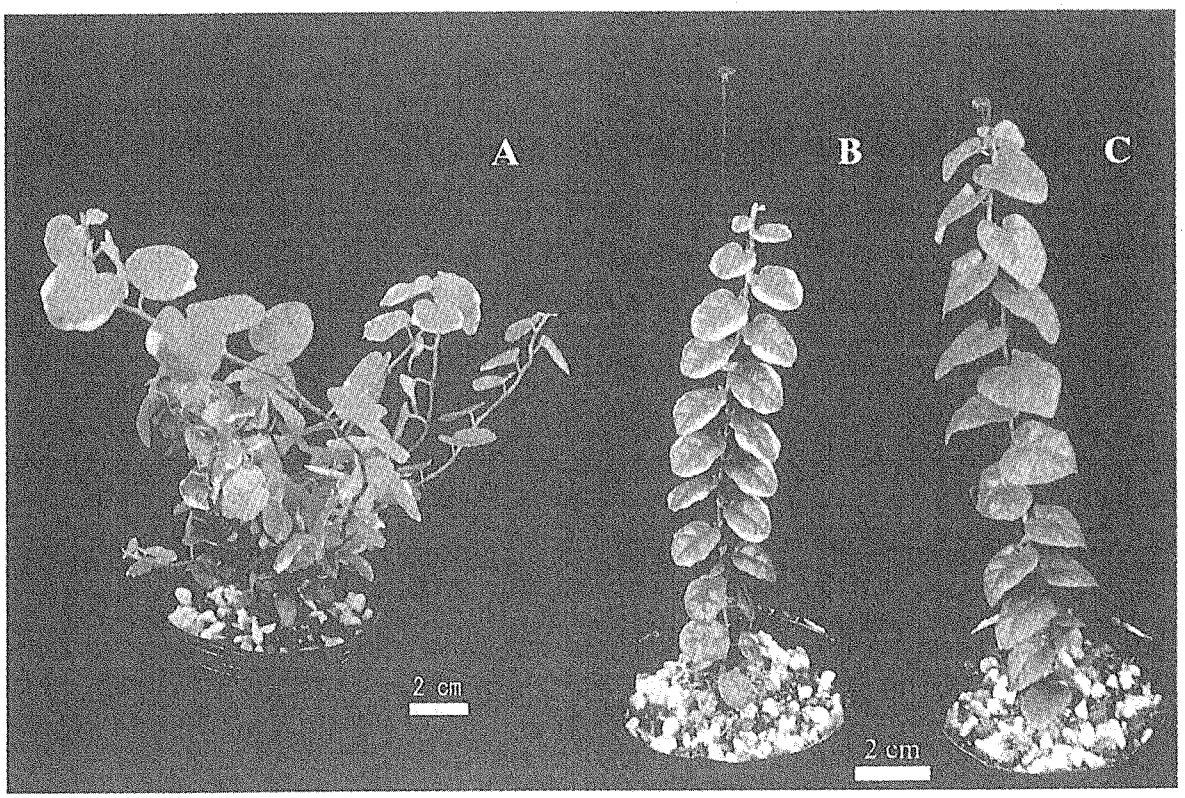

Figure 1. Regenerated plants of *Ficus thunbergii* with variegated leaves that were obtained from irradiated explants (A and B) and a regeneranted plant from non-irradiated explants (C).

2.15 Effect of ion beam irradiation on the growth of netted melon (*Cucumis melo L.*)

H. Yamada*, M.Taneishi*, H. Katai*, H. Otsuka*,
Y. Hase**, N. Shikazono**, and A. Tanaka**
Shizuoka Agricultural Experiment Station*
Department of Ion-beam-applied Biology, JAERI**

1. Introduction

Netted melon (*Cucumis melo L.*) is cultivated as an important fruit in Shizuoka prefecture. As ion beams have higher LET(Linear Energy Transfer) and deposit their energies quite locally, it is considered to be an efficient mutagenic agent applicable to mutation breeding of melon. We started to the mutation breeding of melon in 2000, and melon seeds were irradiated with several doses of carbon ion beam[1)2)].

In this paper, we reported the several mutants which occurred as chlorophyll mutation and others, and the selection of superior plants that had good fruit-net formation and texture of flesh.

2. Materials and Methods

Seeds of melon cultivar `Earls Favorite Kenon Fuyu2' were irradiated with 220MeV carbon ion beam (20 to 70Gy) generated from TIARA AVF cyclotron in JAERI.

M2 seeds obtained by selfing of M1 plants were germinated in a greenhouse. After 10 to 24 days, when the germination rate was over 80%, the frequency of chlorophyll mutation was investigated.

A total of sixteen M2 lines which were irradiated with 0 to 70Gy carbon ion beam were cultured in a heating greenhouse at least 20 ℃ . Several mutants appeared and they were investigated.

3. Results and Discussion

Frequencies of chlorophyll mutation of M2 lines that were irradiated with 0, 20, and 40Gy carbon ion beam were shown in Table 1. There were more mutants in 40Gy than 20Gy, and the maximum frequency was 1.0%. Melon has two kinds of flowers, one is a bisexual flower and the other is a male flower, and those positions are different. But the chlorophyll mutation appeared in M2 germination, thereby fixation of the mutations was considered to be possible in melon.

Table 1 The influence of carbon ion beam dose on the frequency of chlorophyll mutation in M2 generation

Dose (Gy)	No. of lines investigated[1)]	No. of lines chrolophyll mutation	Percent of chrolophyll mutation (%)
0	20	0	0
20	180	1	0.6
40	206	2	1.0

1) When the germination rate was over 80%, the frequency of chlorophyll mutation was investigated.

Other several mutations appeared in M2 lines and typical ones were as follow.

(1) Parachute-like leaves

Because leaf margin didn't elongate normally, the plants which leaf shape changed like parachute appeared. This variation appeared in two lines of 40Gy irradiation, and each number was one, respectively.

(2) Delayed growth

There were three plants which growth were delay in one of 70Gy irradiation lines. These plants showed very slow growth at least the harvest time for normal plants.

(3) Pollen sterility

There was a plant that had incomplete pollen fertility in 70Gy irradiation lines. The pollen fertility of this plant was 58%, while normal one

was 90%. Therefore the fruit of this plant didn't develop and dropped finally.

(4) Stop of fruit enlargement

The plants which fruit didn't enlarge appeared. Usually, non-fertilized fruit changes into yellow, and finally drops. But the fruit of this plant was not yellowing up to one month. And it neither enlarged nor dropped until 50 days(Fig. 1).

The fruit characters of selected lines were shown in Table 2. In investigated lines, there were not only plants that showed abnormal growth, but plants which had superior fruit character. A total of 38 plants were selected mainly because of their good fruit-net formation and good texture of flesh(Fig. 2).

Refernces
1) H. Katai, et al., TIARA Annual Report 2000, (2001) 40-41
2) M. Taneishi, et al., TIARA Annual Report 2001,(2002) 60-61

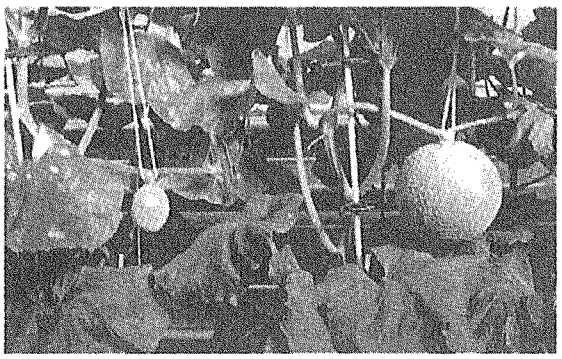

Fig 1 Plant of stopping fruit enlargement
Left: variation plant Right: normal plant

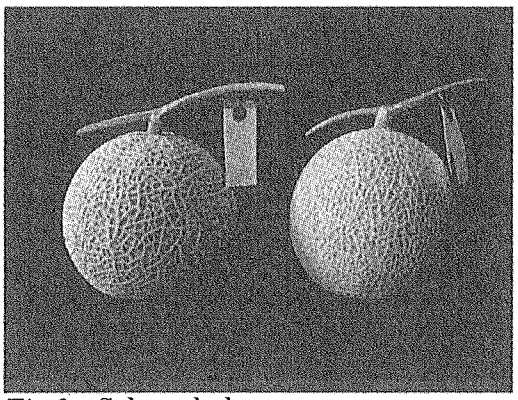

Fig 2 Selected plant
Left: original plant Right: selected plant

Table 2 Fruit characters of selected lines

Line[1)]	Dose (Gy)	Fruit weight (g)	Fruit-net Index[2)]	Flesh width (mm)	Brix (%)	Texture index of flesh [3)]	No. of selected plants
00F-549	20	884	4.3	23	14.5	5.6	2
00F-579	20	845	4.0	22	14.6	5.3	3
00F-590	20	916	4.8	25	14.9	5.4	5
00F-616	20	880	4.5	24	15.3	5.3	2
00A-03	40	1197	3.0	28	12.8	4.7	1
00A-04	40	837	3.4	24	14.4	4.8	1
00A-05	40	1017	3.9	26	14.6	5.4	1
00A-07	40	1002	3.0	25	14.2	4.9	1
00A-08	50	1072	3.1	26	14.1	5.1	2
00A-10	50	985	3.8	25	14.5	5.1	0
00A-13	50	1132	3.3	27	15.0	5.9	2
00A-14	50	958	4.1	25	15.1	5.3	2
00A-15	60	1047	3.7	26	13.9	5.0	1
00A-16	60	972	3.8	24	14.2	4.4	3
00A-17	60	1086	3.9	27	15.4	5.6	4
00A-19	60	1068	3.1	26	15.3	5.5	1
00A-22	70	1049	3.1	25	14.1	4.8	2
00A-25	70	1045	3.8	27	14.8	5.5	1
00A-26	70	990	3.0	26	11.1	5.5	2
00A-28	70	1096	2.6	26	13.9	4.8	2
Kenon fuyu 2	–	1102	3.6	27	14.8	5.6	–

1) Eight plants per each line were investigated.
2) Fruit-net index: 5(excellent)~3(normal)~1(inferior)
3) Texture index of flesh: 10(excellent)~5(normal)~1(inferior)

2.16 Mutation Induction with Ion Beam Irradiation in *Solanum toxicarium*

N. Matsuzoe*, T. Umeda*, Y. Hase** and A. Tanaka**
Faculty of Environmental and Symbiotic Sciences, Prefectural University of Kumamoto*
Department of Ion-beam-applied Biology, JAERI**

Introduction

Solanum toxicarium Lam. has high resistance to the soil-born disease and the rootknoto nematode[1,2]. *Solanum toxicarium* can be used for the rootstock of the tomato because the fruit quantity and quality of the tomatoes grafted on *S. toxicarium* are the same as those of non-grafted tomatoes under the condition of higher soil temperature and more fertilizers than non-grafted tomatoes[3]. On the other hand, it is a problem to use *S. toxicarium* for the rootstock because of it sharp prickles on the stems and the leaves (Fig.1).

Thus we are trying to obtain the individual of *S. toxicarium* without prickles by the ion beam irradiation. In this paper, we describe effects of the ion beam irradiation on germination rate, survival rate and morphological change of *S. toxicarium*.

Materials and Methods

Dry seeds of *Solanum toxicarium* in this experiment were irradiated with 220 MeV carbon ($^{12}C^{5+}$) ion beams from the TIARA AVF cyclotron (JAERI, Takasaki). From the previous result[4], we decided that the irradiation dosage ranged from 25 - 75 Gy. After the irradiation, dry seeds were surface-sterilized with 70% ethanol and 1% sodium hypochlorite solution and washed three times in sterile water. They were put to grow in MS medium with 6% sucrose and 0.8% agar in incubator at the 12h/12h 23/28℃ cycle. Only the germinated plants in MS medium were cultured in the glasshouse for getting the M2 plants. Then, the morphological change and the survival rates of the seedlings were investigated.

Results and Discussion

In *Solanum toxicarium*, the germination rates of the seeds irradiated with ion beam irradiation (220 MeV $^{12}C^{5+}$) were 91% with 25 Gy, 88 % with 50 Gy, and 58% with 75 Gy, the rates decreased at 75 Gy rapidly. The survival rates of them were 90-100% (Table 1). After transplanting the plants in the glasshouse, almost all plants with 25 Gy have grown as vigorously as with 0 Gy. In the irradiations with 50 Gy and 75 Gy, a few individuals of them showed abnormal growths, such as slow growth, plants with shrinking leaves and variegated leaves, respectively (Fig. 2).

These results show that the best dose to obtain mutant of *S. toxicarium* is the vicinity of 25Gy with 220 MeV carbon ($^{12}C^{5+}$) ion beam.

References

1) N. Matsuzoe, H. Okubo and K. Fujieda, J.Japan. Soc. Hort. Sci.61, 865-872 (1993)
2) M. Ali, N. Matsuzoe, H. Okubo and K. Fujieda, J. Japan. Soc. Hort. Sci. 60, 921-926 (1992)

3) N. Matsuzoe, H. Nakamura, H. Okubo and. fujieda, J. Japan. Soc Hort. Sci. 61, 847-855 (1993)
4) N. Matsuzoe, T. Umeda, Y. Hase and A. Tanaka, TIARA Annual Report 2001. 62-63 (2002)

Fig.1 *Solanum toxicarium* used to the experiment

Table 1. Effect of carbon ion beam on the germination and the survival rates of *Solanum toxicarium*

Dose (Gy)	Germination rate (%)	Survival rate (%)
25	91	100
50	88	90
75	58	96

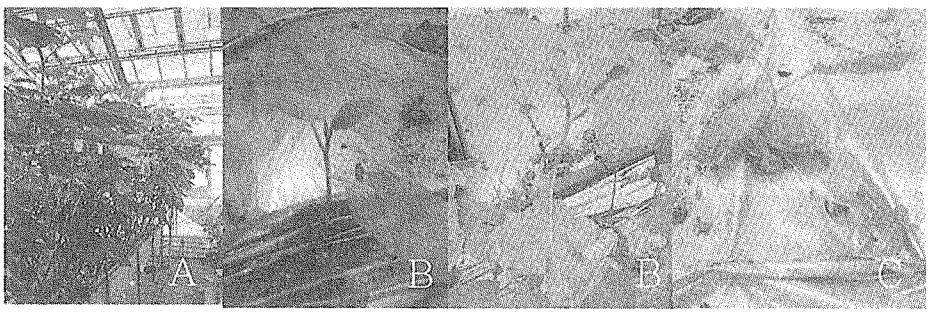

Fig. 2 Effect of carbon ion beam on growth of *Solanum toxicarium*
Irradiation dose :25Gy(A), 50Gy(B) and 75Gy(C)

2.17 Induction of Variegation in Rice Chlorophyl Mutants at M1 by Carbon Ion Beam Irradiation

M. Maekawa*, Y. Hase **, N. Shikazono** and A. Tanaka **
Research Institute for Bioresources, Okayama University*,
Department of Ion-Beam-Applied Biology, JAERI**

1. Introduction

A DNA transposable element (TE) is very useful for gene-tagging in several plant species and maize *Ac/Ds* or *En/Spm* has been utilized for gene-tagging in heterologous plants[1),2)]. Since so far, any class II type active TEs have not been discovered in rice, *Ac/Ds* system in maize was introduced into rice and was tried to be applied for gene-tagging in rice[3)]. If an endogenous active TE were discovered in rice, it could be used easily as a powerful tool for gene-tagging in open environments. As *En/Spm* was discovered in a population of maize exposed to atomic bomb at Bikini[4)] and inactive *Mu* in maize was reactivated by gamma-ray irradiation[5)], it is possible that an active TE may be induced in mutagenized rice. As ion beams are a type of high linear energy transfer (LET) radiation and can deposit high energy on a target compared to low LET radiations such as gamma rays, the novel mutants or large DNA rearrangements are expected to be induced by ion beam irradiation[6),7)]. So, it is expected that inactive transposon may be reactivated by ion beam irradiation in rice. Maekawa[8)] found a variegated yellow leaf (yl-v) mutant in F2 of a cross between distantly related rice varieties. Through the genetic analysis, the yellow leaf character was controlled by a nuclear recessive gene. This mutant was also found to segregate stable yellow leaf (yl-stb) plants and revertants[9)]. This result suggested that the variegation of the yellow leaf mutant might be caused by a class II autonomous element and the stable phenotype was strongly suggested to be caused by defective type of the element. Although a near isogenic line (NIL) for stable yellow leaf with T-65 genetic background was bred, this line did not show any variegations through generations. So, if variegation could be induced by mutation in this NIL and the variegation could be inherited together with segregation of revertants, it was strongly suggested that a cryptic inactive element was restored. Maekawa et al.[10)] obtained one variegated yl plant induced at M1 by carbon ion beam irradiation. Thus, this study aims to induce another variegated chlorophyll mutants at M1 in this stable yellow leaf mutant line with ion beams and examine spikelet fertility at M4 plants derived from one variegated plants induced by carbon ion beam irradiation.

2. Experimental procedure

Seeds of a chlorophyl mutant (referred yl) were derived from a yl-stble (stable yl) plant in T-65 yl-stb BC3F2. Ion beams used were carbon. Irradiated seeds were sterilized with 70% EtOH and sown in planters containing commercial substrate. After three weeks, presence/absence of variegations were examined because yl mutants start withering from this time.

3. Results and Discussion

Although 220 MeV carbon ion beam irradiation drastically reduces germination rates of T-65 yl-stb plants irradiated with increasing dose, the germination rates in 50 Gy or 60 Gy of 320 MeV carbon ion beams were as low as that in 50 Gy of 220 MeV (Table 1). This result

suggested that the median lethal dose with 320 MeV carbon ion might be lower than 50 Gy. In M1 plants irradiated with 220 or 320 MeV C ions, any variegated yl plants were not induced.

In 2001, out of 992 M1 plants survived after carbon ion beam irradiation, one variegated plant was obtained[10] and the clear variegation in stable *yl* plants was heritable. This results suggested that clear variegation induced by carbon ion beam irradiation at M1 plants was caused by germinal conversion of *yl* to *Yl*. This result could be explained by the possibility that *yl* phenotype is caused by non-autonomaous TE inserted into *Yl* gene and inactive autonomous TE which is located at another locus or chromosome. The gene conversion was surmized to be caused by reciprocal translocation. As shown in Table 2, all M3 lines showed partial-fertility segregated semi-fertile and high fertile plants. On the other hand, Pan 6 line fixed high fertility at M3 segregated most of partial fertile plants. Thus, the clear variegated plant induced by carbon ion beam irradiation at M1 plants segregated partial-fertile plants at M4, suggesting that ion beam irradiation induced some mutation(s) for spikelet fertility, such as reciprocal.

References

1) V. Sundaresan, V., Trends in Plant Science 1 (1996) 184-190.

2) R. Kunze, H. Saedler and W.E. Lonnig, Advances in Botanical Research 27 (1997) 331-470

3) T. Izawa, T. Ohnishi, T. Nakano, N. Ishida, H. Enoki, H. Hashimoto, K. Itoh, C. Wu, C. Miyazaki, T. Endo, S. Iida and K. Shimamoto, Plant Molecular Biology 35 (1997) 219-229.

4) P. A. Peterson, Genetics 38 (1953) 682-683.

5) V. Walbot, Molecular and General Genetics 212 (1988) 259-264.

6) A. Tanaka, Gamma Field Symposia 38 (1999) 19-28.

7) N. Shikazono, A. Tanaka, H. Watanabe and S. Tano, Genetics 157 (2001) 379-387.

8) M. . Maekawa, *In* Modification of Gene Expression and Non-Mendelian Inheritance, Oono, K. and F. Takaiwa (eds.). Natl. Inst. Agr. Res., (1995) p. 379-388.

9) M. Maekawa, K. Rikiishi, T. Matsuura and K. Noda, Japan Jpurnal of Breeding 46 (Suppl. 2) (1996) 107.(in Japanese)

10) M. Maekawa, A. Tanaka, N. Shikazono and Y. Hase, JAERI-Review 2001-039 (2001) 64-66.

Table 1. Germination rates and frequencies of variegated*yl* plants in ion beam irradiated T-65 *yl-stb* M1 plants

Radiation	Energy (MeV)	Absorbed dose(Gy)	No. of seeds sown	No. of plants germinated	Germ. rate(%)	No. of var. *yl* plants
$^{12}C^{5+}$	220	30	3362	844	25.1	0
		40	3794	807	21.3	0
		40	3754	645	17.2	0
		50	3836	184	4.8	0
		Total	11384	1636	14.4	0
$^{12}C^{6+}$	320	50	3748	196	5.2	0
		60	3753	316	8.4	0
		Total	7501	512	6.8	0
Control			100	89	89.0	0

Table 2. Segregation of spikelet fertility in M4 plants derived froma variegated-fixed *yl* plant

M4 line	Spik. fert.(%) of M3 plant	Spikelet fertility (%) #1	#2	#3	#4	#5	#6	#7	#8	#9	#10	Seg. fert.[1)]
Pan.2;yl-v-10-3	53.8(PF seg.)	75.8	82.5	89.6	88.0	13.1	17.3	3.9	50.6	1.9	97.5	PF seg.
Pan.5;yl-v-1-1	20.6(PF seg.)	97.4	39.7	42.9	89.5	99.0	80.9	23.3				PF seg.
Revertant		100.0	97.6									
Pan.6;yl-v-1-1	89.1(HF fixed)	12.8	70.0	3.7	4.3	6.3	1.0	25.8	43.0			PF seg.
Pan.8;yl-v-2-4	26.5(PF seg.)	98.6	17.2	97.6	16.5	40.7	96.1	95.5	44.4	50.0		PF seg.
Pan.9;yl-v-3-1	20.7(PF fixed)	7.4	7.7	96.8	58.7	3.0	42.3	41.9	3.1	45.2	2.7	PF seg.
Pan.9;yl-v-4-4	48.9(PF fixed)	39.0	1.6	9.3	4.4	1.2	5.3					PF fixed

1); Segregation of fertility.

PF; Partial fertlity. HF; High fertility.

2.18 *in vivo* Dissection with Ion Beam for Detection of Cis-Acting Regulatory Site for Tissue-Specific Gene Expression -in Regulatory Gene for Biosynthesis of Anthocyanin in Rice as a Model System -

M. Maekawa*, Y. Hase **, N. Shikazono** and A. Tanaka **
Research Institute for Bioresources, Okayama University*,
Department of Ion-Beam-Applied Biology, JAERI**

1. Introduction

Phenotype is carried by the expression of thousands of protein-encoding genes which is subject to complex patterns of spatial and temporal regulation[1]. Although a high-quality draft sequence for entire genome of *Arabidopsis* or rice is now available, regulatory mechanism for tissue-specific gene expression of plants still remains unknown. It is very important to reveal the regulatory mechanism for tissue-specificity of gene expression in order to activate genes properly in transgenic plants. Anthocyanin expression is visible and tissue-specific expression of anthocyanin is characteristic. So, anthocyanin is the best character for studying on tissue-specific gene expression. In rice, anthocyanin character has been studied for a long time as a visible marker. *Pl* locus which governs anthocyanin expression in rice plants consists of three alleles, Pl^j Pl^w and Pl^i. Each allele shows different tissue-specific expression. Especially, Pl^j and Pl^w are complementary and heterozygous state of Pl^j/Pl^w makes aerial parts of rice plant fully pigmented. If a given site of Pl^j or Pl^w is disrupted, fully pigmented heterozygous plant is expected to show partly-greened visibly. Then, the disrupted site of Pl^j or Pl^w is attributed to control tissue-specific expression of anthocyanin. As ion beams are a type of high linear energy transfer (LET) radiation and can deposit high energy on a target compared to low LET radiations such as gamma rays, the novel mutants or large DNA rearrangements are expected to be induced by ion beam irradiation[2),3)]. So, it is expected that ion beam irradiation is useful as a surgical knife for *in vivo* dissection. Thus, this study aims to induce partly-greened plants out of Pl^j/Pl^w M1 plants irradiated with ion beam.

2. Experimental procedure

Pl^j and Pl^w near isogenic lines with T-65 genetic background, T-65 Pl^j lg and T-65 Pl^w were used. T-65 Pl^j lg was crossed with T-65 Pl^w as pollen parents. Selfed plants which showed liguleless were discarded at seedling stage because a female parent carries a recessive gene, *lg* and F1 plants showed normal ligule. Crossed seeds of Pl^j/Pl^w were irradiated with 40 Gy and 50 Gy of 220 MeV carbon-ion beam, from an AVF cyclotron of JAERI, Takasaki, Japan. Irradiated seeds were sterilized with 70% EtOH and sown in planters containing commercial substrate. After 10 days, anthocyanin expression were examined at seedling stage and M1 plants were transplanted at a paddy field of Research Institute for Bioresources, Okayama University, Japan.

3. Results and Discussion

In this study, only carbon ion was used. Because it was reported that only carbon ion beam irradiation induced variegated plant from M1 plants[4)] and number of crossed seeds irradiated was limited. As given in Table 1, 40 Gy or 50 Gy irradiation reduced germination rates slightly. In M1 plants irradiated with 40

Gy or 50 Gy of 220 MeV C ions, partly-greened leaf plants generated as shown in Fig.1. The frequency of partly-greened leaf plants were 2.2 and 1.4 % in 40 Gy and 50 Gy irradiations, respectively. This result indicated that ion beam irradiation is effective for disruption of regulatory site of Pl^{j} or Pl^{w} gene, suggesting that ion beam irradiation is useful as a surgical knife for *in vivo* dissection. New partly-greened plants are being surveyed at the field.

References

1) C. Schwechheimer and M. Bevan, Trends in Plantr Science 3 (1998) 378-383.
2) A. Tanaka, Gamma Field Symposia 38 (1999) 19-28.
3) N. Shikazono, A. Tanaka, H. Watanabe and S. Tano, Genetics 157 (2001) 379-387.
4) M. Maekawa, Y. Hase, N. Shikazono and A. Tanaka, Nuclear Instruments Methods in Physics Research B 206 (2003) 579-585.

Table 1. Number of plants germinated and number of mutants observed in M1 of Pl/Plw F1 irradiated with $^{12}C^{5+}$

Dose	No.seeds irradiated	No.plants germinated	No. mutants
40Gy	661	589(89.1%)	13(2.2%)
50Gy	891	794(89.1%)	11(1.4%)
Cont.	10	6(6.0%)	0

Note; Observation was conducted after 10 days from seeding.

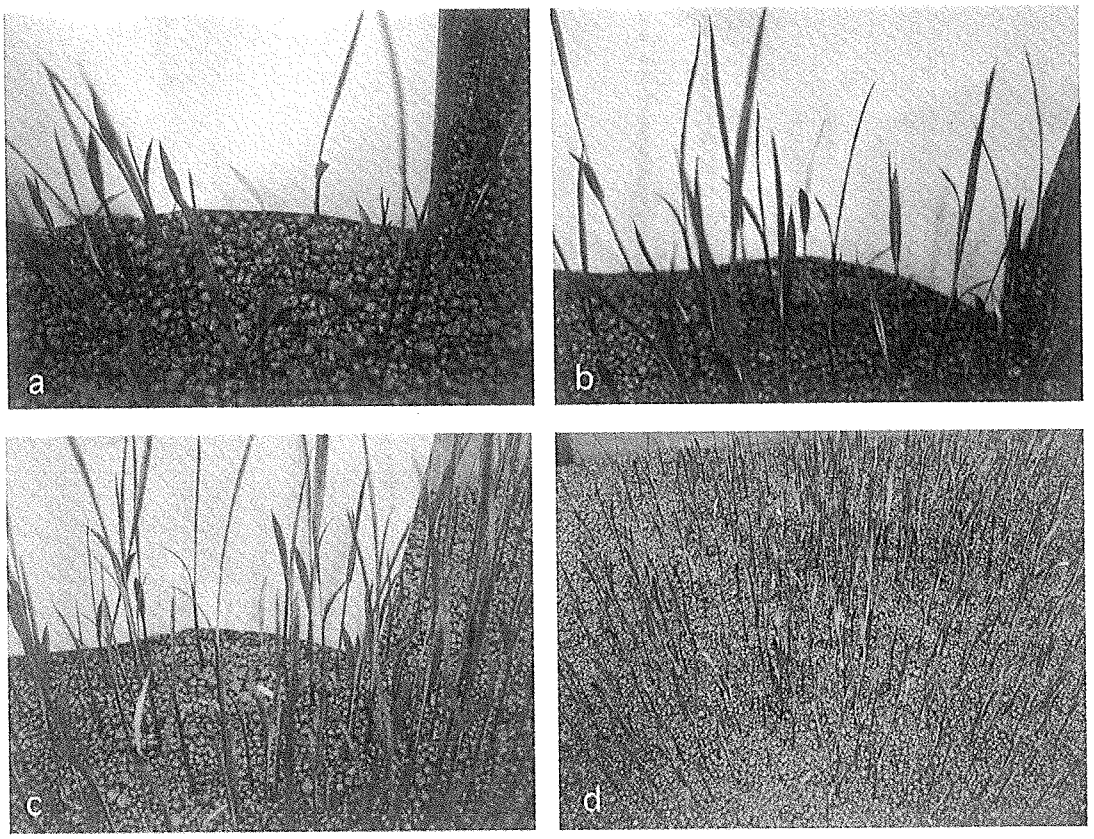

Fig.1. Mutants obtained in M1 plants of Pl/Plw F1 irradiated with carbon ion beam.
a; Green leaf plant by 40 Gy irradiation. b and C; Green leaf mutants by 50 Gy irradiation. d; M1 plants by 50 Gy irradiation.

2.19 Studies on flower color and morphological mutations from chrysanthemum in vitro explants irradiated with ion beams

T.Sato*, Y.Torigoe*, Y.Hase** and A. Tanaka**
Akita prefecture Agricultural experiment station.*
Department of Ion-beam-applied Biology, JAERI**

1. Introduction

Chrysanthemum is important flower in Akita prefecture. Especially chrysanthemum cultivar "Natsuyasumi" (purpulish red flower) is suited for the climate of Akita prefecture. However, producer, market and consumer were demanded for yellow or white color cultivar.

Ion beam is expected as a new and efficient mutagen for plant mutation breeding. In flower color of chrysanthemum, it has been reported that mutants were regenerated from in vitro explants irradiated with ion beam[1].

Last year, we examined an adequate dose of a "Natsuyasumi" flower culture materials. In this paper, we irradiated ion beams to node culture of a "Natsuyasumi" and evaluate a reasonable dose of radiation. In addition, we investigated flower color of regenerated plants which were irradiated with ion beam.

2. Materials and Methods

2.1 Effect of ion beam on plant regeneration from node

Using a chrysanthemum cultivar "Natsuyasumi" the explants of node of the intact plants on medium in petri dish were irradiated with $^{12}C^{6+}$ ion beam from the TIARA AVF cyclotron in JAERI. The energy of $^{12}C^{6+}$ was 320MeV.

After the irradiation, the cultured materials were transferred to a new medium. One month after, we investigated plant regeneration rate.

2.2 Selection of flower Color mutants

In this experiment, we used the regenerated plants. These obtained from chrysanthemum petal culture material which irradiated an ion beam. After acclimation, we transplantated regeneration pants to field. In flowering time, we selected flower color mutant.

3. Results and Discussion

3.1 Effect of ion beam on plant regeneration from nodes

In case of $^{12}C^{6+}$, the irradiation with the dose of 5Gy influenced plant regeneration (Fig.1). LD_{50} of regeneration was about 15Gy. At more than 30Gy, plant regeneration was not observed.

Therefore, we adopted 15Gy as adequate dosage.

3.2 Selection of flower color mutants

We reported that white flower color mutant was obtained with 50Gy by soft X ray irradiation [2,3]. In this experiment, white flower color mutants were obtained with 20Gy $^{12}C^{6+}$ ion beam irradiation (Fig.2). Compared with soft X ray, these ion beam induced mutants were rather

white. However, some red remained at the center and the edge of a flower. Therefore, this white flower color mutant plants are not a goal. In the near future, we will use these for further mutations.

References

1) S.Nagatomi, A.Tanaka, A.Kato, H.Watanabe and S.Tano, TIARA Annual Report (1995) 50-52.
2) T.Sato, Annual of Akita prefecture Agricultural experiment station (2002) in press.
3) T.Sato, H.Naganoma, Y.Hase and A.Tanaka, JAERI-Review 2002-035 (2002) 68-69.

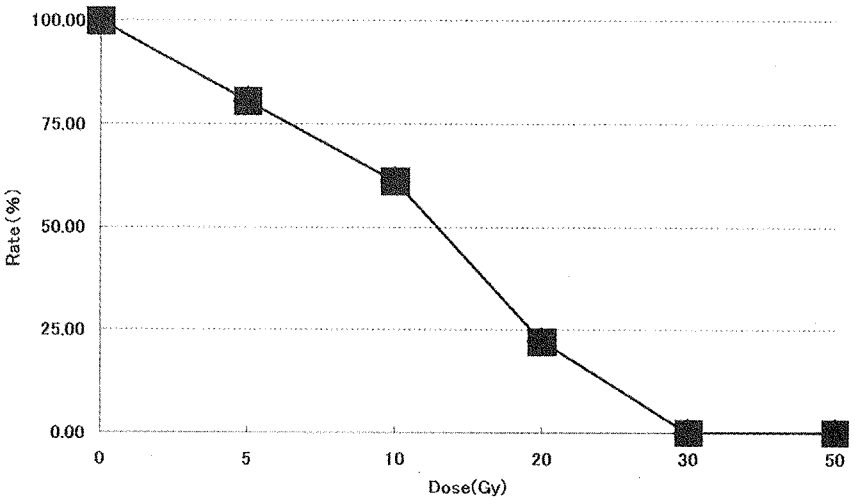

Fig.1 Effect of $^{12}C^{6+}$ ion beam on plant regeneration from node.

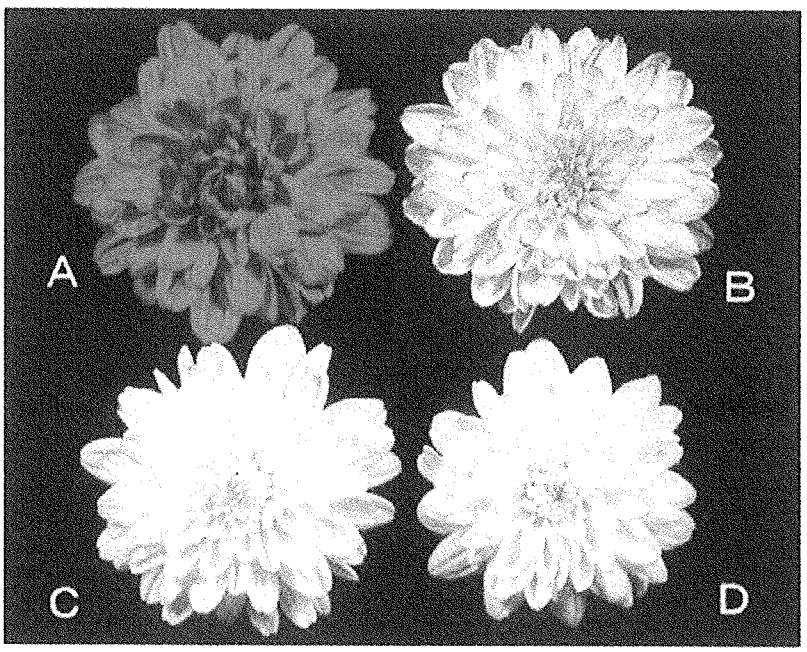

Fig.2 White flower color mutants.
A : "Natsuyasumi" (Control) B : Soft X ray, 50Gy (regenerated from node)
C and D : $^{12}C^{6+}$ ion beam, 20Gy (regenerated from petal)

2.20 Induction of mutation by the ion beam irradiation to the calli of Japanese bunching onion (*Allium fistulosum L.*)

M. Kondo*, Y. Hoshi*, H. Kobayashi*, Y. Hase**, N. Shikazono**, A. Tanaka**

Niigata Agricultural Resarch Institute Biotechnology Division*

Department of Ion-beam-applied Biology, JAERI**

1. Introduction

Japanese bunching onion (*Allium fistulosum L.*) is main vegetable alliums in Japan as well as garlic, onion, etc. In recent years, import of too cheap Japanese bunching onion from China increased rapidly. That has been interfering with Japanese bunching onion market in Japan, and we are forced to take prompt measures to deal with the problem. The flower-bud formation of Japanese bunching onion is induced by encountering low temperature and short-day in winter. And, the bolting and the blooming are induced by encountering high temperature during spring. The bolting lowers the market value of Japanese bunching onion, because the flower stalk is not only too hard to eat but also ruin the appearance. Therefore, a mutant variety of Japanese bunching onion that bolts at late time or does not bolt is profitable for the producers.

Ion beam irradiation is suitable for improving only one property like the bolting-time of Japanese bunching onion because ion beams have higher Linear Energy Transfer (LET), compared to those of X-rays and gamma-rays. And, it has been reported that chimeric plants hardly regenerated from calli after induction of mutation[1]. Therefore, we adopted the calli of Japanese bunching onion as the material for the ion-beam irradiation and regenerated plants from the calli to obtain late- or non-bolting mutants.

2. Materials and Methods

2.1 Plant material

The calli were induced from the seed of Japanese bunching onion cultivar "Tokyo natsuguro nigou".

2.2 Crashing of calli and irradiation

The penetration range of 320 MeV $^{12}C^{6+}$ beam from an AVF cyclotron (JAERI) was 2.2 mm. The diameter of the induced calli was about 10.0 mm or more. Therefore, we crushed the calli to about 1.0 mm diameter by squashing on stainless steel sieves of 0.98 mm mesh (the mesh size of 20 or less) and filtration through them. The crushed calli were covered with sterilized Kapton film (7.5 μm in thickness, 45 mm square in size, Toray-Dupon, Japan), and exposed at a total doses of 0 Gy - 10 Gy of 320 MeV $^{12}C^{6+}$ beams from the AVF cyclotron. The exposed calli were transferred to liquid culture medium and cultivated.

2.3 Determination of appropriate dose

After the ion-beam exposure, the volume of the calli were measured every 7 days.

The 20 calli exposed to 0 Gy and 0.5

Gy of $^{12}C^{6+}$ were transferred to regeneration medium after 21 days from the exposure, and cultured under 16 hr light/8 hr dark at 25°C. After 2 months of the culture on regeneration medium, the number of the calli, which regenerated adventitious buds, were counted.

3. Result and discussion

3.1 Crashing of calli

All calli that were crushed and exposed to 5 Gy and 10 Gy of 320 MeV $^{12}C^{6+}$ beams turned dark brown at 21 days after the exposure. It was noteworthy that the volume of the calli exposed to 10 Gy did not increased between 14 and 21 days after the exposure (Fig. 1). This result indicated that all cells of calli died after the exposure of 10 Gy of $^{12}C^{6+}$ or were at least affected by the exposure. This fact suggested that the thickness of crushed calli were shorter than the penetration range of $^{12}C^{6+}$ beam.

3.2 Determination of appropriate dose for mutation induction

The doses that slightly lowered the increase rate of the volume of calli were 0.5 and 1.0 Gy (Fig. 1). The dose of 0.5 Gy had little effect on the number of the calli that regenerated adventitious buds (Fig. 2). We assumed from these results that the dose of 0.5 Gy of $^{12}C^{6+}$ was appropriate for obtaining mutants, which changed a single property.

At present, the ion beam irradiation, regeneration, acclimatization and planting to a field are in progress to select late- or non-bolting mutants of Japanese bunching onion.

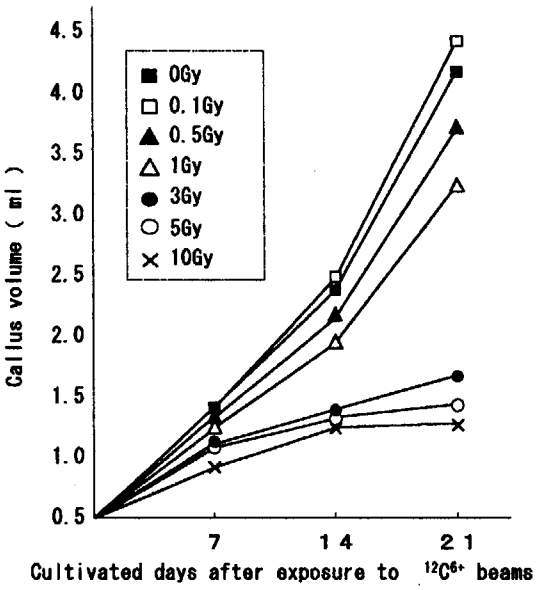

Fig.1 Effects of ion beam exposure on the growth of calli. Values represent the means of 5 calli.

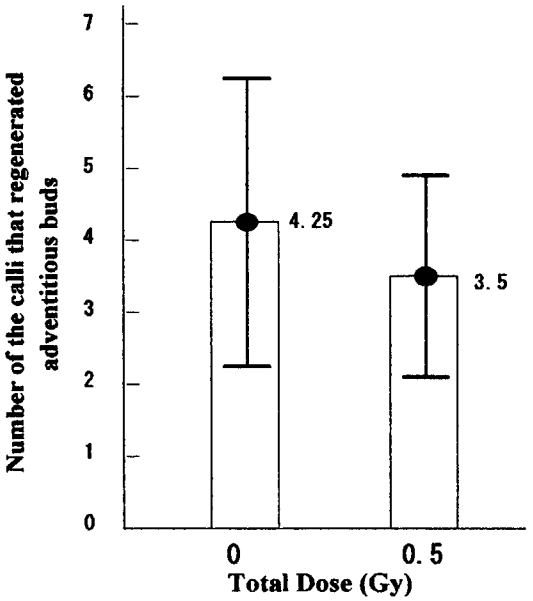

Fig.2 Effects of ion beam exposure on the regeneration of calli. It is the number of the calli that regenerated adventitious buds 2 months after transferred to regeneration medium. Values represent the means of 20 calli. Error bars are standerd deviations.

References

1)S. Nagatomi, E. Miyahira and K. Degi, Gamma Field Symposia, 35 (1996) 51-69.

2.21 Biological Effects of Carbon ion on Rice (*Oryza sativa* L.)

J. Hidema*, M. Yamamoto*, T. Kumagai*, Y. Hase**, A. Sakamoto** and A. Tanaka**
Graduate School of Life Sciences, Tohoku University*
Department of Ion-beam-applied Biology, JAERI**

1. Introduction

The increasing global trend of solar UV-B radiation (290-320 nm) has been confirmed in response to stratospheric ozone loss in mid-latitude Japan[1], in New Zealand in the 1990s[2] and at high and mid-latitudes in both hemispheres[3]. UV-B radiation can damage plants, decreasing growth and productivity[4], [5]. Over a five-year period, we investigated the effects of supplementary UV-B radiation on the growth and yield of Japanese rice cultivars in the field in a cool rice-growing region of Japan[6]. The findings of that study indicated that supplementary UV-B radiation has inhibitory effects on the growth and grain development of rice. Furthermore, we investigated the sensitivity to UV-B radiation of rice cultivars of 5 Asian rice ecotypes, and found that (1) rice cultivars vary widely in UV-B sensitivity[7], (2) among the Japanese rice cultivars, Sasanishiki exhibited resistance to UV-B radiation, while Norin 1 was less resistant, although these cultivars are closely related[8], [9].

To date, we found that (1) two or more genes controlled the difference of sensitivity to UV-B between these rice cultivars[10], (2) putative quantitative trait loci (QTL) associated with the resistance to supplementary UV-B radiation in rice were detected on chromosomes 1, 3 and 10 at least[11], (3) Cyclobutane pyrimidine dimer (CPD), which is major DNA damages induced by UV-B, photolyase may be one of the principal factors in determining the UV-B sensitivity in rice cultivars[12]. However, it is unclear the origin of the differences in UV-B sensitivity among rice cultivars.

The aim of our study is to clarify the molecular origin of the sensitivity to UV-B for improving UV-B resistance in plants by bioengineering or breeding programs. In order to make it, identifying rice mutants with increased or decreased UV-B resistance can help our study powerfully. Heavy ion beams, such as carbon ions, are more effective in plants for inducing mutations compared with electron beam (Shikazono et al. unpublished data). Novel mutants have been obtained by the carbon ion irradiation in several plant species[13]. In this study, we investigated the optimum radiation dosage for producing UV-B hyper-resistant or hypersensitive rice mutants induced by carbon ion irradiation.

2. Experimental procedure

2.1 Plant material and irradiation method

Dry rice seeds of Sasanishiki (*Oryza sativa* L.) were used. About 150 seeds were placed upward embryo on petri dish. The Irradiation Apparatus for Seed, connected to a vertical beam line of the AVF-cyclotron (JAERI, Takasaki), was used for the 320 MeV carbon-ion irradiation. The carbon-ion irradiation with the doses of 20, 40, 60, 80, 100, 120, 140, 160, 180 and 200 Gy were performed under atmospheric pressure within 3 min. At least three independent experiments at different doses of irradiation were performed.

2.2 Growth condition, and measurements of germination rate, survival rate, growth rate and ripening rate

After irradiation, 100 seeds in each lot were placed on wet paper-filter in a petri dish and kept at 30°C for 2 days, and then the seeds were planted in plastic-tray in fertilized soil under visible radiation in a phytotron (12-h photoperiod, day/night temperatures 27/27°C), as described in Hidema et al[14]. The germination rate was measured at 2 days

after planting in tray. The germination rate of unirradiated seeds was generally more than 95%. The survival rate was measured by counting the viable plants at 3 weeks after germination. Survival of the unirradiated seeds was greater than 95%. The growth rate (the ratio of the value for plant length of each irradiated plant to the value for plant length of unirradiated plant) was measured, when the experimental plants were grown for 30 days in a phytotron. The percentage of ripening on the main stem was measured when the experimental plants were grown for 4 months in a phytotron.

3. Results and Discussion

In order to produce a variety of rice mutants induced by carbon-ion beams ($^{12}C^{+6}$; 320 MeV) as one type of mutagen, it is quite important to investigate the effects of the carbon-ion on several biological endpoints such as germination, survival, ripening and subsequent mutations in rice, Sasanishiki cultivar (wild type). Figure 1 shows the effects of carbon-ion beams ($^{12}C^{+6}$; 320 MeV) on germination rate (Fig. 1a), survival rate (Fig. 1b), growth rate (Fig. 1c) and ripening rate (Fig. 1d) in Sasanishiki rice cultivar. The germination rates were more than 90% in the range of 0-200 Gy. A remarkable reduction in the rate at higher dose was not observed in rice. On the other hand, the survival rate marked a sharp decline by carbon-ion irradiation at doses of up to about 140 Gy. The growth rate and ripening rate gradually decreased with increasing the carbon-ion dose.

Table 1 shows the effects of carbon-ion beams on the dry mass, culm length, panicle number and percentage of ripening in rice plant. The dry mass, panicle number and percentage of ripening significantly decreased by carbon-ion irradiation at doses of up to about 80 Gy.

Significant differences in the sensitivity of rice seed to carbon ion dose were observed among relative biological effectiveness (RBE) for germination rate, survival rate, growth rate and ripening rate. The shoulder of dose-response curve for germination rate or ripening rate was 120 (Fig. 1b) or 80 Gy (Fig. 1d and Table 1), respectively. When the carbon ion dose was 120 Gy, the rate of growth or ripening was about 75 or 35%, respectively. In addition, when the carbon ion dose was 100 or 80 Gy, the rate of ripening was about 50 or 67%, respectively. These results suggested the optimum radiation dosage for inducing mutations in rice is 80-100 Gy, because the ripening rate at 120 Gy was less than 50%. Therefore, irradiation with dose of 80 or 100 Gy ($^{12}C^{+6}$; 320 MeV) will be performed for mutagenesis of rice "Sasanishiki".

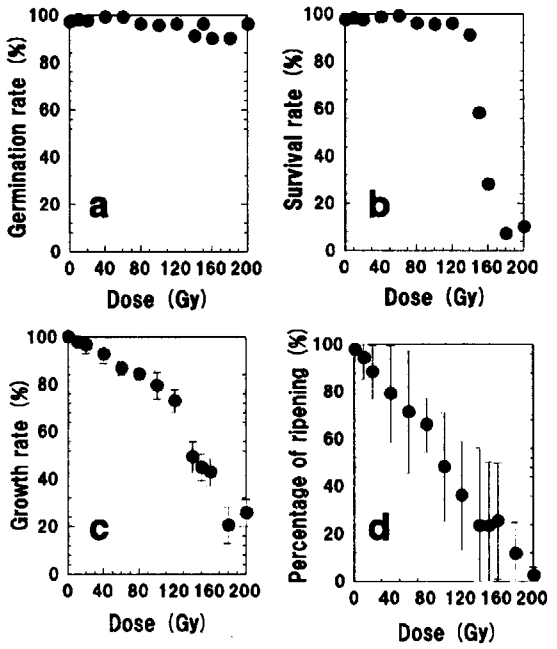

Fig. 1 Dose-response curves for germination rate (a), survival rate (b), growth rate (c) and ripening rate (d) following irradiation by carbon ion ($^{12}C^{+6}$; 320 MeV) with different dose. Points show the mean ± SD of three replication.

Acknowledgement

This work was supported by Grants-in-Aid for Scientific Research from the Ministry of Education, Culture, Sports, Science and Technology, Japan (14704060 and 15201010).

Table 1 Effects of carbon ions ($^{12}C^{+6}$) irradiation (0-120 Gy) on the dry mass, plant length, panicle number and ripening of rice (Sasanishiki).

	Doses (Gy)					
	Control	20 Gy	40 Gy	80 Gy	100 Gy	120 Gy
Dry mass (g/plant)	28.1 ± 3.2	31.1 ± 3.8 (+10.7)^{ns}	27.7 ± 3.5 (-1.4)^{ns}	26.3 ± 2.5 (-6.4)^{ns}	19.0 ± 2.8 (-32.4)**	19.6 ± 3.6 (-30.2)**
Culm length (cm)	99.3 ± 5.3	95.5 ± 3.6 (-3.8)^{ns}	98.5 ± 5.9 (-0.8)^{ns}	98.2 ± 5.1 (-11.8)^{ns}	99.6 ± 5.2 (+0.3)^{ns}	99.8 ± 8.2 (+0.5)^{ns}
Panicle number (no./plant)	12.3 ± 1.4	12.2 ± 1.0 (-0.8)^{ns}	11.4 ± 0.8 (-7.3)^{ns}	9.9 ± 1.1 (-19.5)**	9.6 ± 1.4 (-22.0)**	10.8 ± 2.3 (-12.2)*
Percentage of ripening (%)	97.8 ± 2.2	88.3 ± 11.3 (-9.8)^{ns}	79.0 ± 20.6 (-19.2)^{ns}	65.9 ± 11.3 (-32.6)*	48.2 ± 22.9 (-50.7)**	36.2 ± 22.8 (-63.0)**

* and **: The difference from the control treatment (0 Gy) was significant at P < 0.05 and P < 0.01, respectively (ANOVA).
ns: Not significant.
Numbers in parentheses: percentages showing the ratio to control.

References

1) M. Sasaki, S. Takeshita, T. Oyanagi, Y. Miyake and T. Sakata, Ortical Engineering 41 (2002) 3062-3069.
2) R. McKenzie, B. Connor and G. Bodeker, Science 285 (1999) 1709-1711.
3) S. Madronich, R. L. McKenzie, M. M. Caldwell and L. O. Bjorn, Ambio 24 (1995) 143-152.
4) A. Teramura, Physiol. Plant. 58 (1983) 415-427.
5) M. Jansen, V. Gaba and B. Greenberg, Trends Plant Sci. 3 (1998) 131-135.
6) T. Kumagai, J. Hidema, H. S. Kang and T. Sato, Agriculture, Ecosystems and Environment 83 (2001) 201-208.
7) T. Sato and T. Kumagai, Jpn. J. Breeding 43 (1993) 61-68.
8) T. Kumagai and T. Sato, Jpn. J. of Breed 42 (1992) 545-552.
9) J. Hidema, H.-S. Kang and T. Kumagai, Plant and Cell Physiology 37 (1996) 742-747.
10) T. Sato, H. S. Kang and T. Kumagai, Physiol. Plant. 91 (1994) 234-238.
11) T. Sato, T. Ueda, Y. Fukuta, T. Kumagai and M. Yano, Theor. Appl. Genet. (2003) in press
12) J. Hidema, T. Kumagai and B. M. Sutherland, Plant Cell 12 (2000) 1569-1578.
13) Y. Hase, A. Tanaka, T. Baba and H. Watanabe, Plant Journal 24 (2000) 21-32.
14) J. Hidema, T. Kumagai, J. C. Sutherland and B. M. Sutherland, Plant Physiology 113 (1997) 39-44.

2.22 Induction of Dwarf Mutation in Salvia by Ion Beam Irradiation —Effects on Survival Rates of Seeds and Axillary Buds—

M. Kato*, S.Kageyama*, T. Haketa*, M. Fukushima*,
Y. Hase** , A. Tanaka**
Takii Plant Breeding & Experiment Station*
Department of Ion-beam-applied Biology, JAERI**

1.Introduction

Ion beams have higher LET(linerar energy transfer) and bring intensive RBE(relative biological effectiveness) than γ -rays and X-rays.[1] By the irradiation with heavy ion beams, specific flower color, flower shape, and male sterile mutants were induced in several flowers.[2) 3) 4)] In several crops and vegetables, lethal chlorophyll, sex reverse mutants were induced.[5) 6)]

In this study, we investigated the effect of carbon-ion, helium-ion beam and γ -rays on survival rates of *Salvia coccinea* seeds and Axillary buds for the purpose of production of dwarf *Salvia coccinea* plant.

2.Materials and Methods

2.1 Seed Material

Seeds of *Salvia coccinea* 'Lady in Red' were used in this study. Seeds were irradiated with 320MeV carbon(C), 50MeV helium(He) ion beam and γ -rays at various doses (C-ion:10 to 200 Gy, He-ion:25 to 325 Gy, γ -ray:25 to 400 Gy).

After the irradiation, seeds were allowed to germinate under 30℃ and planted in green house. Survival rate of the irradiated seeds was determined at 60 days after germination.

2.2 Axillary Bud Material

The seed material was same as in 2.1. Seedlings that germinated on filter paper were cut at hypocotyl and roots and testa were removed. After surface sterilization with 70% ethanol and 1% sodium hypochlorite solution, they were cultured on MS(Murashige and Skoog, 1962) solid medium containing 0.1mg/l NAA, 0.1mg/l BAP, 3% sucrose at 30℃ and 12hr-photoperiod. They were subcultured and propagated with each nodal section every 4 weeks.

After three times of subculture, the nodal sections, which have two axillary buds were laid on MS solid medium in 5-cm petri dishes and irradiated with 320 MeV C-ion beam at the doses of 2 to 50 Gy. After the irradiation, they were subcultured on the same medium.

Survival rate of the axillary buds was determined at 60 days after the irradiation.

3.Results and Discussion

3.1 Seed Material

The survival curve had a shoulder. The C-ions showed the greatest effect. The shoulder doses were 125 Gy for C-ions, 200 Gy for He-ions and 225 Gy for γ -rays (Fig. 1, 2, 3). At the doses higher than half of the shoulder doses, seedlings grew unevenly (data not

shown).

From these results, we adopted 60, 80 and 100Gy as the adequate dosages for C-ion, He-ion, and γ -rays to obtain mutants efficiently.

3.2 Axillary Bud Material

In case of axillary bud material, the survival rate was gradually decreased as the dose increased (Fig.4). Uneven growth was observed higher than 5 Gy (data not shown).

We adopted 5 Gy as the adequate dosage for C-ion to obtain mutants efficiently.

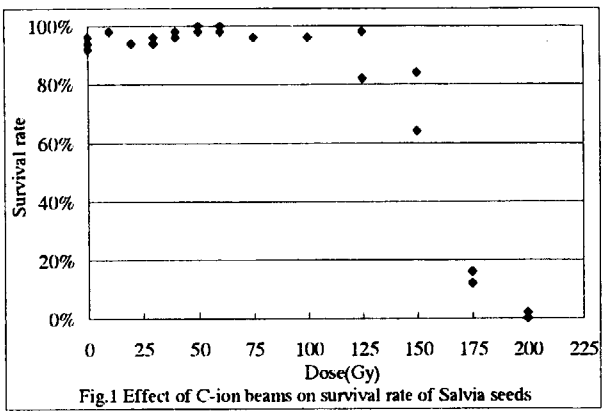

Fig.1 Effect of C-ion beams on survival rate of Salvia seeds

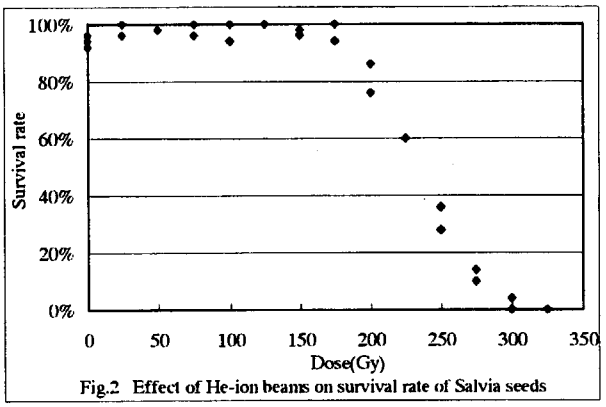

Fig.2 Effect of He-ion beams on survival rate of Salvia seeds

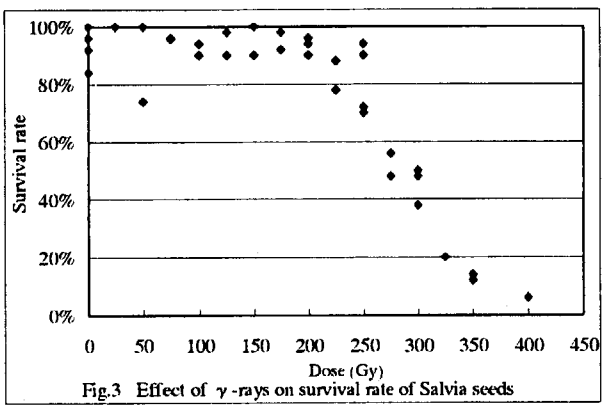

Fig.3 Effect of γ -rays on survival rate of Salvia seeds

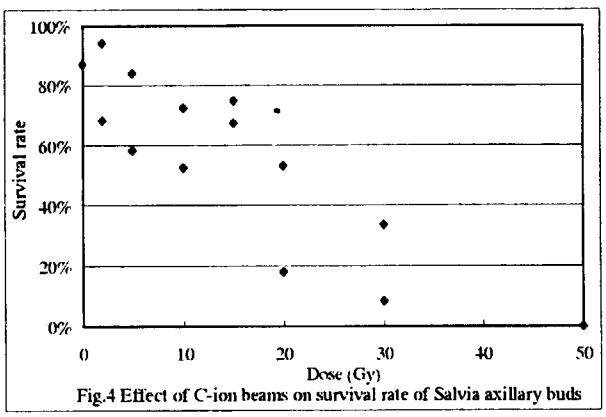

Fig.4 Effect of C-ion beams on survival rate of Salvia axillary buds

References

1) S.Nagatomi, A Tanaka, H.Watanabe and S.Tano, TIARA Annual Report 6:48-50(1997)

2) M.Okamura, M.Ohtsuka N.Yasuno, T.Hirosawa, A.Tanaka, N.Shikazono, Y.Hase and M.Tanase, JAERI-Review 2001-039(2001) 52-53

3) K.Suzuki, Y.Yomo, T.Abe, Y.Katsumoto, K.Miyazaki, S.Yoshida and T.Kusumi, RIKEN Accel.Prog.Rep. 35,129(2002)

4)H.Yamaguchi, S.Nagatomi, A.Tanaka N.Shikazono,T.Morishita and K. Degi, Jaeri-Review 2000-24(2000) 41-42

5) M.Maekawa, A.Tanaka, N.Shikazono and Y.Hase, JAERI-Review 2001-039(2001) 64-66

6) F.Komai, N.Shikazono and A.Tanaka, Plant Cell Rep. 21(2003) 713-717

2.23 Single-Hit Effects on Mammalian Cultured Cells with Heavy-Ion Microbeams (II)

Y. Kobayashi*, T. Funayama*, S. Wada*, M. Taguchi** and H. Watanabe*
Department of Ion-Beam-Applied Biology, JAERI*, Department of Material Development, JAERI**

1. Introduction

Heavy ions transfer their energy to biological organisms through high-density ionization along the particle trajectories. The population of cells exposed to a very low dose of high-LET heavy ions contains a few cells hit by a particle, while the majority of the cells receive no radiation damage. At somewhat higher doses, some of the cells receive two or more events according to the *Poisson* distribution of ion injections. This fluctuation of particle trajectories through individual cells makes interpretation of radiological effects of heavy ions difficult.

Using microbeams, we will be able to overcome this limitation by delivering a counted number of ions to each cell to study a number of important radiobiological processes in ways that cannot be achieved using conventional "broad-field" irradiation. A microbeam can be used for selective irradiation of individual cells, which can be subsequently observed to ascertain what changes occur to that cell and to neighboring un-irradiated cells. The use of microbeam allows direct investigation of cell-to-cell communications such as "bystander effects", that is, radiation effects of heavy ions transmitted from irradiated cells to neighboring un-irradiated cells. Furthermore, a microbeam with sufficient spatial resolution will be useful for analyzing the interaction of damages produced by separate events in an irradiated cell, the dynamics of cellular repair, and the intra-cellular process such as apoptosis by means of highly localized irradiation of a part of a nucleus or cytoplasm.

Therefore, we have developed an irradiation system for targeting cells individually with a precise number of high-LET heavy ions to elucidate radiobiological effects of exactly one particle[1,2].

2. Experimental procedure

The cell irradiation system has been incorporated into the high-energy heavy ion microbeam apparatus which was installed under a vertical beam line of the AVF cyclotron at the TIARA of JAERI-Takasaki.

So far, two inverted optical microscopes are in operation in our cell irradiation system. One of the microscopes is installed below the vertical beam line in the beam room as an "on-line microscope" for cell-targeting and for delivery of a certain number of heavy ions. The other microscope, which is called "off-line microscope", is used in the preparation room before and after irradiation; for cell-finding prior to the irradiation, and for cell-revisiting and observation during post-irradiation incubation, respectively. A local-area-network connects these control systems allowing the object database created at the off-line microscope to be used by the cell-targeting system. Details of the experimental procedure are shown in Fig. 1.

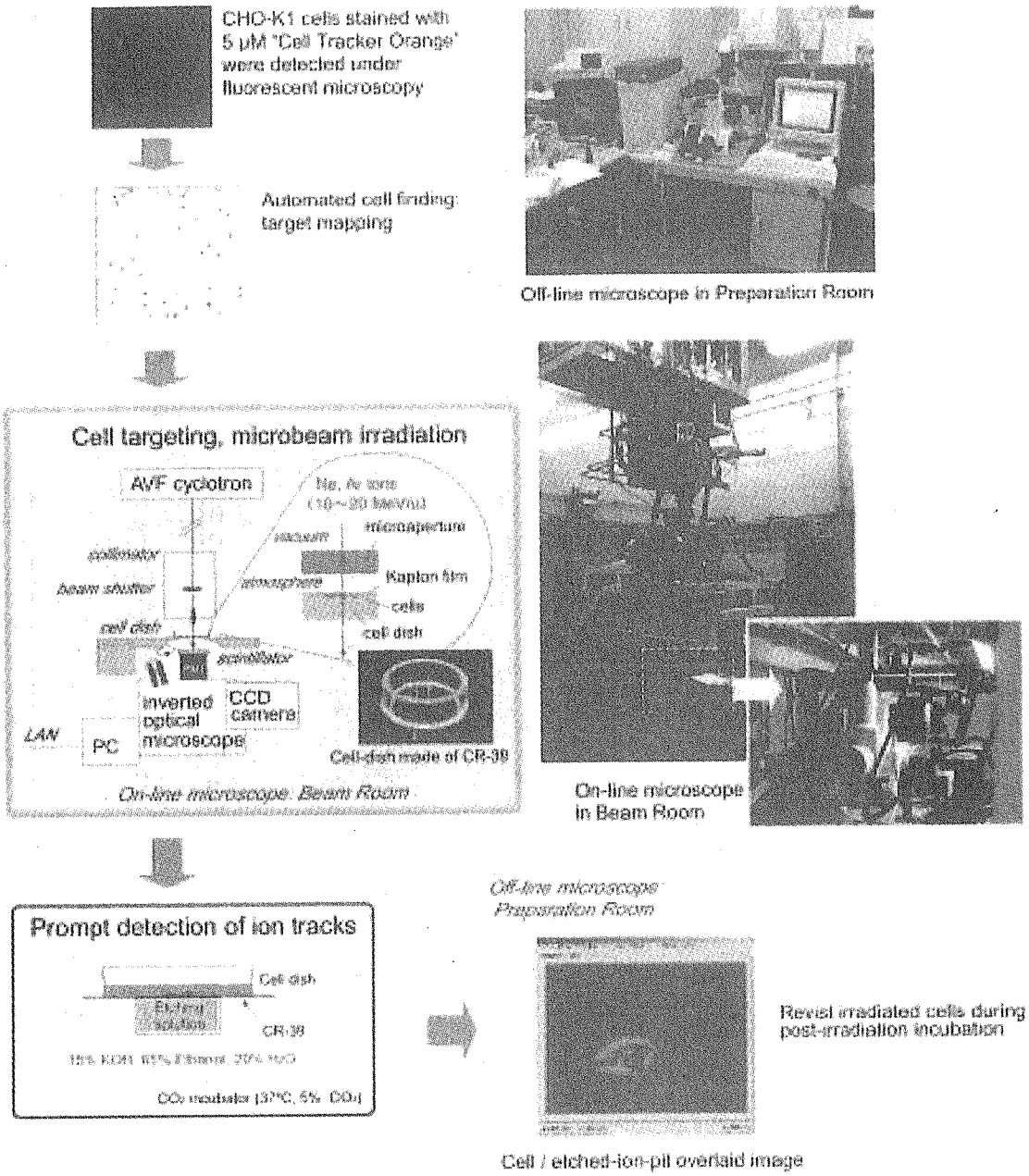

Fig. 1. Procedure of the irradiation of cultured cells with collimated heavy ion microbeam apparatus developed at JAERI-Takasaki. Before irradiation, positional data of the individual cells are obtained at the off-line microscope in the preparation room by microscopically searching the sample dish. Using the object database, targeting and irradiation at the on-line microscope are carried out quickly. Immediately after irradiation, the cell dish is refilled with medium, and then the bottom of the cell dish (100 μm-thick ion track detector CR-39) is etched from the opposite side of the cells at 37°C to detect the accurate position of ion tracks on the cells. It is possible to revisit each irradiated cell repeatedly during post-irradiation incubation according to the object database.

3. Effects of single hit of heavy ions

After irradiation of 11.5 MeV/amu $^{40}Ar^{13+}$ ions (LET=1260 keV/μm), the position and the number of ion tracks penetrating the CHO-K1 cells were detected with prompt etching of CR-39. No significant effect of the etching treatment on the cell growth was observed. The growth of the cells was observed individually at the off-line microscope at every 12 hr up to 60 hr after irradiation, by revisiting the cells according to the object database.

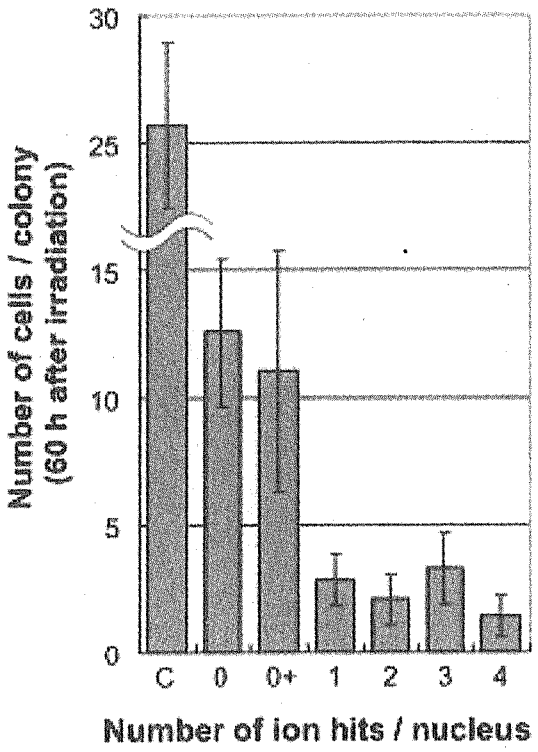

Fig. 2. Effect of targeted irradiation with counted number of 11.5 MeV/amu $^{40}Ar^{13+}$ ions on growth of CHO-K1 cells.

C: control cells in un-irradiated dish.

0: un-irradiated (bystander) cells in the irradiated dish.

0+: cells not hit on nucleus but on cytoplasm.

1-4: cells hit on nucleus with 1 to 4 ions.

In the un-irradiated control dish, average cell number in the mini-colony descended from one target cell was 26 (Fig. 2, column C). Meanwhile, the cells in the irradiated dish but not hit by the ion showed slightly limited cell growth (Fig. 2, column 0). This limited growth might be a bystander effect caused by heavy ion hit cell in the same dish.

The cells irradiated with only one Ar ion on its nucleus showed complete growth inhibition (Fig. 2, column 1). The cells that only hit on their cytoplasm also showed limited cell growth (Fig. 2, column 0+). Radiation damages on mitochondrial DNA or cellular membrane may cause this growth inhibition. Another possible explanation is the effect of delta electrons on cellular nucleus, even if the core of ion track still stands on the cytoplasmic region.

Further investigation is needed to elucidate the effect of cytoplasmic irradiation and the bystander effect. Recently, we had established a method for measuring the DNA damage induced in individual cell[3]. This method will enable us to determine the answer of above question, and also show us the quantitative relationship of the ion-hit position and the yield of induced DNA damages.

References

1) Y. Kobayashi, T. Funayama, S. Wada, M. Taguchi and H. Watanabe, *JAERI-Review* 2002-35 (2002) 74-76.

2) Y. Kobayashi, T. Funayama, S. Wada, M. Taguchi and H. Watanabe, *Nucl. Instr. And Meth.* B210, (2003) 308-311.

3) S. Wada, Y. Kobayashi, T. Funayama, M. Natsuhori, N. Ito and K. Yamamoto, *J. Radiat. Res.* 43 (2002) S153-S156.

2.24 Regeneration Mechanism of Hemopoietic Organs Following Irradiation with Heavy-Ion Beams in the Silkworm, *Bombyx mori* : Phagocytosis of Injured Cells by Invading Hemocytes

K. Kiguchi*, E. Ling*, K. Fukamoto*, K. Shirai*, R. Kanekatsu*,
Y. Kobayashi**, T. Funayama** and H. Watanabe**
Department of Applied Biology, Faculty of Textile Science and Technology,
Shinshu University*
Department of Ion-Beam-Applied Biology, JAERI**

1. Introduction

Local irradiation with heavy-ion beams, or radiosurgery, is an extremely useful tool to inactivate specific organs or tissues such as larval imaginal discs in the silkworm, *Bombyx mori* [1, 2]. For example, deletion of adult wings was induced by local irradiation of the discs at the larval stage with an appropriate dose of carbon-ions. However, we have shown previously that the hemopoietic organs can regenerate following radiosurgery, even after irradiation with 100 Gy of carbon-ions [3]. This interesting phenomenon allows us to study the possible involvement of hemopoietic stem cells in the observed regeneration of hemopoietic organs. We examined the morphological changes during the regeneration of the hemopoietic organs *in vivo* and *in vitro* after selective irradiation with heavy-ions. Our results suggest that the injured cells in irradiated organs are phagocytosed by invading hemocytes from the hemolymph, and that elimination of injured cells by phagocytosis may be the first step in regeneration.

2. Materials and Methods

Insects and ion-beam irradiation

A laboratory colony of the silkworm *pnd* p^s strain was used for the following experiments. Carbon-ion beams ($^{12}C^{+5}$, 220 MeV, 18.3 MeV/u, range in water = 1.2 mm) were generated by the AVF-cyclotron in TIARA, and the hemopoietic organs were selectively exposed to the ion beams *in vivo* or *in vitro* at a dose of 100 Gy as shown in the previous papers [2, 3].

In vitro culturing of the hemopoietic organs

To analyze the effect of irradiation under *in vitro* culture conditions, where there is no contact with circulating hemocytes, 3 hemopoietic organs were cultured in 3 ml of Grace's medium containing 10 % silkworm hemolymph (heated at 60°C for 30 min) and antimicrobial solution in each culture dish. The cultures were kept at 25°C under high humidity in air atmosphere.

Morphological observation

Dissected organs were fixed in Carnoy's medium and embedded in paraffin as usual. The sections (5 μm in thickness) were stained with Hoechst 33342 (2 μg/ml) for 10 min and imaged using a filter for blue fluorescence.

Incorporation of microbeads

A schematic of the procedure is shown in Figure 1. Larvae were injected with fluorescent microbeads (φ 1 μm) and irradiated with 100 Gy of carbon-ions. Then, irradiated organs were dissected out and stained with acridine orange (10 μg/ml). Samples were mounted in coverslip sandwiches and observed by confocal microscopy.

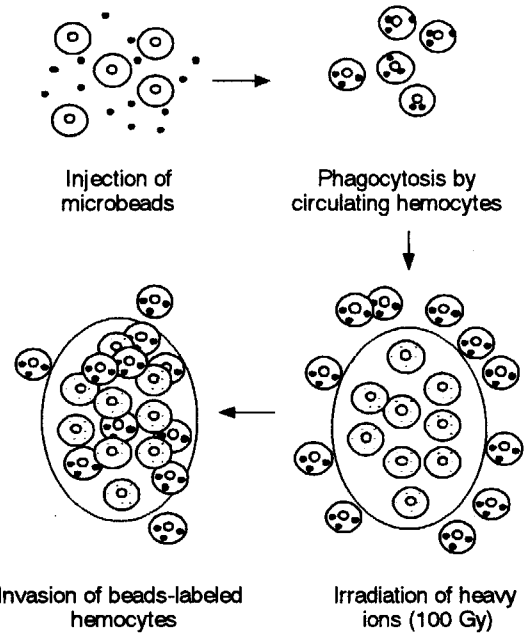

Fig. 1 Scheme of procedures demonstrating invasion of circulating hemocytes into irradiated hemopoietic organs.

3. Results and Discussion

Hemopoietic organs of 5th instar day 0 larvae were selectively irradiated with 100 Gy carbon-ions. Morphology of these organs was examined 6 days following irradiation. As shown in Figure 2, the irradiated hemopoietic organ is composed of many hemocytes which look normal in morphology (Fig.2a), similar to control organs (Fig.2b). This confirmed our previous finding that regeneration occurs in the hemopoietic organs after the irradiation of 100 Gy carbon-ions [3]. Next, dissected hemopoietic organs were irradiated with carbon ions *in vitro* and cultured in Grace's medium for 3 or 6 days. Under our *in vitro* culture conditions, the control organs showed actively proliferating features (Fig.2d). However, the irradiated hemopoietic organ appears to be filled with many small fragments and abnormal, irregular cells (Fig.2c), indicating that the irradiated organs cannot regenerate under *in vitro* condition. We then investigated the possibility that the circulating hemocytes may invade the irradiated organs to phagocytose the injured cells. Following the procedure shown in Figure 1, localization of the injected microbeads was traced using confocal microscopy. The beads were first incorporated into the circulating hemocytes (granular cells). Following irradiation, optical sectioning of the irradiated hemopoietic organs demonstrates that the beads are now localized inside the organs (Fig.3).

These observations, together with our previous observations by electron microscope [2], strongly suggest that the first step for regeneration of irradiated hemopoietic organs is the elimination of injured cells from the organs by phagocytosis by invading hemocytes. Subsequent studies will focus on the origin and fate of the hemopoietic stem cells during regeneration using a transgenic strain of the silkworm.

References

1) Tu Z.-L., Yamasaki S., Shirai K., Kanekatus R., Kiguchi K., Kobayashi Y., Taguchi M., and Watanabe H. (1999a) Effects of general and local irradiation of heavy ion microbeams on the development and morphogenesis of the silkworm, *Bombyx mori*, *J. Seric. Sci. Jpn.*, **68**(6), 443-453

2) Tu Z.-L., Shirai K., Kanekatsu R., Kiguchi K., Kobayashi Y., Taguchi M., and Watanabe H. (1999b) Effects of local heavy ion beam irradiation on the hemopoietic organs of the silkworm, *Bombyx mori*, *J. Seric. Sci. Jpn.*, **68**(6), 491-500

3) Ling, E. , Fukamoto K., Xu S., Shirai K., Kanekatsu R., Kobayashi Y., Tu Z.-L., Funayama T., Watanabe H., and Kiguchi K. (2003) Regeneration of hemopoietic organs in the silkworm, *Bombyx mori*, after locally targeted irradiation with heavy ion beams, *J. Insect Biotechnol. Sericol.*, **72**(2), 95-100

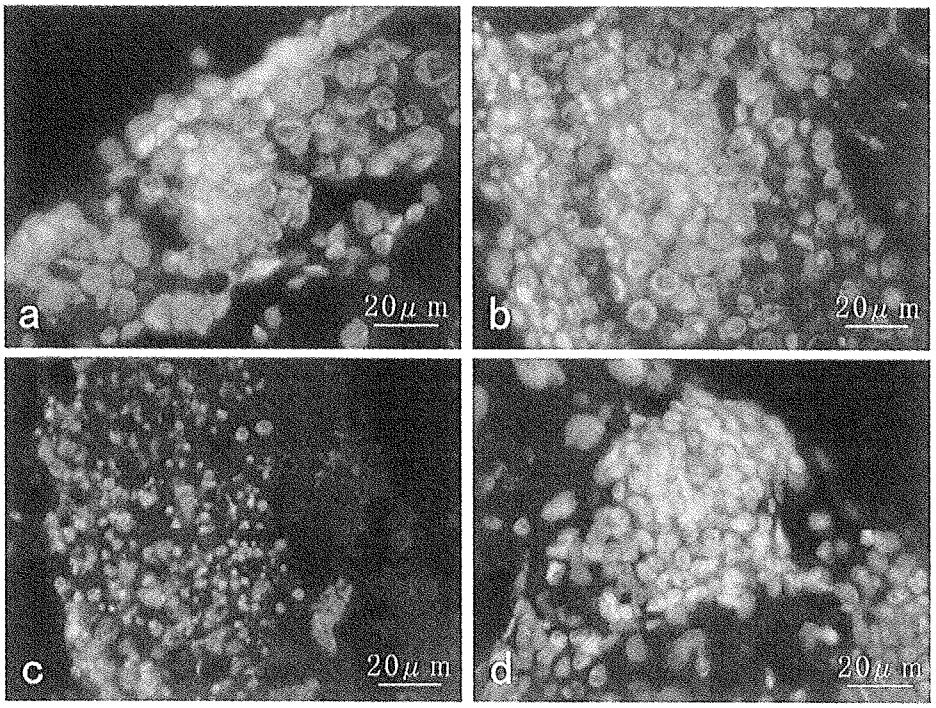

Fig. 2 Paraffin sections of hemopoietic organs irradiated with carbon-ions (stained with Hoechst 33342)

a: Reared on an artificial diet for 6 days after *in vivo* irradiation

b: Reared on an artificial diet for 6 days without irradiation (control)

c: Cultured in Grace's medium for 6 days after *in vitro* irradiation

d: Cultured in Grace's medium for 6 days without irradiation (control)

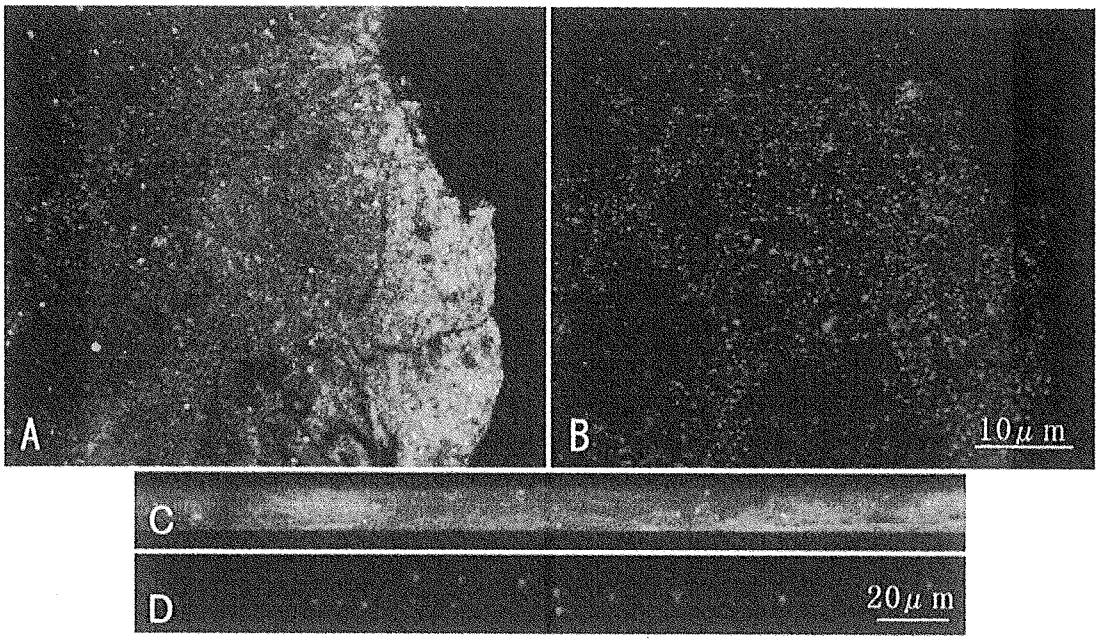

Fig. 3 Optical sections of the irradiated hemopoietic organs

A, B: Scanned approximately 24 μm below the surface in a XY direction

C, D: Scanned approximately 18 μm below the surface in a XZ direction

Beads are localized inside the irradiated hemopoietic organ, indicating that the circulating hemocytes invade into the organ to phagocytose the injured cells.

2.25 Bystander Effect in Confluent Human Fibroblasts Induced by High-LET Particles

Y. Furusawa*, C. Shao*,$, Y. Kobayashi**, T. Funayama**, and S. Wada**
Heavy-Ion Radiobiology Research Group, NIRS*, Department of Ion-beam-applied Biology, JAERI**, Gray Cancer Institute, UK$

1. Introduction

It has been commonly accepted for a long time that damage to DNA, either by direct ionization or by the production of reactive free radicals in water molecules, is required to induce heritable damage in cells. However, considerable evidence has recently been accumulated in support of the existence of a "bystander effect", which cells having received no irradiation show biological consequences from their neighboring irradiated cells. This phenomenon was first reported[1] by Nagasawa et al., then demonstrated by others with various biological endpoints including our results[2]. This suggests that reconsideration may be needed of the current risk assessments for low doses radiation after high-LET exposure.

It is thought that there are two pathways involved in the bystander effects. 1) medium-derived factors such as reactive oxygen species (ROS), nitric oxide[3,4] or the other substances could be released from irradiated cells and then further induce a series of damage in the non-irradiated cells. 2) gap junctional intercellular communication (GJIC) was found to be relevant to the molecular events leading to the modulation of gene expression in non-irradiated bystander cells with a very low dose, and these expressions were effectively reduced when GJIC was inhibited by lindane[5].

Microbeam facilities, in which cells are individually irradiated by a predefined exact number of particle is a very useful tool in the study of bystander responses. In this work, human fibroblast cells were individually hit by heavy ion microbeam of ^{40}Ar or ^{20}Ne. A clear bystander response, independent of these LETs and the number of charged particles delivered to the targeted cells was observed[6].

2. Materials and Methods

2.1.Cell culture and treatments

AG1522 human fibroblasts were cultured in Eagle's MEM supplemented with L-glutamine and fetal bovine serum with antibiotics. Cells in full confluence (~7×10^5 cells/dish) were prepaired in specially made dishes with a thin Kapton® film bottom, and irradiated. In some dishes, the cell culture medium was replaced with the medium containing 1 nM PMA (4 β, 9 α, 12 β, 13 α, 20 - pentahydro-xytiglia - 1, 6 - dien - 3 - one 12 β - myristate 13 -acetate) 1 hr before irradiation in order to prohibit GJIC, but 14 mM DMSO as the solvent was contained in the medium. In some other dishes, the culture medium was replaced with one containing 14 mM DMSO also 1 hr before irradiation.

Just before irradiation, the medium was removed and cells were covered with a Kapton® film to kept the cells hydrated during irradiation. After irradiation, fresh medium was immediately supplied to each dish and cells were subsequently cultivated for 15 hr until they were harvested for the micronuclei (MN) assay. During this process, the drugs with a reduced concentration (1/4) was added in the medium to keep the inhibition of GJIC. The GJIC situation (Fig.1.) in confluent culture was tested by the scrape-loading and dye transfer technique[7].

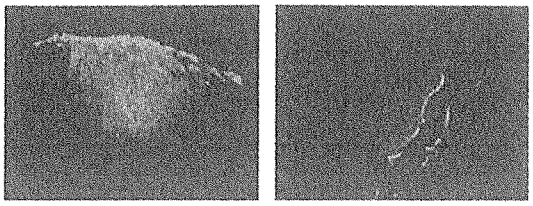

Fig.1. Transfer of the dye through gap junctions in confluent cells with (right) or without (left) PMA treatment (1 nM).

2.2. Cell irradiation

A heavy-ion microbeam apparatus at TIARA was used to deliver precise number of heavy ions of 260 MeV ^{20}Ne or 460 MeV ^{40}Ar with the calcurated LET values of ~380 or ~1260 keV/μm, respectively. The cells in confluent culture were irradiated in two ways; on the one hand, 1 to 121 cells with a matrix distribution of 11×11 mm^2 in the culture center were individually hit by 1 particle; on the other hand, 7×7 matrix-distributed cells were individually hit by from 1 to 4 particles.

2.3. MN assay

The formation of MN was assayed by using the cytokinesis-block technique[8]. Briefly, the cells were incubated in the presence of cytochalasin-B. After 48 hr, the cells were treated with a hypotonic solution and fixed by methanol. For the observation, a potion of the cells was placed on a glass slide and stained with acridine orange. Following this treatment, approximately 20% of the cells became to be binucleated (BN) cells. MN in BN cells was checked by fluorescence microscopy and morphologically identified.

3. Results and Discussion

3.1. Effect by number of the targeted-cells

When a few selected cells in the dish were individually hit by a precisely numbered particle, additional MN was significantly produced in the BN cells. Most of micronucleated BN cells had one MN and few of them contained two or three MNs. Yield of micronucleated cells, where 1 to 121 cells are individually targeted by one ^{20}Ne particle were shown in Figure 2. A very similar result was observed also for ^{40}Ar particles (data not shown). Even when only a single cell in a dish was targeted with one particle, the level of MN was increased about 1.4-fold to that of unirradiated control. Based on the observed yield of MN and the frequency of BN formation, it was calculated that additional MN could be produced in about 3000 BN cells when only one cell was actually hit in the dish. This additional MN induction must result from the bystander response.

To investigate the possible pathways of the bystander effect, we treated the cells with PMA or DMSO before and after irradiation as described above. Neither of the treatments themselves significantly changed the MN background. It is seen from Figure 2 that the yield of MN of the PMA-treated cßells was reduced to a very low level comparable to the control without any irradiation, and the MN yield was partly reduced (1/2) by DMSO. These results indicate that both GJIC and ROS contribute to the microbeam radiation-induced bystander effect.

Although the LET values of ^{40}Ar and ^{20}Ne

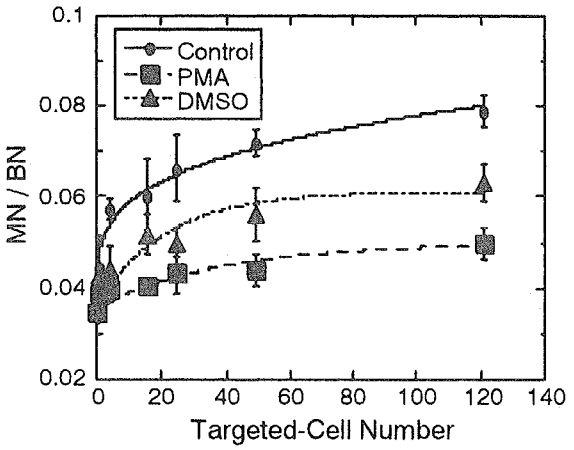

Fig.2. Yield of MN to the number of targeted cells. Cells with a matrix distribution in a dish were treated by PMA (■), DMSO (▲), or without drugs (●) before and after irradiation, and individually hit by one ^{20}Ne particle then incubated for 15 hr before MN assay.

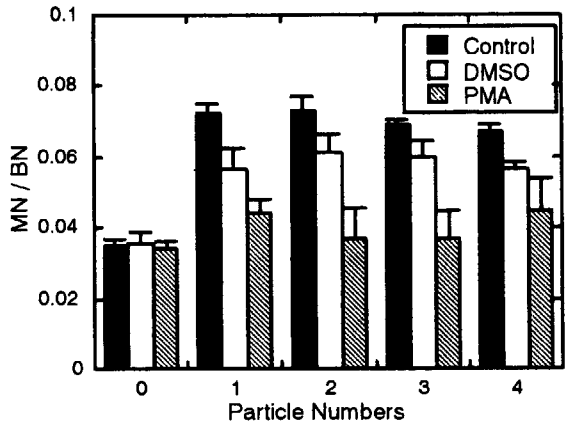

Fig. 3. Yield of MN to the number of particles delivered in 49 cells in a dish. Cells were treated with PMA (net), DMSO (open) or without treatment (fill), and individually hit by ^{20}Ne-ions, then incubated for 15 hr before MN assay.

were quite different (×3), the yields of MN induced had no significant difference (data not shown). For instance, when 49 cells in the dish were hit by one particle, the yield of MN was 0.074 and 0.072 for ^{40}Ar and ^{20}Ne, respectively. Thus, the MN induction was independent of the LET of these particles delivered to the selected cells in a dish.

The yields of MN have biphasic responses to the number of targeted-cells (Fig.2.). When the number of targeted-cells increased from 0 to 4, the yield of MN increased steeply than that when the number of targeted-cells increased from 16 to 121. The highest efficiency of MN induction was generated in the case of single cell irradiated by one particle. When the number of targeted-cells increased, the efficiency of MN induction drastically decreased.

3.2. Effect of particle number in a cell

We further studied the dose effect of MN induced by counted particle irradiation, 49 cells in a dish were respectively hit by 1 to 4 particles. Yields of MN in the irradiated cultures are approximately 2-fold higher than the unirradiated control (Fig.3.), which means that additional MN are produced in about 4500 BN cells since a bystander response even though only 49 cells are actually irradiated. Moreover, the effects were not significantly influenced by number of the particle. However it was partly reduced by DMSO and totally inhibited by PMA. In general, with direct effects, the higher the LET and dose of radiation, the more serious the cellular damage. However, the results in Figure 3 indicate that the level of bystander-induced MN does not depend on the amount of direct damage induced in the targeted cells. Thus the bystander phenomenon is quite different to broad beam irradiation induced damage[9] that has a positive relationship to radiation dose and LET and illustrates that the bystander effect is dominated by signaling type of behavior whereas direct damage is governed by stochastic mechanisms.

References

1) H. Nagasawa, J.B. Little, *Cancer Res.* 52 (1992), 6394-6396.

2) C. Shao, M. Aoki, Y. Furusawa, *J. Radiat. Res.* 42 (2001), 305-316

3) H. Matsumoto, S. Hayashi, M. Hatashita, K. Ohnishi, H. Shioura, T. Ohtsubo, R. Kitai, T. Ohnishi, E. Kano, *Radiat. Res.* 155 (2001), 387-396.

4). C. Shao, Y. Furusawa, M. Aoki, H. Matsumoto, K. Ando, *Int. J. Radiat. Biol.* 78 (2002), 837-844.

5) E.I. Azzam, S.M. de Toledo, B.J. Little, *Proc. Natl. Acad. Sci. U S A* 98 (2001) 473-478.

6) C. Shao, Y. Furusawa, Y. Kobayashi, T. Funayama, S. Wada, *FASEB J* (2003.8) 0000-0000, (in Press)

7) M.H. El-Fouly, J.E. Trosko, C.C. Chang, *Exp. Cell Res.* 168 (1987), 422-430.

8) M. Fenech, A.A. Morley, *Mut. Res.* 161 (1986), 193-198.

9) Y. Furusawa, K. Fukutsu, M. Aoki, H. Itsukaichi, K. Eguchi-Kasai, H. Ohara, F. Yatagai, T. Kanai, K. Ando, *Radiat. Res.* 154 (2000), 485-496.

2.26 Effect of Mammalian Nucleus Irradiation with Heavy-Ion Beams

S. Wada*, T. Funayama*, Y. Kobayashi*
M. Natsuhori**, N. Ito**
Department of Ion-Beam-Applied Biology, JAERI *
Department of Veterinary Medicine, Kitasato University**

1.Introduction

Radiation of high linear energy transfer (LET) has greater biological effectiveness than the same absorbed dose of low LET radiation. Thus, LET is used to describe radiation quality. However, it is considered that the different particles with the same LET induce different biological effects and the difference in the biological effects is caused by a difference in track structures. Because the different particles with the same LET differ in their pattern of energy deposition in the target materials, it is considered that the different damage was produced.

For mammalian cells exposed to high LET heavy charged particles DNA double strand breaks (dsbs) have an important role in the biological effects. At present, there are many studies with regard to the measurements of DNA dsbs induced by the heavy ions that deposit energy at very high LET. The quantitative analysis of every approach relies on the assumption that ions hit randomly to the cells and the biological effects were evaluated with the absorbed dose. To analyze the track structures in detail, the biological effects should be evaluated not with the absorbed dose but the number of the hit ions.

Recently we established a method of simultaneous detection of ions traversing the cellular nuclei and DNA damage in the individual cells[1]. So by this method we investigated the biological effects of the track structure of the ion beams with the same LET value but different particles.

2.Materials and methods

CHO-K1 cells were grown in Ham's F12 medium supplemented with 10% serum and 0.1 mg/ml kanamaycin in 10 cm diameter culture dishes. Cells were incubated at 37℃ in humidified atmosphere of 5% carbon dioxide and 95% air.

Accelerated heavy ions of 17.3 MeV/u $^{12}C^{5+}$, 10.4 MeV/u $^{20}Ne^{7+}$ were provided by the AVF cyclotron at TIARA JAERI-Takasaki. The energy of C ion beam was reduced by nickel plates.

To examine the rates of cell

survival, colony formation assay was preformed. The cells were irradiated at a given dosage at a room temperature and plated on 6-cm tissue culture dishes at a given density to calculate the rate of surviving cells. About 7 days after the irradiation, colonies of the cells were stained and counted.

To evaluate DNA damage, comet assay was applied. Cells were attached on the CR-39 plate that is particle track detector. Then, the cells were incubated for 12 hr with medium containing 1 mM Hydroxyurea. Immediately After irradiation the CR-39 plate on which cells were attached was placed in chilled PBS. The CR-39 plate was placed on the slide glass and then was embedded in 1% agarose. Finally 100 μl of 1% agarose was quickly layered. The slide glasses were placed immediately in a chilled nucleus lysing solution of 2.5 M NaCl, 100 mM Na_4EDTA, 1% sarkosyl, 10% DMSO, and 1% Triton X-100 and kept at 4℃ in the dark for 60 min. Under the neutral condition for comet assay the slides were placed on a horizontal gel electrophoresis platform and covered with chilled neutral solution made up of 90 mM Tris, 2 mM Na_2EDTA and 90 mM boric acid (pH 8) for 1 hour. Electrophoresis was conducted at 4℃ in dark for 30 min at 25 V (0.89 V/cm).

The slide glasses were washed with 300 mM NaOH and 1 mM Na_2EDTA and then rinsed gently with 400mM Tris (pH 7.5) to neutralize the excess alkali. After air drying the CR-39 plate was take off from the slide glass. The agarose gel on the CR-39 was stained with 50 μl of 0.4 μg/ml ethidium bromide and the opposite side of the CR-39 plate was etched with KOH-ethanol solution at 37°C. Using a fluorescence microscope equipped with a green filter we examined about comet images on one slide at 400 magnification. The comet images were stored using CCD camera. Then the microscope was focused on the image of pits etched on the CR-39 plate, and the image was also stored using CCD camera. Because the area of cellular nucleus was identified with the area of high fluorescent intensity of comet image, the number of ions traversing individual cellular nuclei was counted by merging both images. The comet images were analyzed using a Komet software (Komet 4.0, Kinetic imaging, LTD, UK). The parameter used as an index of DNA damage was tail moment, which combines a measure of the length of comet tail and the proportion of DNA to migrate into the tail.

3.Result and discussion

Fig. 1 shows the effect of radiation on the survival rates of CHO-K1 exposed to C and Ne ion corresponding to LET of 430 keV/μm. Lethal effect was much higher by C ion than Ne ion irradiation. It was observed that

the different particles with the same LET induced the different lethal effect.

Fig. 2 shows the relationship between the number of ions traversing the cellular nuclei and tail moment evaluated as DNA dsbs after C and Ne ion irradiation of 430 keV/μm. The tail moment increased with the number of ions traversing the cellular nuclei. Those data was fitted by linear regression. The slopes of the fitted curves indicated induction of DNA damage per a particle in CHO-K1 cell. The induction of DNA damage per a particle for C ion was higher than that for Ne ion.

These results indicate that the difference in cell killing and the induction of DNA damage were caused by the difference in the track structure. Because the ion track radius for C ion is narrower than that for Ne ion, it was considered that the efficient induction of DNA damage for C ion irradiation induced high lethal effect.

Reference

1) S. Wada et al., Journal of Radiation Research 43: (2002) S153-156

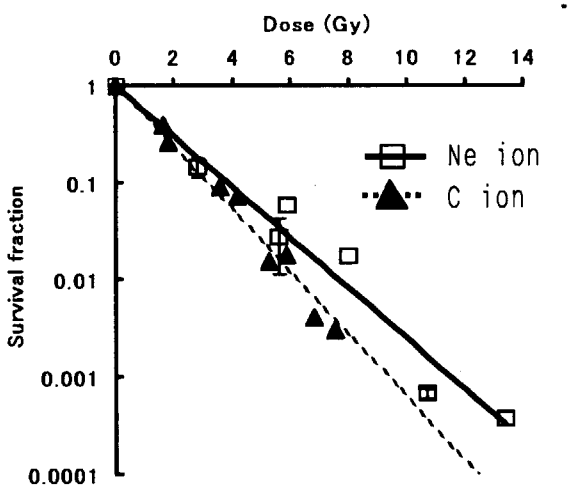

Fig.1. Survival curves of CHO-K1 cells exposed to C and Ne ion of 430 keV/μm.

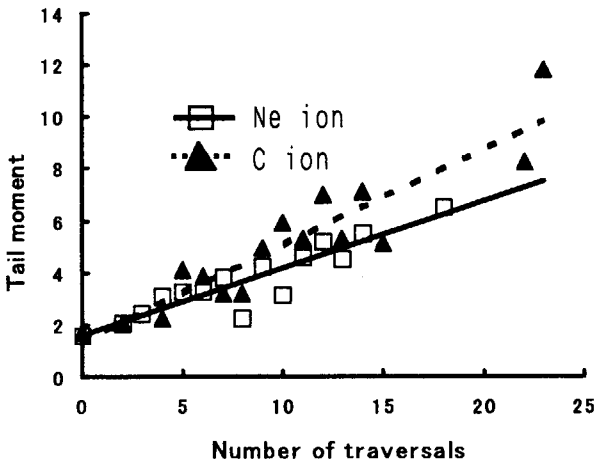

Fig.2. Induction of DNA damage of CHIO-K1 cells exposed to C and Ne ion of 430 keV/μm. Tail moment was plotted as a function of the number of ions traversing.

2.27 Study on Signal Transduction by Local Damage Using Penetration Controlled Ion Beam Exposure

S. Wada and Y. Hase
Department of Ion-Beam-Applied Biology, JAERI

1.Introduction

Radiation-induced cell death is thought to result from damage to two cellular targets: the DNA damage and the plasma membrane.

Especially, DNA is most important target. DNA damage includes single and double strand breaks, residual unrepaired and misrepaired DNA damage lead to genetic instability and cell death. Radiation-induced DNA damage can also induce death by apoptosis through activation of an apoptosis pathway. Now research of the pathway is proceeding.

Several recent studies have suggested that radiation could also generate signals at the cell membrane that led to apoptosis. It is considered that radiation induce two different signaling system for apoptosis in signal of the cell membrane. One pathway is the sphingomyelin–ceramide signal transduction pathway. Radiation activates sphingomyelinases that convert sphingomyeline into ceramide. Ceramide serves as a second messenger in inducing apoptosis. Other pathway is the ceramide synthase pathway. Radition-induced DNA damage can also increase ceramide level by activating the synthesis pathway, through the activation of the ceramede synthase enzyme. To elucidate radiation-induced apop-tosis in detail, we investigated the induction of apoptosis on cells with non-DNA damage by selective irradiation using the penetration controlled irradiation apparatus.

2.Materials and methods

Accelerated heavy ion of 1.5 MeV/u $^{12}C^{5+}$ was provided by the tandem accelerator at TIARA JAERI-Takasaki.

CR-39 plates were used for the measurement of ion beam fluence. The irradiated CR-39 plates were treated in KOH-ethanol solution at 37°C.

CHO-K1 cells on a kapton film were grown in Ham's F12 medium supplemented with 10% serum and 0.1 mg/ml kanamaycin. The cells on a kapton film were exposed to C ions.

To evaluate radiation-induced DNA damage, comet assay was applied. After irradiation cells were removed from a kapton film and suspended in chilled PBS. The cell

solution was mixed with 2% agarose. The mixture was quickly layered on the glass slides. The glass slides were placed immediately in a chilled nucleus lysing solution. Then electrophoresis was conducted under the alkaline condition at 4℃ in dark for 15 min at 25 V (0.89 V/cm). The agarose gel on the glass slide was stained with ethidium bromide and radiation-induced DNA damage was observed using a fluorescence microscope in individual cells.

To evaluate induction of apoptosis, apoptosis fraction was detected by the TUNEL assay. After irradiation cells were removed from a kapton film and were incubated in the culture dishes at 37°C in humidified atmosphere of 5% carbon dioxide and 95% air. After 72 hr the cells were harvested from culture dishes and fixed in 1% paraformaldehyde. Apoptosis cells were detected by labeling 3'-OH ends of fragmented DNA with TDT.

3.Result and discussion

When CR-39 plates were irradiated at the distance of 13, 17 and 18mm from the beam window, the fluence at the distance of 17mm reduced to one tenth of the fluence at the distance of 13 mm and etched pits were not observed at the distance of 18 mm.

Radiation-induced DNA damage was detected at the distance of 13 mm. When cells at the distance of 17 mm were irradiated at tenfold of fluence at the distance of 13 mm, DNA damage was not detected. This result indicates that cells can be selectively irradiated without DNA damage using the penetration controlled irradiation apparatus.

Fig. 1 shows change of apoptosis fraction as a function of the distance from the beam window. Apoptosis fraction was 2.5% at the distance of 13 mm and similar to control at the distance of 18 mm at which etched pits were not observed on the CR-39. However, apoptosis fraction was higher than control level at the distance of 17mm at which DNA damage was not observed. This result indicates that one of the signal transductions of radiation-induced apoptosis do not mediate DNA damage.

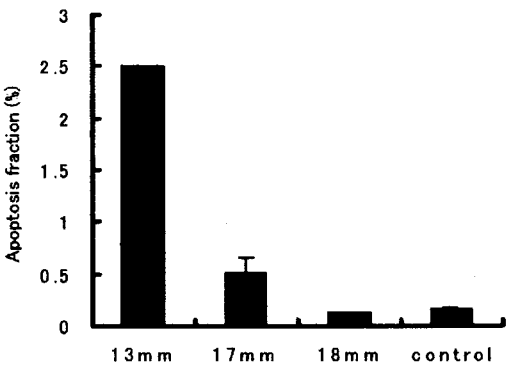

Fig.1. Change of apoptosis fraction as a function of the distance from the beam window. Cells were irradiated at a fluence of 5×10^7 p/cm^2. At the distance of 13 mm, both etched pits and DNA damage were detected. At the distance 17 mm, etched pits were detected, but DNA damage was not detected. At the distance of 18 mm, etched pits were not detected.

2.28 Establishment of a cell system to be used for isolation of human cell mutants, induced by heavy-ion irradiation, resistant to human immunodeficiency virus

H. Hoshino*, T. Ohtsuki*, N. Shimizu*, A. Tanaka*, M. Shinagawa*,
S. Wada**,T. Funayama**, and Y. Kobayashi**
Department of Virology and Preventive Medicine, Gunma University Graduate School of Medicine*
Department of Ion-Beam-Applied Biology, JAERI**

1. Introduction

The aims of this study are to (1) establish a cell system to be used to examine effects of heavy-ion irradiation on cellular genes and (2) to isolate human cell mutants resistant to human immunodeficiency virus type1(HIV-1) using this system. In order to judge changes of gene expression in irradiated cells easily as well as rapidly, cells that become green fluorescence protein (GFP)-positive after HIV infection will be established. Further, we shall isolate cell mutants that will not become GFP-positive even after HIV-1 infection using this system. Mutant cell sublines thus obtained after heavy-ion irradiation will be used to identify a cellular factor(s) necessary for eestablishment of HIV-1 infection.

Viral genes and cellular factors necessary for establishment of HIV-1 infection and the process of HIV-1 infection have been studied well. For example, the expression of CD4 and one of coreceptors, which mainly belong to the chemokine receptor family, e.g, CCR5 or CXCR4, on the cell surface are almost absolutely required for the entry of HIV-1 into target cells. In addition to them, other cellular factors will be necessary, as the life cycle of HIV-1 in the cell has been not precisely understood. Recently several factors have been identified as new factors necessary for the establishment of HIV-1 infection. There may still be other cellular gene products necessary for HIV-1 infection.

On the other hand, there are only a few reports on quantitive analyses of the effects of heavy ion ($^{4}He^{2+}$, $^{12}C^{5+}$ or $^{20}Ne^{8+}$) irradiation on induction of mutation in human genes [1)-4)]. For this, a cell system that enables us to detect cellular gene mutation induced by heavy-ion irradiation easily is desirable. Thus, we shall isolate a new cell line after transduction of CD4, CR5 and GFP expression vectors and then selection as described below.

By the use of mutant cell lines resistant to HIV-1 infection, another new cellular factor required for HIV-1 infection can be identified. This type of a gene will be a target for the development of a new type of anti-HIV drugs.

2. Experimental protcedure

2.1 Generation of irradiation target cells

A human glioma cell line, NP-2, has been found to be completely resistant to HIV-1 infection. NP- 2 cells were transduced with CD4, EcoR (a receptor gene for ecotropic murine leukemic virus), and CCR5, using the resistance to neomycin, hygromycin, and puromycin, respectively, as selectable markers. Thus, NP2/CD4/CCR5 cells were isolated [5)]. To them, a GFP- expressing vector containing. HIV-1 long terminal repeat (LTR) promoter and the GFP gene fused with the nuclear localization signal sequence of HIV-1 *rev* gene was transduced, and suitable cellular clones for the assay were obtained as described below. For tranduction of DNA, Fugene 6 (Roche) was used.

2.2 Heavy ion irradiation and cell cloning

NP-2/ CD4/CCR5/GFP cells were seeded into 35-mm culture dishes. On the following day, the culture medium was removed, the dishes were covered with Kapton (8 μm thick polyimide) films, and the cells were irradiated with $^{4}He^{2+}$, (50 MeV), $^{12}C^{5+}$, (220 MeV) or $^{20}Ne^{8+}$ (350 MeV). Next day the cells in the dishes were counted and re-seeded into wells of 96-well multi-well plates in an amount of 0.3-30,000 cells/well. The number of wells showing cell growth were judged and scored during observation for 1-2 months.

2.3 Establishment of irradiation target cells

NP-2/CD4/CCR5 cells were transduced with the GFP vector that would induce the expression of GFP in the cell nucleus under the control of the HIV-1 LTR promoter. As GFP had been fused with the nuclear localization signal to its downstream, fluorescence was mainly detected in the cell nuclei of the GFP-transduced cells. The cells that did not become GFP-positive even after transduction were cloned. Clonal cells were infected with HIV-1. Some clones that did not express GFP before HIV-1 infection, namely, cell clones showing low background fluorescence, became GFP-positive after HIV-1 infection. These clones were used for the further experiment.

3. Results and Discussion

3.1 Effects of heavy-ion irradiation on the growth of the cells

Irradiated cells were seeded into multi-well plates (0.3-30,000/cell) and cultured for up to two months. D10's (an irradiation dose that would reduce plating efficiencies of cells to one tenth of the control.) were estimated after determination of colony-forming efficiencies of each irradition: for He and C ions irradiation, 2.6 and 0.9 Gy, respectively were obtained (Tables1 and 2). As for Ne ion irradiation, there was not an apparent correlation between irradiation doses and colony-forming efficiencies: this discrepancy was probally due to a short penetration range of Ne ions and the presence of a small amount of culture medium remaining in dish corners even after its removal by aspiration.

3.2 Effects on HIV-1 infection

Irradiated cells in different dishes were harvesred and pooled and re-seeded into multi-well plates at the indicted cell concentrations (Tables 1 and 2). Irradiated cells growing in wells of 96-multi-well plates with a colony forming efficiency of 0.3 or lower were considered to originate from a single or a few cells. These clonal or oligoclonal cells were infected with HIV-1. Almost all irradiated cell clones became GFP positive after cultivation for 1-2 weeks. Some cells did not become GFP positive. However, most of them showed many syncytia indicating that these NP-2 cell sublines were susceptible to HIV-1, although they did not express GFP after HIV-1 infection.

HIV-1-resistant mutant cells were hardly isolated after random cloning more than a few hundred cells. However, cells lacking GFP expression were isolated much more frequently than expected before the experiment: a few percents of irradiated cells were judged to each GFP expression. It remains to be determined whether this phenomenon, frequent isolation of GFP-negative clones, is specific for heavy-ion irradiation. Therefore, for isolation of HIV-1-resistant cells, a large number of irradiated cells should be examined.

References

1) Morimoto S, Honma M, Yatagai F. Sensitive detection of LOH events in a human cell line after C-ion beam exposure. J Radiat Res (Tokyo). 43 (2002) Suppl: S163-167.
2) Grosovsky A, Bethel H, Parks K, Ritter L, Giver C, Gauny S, Wiese C, Kronenberg A. Genomic instability in human lymphoid cells exposed to 1 GeV/amu Fe ions. Phys Med. 17 (2001) Suppl 1: 238-240.
3) Shigematsu N, Ihara N, Kawata T, Kawaguchi O, Takeda A, Ishibashi R, Kutsuki S, Kubo A, Kanai T, Furusawa Y, Isobe K, Uno T, Ito H. Cell killing and mutation induction by heavy ion beams. Int J Mol Med. 7 (2001) 509-513.
4) Piao CQ, Hei TK. Gene amplification and microsatellite instability induced in tumorigenic human bronchial epithelial cells by alpha particles and heavy ions. Radiat Res. 155 (1 Pt 2) (2001) 263-267.
5) Soda Y, Shimizu N, Jinno A, Liu HY, Kanbe K, Kitamura T, Hoshino H. Establishment of a new system for determination of coreceptor usages of HIV based on the human glioma NP-2 cell line. Biochem Biophys Res Commun. 258 (1999) 313-321.

Table 1 Colony-forming efficiency (%) of NP-2/ CD4/ CCR5/ GFP cells after $^{4}He^{2+}$ ion irradiation

Irradiation dose (Gy)	Number of inoculated cells /well											Number of cells required for their growth in 66% of wells.
	0.3	1	3	10	30	100	300	1,000	3,000	10,000	30,000	
0	33*	38	83	96								2.0
2	-	0	33	67	88							10.0
4	-	-	-	13	38	83	100					62
6	-	-	-	-	-	21	63	100				330
8	-	-	-	-	-	0	0	4	46	83		4,200
10	-	-	-	-	-	-	0	8	38	63	100	11,000

*Colony-forming efficiency (%) in multi-well plates
D_{10} determined by colony-forming efficiency was 2.6 Gy
Number of clones that were GFP-negative, but syncytia-positive after infection: 20.
Number of clones that were GFP-negative as well as syncytia-negative after infection: 0.

Table 2 Colony-forming efficiency (%) of NP-2/ CD4/ CCR5/ GFP cells after $^{12}C^{5+}$ ion irradiation

Irradiation dose (Gy)	Number of inoculated cells /well										Number of cells required for their growth in 66% of wells.
	0.3	1	3	10	30	100	300	1,000	3,000	10.000	
0	13*	71	96	100							0.9
2	-	8	33	83	92						6.6
4	-	-	13	8	71	100	100				28
6	-	-	-	0	13	17	71	96			270
8	-	-	-	-	0	21	58	88	92		420
10	-	-	-	-	-	0	29	29	8	25	-

*Colony-forming efficiency (%) in multi-well plates
D_{10} determined by colony-forming efficiency was 0.9 Gy
Number of clones that were GFP-negative, but syncytia-positive after infection: 10.
Number of clones that were GFP-negative as well as syncytia-negative after infection: 0.

2.29 The preservation of the organ-cultured Ciliary body by gamma ray irradiation

K. Akeo*, T. Funayama**, A. Ogawa***, R. Inoue*, Y. Kobayashi**
Department of Ophthalmology, Takasaki National Hospital*
Department of Ion-Beam-Applied Biology, JAERI**
Department of Research and Examination, Takasaki National Hospital***

INTRODUCTION

Morphology of the tissue should be damaged due to necrosis by the cease of blood flow after dissection from living body. If the radiation induced preventive reaction into the cells and quit the destruction of the living tissue by necrosis, the long-time preservation of the internal organs and the living tissue would be possible and leaping contributed to the medical field.

Especially, the labyrinth of the blood vessel in the ciliary processes does not make the blood supply spread entirely because of the more complicated structure than the ciliary folds. It is necessary to know which part of the ciliary body is damaged at the initial phase by the cease of blood. We thought that the ciliary body was most useful to investigate the inflammatory reaction by gamma radiation because of the complicated vascular structure. Gamma radiation of blood products is considered the mainstay of transfusion-associated graft-versus-host disease prevention. Recently it is reported that there is evidence of cellular variability with production of cytokines at different storage time which could be related with irradiation activity and cellular damage repair but not lymphocyte inhibition rate in blood components just one time after irradiation, and the cytokines had a central role in the stimulation of cellular and inflammatory reactions [1].

As for as we know, this is the first report concerned with the preservation of the organ-cultured ciliary body without blood flow by gamma ray irradiation.

We are now submitting materials and methods, results, and discussion to an article.

References

1) E. Fagiolo, C. Toriani-Terenzi, Transfus Apheresis Sci 27 (2002) 225-231.

2.30 Effect of Various Radiations with Different LET on Survival of *Euglena gracilis*

H. Hayashi*, M. Furuta*, K. Uehara*, T. Funayama**, S. Wada**,
Y. Kobayashi**, H. Watanabe**
Research Institute for Advanced Science and Technology, Osaka Prefecture University*
Department of Ion-Beam-Applied Biology, JAERI **

1. Introduction

Euglena is a photosynthetic unicellular organism, which is classified both as animal and as plant. *Euglena gracilis* Z strain has a very high photosynthetic efficiency [1], and the nutritional value of its cellular components is higher enough to support animal life [2-4]. In near future, it would be expected that humankind rush into the cosmic era where we are forced to live in Closed Ecological Life Support System. Considering living in such environment, it is necessary to establish an effective support system for supplying food and air. Because of its high photosynthesis ability and nutritional value, *E. gracilis* can be a good biological component for utilizing in such a closed system.

Nevertheless, in using *E. gracilis* for the purpose in space, the radiation damage caused by cosmic rays that includes high LET particles will be problematic. Therefore, as the first step to solve this problem, we assessed the radiation effect of heavy ion beams on *E. gracilis*, and compared its property with previously reported data [5-10].

2. Experimental procedure

2.1 Organism and Cultivation conditions

E. gracilis strain Z was used. The cells were grown at 25℃ in 150 ml of Koren-Hutner (KH) medium[11] in a 500-ml Sakaguchi flask to stationary growth phase (for 5 days) with agitation under the illumination of fluorescent light (5,000 lx).

2.2 Irradiation conditions

The light-grown cells of *E. gracilis* Z strain were harvested by centrifugation. Then the cells were washed, and resuspended in a fresh KH medium. The cell suspension (containing 2×10^6 cells) was poured on the surface of KH agar medium in a sterile 3.5-cm plastic culture dish. Before irradiation, the surface was covered with a Kapton (7.5μm thick polyimide) film to avoid drying-out and contamination. The cells were then exposed to various heavy ion beams at room temperature. In the present study, 7 kinds of heavy ion beams that can be generated by AVF-Cyclotron (JAERI Takasaki, dose rates: 1.1 to 11 Gy/sec) were used. The properties of heavy ions used in the experiment are shown in Table 1.

Irradiation of γ-ray was carried out by using ^{60}Co γ-ray source at JAERI Takasaki (dose rates:

100 to 500 Gy/h).

Table 1. Physical properties of ^{60}Co γ-ray and heavy ion beams

Radiation	Energy (MeV/n)	LET (keV/μm)
^{60}Co γ- ray	–	0.2
H^{+}	19.8	2.8
$^{4}He^{2+}$	12.5	16.2
$^{12}C^{6+}$	26.7	70
$^{12}C^{5+}$	18.3	108
$^{12}C^{5+}$	18.3	196 *
$^{20}Ne^{8+}$	17.3	321
$^{20}Ne^{7+}$	12.9	437
$^{40}Ar^{13+}$	11.5	1,610

* LET value was increased using nickel plates as absorbers

2.3 Measurement of Cell survival

The survival rates of *E. gracilis* Z strain following irradiation were determined on the basis of colony-forming ability according to the procedure of Lyman, Epstein and Schiff [12]. The irradiated cells were grown on KH agar medium at 28°C under the illumination of fluorescent light (5,000 lx) for 7 to 10 days. RBE values were calculated from LD_{10} values using the value of γ-irradiated cells as a standard.

3. Results and Discussion

We irradiated light-grown *E. gracilis* Z strain by 7 kinds of heavy ion beams with different LET, and the cell survival rates were determined. As shown in Fig. 1, all survival curves have a "shoulder" part in their curves. It was reported that in animal cells, LD_{10} value of X-rays were 4.1 to 7.8 Gy [5-7]. In this study, LD_{10} value of γ-rays was 300 Gy (Fig.1), suggesting that the radioresistence of *Euglena* was about 40 to 70 times higher than that of animal cells. The RBE values based on LD_{10} were increased with increasing LET value, peaked at 196 keV/μm, and then decreased with increasing LET value (Fig. 2). This result suggests that the LET effect of *E. gracilis* is analogous to that of animal cells and plant seeds [5-10]. We estimated the dose at the shoulder of survival curve. At the dose almost all cells can survive after irradiation. As shown in Table 2, *Euglena* was capable of growth without any lethality after the exposure to the high LET radiation up to 40 Gy. This result suggests that *E. gracilis* may grow under the space environment where the cosmic radiation level is kept at less than 40 Gy.

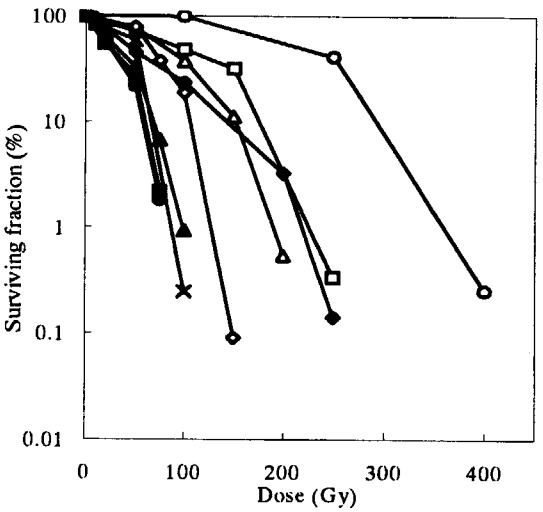

Fig. 1. Survival of *E.gracilis* Z strain exposed to heavy ion beam at different

○:γ-ray, □:H^{+}, △ : He^{2+}, ◇:C^{6+}, ×:C^{5+} (108 keV/μm), ● : C^{5+} (196 keV/μm), ■ : Ne^{8+}, ▲ : Ne^{7+}, ◆Ar^{13+}

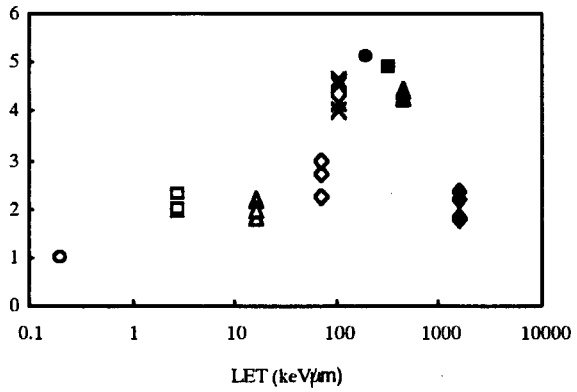

Fig.2. Relationship between LET and RBE based on the killing effect of heavy ion radiation

○:γ-ray, □:H^{+}, △ : He^{2+}, ◇:C^{6+}, ×:C^{5+} (108 keV/μm)

● : C^{5+} (196 keV/μm), ■ : Ne^{8+}, ▲ : Ne^{7+}, ◆Ar^{13+}

Table 2. The dose at shoulder of the survival of *E. gracilis* Z strain exposed to heavy ion beam at different doses.

Radiation	LET (keV/μm)	Dose at shoulder (Gy)
H^{+}	2.8	130
He^{2+}	16.2	120
C^{6+}	70	90
C^{5+}	108	50
C^{5+}	196 *	40
Ne^{8+}	321	40
Ne^{7+}	437	40
Ar^{13+}	1,610	160

* LET value was increased using nickel plates as absorbers

References

1) Y. Kitaya, S. Kibe, M. Oguchi, H. Tanaka, K. Miyatake, Y. Nakano, *Life Support Biosph. Sci.*, 5, 243 (1998)

2) Y. Kott, A. M. Wochs, *Appl. Microbiol.*, 12, (1964)

3) S. Kitaoka, K. Hosotani, *Nippon Nogeikagaku Kaishi,* 51, 477 (1977)

4) K. Hosotani, S. Kitaoka, *Nippon Nogeikagaku Kaishi,* 51, 483 (1977)

5) G. Raft, *Nuclear Science Application* I, 3, 1 (1987)

6) D. T. Goodhead, J. Thacker, R. Cox, *Int. J. Radiat. Biol.*, 63, 543 (1993)

7) M. Aoki, Y. Furusawa, T. Yamada, *J. Radiat. Res.*, 41, 163 (2000)

8) A. Tanaka, N. Shikazono, Y. Yokota, H. Watanabe, S. Tano, *Int. J. Radiat. Biol.*, 72, 121 (1997)

9) Y. Hase, M. Yamaguchi, M. Inoue, A. Tanaka, *Int. J. Radiat. Biol.,* 78, 799 (2002)

10) N. Shikazono, A. Tanaka, S. Kitayama, H. Watanabe, S. Tano, *Radiat. Environ. Biophys.* , 41, 159 (2002).

11) L. E Koren, S. H. Hutner, *Protozool. J.* 14, Suppl., 17 (1967)

12) H. Lyman, H. T. Epstein, *Biochem. Biophys. Acta.*, 50, 301 (1961)

2.31 Study on Transportation of Photoassimilates in Higher Plants under CO_2 Enrichment

S. Matsuhashi, S. Fujimaki, S. Watanabe, N. S. Ishioka and T. Kume
Department of Ion-beam-applied Biology, JAERI

Introduction

CO_2 enrichment increases fruit harvest in plant cultivation[1]. It acts as additional fertilizer, and changes efflux from a leaf and/or transportation through phloem of photoassimilates in a plant. However, the regulation mechanism of such dynamics is not clear yet. Our objective is to elucidate the regulation mechanism of photoassimilate transportation in a plant under CO_2-enriched conditions. For this purpose, we have been using the Positron Emitting Tracer Imaging System (PETIS), which enables real-time observation of transportation of photoassimilates labeled with a positron emitting tracer. We have previously reported influence of CO_2 enrichment on the photoassimilate transportation in a broad bean (*Vicia faba* L.) plant using ^{11}C-labeled carbon dioxide ($^{11}CO_2$)[2),3)]. The treatment of enriched CO_2 on leaves of the broad bean plant enhanced efflux of photoassimilates from the $^{11}CO_2$-fed leaves to the stem. In the present study, we applied the transfer function analysis to evaluate quantitatively the effect of CO_2 enrichment on the transportation of ^{11}C-labeled photoassimilates in phloem.

Experiment

Broad bean (*Vicia faba* L.) plants were cultivated in the same manner of a previous report[3].

For positron imaging, the plant was placed in a chamber conditioned with 350 ppm of CO_2 (normal atmospheric condition). The fourth foliage leaves of the plant were inserted into a cuvette, which is a clear acrylic box with inside dimensions of 12 cm in length, 8 cm in width and 1 cm in depth, for feeding $^{11}CO_2$. The cuvette was sealed at the petiole of the leaves with dental plastic filling, and connected to a $^{11}CO_2$ gas circulating system.

Soon after the $^{11}CO_2$ gas was introduced to the cuvette, imaging by PETIS was started and continued for two hours. The $^{11}CO_2$ gas was supplied for the first one to two minutes and then drained off and substituted with standard gas without $^{11}CO_2$. During the experiment, total CO_2 concentration in the cuvette was controlled to keep 350 ppm by introducing a CO_2 standard gas, at a flow rate of 60 ml/min.

Three hours after the imaging was finished, the CO_2 concentration in the cuvette was increased to 1000 ppm (enriched condition), and kept for approximately 2 hours. The next PETIS imaging was done in the same way as the first one, but the total CO_2 concentration in the cuvette was kept 1000 ppm during the experiment.

Transfer function analysis was applied to the obtained imaging data, according to a previous study[4]. Figure 1 shows the broad bean plant, which was used for the PETIS imaging. ^{11}C tracer profiles at the two points on the stem, A and B, were extracted from the obtained two-dimensional data, and analyzed as "input" and "output", respectively. The translocated fractions and average transport speeds of the photoassimilates in the stem of the plant were also estimated.

Results and Discussion

According to the previous report[4], the model of input-output relationship in this study could be described by a simple equation:

$$B(n) = a\,B(n-1) + b\,A(n-d) + e(n), \qquad (1)$$

where $B(n)$ and $A(n)$ mean observed tracer intensities at the point B and A at the n-th cycle of PETIS imaging, a and b are parameters, d is "delay factor" with a positive integral value, and $e(n)$ is the residual.

We performed multiple regression analysis to estimate the best fitting model for each experiment. First, the observed values were substituted for $B(n)$, $B(n-1)$ and $A(n-d)$ in the cases with $d = 0$ to $d = 5$, where if $k \leqq 0$ then $A(k) = B(k) = 0$. Then the least-squares method was employed, that is, the values of parameters a and b which give the minimum sum of squares of $e(n)$ were calculated for the respective cases. Finally, the best fitting case with the best parameters was selected.

The optimum models for 350 ppm and 1000 ppm of CO_2 were respectively determined as

$$B(n) = 0.393\,B(n-1) + 0.168\,A(n-3) \qquad (2)$$
$$(R^2 = 0.988)$$

and

$$B(n) = 0.547\,B(n-1) + 0.129\,A(n-1) \qquad (3)$$
$$(R^2 = 0.996)\,.$$

Figure 2 shows the time-course changes of observed tracer intensities at the point A ($A(n)$) and B ($B(n)$), and the estimated values for $B(n)$ from the models ($M(n)$), in the respective experiments with 350 and 1000 ppm of CO_2. The observed intensities with 1000 ppm were obviously higher than those with 350 ppm. The models showed very good fitting to the observed data in the both experiments.

From these equations, we estimated the fractions of translocated tracer and the average transport speeds from the origin point A to the terminal point B in the respective conditions.

The fraction of tracer at B translocated from A is generally called "system gain", G. The system gain is defined as the equation (4) when the input is provided as "unit impulse" defined as the equation (5):

$$G = \sum_{k=1}^{n} B(k)\,. \qquad (4)$$

$$\begin{cases} A(0) = 1 \\ A(k) = 0 \quad (k > 0)\,. \end{cases} \qquad (5)$$

The average transport speed is the quotient of the distance between A and B divided by "average transit time", T, which is defined as

$$T = T_i \sum_{k=1}^{n} k\,B(k) \,/\, G\,, \qquad (6)$$

where T_i is data sampling interval. In this study, the imaging data was collected and compiled every one minute by PETIS, thus the T_i value equaled to one. The approximate value of G and T can also be obtained from the following equations,

$$G = b / (1 + a)$$
$$T = T_i \{d - a / (1 + a)\}\,. \qquad (7)$$

The calculated values of the fractions of translocated tracer and the average transport speeds were 0.28 and 3.4 cm/min under 350 ppm of CO_2, and 0.29 and 5.7 cm/min under 1000 ppm of CO_2.

The estimated average transport speed under 350 ppm of CO_2 (normal atmospheric condition) was similar to flow speeds of phloem known in other higher plants. In this study, we used the same plant for the serial experiments under the two CO_2 conditions. Therefore, the difference of the average transport speeds was not attributed to individual difference. Our results suggest that the treatment of enriched CO_2 on the foliage leaves increases the speed, as well as the amount, of phloem transport of photoassimilates. In contrast, the treatment did not change the system gain; in other words, it is suggested to have no effect on the efficiency of phloem transportation.

In this study, we used data profiles from only two points for the analysis, though PETIS measures the time course of radioactivity at every area of 1.1 mm square in its whole field of view. Thus, in the next step, the analysis should be extended to treat two-dimensional data and done more in detail on a plant body. The transfer function analysis will be a powerful technique to analyze PETIS data quantitatively.

References

1. T. Sakashita, *Annual Report of Agricultur. Res. Center*, (1997) 42-43.
2. S. Matsuhashi, S. Watanabe, N. S. Ishioka, C. Mizuniwa, T. Ito, T. Sekine, *TIARA Annual Report 2000*, JAERI-Review 2001-039 (2001) 90-92.
3. S. Matsuhashi, S. Watanabe, N. S. Ishioka, C. Mizuniwa, T. Ito, T. Sekine, *TIARA Annual Report 2001*, JAERI-Review 2002-035 (2001) 86-88.
4. N. Keutgen, S. Matsuhashi, C. Mizuniwa, T. Ito, T. Fujimura, N. S. Ishioka, S. Watanabe, T. Sekine, H. Uchida, S. Hashimoto, *Appl. Radiat. Isotopes*, 57 (2002) 225-233.

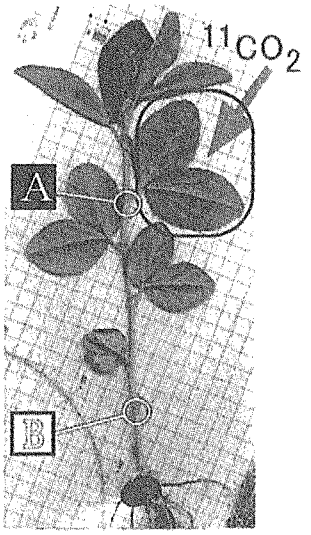

Fig. 1 The broad bean plant used for the positron imaging. The data on the points A and B were used for the transfer function analysis. The point A is the base of the 4th foliage leaves which $^{11}CO_2$ and cold CO_2 gas were fed with controlled concentrations. The distance between the point A and the point B was 12.5 cm.

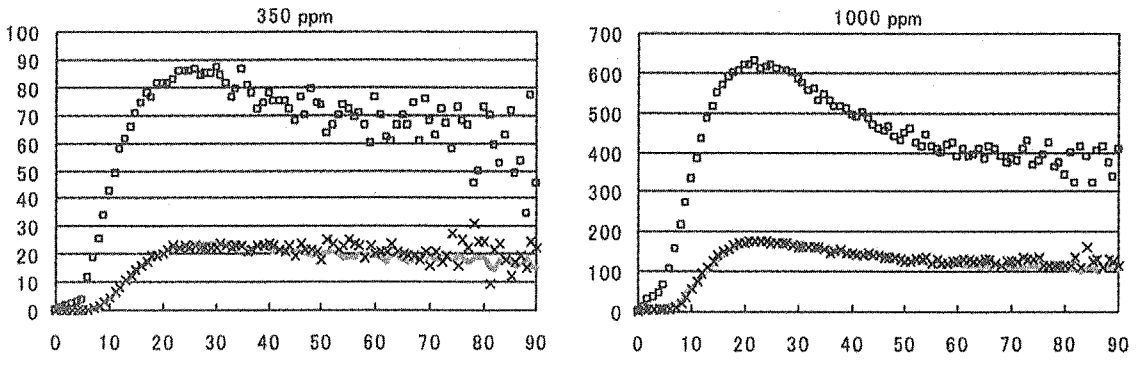

Fig. 2 Time course of ^{11}C-intensity at the two points in the broad bean plant, extracted from PETIS imaging data.

The symbols: □ A*(n)*; at the position A, × *B(n)*; at the position B, — *M(n)*; the estimated value for ^{11}C-intensity at the position B from the model obtained from the transfer function analysis.

2.32 Translocation and Distribution of Photosynthetic Products in Soybean 'Williams' and its Hypernodulating Mutant 'NOD1-3'

N. Ohtake*, S. Ito*, A. Yamazaki*, H. Fujikake*, K. Sueyoshi*, T. Ohyama*
S. Fujimaki**, N. S. Ishioka**, S. Matsuhashi**, T. Sekine** and T. Kume**
Faculty of Agriculture, Niigata University*
Department of Ion-Beam-Applied Biology, JAERI**

1. Introduction

Soil bacteria belonging to the genera *Rhizobium* and *Bradyrizobium* are able to invade the roots of their leguminous host plants and trigger the formation of new organ, the root nodule. In rhizobium-legume symbioses, considerable metabolic energy is invested by the plant to produce nitrogen fixing nodules and to maintain nitrogen fixation. Nodule number in soybean appears to be regulated by host plant through variety of mechanisms, the major one known as autoregulation, being inhibition of further nodule formation by existing or developing nodules. In this study, we examined autoregulation of nodulation in soybean by using cv. Williams and NOD1-3 at the point of distribution of photosynthetic products. The NOD1-3 is a hypernodulatig mutant derived from *N*-nitroso-*N*-methylurea mutagenesis of cv. Williams. Experiments were designed to compare ^{11}C distribution in the Williams and NOD1-3 plant of different periods after inoculation, seed inoculation or non-inoculation.

2. Experimental Procedure

Soybean (cv. Williams and NOD1-3) seeds were non-inoculated or inoculated with *Bradyrizobium japonicum* strain USDA 110 and they were cultivated hydroponically. Seed inoculated plants were supplied with N free medium and non-inoculated plants were supplied with 5 mM sodium nitrate. Nitrate application was stopped from 22 days after sowing (DAS) to sampling time. Some of the non-inoculated plants (both Williams and NOD1-3) were inoculated with liquid cultured of USDA 110 (about 10^8 cells) from 25 DAS (4 days after inoculation) or 27 DAS (2 days after inoculation). Another plants were kept to culture rhizobium free medium. At 29 DAS, these plants were used for $^{11}CO_2$ feeding experiment in TIARA. The ^{11}C atoms were produced by bombarding a nitrogen gas target with 10 MeV protons at a current of 1mA using the TIARA AVF cyclotron, and the $^{11}CO_2$ was produced from the ^{11}C atoms and O_2 present in target chamber. $^{11}CO_2$ was supplied to a

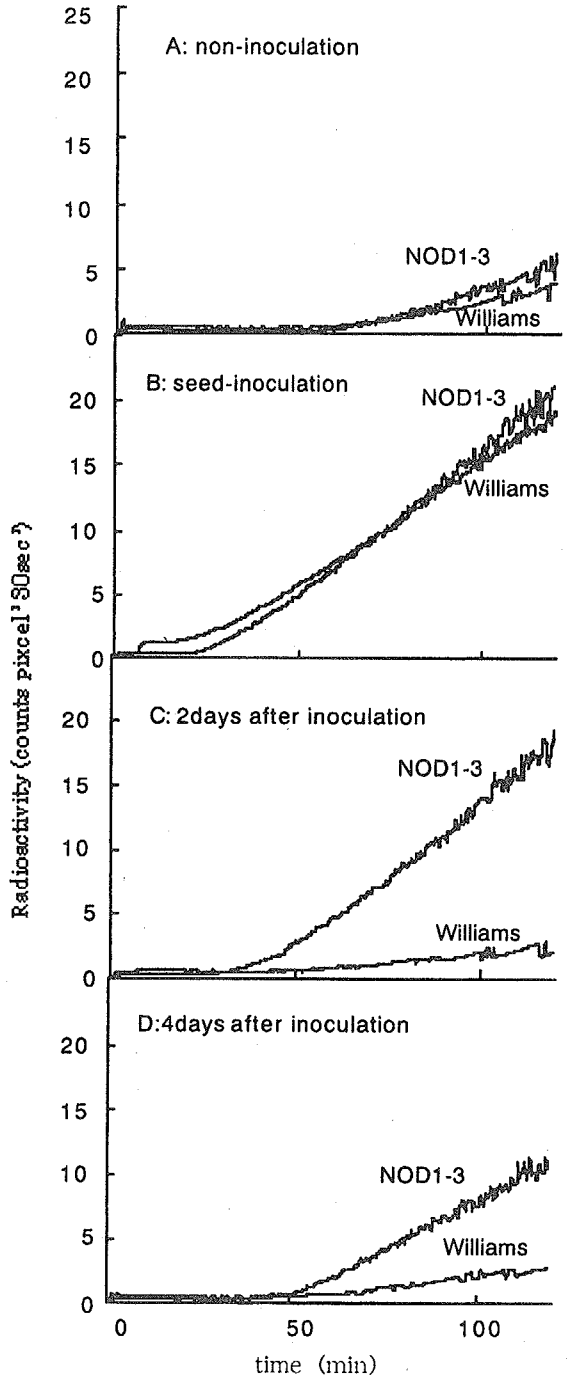

Figure1 Comparing radioactivity in root position of each treated NOD1-3 and Williams. $^{11}CO_2$ were supplized to first trifolite for 5 min then changed atomospheric air. The radioactivity was detected fro 120 min.

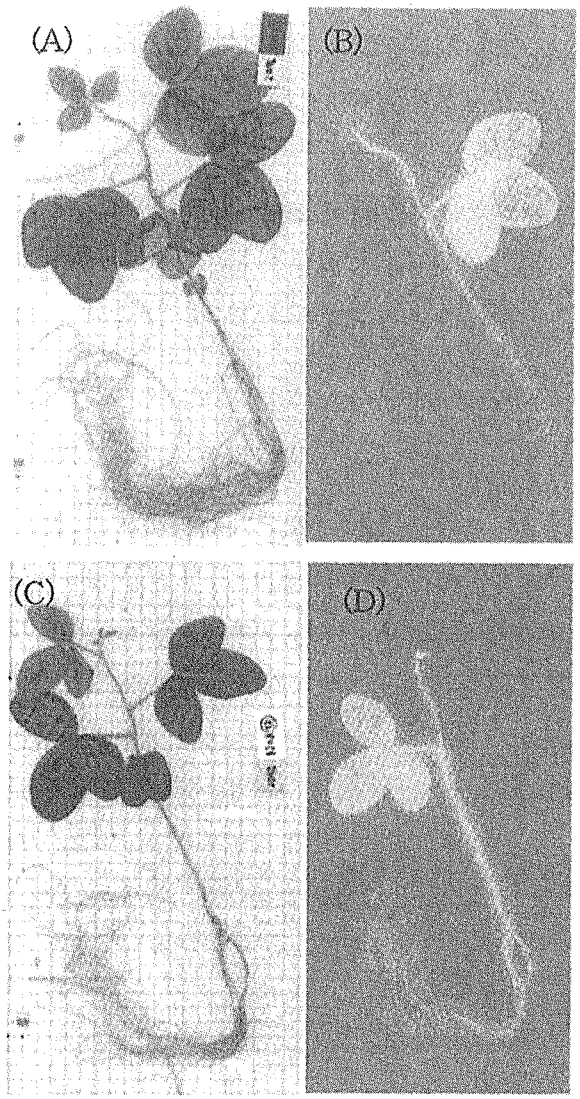

Figure 2 Distribution of radioactivity of whole plants 2 days after inoculate. (A) and (C) were the photo, and (B) and (D) were the BAS image of Williams and NOD1-3, respectively.

first trifoliate for 5 min, and transport of ^{11}C in the root and shoot was monitored using a PETIS for 120 min. The distribution of radioactivity in whole plants was detected by bio imaging analyzer system (BAS).

3. Results and Discussions

By application of $^{11}CO_2$ to the first trifoliate leaf of the non-inoculated Williams and NOD1-3, ^{11}C was scarcely detected in the

root. When $^{11}CO_2$ was supplied to the first trifoliate of seed inoculated Williams and NOD1-3 which had active nodule, the radioactivity was detected high level in the root position. This result indicates that a high level of photosynthetic products was supplied to the nodulated root (Fig 1). On the other hand, application to NOD1-3 trifoliate of the 2 and 4 days after inoculation resulted in high translocation of ^{11}C to the root position compared with Williams. Figure 2 shows the BAS images of distribution of radioactivity in whole plant treated 2 days after inoculation of Williams (A and B) and NOD1-3 (C and D). The radioactivity was highly accumulated in root position in NOD1-3 compared with Williams.

Calvert et al.[1] reported the early nodule development as follows; Stage I is characterized by the anticlinal division of a hypodermal cell into four to eight daughter cells (within 6 hours). By stage II, cortical cells in the outermost layers had divided anticlinally six to eight times (within 36 hours). By stage III, cell division activity was evident in the inner cortex as well (within 48 hours). By stage IV, divisions within the inner and outer cortex were relatively equal and a nodule meristem had formed (within 60 hours). At stage V the meristem had enlarged to involve a volume with a radius of 75 μm (within 72 hours). Gerahty et al.[2] showed that major control points appear to be correlated with significant changes in root cell activity such as an increase in cytoplasmic content of dividing cortical cells and cell division activity in the inner cortex (cell division stage III) and the formation of a meristem and onset of periclinal cell division (cell division stage IV-V).

In our experiments, it was suggested that there is some relationship between autoregulatory control and distribution of photosynthetic products in early inoculation stage.

References

1) Calvert H. E., Pence M. K., Pierce M., Malik N. S. A. and Bauer W. D., 1984. Can. J. Bot., 62, 2375-2384.

2) Gerahty N., Caetano-Anolles G., Joshi P. A. and Gresshoff P. M., 1992. Plant Sci., 85, 1-7.

2.33 Phloem Transport of ^{52}Fe from the Discrimination Center to Immature Sink was Suggested by ^{52}Fe Translocation in Barley Plants under Dark Condition

T. Tsukamoto*, H. Nakanishi*, S. Kiyomiya*, S. Watanabe**,
N. S. Ishioka**, S. Fujimaki**, S. Matsuhashi**, T. Kume**,
N. K. Nishizawa***, **** and S. Mori*
Department of Applied Biological Chemistry, The University of Tokyo*,
Department of Ion-Beam-applied Biology, JAERI**,
Department of Global Agricultural Sciences, The University of Tokyo***
Core Research for Evolutional Science and Technology (CREST)****

1. Introduction

Iron is required for many functions in plants, including heme and chlorophyll biosynthesis, photosynthesis, and as a component of Fe-S cluster containing enzymes. Although abundant in soils, iron often forms highly insoluble ferric-hydroxide precipitates that limit its availability for plants. Therefore, plants have evolved mechanisms to solubilize and to efficiently take up iron. Graminaceous plants release mugineic acid family phytosiderophores (MAs) into the rhizosphere that bind Fe(III) ion and are then taken up into the roots. Then, Fe is transferred to the shoot via xylem transport driven by transpiration and root pressure and unloaded to the leaves. However, the mechanism of Fe translocation in intact plants is still unclear.

We compared the real time ^{52}Fe translocation in the intact barley plants by a Positron-Emitting Tracer Imaging System (PETIS) under light and dark condition.

2. Experimental procedure

2.1 Plant material

Barley (*Hordeum vulgare* L. cv. Ehimehadaka no.1) seeds were germinated at room temperature (ca 24°C) on paper towels soaked with distilled water. After germination, the plantlets were transferred to a plastic net floating on water in a growth chamber under a mixture of incandescent and fluorescent lamps with a 14 h light (20 °C)/10 h dark (15 °C) regime and a photon flux density of 320 μmol $m^{-2} s^{-1}$. After two days, the plants were transferred to modified Kasugai's medium: 0.7 mM K_2SO_4, 0.1 mM KCl, 0.1 mM KH_2PO_4, 2.0 mM $Ca(NO_3)_2$, 0.5 mM $MgSO_4$, 10 μM H_3BO_3, 0.5 μM $MnSO_4$, 0.2 μM $CuSO_4$, 0.5 μM $ZnSO_4$, 0.01 μM $(NH_4)Mo_6O_{24}$, 0.1 μM Fe-EDTA. The pH was adjusted daily to 5.5 with 1 N HCl or NaOH, and the nutrient solution was renewed once a week. For Fe deficiency, the plants were transferred to the culture solution without Fe, respectively, one week before the beginning of the experiments. The absorption experiments were performed at about 3 weeks after germination.

2.2 Production of ^{52}Fe

^{52}Fe (half life: 8.27 h) was produced by the ^{52}Cr (α, 4n) ^{52}Fe reaction by bombarding a 1.5 mm thick Cr foil (natural isotopic composition, 99.9% purity, Goodfellow Metals Ltd.) with a 100-MeV α beam from the TIARA AVF cyclotron.

Using a beam current of 3 μA for 2 hours, about 1 MBq of ^{52}Fe was produced. The radiochemical separation of the ^{52}Fe from the target was carried out with a method described by Watanabe et al. (2002)[1]. After the pH of the $^{52}Fe^{3+}$ solution without cold Fe was adjusted to about pH 3 with 1 M KOH, the $^{52}Fe^{3+}$ was chelated with 197.4 μmol of deoxymugineic acid (DMA) in the dark for one hour.

2.3 Experimental setting up for ^{52}Fe translocation in the plant

An Fe-deficient barley plant in the culture solution was kept in the dark for 13 hours. Then $^{52}Fe^{3+}$-DMA (0.54 MBq, 38.5 fmol) was supplied from the roots under dark condition. Another Fe-deficient barley plant was also prepared and analyzed simultaneously under light condition (320 μmol m^{-2} s^{-1}) in another chamber. The 'DC' (discrimination center) [3),6)] parts were monitored by PMPS (positron multi-probe system) [4]. After 6 hours PETIS-analysis, BAS image-analysis of whole body and quantitative analysis of plant parts by Gamma-ray spectrometry were performed. In Fe-sufficient barley plants, the simultaneous experiments were performed as Fe-deficient barley plants. In PETIS analysis, the experiments were repeated at least three times for one treatment to confirm the reproducibility of the results.

3. Results and discussion

Although ^{52}Fe translocation from the roots to the old leaves was suppressed under dark condition in both Fe-sufficient and Fe-deficient barley, ^{52}Fe translocation to the basal parts of the shoot known as DC, the leaf sheath and the youngest leaf was not suppressed (Fig. 1A, 1B). The translocation pattern of ^{52}Fe in Fe-deficient barley under dark and light conditions (Fig.1C, 1D) was also the same as in Fe-sufficient barley. Therefore, in order to analyze by the better SN ratio, we analyzed Fe-deficient barley. In the DC, while the rate of ^{52}Fe accumulation of Fe-deficient barley under light condition has decreased from after 120 min, the rate of ^{52}Fe accumulation under dark condition was constant (Fig. 2A). In the parts of main shoot, the rate of ^{52}Fe accumulation under light condition was more than that under dark condition (Fig. 2B). Interestingly in the youngest leaf, ^{52}Fe

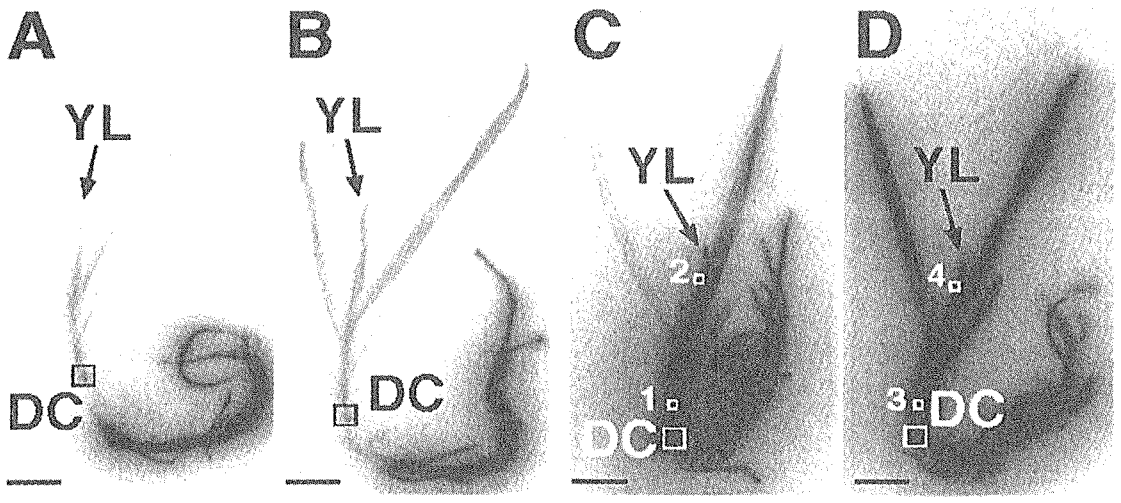

Figure 1. BAS images of ^{52}Fe translocation in barley plants under dark or light conditions.

YL, youngest leaf; DC, discrimination center; bar =4 cm. A.Fe-sufficient barley under dark condition. B.Fe-sufficient barley under light condition. C.Fe-deficient barley under dark condition. D.Fe-deficient barley under light condition.

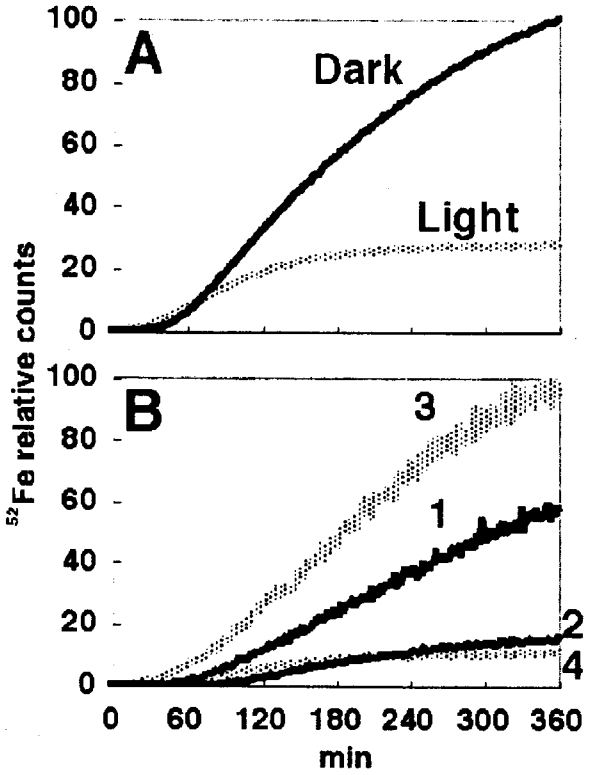

Figure 2. Time-course of ^{52}Fe translocation in Fe-deficient barley under dark or light conditions. **A**,Time-course study for the incorporation of radioactivity into the DC. Dark, dark condition; Light, light condition. **B**,The curve showing the accumulation of radioactivity for each position in Fig. 1C and 1D using PETIS analysis. No. 1 and No. 3 are the parts of the main shoot of Fe-deficient barley under dark and light conditions, respectively. No. 2 and No. 4 are the parts of the youngest leaf of Fe-deficient barley under dark and light conditions, respectively.

accumulation was not decreased by dark treatment.

We show ^{52}Fe content in each part of the plants by Gamma-ray spectrometry (Fig. 3). ^{52}Fe was accumulated in the DC of Fe-deficient barley under dark condition about 2 times higher than under light condition. While ^{52}Fe translocation in Fe-deficient barley under dark condition was suppressed in the oldest leaf blade, the second oldest leaf and the 3rd leaf blade, it was not suppressed in the oldest leaf sheath, the second youngest leaf sheath and the 4th (youngest) leaf.

These results suggest that barley plants

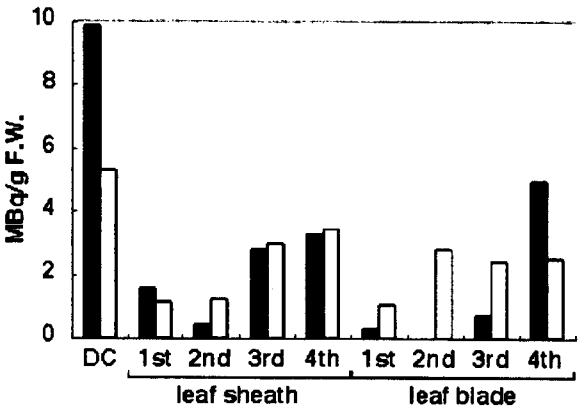

Figure 3. Distribution of ^{52}Fe into each parts of Fe-deficient barley plants. black bar, dark condition; white bar, light condition.

absorb iron under dark condition and iron translocation to the DC, the leaf sheath and the youngest leaf blade is not affected by dark condition. We have already shown that $H_2{}^{15}O$ translocation from the roots to the shoot of rice under dark condition was almost completely suppressed[2,5]. Therefore, Fe translocation from the roots to the strong sink such as the youngest leaf blade was less affected by the transpiration stream, suggesting the phloem transport of ^{52}Fe is the dominant routes from the roots throughout DC to the immature organ(s).

References

1) S. Watanabe et al., *Radiochimica Acta* 89: 853-858 (2001)
2) S. Kiyomiya et al., *Physiologia Plantarum* 13: 359-367 (2001)
3) H. Nakanishi et al., *J. Exp. Bot.* 50: 637-643(1999)
4) S. Kiyomiya et al., *Plant Physiology* 125: 1743-1753(2001)
5) S. Mori et al., *Soil Sci. Plant Nutr.* 46:975-979(2000)
6) H Nakanishi et al., *Soil Sci. Plant Nutr.* 48: 759-762(2002)

2.34 Effects of heavy-metal (Cd) stress on ^{11}C distribution and the detection of ^{105}Cd and ^{107}Cd distribution in rice plants

H. Hayashi*, N. Suzui*, S. Matsuhashi**, N. S. Ishioka**,
S. Fujimaki, T. Watanabe**, T. Kume**
Department of Applied Biological Chemistry, Univ. Tokyo*,
Department of Ion-Beam-Applied Biology, JAERI**

1. Introduction

Sieve tubes are the main routes for long distance transport of photoassimilates, such as sucrose and amino acids, in plants. This phloem transport process of photoassimilates is affected by the surrounding conditions. Other than these main transport materials, Cd is also thought to be transported to grains through sieve tubes when rice plants grew on Cd contaminated soils.

Cd accumulation in rice grains represents a concern to consumers. To understand the mechanisms of internal translocation of Cd in rice plants may offer a way to reduce Cd accumulation in grains.

To know the effects of Cd on the phloem transport in rice plants, we have established the experiments for detailed analysis of phloem transport, such as photoassimilate-partitioning patterns, by a positron-emitting tracer imaging system (PETIS). Moreover, we produced ^{105}Cd and ^{107}Cd for the application to rice roots and the detection of Cd transport in rice plants.

2. Experiments

Rice plants (*Oryza sativa* L. var. Kantou) were grown in a complete nutrient solution. The plants at 9th-leaf stage and at 10 days after anthesis were used for the experiments. Cd was applied to rice roots at the concentration of 10 or 100 μM in the nutrient solution for 1 day before experiments.

Around 100 MBq of $^{11}CO_2$ ($^{14}N(p,\alpha)^{11}C$) was applied to the small absorption chamber containing the tip of 7th leaf blade of rice plant for 10 min. Just after the absorption started, the ^{11}C-compounds distribution was detected by PETIS at the leaf sheath position.

^{105}Cd and ^{107}Cd ($^{107}Ag(p,3n)^{105}Cd$, $^{109}Ag(p,3n)^{107}Cd$) was applied to rice root of 10 days after anthesis. ^{105}Cd and ^{107}Cd were applied at 0 and 24 hrs of experiment start and at 48hrs, Cd distribution to shoots was detected by BAS.

3. Results and discussion

Detection of ^{11}C-compounds by PETIS is useful to discuss the effects of environmental stress on the long distance phloem transports of photoassimilates, specially the rate of transport and the pattern of photoassimilate distributions. In this experiment, effects of Cd on the ^{11}C distribution were measured directly by PETIS.

Figure1-B and C show the PETIS images of the absorption and translocation of ^{11}C-compounds during experiments. The absorbed ^{11}C-compounds at the leaf blade were transported only to the leaf sheath direction,

namely to the leaf sheath, not to the tip of the leaf blade. Absorbed $^{11}CO_2$ was metabolized at the leaf blade and translocated to the bottom of the leaf sheath within 16 min. in control plant (Fig.1 B control, position b). On the other hand, activity in position b in the Cd treated plant started to increase at 21 min. after ^{11}C application start (Fig.1 C Cd-treated, position b).

When Cd was applied to plants through roots, many metabolic pathways in plants were affected, for example, nitrogen assimilation (Chien et al. 2002)[1]. In this experiment, we found that the arrival of ^{11}C assimilates to the base of leaf sheath of Cd treated rice plants delayed around 5 min compared with that of control rice plants when the $^{11}CO_2$ was applied to the leaf blade. This delay suggested that Cd treatment affected the processes of photoassimilate and/or translocation although the visible damages of 10 μM Cd treatment was not observed in rice plants.

As shown in Fig.2 B, Cd transported from root was accumulated at the node and the Cd movement beyond the node was hardly inhibited.

We recently analyzed the Cd concentrations in both xylem exudate and phloem sap of rice plants treated with 10 and 100 μM Cd for 3days. From that experiments, Cd concentration in the phloem sap (4.6 ± 3.4 and 17.7 ± 9.8 μM, respectively), was significantly lower than that in the xylem exudates (18.9 ± 6.4 μM and 64.2 ± 14.6 μM, respectively), indicating that Cd is not concentrated during the transfer from xylem to phloem (Tanaka et al. 2003)[2]. Our present results is consistent with the analysis of saps above, namely that the Cd transported through xylem vessels are thought to be precipitated at the node and lower concentration of Cd in xylem vessels are moved to leaf where Cd may be transferred to phloem. Alternatively, Cd after precipitated at node directly move to phloem there.

In rice plants, most of Cd absorbed from roots was accumulated in root and only small parts of Cd in roots were transported to shoots, indicating the existence of a barrier between root and shoot. In shoots, Cd translocation was inhibited at the node, indicating that the node is also a barrier for the translocation of Cd, possibly for xylem transport.

It is very important to know the Cd distribution in rice plant more detail. In this experiments, we can not detect the Cd distribution patterns in rice shoots by PETIS. We need to apply more concentrated positron emitting Cd tracer for PETIS or, to accelerate the Cd absorption in root by applying an appropriate chelator.

4. References

1) Chien HF, et al. Plant Growth Regul. 36:41-47 (2002)

2) Tanaka K, et al. Soil Sci. Plant Nutr. 49:311-313 (2003)

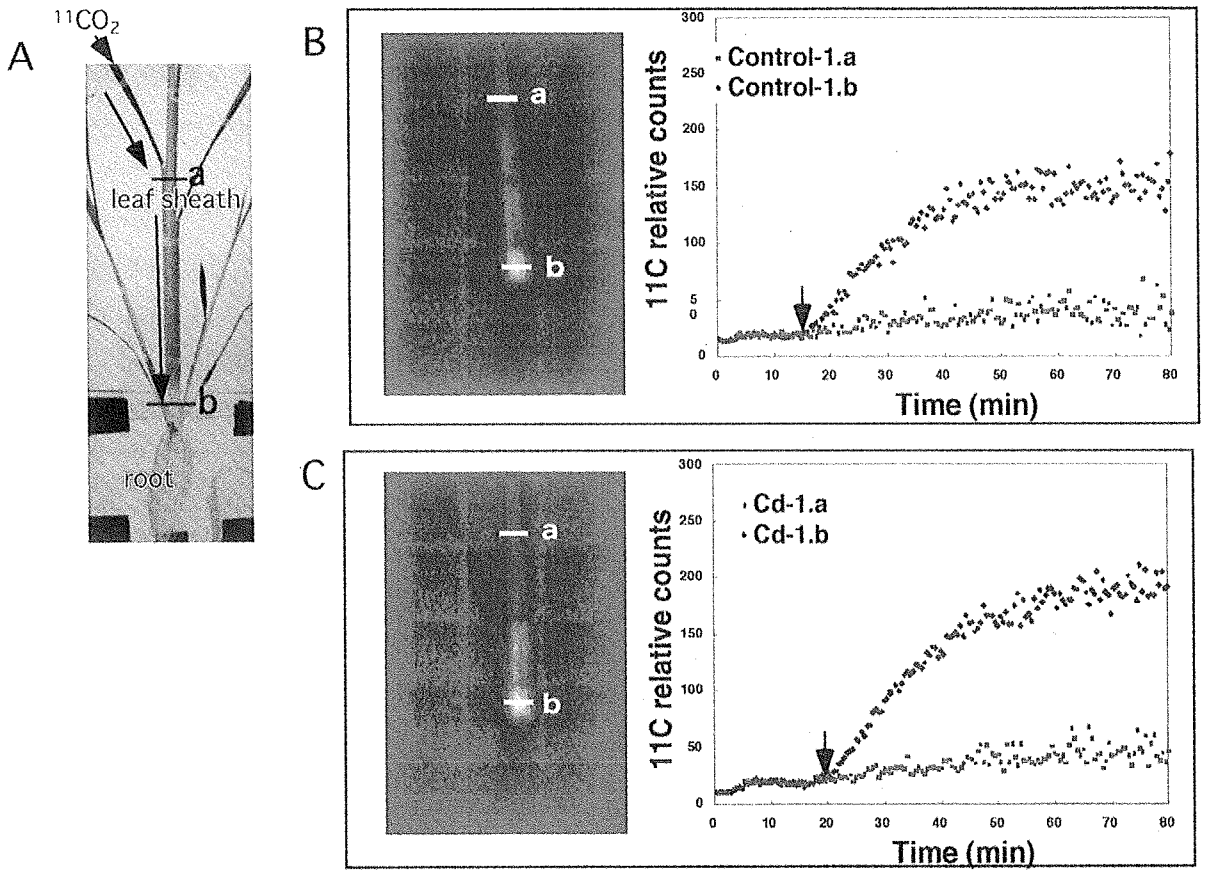

Fig.1 Effects of Cd on the long distance transport of ^{11}C assimilates in rice plants

A: Picture of experiment. $^{11}CO_2$ was applied to leaf blade. This area was mesured by PETIS. B: PETIS image of control plants.At position a and b in leaf sheath, activity was measured and plotted. C: PETIS image of Cd treated plants. Arrows in B and C showed the time when activity at b started to increase.

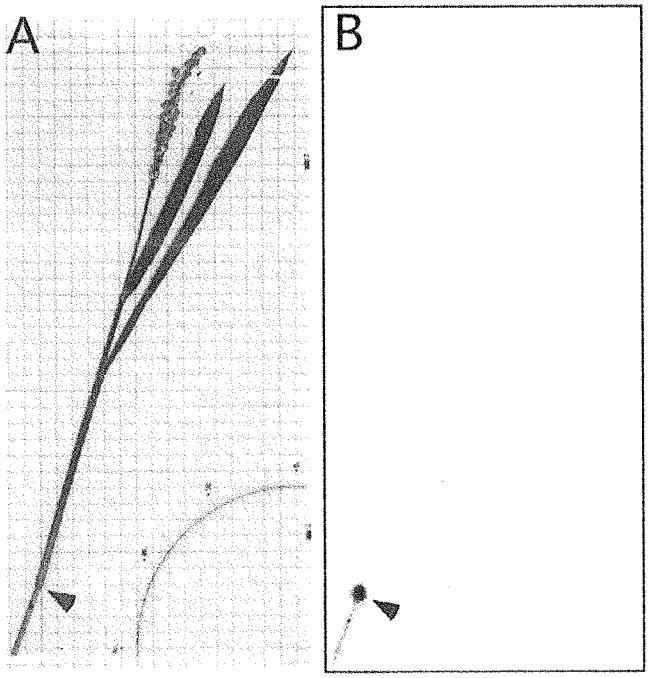

Fig.2 Distrbution of Cd in rice shoot

A: Picure of rice shoot. B:BAS image of the shoots Arrow indicated the node.

2.35 The uptake pattern of ^{48}V labeled vanadate in phosphate-deficient soybean

Y. Hayashi*, J. Furukawa**, T. M. Nakanishi*, N. S. Ishioka***,
S. Fujimaki***, S. Matsuhashi***, T. Sekine****, and T. Kume***
Department of Applied Biological chemistry, The University of Tokyo*
Faculty of Agriculture, Kagawa University**
Department of Ion-Beam-Applied Biology, JAERI***
Department of Irradiation Technology and Public relation, RADA****

1. Introduction

Phosphate plays an important role in plant metabolism. However, P is the least accessible macronutrient in many ecosystems and its low availability often limits plant growth[1]. Plants have evolved an array of molecular and morphological adaptations to cope with P limitation, but they have not been clarified yet. Since P has no positron emitting nuclides, it has been impossible to perform real-time studies with intact plants to analyze phosphate uptake through a Positron Emitting Tracer Imaging System (PETIS). We selected vanadate labeled by ^{48}V, as an analog for phosphate, and tried to examine phosphate uptake mechanism, especially focusing on expression of root phosphate transporters and phosphate distribution system.

2. Experimental Procedure

Soybean (*Glycine max* (L.) Merr.) seeds were germinated on vermiculite and cultured hydroponically in a growth chamber at 28℃ with 70% humidity, under 12h-light / 12h-dark condition. Plants were transferred to P-deficient solution for 5 days before experiments, and to study the recovery of phosphate uptake, plants cultured in P-deficient solution for 4 days, were supplied with phosphate solution which concentration was 5 times higher than that of control solution a day before the experiment. The ^{48}V uptake experiments were observed after three weeks of germination.

A Sc target, 500 μm in thickness, was irradiated by a proton beam (18.2MeV) to produce ^{48}V through by a TIARA AVF cyclotron. After 12.5 hours irradiation with the beam current of 2.6 μA, about 30MBq of ^{48}V was produced. The chemical separation of the ^{48}V from the target was carried out using a cation exchange column.

Two sample plants were supplied with 15ml of culture solution in respective polyethylene bags, and they were fixed on an acrylic board. The board was placed at the center, between a pair of PETIS detectors. Then ^{48}V was added to the culture solution. To prepare a dark condition, the detection chamber was covered with aluminum foil. After 8h measurements, the plants were

removed from the polyethylene bags and the roots were cut down. The upper part of each plant was placed on an IP, imaging plate (Fuji Film, Tokyo, Japan) inside a cassette. After 2 hours, the image in the plate was scanned by an image analyzer (BAS-1500, Fuji Film, Tokyo, Japan).

3. Results and Discussion

In soybeans, ^{48}V labeled vanadate was absorbed and translocated to the whole plants after 8h treatment, suggesting that phosphate was replaced with vanadate on its absorption mechanism in plant. The ^{48}V radioactivity in a plant was detected 30minutes after the supply of ^{48}V. Phosphate-deprived plants absorbed ^{48}V labeled vanadate more quickly than that of the control (Fig. 1). On the contrary, the vanadate uptake activity by P-deficient plant was the same level as that of control under dark condition (data not shown). The results indicated that vanadate (as phosphate) was distributed to shoot and

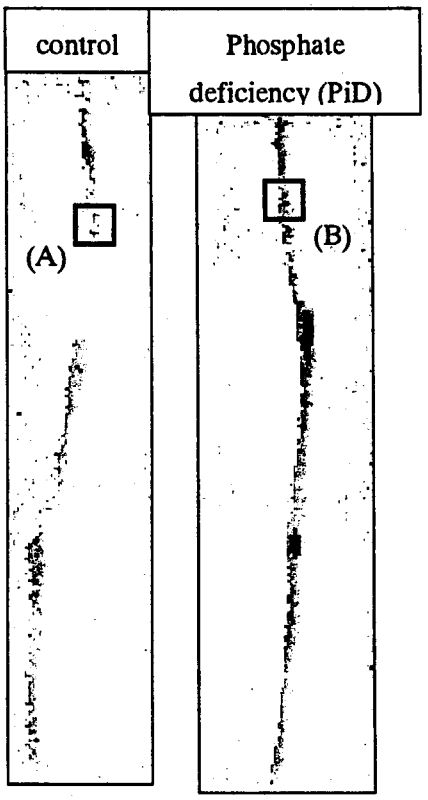

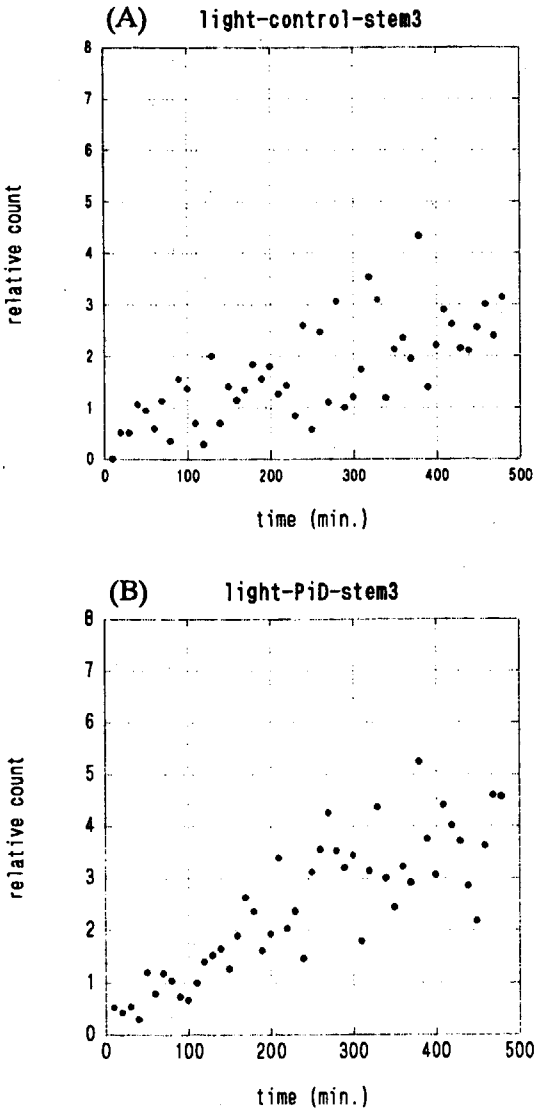

Fig.1 ^{48}V uptake manner in a soybean plant. The counts of ^{48}V were detected with IP in every 10 minutes under light condition. Left: control. Right: phosphate-deprived plant.

leaves mainly by transpiration current.

Enhanced vanadate uptake activity was continued for at least 8 hours. In the case of the plants, cultured in P-deficient solution and then supplied with phosphate again at the day before the experiments, ^{48}V radioactivity detected in P-deficient plants was apparently higher than that of control after 8 hours (data not shown).

It has been reported that to resupply phosphate to phosphate-deprived plants, the expression of genes encoding phosphate transporters found in *Arabidopsis* was down-regulated and the steady-state mRNA levels corresponding to these genes were decreased rapidly [2),3)]. However, we could not confirm the negative feedback regulation system on this experiment. The different phosphate concentration or treatment time should be taken in account for the next experiment.

Though the image taken by IP provides higher resolution than that by PETIS, PETIS was shown to be an effective method for real-time observation with intact plants. To study the distribution and accumulation manner of vanadate related to phosphate and the other nutrients, more in detail, it is necessary to carry out repeated experiments with this system.

References

1) F. D. Dakora, and D. A. Phillips, Plant and Soil 245: 35-47, 2002

2) F. W. Smith, A. L. Rae, and M. J. Hawkesford, Biochimica et Biophysica acta Biomembranes 1465: 236-245, 2000

3) F. W. Smith, Plant and Soil 245: 105-114, 2002

2.36 Negative-feedback Regulation of Ammonium Uptake and Translocation in Rice under Ambient and Elevated CO_2 Conditions

J. Yamaguchi*, S. Ohtsuki*, Y. Sonoda*, C. Yamamuro*, A. Ikeda*,
S. Fujimaki**, N. S. Ishioka**, S. Matsuhashi**, T. Sekine** and T. Kume**
Division of Biological Sciences, Graduate School of Science, Hokkaido University*
Department of Ion-Beam-Applied Biology, JAERI**

1. Introduction

Inorganic nitrogen (N) uptake by plant roots is subject to strict regulation according to whole plant demand[1]. The enhancement of NH_4^+ uptake is reported in whole plant level of rice by real time using Positron Emitting Tracer Imaging System (PETIS) [2]. Increase in 25 to 40 % for nitrogen influx of root peaked at 2 h exposure to NH_4^+ after nitrogen deprivation was correlated with a 4- to 5-fold enhancement in the translocation of shoot in rice. Evidently, when nitrogen supply is sufficient, negative-feedback mechanisms which down-regulate the uptake in roots would be expected, while de-repression of plasma membranc transport occurs when nitrogen is withdrawn during starvation[3]. There has been much debate in the literature as to whether NO_3^- and NH_4^+ themselves or rather downstream products of nitrogen assimilation, such as glutamine and other amino acids, are the more potent negative-feedback factors in this regulation of the membrane transport[1].

We report in this communication the effect of elevated CO_2 on nitrogen uptake and translocation to the shoot of rice.

2. Experimental procedures

2.1 Plant Materials and Growth Conditions

Rice (*Oryza sativa* L. cv Nipponbare) plants were grown hydroponically in an environmentally controlled growth chamber equipped with a CO_2 partial pressure controller. The chamber was maintained with a 14-h photoperiod, 25/20°C day/night temperature. Rice seeds were soaked in tap water at 28°C for 2 d, and the seedlings were grown for 19 d on a net floating on a tap water.

Four seedlings were transplanted to each of 3.5-L plastic pots containing nutrient solution. The basal nutrient solution was as previously described by Makino et al[4]. The solution was renewed once a week. The plants that prepared for long-term CO_2 enrichment experiments were grown under two CO_2 partial pressures, 36 and 110 Pa for 2 to 3 weeks.

2.2 $^{13}NH_4^+$ Synthesis

The radiotracer ^{13}N (half-life = 9.96 min) was produced in the cyclotron at TIARA by proton irradiation of water. This procedure was described in detail [2].

2.3 Ammonium translocation activity measurement under distinct CO_2 partial pressures

To study $^{13}NH_4^+$ uptake and translocation from roots to whole plant, the roots of a single plant were placed in a 16 cm height glass test tube that contained 20 mL of culture solution without nitrogen source. $^{13}NH_4^+$ (50 MBq, carrier-free in 5 mL) was added to the culture solution after synthesis with gentle aeration for immediate mixing. The light intensity was 500 μmol $m^{-2}s^{-1}$ unless otherwise described. The PETIS analysis performed under ambient conditions described in detail[2]. For nitrogen-deficiency treatment,

plants were transferred to culture solution without nitrogen source for 2-3 d under continuous CO_2 partial pressures of 36 and 110 Pa, respectively. After nitrogen-deficiency experiments, the same rice plant was treated with 1 mM NH_4NO_3 or 2 mM glutamine for 2 h as the nitrogen source under ambient conditions.

3. Results and Discussion

Uptake and translocation for NH_4^+ was sequentially measured to the rice plant with nitrogen-deficient treatment and 2 h pretreatment with 1 mM NH_4NO_3 application. The translocation of NH_4^+ in rice with NH_4NO_3 treatment was down-regulated as a half amount to that in nitrogen-deficient plant under 36 Pa CO_2 conditions (Fig. 1A), while the NH_4NO_3 treatment enhanced the translocation to 4-fold than the control (nitrogen-deficient) under 110 Pa CO_2 conditions (Fig. 1B).

Enhancement of nitrogen uptake and translocation was observed for both NO_3^-- and NH_4^+-pretreated plants after nitrogen deprivation[2]. The enhancement of nitrogen uptake and translocation by the NH_4^+ application was observed in the experiments using the plants under both ambient and elevated CO_2 conditions (data not shown). It has been also reported that 4- to 5-fold enhancement to nitrogen translocation to shoot by following re-exposure to NH_4^+ after nitrogen deprivation in rice. When nitrogen supply is sufficient, the uptake would be down-regulated by negative-feedback manners. After NH_4NO_3 treatment was exposed to the nitrogen-deprived plant for 2 h, the NH_4^+ translocation was down-regulated to 50% of the control levels of nitrogen deficiency under 36 Pa CO_2, while the translocation increased to 4 times of nitrogen deficiency under 110 Pa CO_2 (Fig. 1). Elevated CO_2 may provide enough carbon skeletons to assimilate NH_4^+ for plants. This negative-feedback might be caused by lack of the

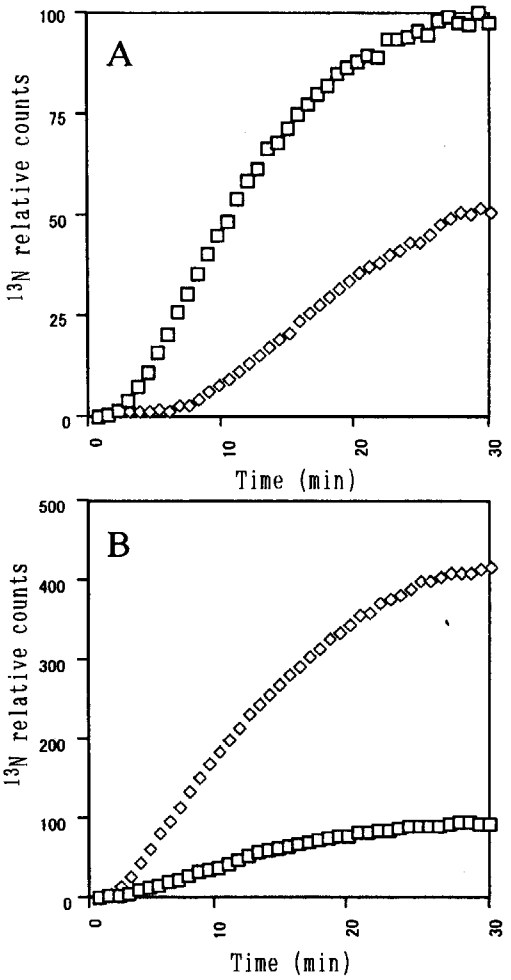

Fig. 1 Effect of NH_4NO_3 on $^{13}NH_4^+$ translocation conditions of 36 Pa (A) and 110 Pa (B). Nitrogen deficiency (□) and 1 mM NH_4NO_3 treatment (○) for 2 h.

carbon skeletons in nitrogen-depleted rice under ambient conditions, while enhanced nitrogen translocation under elevated CO_2 conditions would be still promoted by saturation of the pool for carbon skeletons derived from activation of photosynthesis.

Uptake and translocation for NH_4^+ was sequentially measured to the rice plant with nitrogen-deficiency treatment and 2h pretreatment with 2 mM glutamine (Fig. 2). Under 36 Pa CO_2 conditions, glutamine enhanced the NH_4^+ translocation to the shoot to 2-fold than that of control (nitrogen deficiency) (Fig. 2A), while glutamine suppressed the

translocation under 110 Pa CO_2 conditions (Fig. 2B). Moreover NH_4^+ translocation was sequentially measured to the same plant treated with 2 mM $(NH_4)_2SO_4$ for 1 h after 1.5 h incubation in nitrogen-free medium for cooling down of ^{13}N activity. The up-regulated translocation under 36 Pa CO_2 declined to 50% of that of the control (nitrogen-deficient plant) (Fig. 2A), while the down-regulated translocation restored to the control levels under 110 Pa CO_2 (Fig. 2B).

Suppression to the nitrogen translocation by $(NH_4)_2SO_4$ treatment under 110 Pa CO_2 in Fig. 2B may result in the similar negative-feedback to the ambient-grown rice under nitrogen starvation as shown in Fig. 1A. The capacity to uptake and translocation of NH_4^+ to shoot might be influenced by the availability of carbon skeletons (in particular α-ketoglutarate) and thus depend upon photosynthetic activity when the plant is subjected to nitrogen deprivation. Glutamine treatment would not reduce the accumulated carbon skeletons. Negative-feedback regulation was only observed in the plant under elevated CO_2 with 2 h glutamine treatment followed to the nitrogen starvation (Fig. 2B). Because limited levels of photosynthesis activity in the ambient rice may lead the plant to keep insufficient status for nitrogen sources, and glutamine treatment would not be enough to saturate the nitrogen demand without any feedback inhibition. However under elevated CO_2 conditions, negative-feedback regulation to the translocation might occur by glutamine treatment because of the saturation of nitrogen demand.

Further experiments will be needed to evaluate the hypothesis.

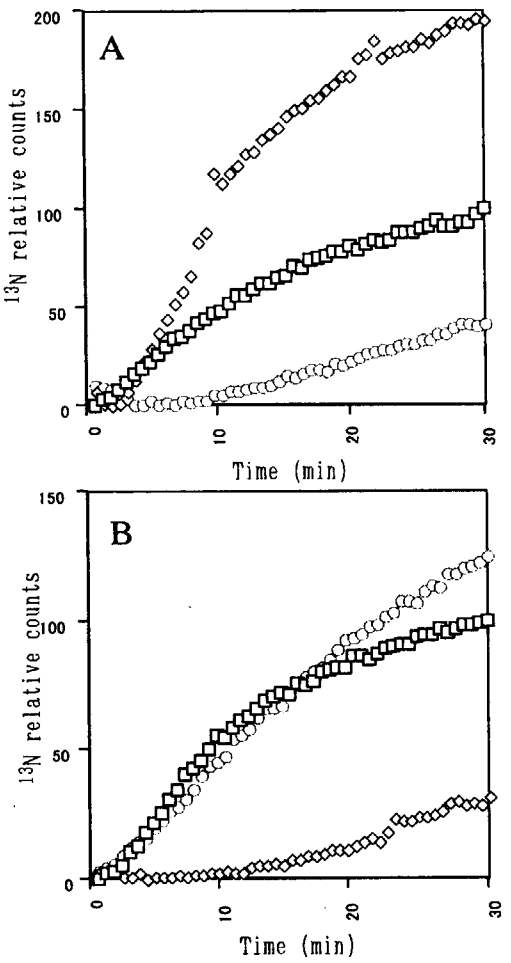

Fig. 2 Effect of glutamine on $^{13}NH_4^+$ translocation in rice under 36 Pa (A) and 110 Pa (B) CO_2 conditions. Nitrogen deficiency (□), 2 mM glutamine treatment for 2h (◦) and subsequently 2mM $(NH_4)_2SO_4$ treatment for 1h ( ).

References

1) N. M. Crawford, A.D. M. Glass, Trends in Plant Science 3 (1988) 389-395.
2) S. Kiyomiya, H. Nakanishi, H. Uchida, A. Tsuji, S. Nishiyama, M. Futatsubashi, H. Tsukada, N. S. Ishioka, S. Watanabe, T. Ito, C. Mizuniwa, A. Osa, S. Matsuhashi, S. Hashimoto, T. Sekine, S. Mori, Plant Physiology 125 (2000) 1743-1754.
3) Y. Sonoda, A. Ikeda, N. Von Wiren, T. Yamaya, J. Yamaguchi Plant Cell Physiology 44 (2003) 726-734.
4) A. Makino, T. Mae, K. Ohira Planta 174 (1988) 30-38.

2.37 Real time-monitoring for translocation and perception of signal molecules in *Arabidopsis thaliana* mature plant

Takuya Furuichi*, Shinpei Matsuhashi**, Noriko S. Ishioka**,
Syu Fujimaki**, Shigeo Ohtsuki**, Toshiaki Sekine**, Tamikazu Kume**
and Shoshi Muto*
Nagoya University Bioscience Center, Nagoya University*
Department of Ion-beam-applied Biology, JAERI**

1. Introduction

In planta, photosynthesized sugars are utilized not only as carbon sources but also as signal molecules for growth and development. We have shown that sucrose fed to the root of an autotrophically grown *A. thaliana* intact whole plant containing aequorin in its cytosol caused weak luminescence moving from the lower to the upper leaves.[1] The moving rate of aequorin luminescence was roughly comparable to that of ^{14}C-labeled sucrose, suggesting that sugar signal was converted to Ca^{2+} signal. However, precise relationship between sugar transport and aequorin luminescence was obscure. In the present study, we have established a simultaneous real time imaging system for movements of sugar molecules and aequorin luminescence in *A. thaliana* mature plants, which consists of a PETIS (positron emitting tracer imaging system) for measuring radioactivity of ^{18}F-deoxyglucose (^{18}FDG) and a VIM-camera system (a CCD camera equipped with an intensifier) for detecting aequorin luminescence.

2. Experimental procedure

2.1. Plant material

Seeds of *A. thaliana* (cv. Wassilewskija) expressing apoaequorin were sown on 0.3% gellan gum plate containing GM medium[2] with 1% sucrose (GM+Suc medium) and grown at 22°C under continuous light at 4,000 lux with day-light fluorescent lamps. Two-week-old intact plants were transplanted onto fresh plates containing GM medium deficient of sucrose (GM-Suc medium) and grown further 3 - 4 weeks under the same condition. In order to reconstitute aequorin, the roots of intact plants were washed with liquid GM+Suc or GM-Suc medium, and immersed in the same medium containing 2.5 μM coelenterazine overnight in the dark.[1]

2.2. Production of ^{18}FDG

^{18}FDG was synthesized at TIARA as following the method of Hmmacher *et al.*[3] with minor modification. After the synthesis and quantification of the product, ^{18}FDG was

immediately used for imaging by PETIS.

2.3. Absorption and Translocation of ^{18}FDG in plants

To study ^{18}FDG absorption from roots, the roots of a single plant were placed in a bottle containing 10 ml of the culture medium without sucrose. To maintain geometry, the stem and the canline leaves were settled onto a flexible net fixed by acrylic frames, and centered between the PETIS detectors[4]. To start positron-imaging, 5 ml of the medium was replaced with equal volume of flesh media containing 100 mM glucose and ^{18}FDG.

The PETIS detectors covered whole of the plant. The γ-rays emitted from decaying positrons from ^{18}F were counted over time using the coincident method with the paired detectors for 120 min. The data were automatically corrected using 110 min as the half-life of ^{18}F. To monitor $[Ca^{2+}]_{cyt}$ at the same time, positron-imaging was performed in the dark room kept at 22°C and 60% relative humidity.

2.4. $[Ca^{2+}]_{cyt}$ monitoring

The $[Ca^{2+}]_{cyt}$ (cytoplasmic Ca^{2+} concentration) level in the ^{18}FDG -treated plant was monitored with a ultra-sensitive VIM camera system (a charge coupled device camera equipped with an intensifier, Model C-1400-47; Hamamatsu Photonics Co., Hamamatsu, Japan). Luminescence images were processed with an Argus 50 imaging analyzer (Hamamatsu Photonics. Co.). For the dual-monitoring, the VIM camera and PETIS detectors were arranged as shown in Fig. 1. Experimental condition is as described above.

3. Results and discussion

Using this system, the movement of sugar molecules and the aequorin luminescence in leaves were simultaneously analyzed.

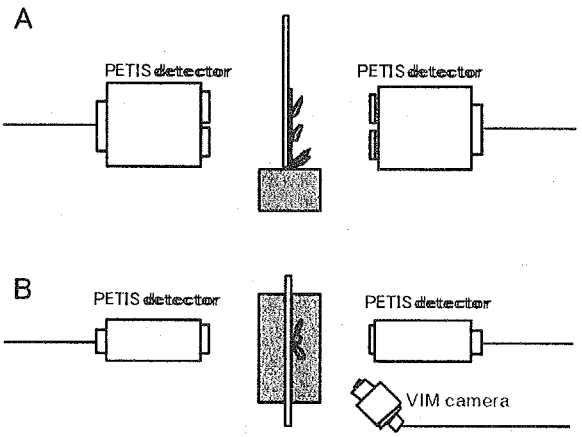

Fig. 1 Real-time imaging system combined with PETIS and ARGUS-50 imaging analyzer. **A,** Side view. **B,** Top view.

As shown in Fig. 2, ^{18}FDG was gradually taken up from root to upper part through the stem.

The uptake rate in the lowest pert (ROI-1) seems to be oscillated with periodicity (Fig. 3).

Because sugar molecule is co-transported into cells with H^+ and immediately phosphorylated in cytoplasm, we assumed that this periodicity is caused by the limitation of sugar uptake from media into roots. Interestingly, this periodicity was not observed in the knot (ROI-2) and upper part of the stem (ROI-3). Apparently the amount

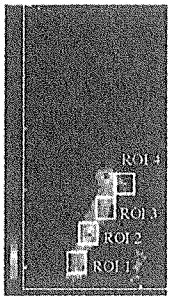

Fig. 2 ^{18}FDG distribution after 2 h absorption experiment in *A. thaliana* mature plant. Squared areas were; ROI-1 and 3; stem, ROI-2; knot, ROI-4; leaf.

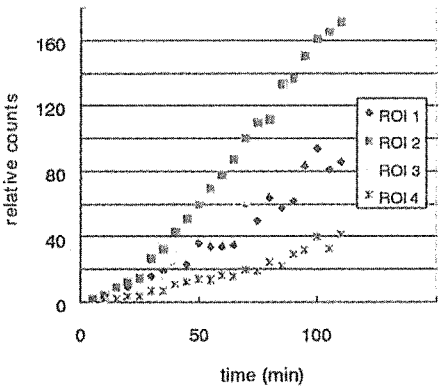

Fib. 3 Time-course study of the translocation of ^{18}FDG into the stem and the leaf. ^{18}FDG radioactivity curves at the numbered positions in Fig. 2.

of ^{18}FDG accumulated in the knot was higher than that of in the stem part. So we assumed that the knot part has the buffering capacity for sugars and minerals translocating in the plant, and regulates supply of solutes to the developing part. The time course of ^{18}FDG translocation in leaf (ROI-4) was roughly comparable to aequorin luminescence reflecting an increase in $[Ca^{2+}]_{cyt}$, though the intensity of the aequorin luminescence was very weak (data not shown). For detailed analysis of this, improvement of the monitoring system and analysis of the expression level of the genes for the sugar-transport and –metabolism are required.

References

1) Furuichi, T., Mori, I. C., Takahashi K. and Muto, S. (2001b) Plant Cell Physiology 42, 1149-1155.

2) Valvekens, D., Van Montagu, M. and Van Lijsebettens, M. (1988) Proceeding of the National Academy of Science of the United States of America 85: 5536-5540.

3) Hmmacher, K., Coenen, H. H. and Stoucklin, G. (1986) *J. Nucl. Med.*, 27, 235-238

4) Kiyomiya, S., Nakanishi, H., Uchida, H., Tsuji, A., Nishiyama, S., Futatsubashi, M., Tsukada, H., Ishioka, N., Watanabe, S., Ito, T., Mizuniwa, C., Osa, A., Matsuhashi, S., Hashimoto, S., Sekine, T. and Mori, S. (2001) Plant Physiology 125, 1743-1754

This is a blank page.

3. Radiation Chemistry / Organic Materials

This is a blank page.

3.1 SEM and conductometric studies of evolution of heavy ion tracks in PET during chemical etching

M. Asano, T. Yamaki, and M. Yoshida
Department of Material Development, JAERI

1. Introduction

Etching of ion tracks is a well-known method used for the production of nano- and micro-porous structures in commercial polymers[1,2]. The applications based on the ion track etching include microfiltration membranes, porous substrates, templates for the fabrication of small wires, tubules, capsules, sensors, microdevices, etc[3-7]. Most frequently, polyethyleneterephthalate (PET) and polycarbonate (PC) films have been employed as matrices, in which the ion tracks with desired sizes and geometries are chemically developed. A precise control of the track shapes requires a better understanding of the radiation chemical reactions induced by ion beams and the post-development processes. So far, much effort has been devoted to the investigations of pore growth in the nanometer and submicrometer range. Electrical conductivity was obtained for the ion-irradiated plastic films in the course of etching to evaluate transversal dimensions and morphologies of the damaged zone in the latent track[7-8]. These previous studies revealed that bombardment with heavy ions produced a track core and a track halo. The track core is a narrow cylinder with high-density defects, where the etch rate is considerably higher compared to the virgin material. The track halo is a region extended further in the radial direction; the etch rate in this region changes slowly with the increasing radius. As found from the conductometric experiments, the halo is large enough to be analyzed by other techniques, for example, scanning electron microscopy (SEM). Such a microscopic study of the tracks would be essential because the conductometric analysis is one of the indirect methods and the resulting data remain unconfirmed. In principle, the effective pore size estimated from the conductometry is the average of the radii all over the etched track. Some tracks appear not to be ideally cylindrical when their chemical etching stops just after the breakthrough time of the film (Tb), and this leads to large and serious experimental errors in radius estimations. Direct observations of the track-etch pores, therefore, will be of great importance.

According to our conductometric measurements, the damaged region was found to consist of the track core and halo as mentioned above. In order to confirm this result, it is necessary to examine changes in the membrane morphology during the etching process. The present work aims to clarify the existence of the track core and halo by a direct observation of the track-etched membranes using a SEM. A conductometric method was also used to determine Tb of our ion track etched samples.

2. Experimental

The PET films were irradiated with $^{84}Kr^{20+}$, $^{84}Kr^{17+}$, $^{129}Xe^{23+}$ and $^{197}Au^{31+}$ ions of 6.2, 3.8, 3.5 and 2.5 MeV/n, respectively, from an AVF cyclotron in the TIARA, JAERI (Takasaki, Japan) and $^{197}Au^{30+}$ ions of 11.4 MeV/n from a linear accelerator, UNILAC, of GSI (Darmstadt, Germany). The irradiated films were etched in a 0.2 M NaOH aqueous solution at 70 °C without stirring. The samples were etched in a

conductometric cell made of Teflon. The etching was monitored by simultaneous measurements of the electric conductivity through the membranes using a conductometer (712, Metrohm Ltd., Switzerland) to determine the Tb value. The pore diameter was estimated by the SEM observations.

3. Results and discussion

Figure 1 shows the plot of average pore diameters determined by SEM against etching time. There is a difference in the etch rate between the damaged and non-damaged areas and it causes this plot to break at the transition point. Apparently, these points were dependent on the ions and their energies. The time required to reach the transition from the beginning of the etching was 11.0 h for 3.8 MeV/n of ^{84}Kr, 12.7 h for 6.2 MeV/n of ^{84}Kr, 10.8 h for 3.5 MeV/n of ^{129}Xe, 9.1 h for 2.5 MeV/n of ^{197}Au, and 10.4 h for 11.4 MeV/n of ^{197}Au. The pore diameters at the transition point, Dtp, were 370, 400, 300, 200, and 230 nm, respectively.

The pore diameter changed linearly beyond the transition point, and the slope of the plot was not influenced by the kind and energies of irradiated particles. This means almost the same rate of pore growth (35 nm/h) at the present etching stage. The bulk etch rate (Vb) of the PET film was determined to be 17.9 nm/h at 70 °C in the 0.2 M NaOH solution. The rate of the pore growth approximately corresponds to twice Vb in the PET film, indicating that chemical etching proceeds in the non- damaged region.

Figure 1 further demonstrates the important result that the pore grew in different ways *before* the transition point; the slope appeared to be varied by the irradiated conditions. The rates of the track etch are 46.7, 40.3, 32.0, 24.2, and 26.1 nm/h for 3.8 MeV/n ^{84}Kr, 6.2 MeV/n ^{84}Kr, 3.5 MeV/n ^{129}Xe, 2.5 MeV/n ^{197}Au, and 11.4 MeV/n ^{197}Au, respectively. Interestingly, the etch rates are either larger or smaller than twice Vb (35.8 nm/h), depending on the irradiated ions. The mechanism determining the formation of the tracks seems to be rather complicated, but we consider that it is related to the crosslinking or decomposition of the polymer chains induced by the ion bombardment. The crosslinking may occur in the film irradiated with heavier ions such as ^{129}Xe and ^{197}Au (also having a large restricted energy loss, REL), thereby decreasing the etch rate, while the etching is fast around the trajectories of ^{84}Kr ions due to the

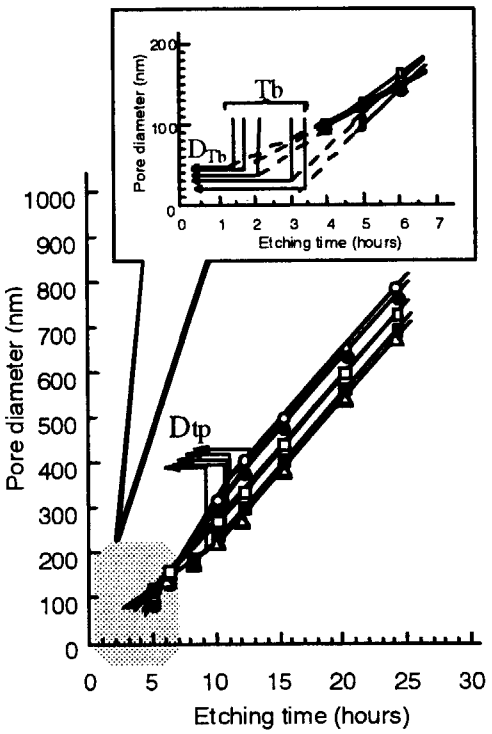

Fig. 1 Changes of pore diameter obtained from SEM observation as a function of etching time for the PET films irradiated with different ions: (○) ^{84}Kr 3.8MeV/n, (●) ^{84}Kr 6.2MeV/n, (□) ^{129}Xe 3.5 MeV/n, (■) ^{197}Au 2.5 MeV/n, (△) ^{197}Au 11.4 MeV/n.

decomposition of the polymer. In Figure 1 there is shown the extrapolation of the linear plot to Tb for each track membrane sample. The diameters at this point, defined as D_{Tb}, were 25, 30, 39, 45, and 50 nm for 6.2 MeV/n ^{84}Kr (REL = 33.4 MeV cm^2/mg), 3.8 MeV/n ^{84}Kr (38.7 MeV cm^2/mg), 3.5 MeV/n ^{129}Xe (60.9 MeV cm^2/mg), 11.4 MeV/n ^{197}Au (64.9 MeV cm^2/mg), and 2.5 MeV/n ^{197}Au (83.2 MeV cm^2/mg), respectively. There was an increasing tendency for the D_{Tb} value as the REL of the introducing particles increased.

As illustrated in Figure 2, the results of morphological chanse of the track formation obtained from the conductometric analysis and SEM observations can be clearly rationalized. We consider here a simple three-zone model, consisting of (1) an atomic damage core near the ion path, (2) a mixed phase of an electronic damage track outside the core (i.e., a penumbra region) and non-damaged part, and (3) a non-irradiated, virgin material only. At the initial etching stage, the core region is most sensitively developed until Tb. The next etching stage proceeds to reach the transition point shown as tp in the figure. At this stage, whether the crosslinking or decomposition of the polymer molecules preferentially occurs in the latent track is a key factor related closely to the etching behavior. Beyond the transition, the outermost non-irradiated zone undergoes the etching at a constant rate of Vb, irrespective of the irradiation conditions.

4. Conclusions

PET films were irradiated with ions of different nucleons and energies and then etched in the NaOH aqueous solution to prepare the track-etched membranes. The Tb value and the diameter of the track were determined by the conductmetric measurement during the etching

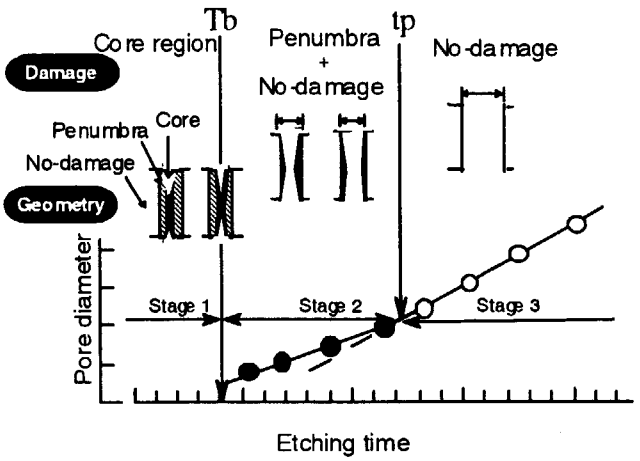

Fig. 2 Morphological change of the PET film during the etching process, together with the pore diameter vs. etching time plot. This explains our experimental results obtained from the conductometric analysis and SEM observations.

and by the SEM observations, respectively. We rationalized the results from such analyses by considering that the etching occurred in the following three phases: (1) the heavily damaged region called the track core, (2) the electronical ly damaged penumbra region mixed with the non-damaged part, and (3) the non-irradiated zone.

References

1) R.L.Fleischer, P.B.Price, R.M.Walker, Nuclear Tracks in Solids. Principles and Applications. Univ. of califonia Press, Berkeley, 1975.
2) R.Spohr, Ion Tracks in Microtechnology. Priciples and Applications. Vieweg Verlag, Braunschweig, 1990.
3) P.Apel, Radiat. Measurements, 34, 559 (2001).
4) T.N.Whitney, J.S.Jiang, P.C.Searson, C.L.Chien, Science, 261, 1316(1993).
5) C.R.Martin, Science, 266, 1961(1994).
6) L.Piraux, J.M.George, J.F.Despres, C.Leroy, E.Ferain, R.Legras, K.Ounadjela, A.Fert, Appl. Phys. Lett., 65, 2484(1994).
7) P.Apel, Nucl. Tracks Radiat. Meas., 19, 29(1991).
8) F.Petersen, W.Enge, Radiat. Meas., 25, 43(1995).

3.2 Preparation of hybrid membranes consisting of thermally stable polyimide and copper nanowires

H. Koshikawa*, Y. Maekawa*, M. Yoshida*, Y. Suzuki** and N. Yonezawa**
Department of Material Development, JAERI* Tokyo Univ. of A&T**

1. Introduction

When polymeric membranes are irradiated by heavy ion beams, each single heavy ion particle deposits its energy to a substrate in a region of less than 10 nm in diameter along the ion-path through membranes. The damaged region is susceptible to a proper etchant, resulting in the formation of through-holes with nanoscopic diameters, which are called "ion track membrane".[1] We have developed the ion track membranes made of high performance (thermally and mechanically stable) polymers, which can be applied to nanoscopic electronic devices such as anisotropic conductive films and field emitters through hybridization with conducting metals and semiconducting alloys by electroplating.[2-4] In this paper, anisotropically conducting membranes possessing copper wires of less than sub-micron in diameter are prepared by electrochemical plating of copper into the cylindrical pores in diameters ranging from 0.20 to 2.9 μm in the ion track membrane made of polyimide (PI).

2. Experimental

Commercial PI (Kapton, thickness 12 μm) was irradiated by $^{129}Xe^{23+}$ (450 MeV) ions with fluences of $3x10^5$ and $3x10^7$ ions/cm^2. The PI ion track membranes with cylindrical pores were prepared by etching in pH12 and pH9 sodium hypochlorite (NaClO) at 60 °C (Fig. 1-a). Successive layers of gold (25nm) and copper (20μm) were coated at one side of the PI ion track membranes as a cathode.[5,6] Then, the copper wires were deposited within the pores of ion track membranes onto the copper cathode by electrochemical plating in a pH1 aqueous solution of 1.3M copper sulfate ($CuSO_4$) with periodic potential modulation (-0.2V; 6sec, 0.2V;1sec)(Fig. 1-b).[7] The PI film was removed from the copper electrode with copper wires using a NaClO solution at 60 °C for 30 min. (Fig. 1-c); then, the geometry of copper wires on copper electrode were estimated by SEM measurement. The resistance of the membranes was measured by attaching a needle probe with 0.18 μm in diameter (2.5×10^{-4} cm^2 in area), which was connected with the multimeter.

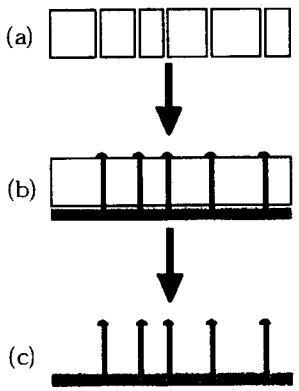

Fig. 1 The fabrication of conductive and insulating hybrid membranes consisting of copper wires in PI ion track membranes.

3. Results and discussion

The PI ion track membranes with 9.0 μm in thickness were prepared by $^{129}Xe^{23+}$ ion irradiation (fluence : 3.0×10^5 ions/cm^2), followed by etching in a pH12 aqueous NaClO solution. The clear hole patterns with 2.9 μm in diameter were observed in the SEM image of the surface, as shown in Fig. 2-a.

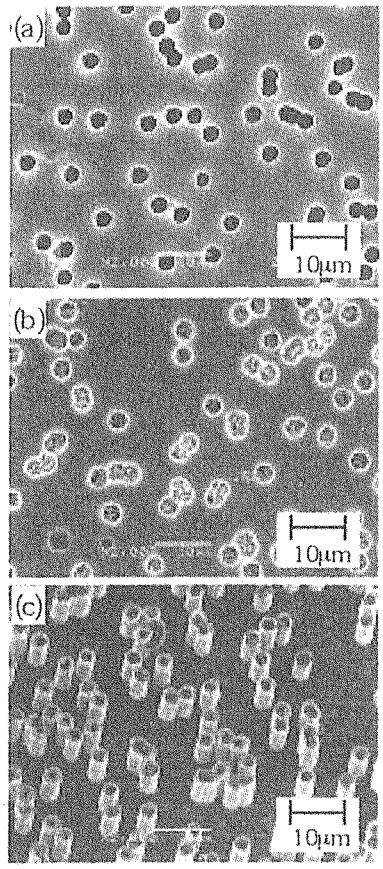

Fig. 2 (a) The PI ion track membrane; 2.9 μm in diameter. (b) The polyimide / copper nanowires hybride membranes. (c) The copper nanowires with 2.9 μm in diameter and 9 μm in height .

The copper wires were deposited into the pores of 2.9 μm in diameter by electrochemical plating in aqueous $CuSO_4$. As shown in Fig. 2-b, the most of the pores was filled with copper wires. In order to observe the copper wires which grew into the pores of the ion track membranes, only the PI films were removed from the cupper electrode using pH12 NaClO; then, the geometry of the wires were confirmed to be almost the same as that of the pores as shown in Fig. 2-c.

The PI ion track membranes with smaller pores were prepared by $^{129}Xe^{23+}$ ion irradiation, followed by etching in pH9 NaOCl. The clear hole patterns with 200 nm in diameter were observed in the SEM image of the surface of the PI membranes with 12 μm in thickness. The copper wires were deposited into the pores of 200 nm in diameter by the same plating method. After removing the PI film from the copper electrode in the same solution, the geometry of the copper wires was observed by SEM and found to be 200 nm in diameter, which are in good agreement with the size of the pores as shown in Figure 3-b.

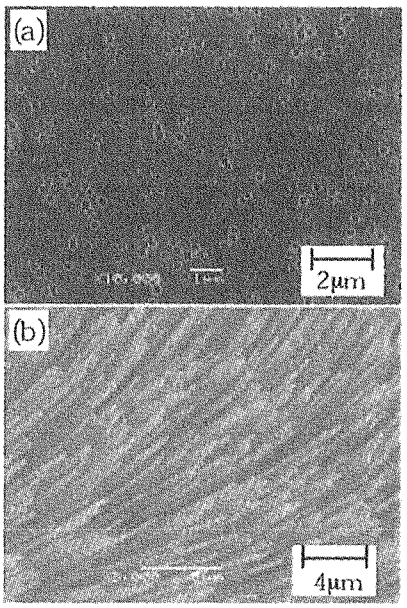

Fig. 3 (a) The PI ion track membrane; 200 nm in diameter. (b) The copper nanowires; 200 nm in diameter, 12 μm in height .

Next, we evaluated the conductivity of the membranes consisting of PET film and perpendicularly aligned cylindrical copper wires with 36 μm in height and 2.2 μm in diameter (the preparation was reported previously in

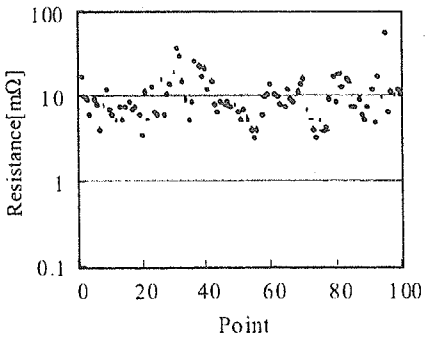

Fig.4 The perpendicular resistance to the membrane consisting of PET film and perpendicularly aligned cylindrical copper wires.

TIARA report in 2002) by the measurement of the membrane resistance in the directions perpendicular and parallel to the surfaces by four terminal resistance method. As shown in Figure 4, the resistances at these points were in the ranges from 3.10 to 55.3 mΩ and the average was 10.2 mΩ. The smallest of resistanc are in similar order to the theoretical resistance (2.8 mΩ). In contrast, the conductivity of the membrane parallel to the surfaces were zero at any points. From these results, it should be noted that anisotropically conducting membranes possessing copper wires are prepared by electrochemical plating of copper into the cylindrical pores in the ion track membrane made of PET.

References

1) R. Spohr, Ion tracks and Microtechnology, Principles and Applications, Vieweg & Sohn Verlagsgesellschaft mbH: Braunschweig, 1990.
2) C. R. Martin, Science 266 (1994) 1961.
3) Y. Suzuki, Y. Maekawa, M. Yoshida, K. Maeyama and N. Yonezawa Chem. Mater., 14 (2002) 4186-4191.
4) Y. Suzuki, Y. Maekawa, M. Yoshida, K. Maeyama and N. Yonezawa, Polymer, 44 (2003) 2307-2312.
5) C. Trautmann, W. Brüchle, R. Spohr, J. Vetter and N. Angert, Nuclear Instruments and Methods in Physics Research B 111 (1996) 70-74.
6) T. Molares, V. Buschmann, D. Dobrev, R. Neumann, R. Scholz, I. U. Schuchert and J. Vetter, Adv. Matter., 13, 1 (2001) 62.
7) D. Dobrev, J. Vetter, N. Angert, Nuclear Instruments and Methods in Physics Research B 149 (1999) 207-212.

3.3 Differential analyses of transient species initially produced in single heavy ion track - nuclear and specific energy dependence –

Mitsumasa Taguchi, and Takuji Kojima
Department of Material Development, JAERI

1. Introduction

The heavy ion-induced chemical reactions in aqueous solutions are strongly dependent on distributions of transient species, especially OH radicals. Understanding of reaction mechanisms of OH radicals is very important theme not only for radiation chemistry but also radiation biology. The heavy ion deposits its kinetic energy concentrically around the trajectory. The initial distributions of OH radicals depend on the energy distribution, which differs along the trajectory, and subsequent chemical reactions are very complicated. Therefore, 'average LET' and 'average yield' are not suitable parameter for detailed investigation about irradiation effects. The purpose of this study is to understand chemical reactions on the basis of physical track structure by measuring radical yield depending on nuclear and specific energy of the incident ion. We investigated the differential *G*-value of oxidized products from aqueous phenol solutions irradiated with several tens of MeV/n C and Ne ions, and tried to find consistency between physical and chemical aspects.

2. Experimental

Water containing 10-mM phenol was saturated with oxygen, or with helium gas to purge dissolved oxygen by 30-minute bubbling. The solution was put into an aluminum irradiation cell with a magnetic stirrer chip. The cell has an aluminum window of 15-μm thickness and 40-mm diameter.

Heavy ions used in this study were 220-MeV $^{12}C^{5+}$ and 350-MeV $^{20}Ne^{8+}$ provided from an AVF cyclotron in TIARA facility. Fluence rates were about 5×10^{8} ions/cm^2/s for C ion, and 3×10^{8} ions/cm^2/s for Ne ion at the surface of the sample solution. The irradiations were performed in the same manner as the references [1,2].

The irradiated aqueous solutions were analyzed by High Performance Liquid Chromatography (HPLC) with a reversed phase column (Shodex, Rspak DE-613) at 40 ℃. Acetonitrile mixed with 70-%(v/v) aqueous H_3PO_4 solution (0.01 M) was used as an eluent at a flow rate of 1.0 mL/minute.

3. Results and discussion

Hydroquinone, resorcinol and catechol, which are irradiation products by addition of one OH radical to *p*-, *m*- and *o*- position in phenol, were identified on the HPLC chromatogram. The number of these oxidized products by a single ion (N) increased super-linearly with an incident energy of the ion as shown in Figure 1. N corresponds to the value of the differential G-value (G'-value) integrated entirely over the trajectory. The G'-values are obtained by differentiating in a polynomial function of the energy. The G'-values of oxidized products were in the range of 1/10 to 1/2 of the G-value obtained by γ-ray irradiation. In the case of γ-ray irradiation, total G-value of the whole oxidized products is larger than 90 % of the G-value of OH radical. The G'-value of OH radicals was estimated using following equation;

$$G'(\mathrm{OH}) = \frac{\Sigma G'(\mathrm{product})}{\Sigma G(\mathrm{product})} \times G(\mathrm{OH}) \quad (1)$$

The G'-values estimated for C and Ne ions were plotted against specific energy as shown in Figure 2. The G'-values of OH radicals increase monotonously with the specific energy for both ion. The G'-values will approach to a limited value (2.8) obtained for γ-rays. The G'-values for C ion in this work are in consistency to those

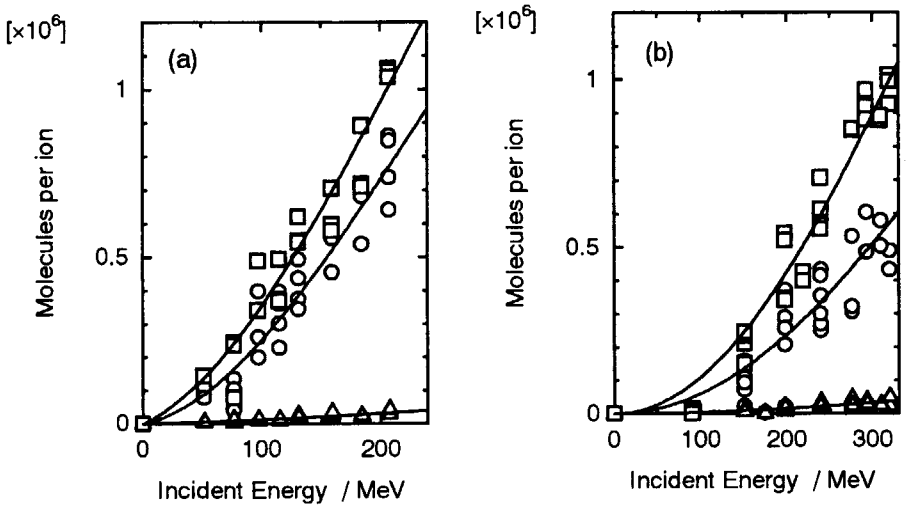

Figure 1 Number of molecules of hydroquinone (circle), resorcinol (triangle) and catechol (square) in the oxygen-saturated aqueous phenol solution per single C ion (a) and Ne ion (b) at different incident energies, the energies just before entering the sample solution.

obtained by LaVerne [3]. The G`-values for Ne ion are smaller than those for C ion at the same specific energy. C and Ne ions have the same physical track radius at the same specific energy. Therefore, this atomic number dependence is considered to be attributed to the increment of radical-radical recombination probability under the high density energy deposition in the center part of the track.

The G`-values of the oxidized products were also evaluated for oxygen-purged phenol solution. The $G$`-values of hydroquinone and catechol increase with increasing specific energy of the ions. The G`-values of these oxidized products are several times those expected from the $G$`-value of OH radicals and oxidation efficiency obtained by γ-ray irradiation. Furthermore, the G`-value of catechol in the higher specific energy region is larger than the $G$-value (0.14) of catechol obtained for γ-rays. Larger $G$`-values by heavy ions under oxygen-purged condition was also observed for the oxidation of phenylalanine in water [1]. These phenomena are considered to be induced by the oxidative species, e.g. oxygen and superoxide anions, produced in the center part of the track.

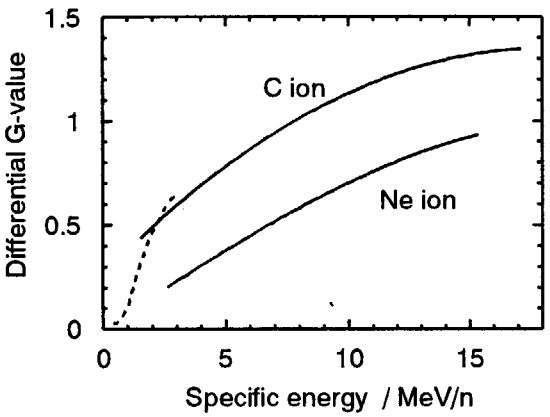

Figure 2 Differential G-values of OH radicals determined using the equation (1) as a function of the specific energy in the phenol solution. Dashed line shows the differential G-values of OH radicals estimated by LaVerne [3] for C ion irradiation of acidic aqueous solutions.

References

[1] M. Taguchi, et al., *Radiat. Phys. Chem.*, **60**, 263 (2001).

[2] M. Taguchi, et al., *JAERI-Review*, **2002-035**, 117 (2002).

[3] J. A. LaVerne, *Radiat. Phys. Chem.*, **34**, 135 (1989).

3.4 Crosslinking of Polymers in Heavy Ion Tracks

H. Koizumi*, M. Taguchi**, T. Kojima**, and T. Ichikawa*
Division of Molecular Chemistry, Graduate School of Engineering, Hokkaido University*, Department of Material Development, JAERI**

1. Introduction

Ions deposit energy along their tracks with high density. The high local dose can cause effects different from γ-rays and fast electrons[1]. In previous papers,[2,3] we have demonstrated formation of "gel string" of polydimethylsiloxanes by ion irradiation. Polydimethylsiloxane is a typical polymer that predominantly crosslinks by ionizing radiation. The dose near the center of heavy ion tracks exceeds the gelation dose. A gel string is hence generated in each ion track.

In the present study, we studied formation of gel string in polydimethylsiloxane irradiated with 256 MeV Ar, 306 MeV Ne, and 204 MeV C ions.

2. Experimental

Polydimethylsiloxane (KF96, Mn 60,000) supplied by Shin-Etsu Chemical Co., Ltd. was degassed under vacuum. They were put in metal cells with aluminum window of 25 μm thickness. 460 MeV $^{40}Ar^{13+}$, 350 MeV $^{20}Ne^{8+}$ and 220 MeV $^{12}C^{5+}$ ions from the cyclotron of TIARA were irradiated at HY1 port. The ion passes through a titanium window of 30 μm thickness, distance of 80 mm in 1-atom helium gas, and the aluminum window of the cells. The initial energy of the Ar, Ne, and C ions at the surface of polydimethylsiloxanes are 256 MeV, 306 MeV, and 204 MeV, respectively. Thickness of liquid polydimethylsiloxanes was sufficiently larger than the ranges of the ion beams. The irradiated samples were dissolved in hexane. The insoluble residue was separated with membrane filters (Millipore, LSWP04700, pore size 10 μm). The weight of the insoluble residue was measured.

3. Results and Discussion

Gel fractions for the ion- and γ-irradiated polydimethylsiloxanes are plotted as a function of dose in Figure 1. The doses for the ion-irradiated polydimethylsiloxanes are average doses within the ion range. The gel fraction is the ratio between the weight of the insoluble residue and that of polydimethylsiloxane within the ion range. The gel fraction for γ-irradiation was calculated with the G-value reported in the literature[4] and Charlesby-Pinner equation.

The gel fraction depends on radiation quality. The gel fraction for γ-irradiated polydimethylsiloxane is zero at lower than gelation dose. It abruptly increases at doses higher than the gelation dose and approaches unity. In contrast, the gel fractions for the ion-irradiation are proportional to dose, and lower than 0.1 at the doses in Figure 1.

This result indicates that gelation occurs in each ion track and gel strings are generated by the ion irradiation. The gel

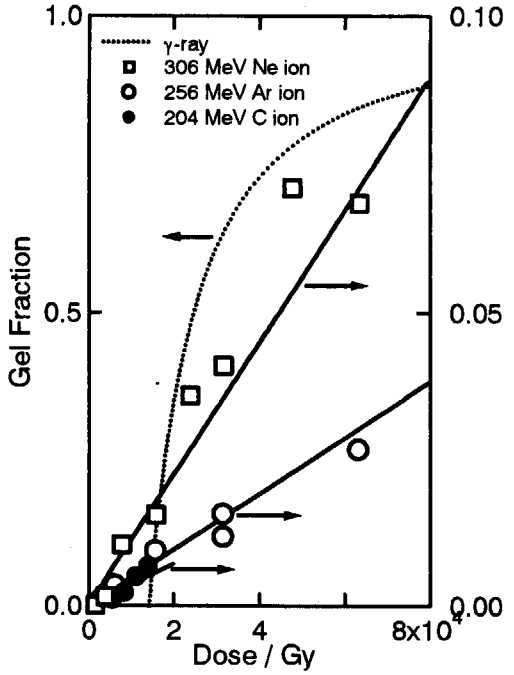

Figure 1. Gel fraction for polydimethylsiloxane irradiated with 256 MeV Ar, 306 MeV Ne and 204 MeV C ions and γ-rays as a function of absorbed dose.

fraction is hence proportional to dose, which is proportional to number of irradiated ions.

The weights of the insoluble residue per incident ions are 2.0 x 10^{-14} g ion^{-1} for the Ar ion, 5.7 x 10^{-14} g ion^{-1} for the Ne ion and 1.1 x10^{-14} g ion^{-1} for the C ion. Average radius was calculated under the assumption that the lengths of the gel strings are equals to the range of the ions. It is 6.9 nm for Ar ion, 5.4 nm for Ne ion, and 1.7 nm for C ion. This difference arises from different dose distribution in the ion tracks. The radial dose distributions for the ions are shown in Figure 2. It was calculated with equation proposed by Chatterjee and Schaefer[5]. In the radiolysis by γ-rays, gel fraction is 90%

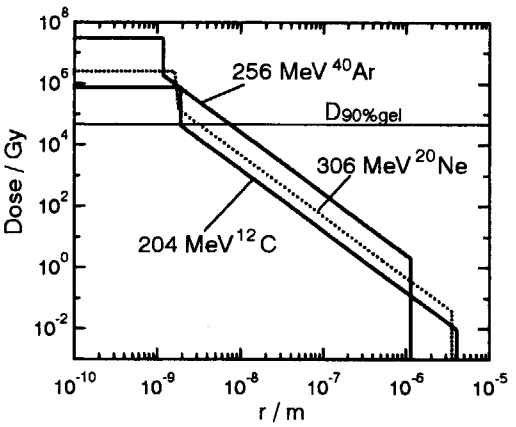

Figure 2. Radial dose distribution for 256 MeV Ar, 306 MeV Ne and 204 MeV C ions in polydimethylsiloxane.

at 5x10^4Gy. This dose ($D_{90\%}$) is indicated as a solid line in Figure 2. If we assume gelation in the ion tracks occurs with the same dose-yield relationship as for low-LET radiation, the gel strings are generated in the region higher dose than $D_{90\%}$. The radius of $D_{90\%}$ is 7.5 nm for the Ar ion, 3.1 nm for the Ne ion and 1.9 nm for the C ion. It well explains the experimental radii of the gel strings.

References

1) H. Koizumi, M. Taguchi, H. Namba, T. Ichikawa, H. Yoshida: Nucl. Instr. and Meth. B 132 (1997) 633-638.
2) H. Koizumi, M. Taguchi, Y. Kobayashi, T. Ichikawa: Nucl. Instr. and Meth. B 179 (2001) 530-535.
3) H. Koizumi, M. Taguchi, Y. Kobayashi, T. Ichikawa, Nucl. Instr. and Meth. B 208 (2003) 161-165.
4) C. G. Delides, I. W. Shepherd, Radiat. Phys. Chem. 10 (1977) 379-385.
5) A. Chatterjee and H. J. Schaefer, Radiat. Environ. Biophys. 13 (1976) 215-227.

3.5 Primary Process of Radiation Chemistry Studied by Ion Pulse Radiolysis

Y. Yoshida*, J. Yang*, S. Seki*, A. Saeki*, S. Tagawa*, H. Shibata**,
M. Taguchi***, T. Kojima***, H. Namba***
ISIR, Osaka University*
Faculty of Engineering, Kyoto University**
Department of Material Development, JAERI***

1. Introduction

Radiation effect of high energy high LET ion beams on the material is very interesting and was investigated by many researchers, because the highlly-densed irradiation makes the different effect from that by low-LET radiation, such as γ rays. We have studied the primary process of the ion beam-induced radiation chemistry by using the technique of ion beam pulse Radiolysis for emission spectroscopy[1-3].

The LET effect on the time-dependent emission could be discovered by using the ion beam pulse radiolysis of the polystyrene. However, the whole mechanism of LET effect can not be elucidated, because the information on the other important short–lived species, such as electron and cation radical, can not be obtained by the emission spectroscopy. The behavior of other short-lived species can be detected by using absorption spectroscopy. However, there are many difficulties to the absorption spectroscopy, such as the ion beam intensity, the penetration of the ion beam into material, the light source, and so on.

A new idea on the absorption spectroscopy system is proposed to overcome the difficulties. The points of the system are the production and the detection of the analyzing. The preliminary time-dependent absorption data has been obtained.

2. Experimental

Figure 1 shows the system for ion beam pulse radiolysis for absorption spectroscopy. A liquid sample is irradiated by 220MeV C^{5+} pulsed ion beam from the AVF cyclotron. A thin scintillator floats on the liquid sample. The pulsed ion beam produces the emission through the scintillator, which is used as analyzing light. The analyzing light is introduced to an optical

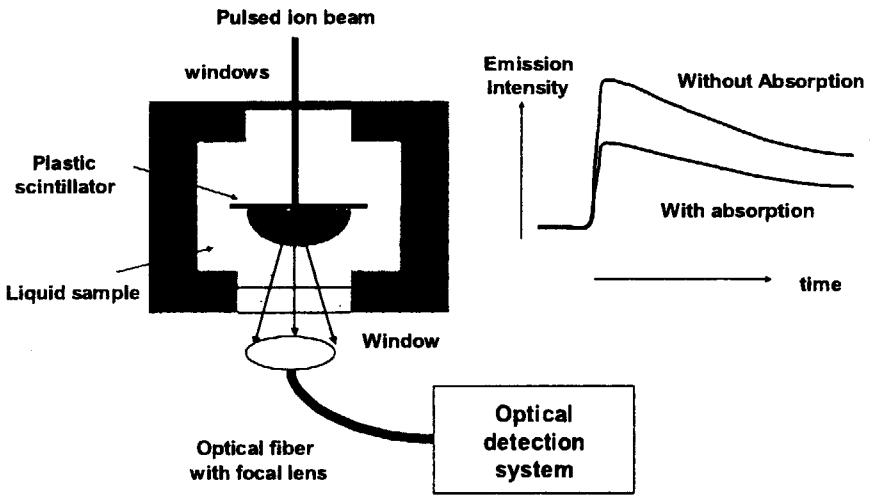

Fig. 1 Absorption spectroscopy system for ion beam pulse radiolysis

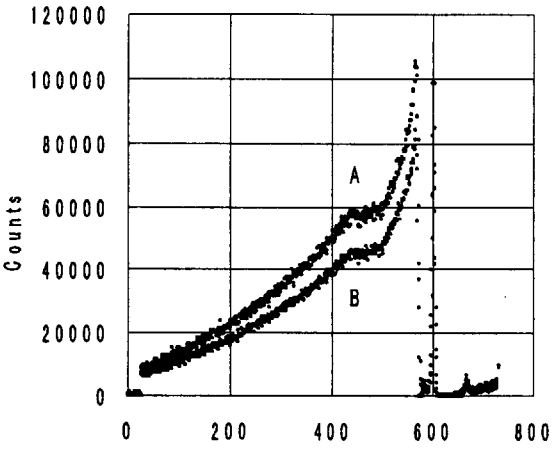

Fig. 2 typical outputs from the photon counting system obtained in the 220MeV C5+ion beam pulser adiolysis of water

detection system through a lens and an optical fiber. The single photon counting technique is used in the optical detection system, because the ion beam intensity is very small.

Figure 2 shows the typical outputs from the photon counting system obtained in the 220MeV C^{5+} ion beam pulse radiolysis of water. Signals A and B mean the intensity of analyzing light and that s containing absorption, respectively. Optical density was calculated by using both data.

BGO (Bismuth Germanate; $Bi_4Ge_3O_{12}$) was used as the scintillator. The lifetime and band of the emission are 300 ns and 480 nm, respectively.

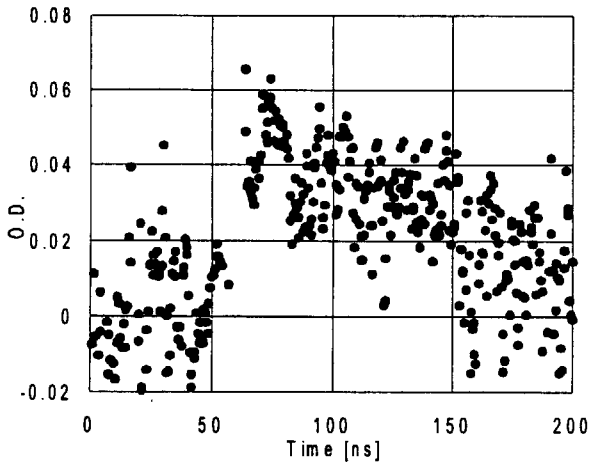

Fig. 3 Time-dependent behavior of hydrated electron obtained in 220 MeV C^{5+} pulse radiolysis of water monitored at 480 nm

3. Results and Discussion

Figure 3 shows the time-dependent optical absorption of the hydrated electron obtained in the 220MeV C^{5+} ion beam pulse radiolysis of water monitored at 480 nm. The raise of the absorption was 20 ns, which was equal to the time resolution of the system. The decay consisted of two components, very rapid decay with the lifetime of about 10 ns, and a slow component. The similar result was reported by W. G. Burns et al [4]. The kinetics is very different from that observed in the case of low LET radiation. Two-components decay is often observed in the ion beam pulse radiolysis for emission spectroscopy. The rapid decay is caused by highly-densed excitation of the ion beam.

4. Conclusion

Although either H^+ or He^+ was used in most of the previous ion beam pulse radiolysis, the present system enabled the heavy ion pulse radiolysis for absorption spectroscopy in the nanosecond time region. By using the new method, primary processes of ion beam irradiation will be elucidated near future.

References

1) H. Shibata et al., Nucl. Instrum. Meth., A327, 53, 1993
2) Y. Yoshida et al., Nucl. Instrum. Meth, A327, 41, 1993
3) H. Shibata et al., Nucl. Instrum. Meth., B105, 42, 1995
4) W. G. Burns et al., Faraday Diss. Chem. Soc. 63 (1977) 47.

3.6 3-D Structure Control of Nanowires Formed by Single Ion Hitting to Si-Based Polymers

Shu Seki*, Satoshi Tsukuda*, Yoichi Yoshida*, Seiichi Tagawa*,
Masaki Sugimoto**, Akira Idesaki**, and Shigeru Tanaka**
The Institute of Scientific and Industrial Research, Osaka University*
Department of Material Development, JAERI**

Abstract

Nano-wire formation by single ion hitting to Si-based polymer thin films is discussed in the present paper. Gelation of the polymers at the inside of single ion track gives crosslinked polymer nano-wires whose sizes (length, thickness) and number densities are completely controlled by changing parameters of incident ions and polymer materials. Ion hitting to polycarbosilane (**PCS**), **PCS**-polyvinylsilane (**PVS**) blend polymer, and polymethylphenylsilane (**PMPS**) produces nano-wires with their radii of cross sections as 30 nm ~ 7 nm for 450 MeV ^{129}Xe and 500 MeV ^{197}Au ion irradiations. The difference in the size is well interpreted by the efficiency of crosslinking reaction (G value of crosslinking: G(x)) as G(x) ~1.0 $(100\ eV)^{-1}$ in **PCS** and G(x) = 0.12 $(100\ eV)^{-1}$ in **PMPS** based on the physical aspects of deposited energy distribution in the ion tracks.

Introduction

1-D nano-sized materials such as carbon nanotubes have attracted much attention as ideal quantum wires for future manufacturing techniques of nano-scaled opto-electronic devices. However it is still difficult to control the sizes, spatial distributions, or positions of nanotubes by conventional synthetic techniques to date.

The MeV order heavy ion beams cause ultra-high density energy deposition which can not be realized by any other techniques (lasers, ΔH, etc.), and penetrate the polymer target straightforward as long as 1~100 μm depth[1-4]. The energy deposited area produces non-homogeneous field of chemical reactions, so-called a chemical core of an ion track[5-9]. The dimension of the field can be controlled by changing the energy deposition rate of incident ions (LET: linear energy transfer, eV/nm).

We found that cross-linking reaction of polysilane derivatives was predominantly caused and gave "nano-gel" in the chemical core, unlike main chain scission occurring at the outside of the area[10,11]. Based on the concept of the "single track gelation", the present study demonstrates the formation of cross-linked polymer nano-wires with the fairly controlled sizes for not only polysilanes but also a variety of Si based polymers. The size controllability of the nano-wires is also discussed in relation with the efficiency of the cross-linking reaction of the polymer materials.

Experimental

Poly(methylphenylsilane) (**PMPS**) was synthesized by the Kipping reaction with sodium in refluxing toluene or *n*-undecane from a doubly distilled monomer of methylphenyldichlorosilane purchased from Shin-Etsu Chemical Co. LTD.[12] The reaction was carried out under an atmosphere of predried nitrogen with or without 12-crown-4 ether. The obtained **PMPS** was purified by passing the toluene solution through a PTFE filter with 0.45 μm pore size, followed by the precipitation with toluene – isopropylalcohol (IPA) and methanol systems. The **PMPS** was fractionated by separatory precipitation leading to **PS1** (Mn = 1.5 ~ 1.1 x 10^5), **PS2** (Mn = 2.6 ~ 2.1 x 10^4), **PS3** (Mn = 1.1 x 10^4~ 9.0 x 10^3), **PS4** (Mn = 5.0 x 10^4~ 3.9 x 10^3), with small dispersion less than 1.5. Molecular weight of **PCS**, supplied by Nippon Carbon Co., Ltd., is 1.5 x 10^3. **PVS** is synthesized by radical polymerization of vinylsilane in an autocrave.[13]

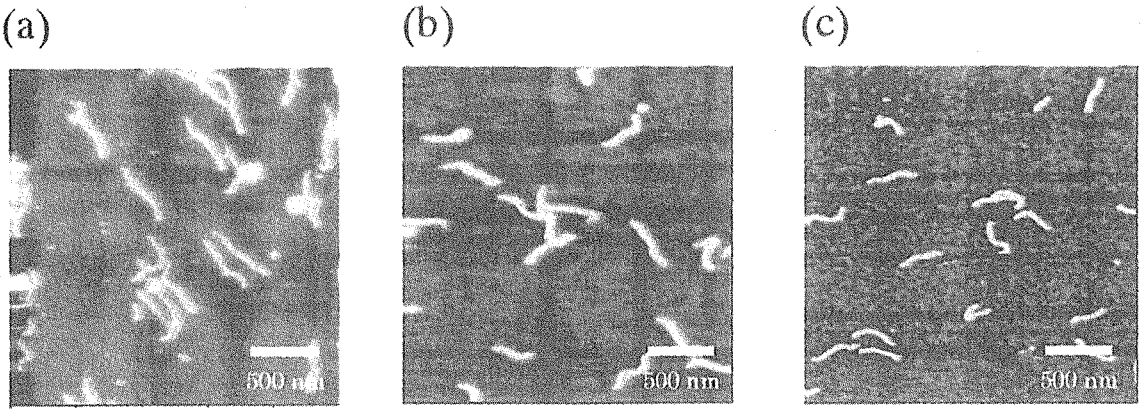

Fig 1.AFM images of the nano-wires changed the sizes for each molecular weight. a-c) The nano-wires were formed by the 450 MeV $^{128}Xe^{23+}$ irradiation to a **PS1** thin film (350 nm thick) at 5.0 x 10^8 ions/cm^2, a **PS2** thin film (250 nm thick) at 5.0 x 10^8 ions/cm^2 and a **PS3** thin film (250 nm thick) at 5.0 x 10^8 ions/cm^2, respectively.

The polymer, which contains 20 wt% of **PVS** in **PCS**, was prepared by freeze-drying of benzene solution under vacuum.

The polymers were spin-coated on Si substrates after O_2 plasma etching. The irradiation was carried out by using Xe, and Au ions from "TIARA" cyclotron accelerator at Japan Atomic Energy Research Institute, Takasaki Radiation Chemistry Research Establishment, followed by adequate development by ether and benzene.

The observation of the nano-wires was carried out by using Seiko Instruments Inc. SPI-3800 atomic force microscope (AFM).

Results and Discussion

When MeV order heavy ion beams irradiate to thin polymer film, an incident ion penetrates the target polymer and deposits only its energy within a limited area. Its irradiation to silicon backbone polymer causes cross-linked reaction in an ion track and forms one cylinder-like structure (nano-wire) along projectile of single ion. Because of changes in solubility induced by gelation of the polymers, development by using benzene eliminates uncross-linked part, and the nano-wires completely isolated on a Si substrate. Figure 1 shows a series of AFM images of nano-wires on a Si substrate formed in **PMPS** of different molecular weights (**PS1-PS3**). The sizes become small with a decrease in the molecular weight (from a to c). Thus the radii of nano-wires can be controlled by changing molecular weight.

Figure 2 shows a series of AFM images of nano-wires produced in **PMPS**, **PCS** and **PCS-PVS** for different ion beams. We observe the nano-wires formed in **PCS**(b,e) and **PCS-PVS** (c,f). Changing target material also controls the sizes of the nano-wires.

These radii of nano-wires for all the polymers and ion beams are summarized in Table 1. The radii in **PMPS** change within the range of 6.9-19.4 nm by changing molecular weight and ion beams. The values of nano-wire radii for **PCS** are 22.4 and 29.6 nm, respectively by Xe and Au ion beams irradiation.

The following formula were already given on the values of the coaxial energy in an ion track [1],

Table 1. Radii of nano-wire cross section

	$r+dr$ [a] (nm)					
Ion Beams	PS1	PS2	PS3	PS4	PCS	PCS+PVS
500 MeV $^{197}Au^{31+}$	19.4	16.2	12.5	10.7	29.6	24.2
450 MeV $^{129}Xe^{23+}$	10.5	—	—	6.9	22.4	19.0

[a] $r+dr$ denotes the radius of nano-wire formed by each ion beam. The values are estimated by sizing half band width of nano-wire cross section.

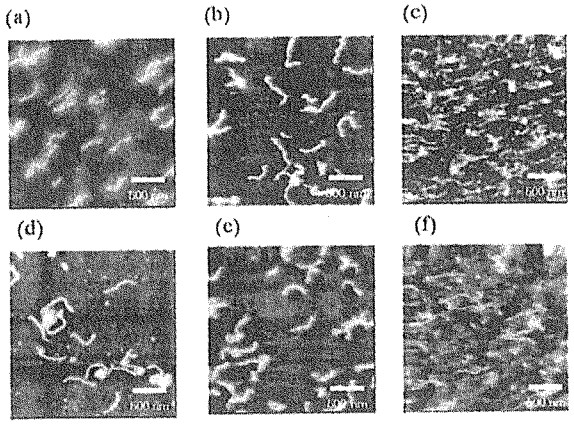

Fig. 2. AFM images of the nano-wires changed the sizes for each ion beams and target molecules. a-c) The nano-wires were formed by the 450 MeV $^{128}Xe^{23+}$ irradiation to **PS2** thin film (250 nm thick) at 1.0 x 10^9 ions/cm^2, a **PCS** thin film (400 nm thick) at 1.0 x 10^9 ions/cm^2 and a **PCS-PVS** thin film (200 nm thick) at 3.0 x 10^9 ions/cm^2, respectively. d-f) The nano-wires were formed by the 500 MeV $^{197}Au^{31+}$ irradiation to **PS1** thin film (350 nm thick) at 5.0 x 10^8 ions/cm^2, a **PCS** thin film (410 nm thick) at 5.0 x 10^8 ions/cm^2 and a **PCS-PVS** thin film (270 nm thick) at 5.0 x 10^8 ions/cm^2, respectively.

$$\rho_c(r) = \frac{LET}{2}\left[\pi r_c^2\right]^{-1} + \frac{LET}{2}\left[2\pi r_c^2 \ln\left(\frac{e^{1/2} r_p}{r_c}\right)\right]^{-1} \qquad r \le r_c \qquad (1)$$

$$\rho_p(r) = \frac{LET}{2}\left[2\pi r^2 \ln\left(\frac{e^{1/2} r_p}{r_c}\right)\right]^{-1} \qquad r_c < r \le r_p \qquad (2)$$

where ρ_c and ρ_p are the deposited energy density at core and penumbra area, respectively, r_c and r_p are the radii of core and penumbra area, e is an exponential factor. The equations give a value of deposited energy density at a boundary of a nano-wire by using its radii. The each deposited energy density at a boundary of a nano-wire is estimated as 2.4, 0.35 eV/nm^3 for Au ion beam and 4.1, 0.43 eV/nm^3 for Xe ion beam in **PS4** and **PCS**. These values reflect G values of cross-linking for **PMPS**[14] and **PCS**[15] (**PMPS**: G(x) = 0.12 (100 eV)$^{-1}$,**PCS**: G(x) = ~1.0 (100 eV)$^{-1}$).

The radii of nano-wires of **PCS-PVS** were smaller than **PCS**. The values of deposited energy density at a boundary of a nano-wire in **PCS-PVS** are 0.53 and 0.60 eV/nm^3 for Au and Xe ion beams irradiation. Idesaki et al., already reported that the efficiency of cross-linking reaction in **PCS-PVS** by using **EB** decreased than **PCS**.[14, 15] Therefore we regarded that the radii in **PCS-PVS** become smaller than **PCS** because crosslinking reactions for same energy is dominated the efficiency cross-linking reaction. Those results strongly suggest that cross-linking reactions of polymer at a boundary of a nano-wire are maximum factor to determine the size.

Conclusion

We observed the nano-wires formed in PCS and PCS-PVS without polysilane derivatives for the first time by high LET ion beams irradiation. For formation reaction of nano-wires along the projectile ion freedom control of the sizes are capable by particularly selecting particularly polymer materials of different crosslinking reaction characteristica.

References

1) L. Calcagno, G. Foti, A. Licciardello, O.Puglisi, *Appl. Phys. Lett.* **51**, 907-909 (1987).
2) L. Calcagno, G. Foti, *Nucl. Instrum. Methods* **B59/60**, 1153-1158 (1991).
3) M. B. Lewis, E. H. Lee, *Nucl. Instrum. Methods* **B69**, 341-348 (1992).
4) Z. Chang, J. A. LaVerne, *J.Phys Chem. B* **104**, 10557-10562 (2000).
5) J. L. Magee, A. Chattarjee, Kinetics of Nonhomogenious Processes, G. R. Freeman Ed., Chapter 4, p.171 (1987) (John Wiley & Sons, New York).
6) J. A. LaVerne, R. H. Schuler, *J. Phys. Chem.* **98**, 4043-4049 (1994).
7) E. Kobetich, R. Katz, *Phys. Rev.* **170**, 391-396 (1968).
8) W. E. Wilson, *Radiat. Res.* **140**, 375-381 (1994).
9) M. N. Varma, J. W. Baum, A. J. Kuehner, *Radiat. Res.* **62**, 1-11 (1975).
10) S. Seki et al., *J. Phys. Chem.* **B103**, 3043-3048 (1999).
11) S. Seki,et al.,*Adv Mater.*13 ,1663-1665 (2001).
12) S. Seki,et al., *Macromolecules,* **32**,1080 (1999).
13) M. Itoh, et al, *Macromolecules,* **31**,5609-5615 (1998).
14) A. Idesaki,et al., *Radiat. Phys. Chem.* 60,483-487(2001). S. Seki,et al., *Radiat. Phys. Chem.* **48**,539-544(1996).
15) T. Seguchi, *Radiat. Phys. Chem.* 57,367-371 (2000).

3.7 Separation of Dioxin using heavy ion-irradiated membranes

Shuichi Takahashi, Satoshi Iida and Yoshitaka Obayashi
Department of Industrial Chemistry, Meiji University

1. INTRODUCTION

Much research has already been done on polymers irradiated by heavy ions. It has been proven that interaction occurs between the heavy ions and polymer materials, in which the degree of damage to the polymer material differs with the kind of irradiating ions [1-3]. The high stability of the mechanical properties and chemical structure should be assigned a very important significance. Therefore, the effects of heavy ion irradiation on Poly(ethylene terephthalate) (PET) membranes were chemically and mechanically investigated in this study. PET and 3,3`,4,4`-diphenylhexafluoroisopropylidene tetracarboxylic dianhydride-based polyimide (6FDA-PI) membrane was irradiated with a fluence of 3×10^9 ions/cm^2 and used in this study with a view to separation of the dioxin from the aqueous solution using the pervaparation (PV) system.

2. EXPERIMENTAL

2.1 Material

The membrane used in this study, PET, was obtained from Hoechst Japan Co., Ltd. The thickness of the PET membrane was 38μm. Also, 6FDA-PI was synthesized by a chemical imidization method. 6FDA-PI membrane was prepared by pouring the casting solutions onto a glass plate. The thickness of the 6FDA-PI membrane was about 40μm. Figure 1 shows the chemical structures of the precursor polymers used in this work.

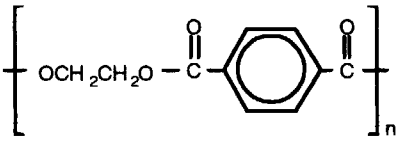

[PET]

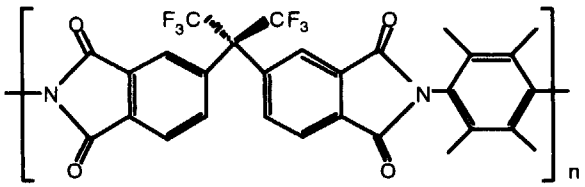

[6FDA-PI]

Figure 1. Chemical structures of PET and 6FDA-PI

2.2 Heavy Ion Irradiation

For heavy ion irradiation, PET and 6FDA-TeMPD membranes were cut into a square of 50 × 50 mm^2 and attached to a glass plate. The chamber for the formation of the ion-track pores in the membrane, which is connected to the AVF cyclotron in the TIARA, was designed for the alternate use of turntable-type and roll-type film-carrying systems. All the irradiation was performed in vacuum at room temperature. The $^{129}Xe^{23+}$ (450MeV) was supplied in this study. The fluence of the ion irradiation was changed ranging from 3×10^3 to 3×10^9 ions/cm^2 to observe the effect of the fluence on the various characterizations. In the case of dioxin separation, the fluence was fixed at 3×10^9 ions/cm^2.

2.3 Measurement

Dynamic loss tangent (tanδ) was measured within the range of 25 ~ 160°C at a frequency of 1 Hz using a dynamic modulus Perkin-Elmer Dynamic Mechanical Analyzer,

DMA-7e. The programmed heating rate was 3°C/min, and the dynamic and static stresses were 4.00e+5Pa and 4.80e+5Pa, respectively.

The tensile modulus at room temperature was obtained with a tensile testing machine (SHIMADZU AGS-H 5kN AUTOGRAPH) having a crosshead speed of 5 mm/min. The capacity of the clamp assembly was 5kN/500kgf.

PV measurement was performed with a stainless steel cell at 75°C. The feed solution of Dioxin-Water mixtures was circulates using a microtube pump on the upper side of the membrane in order to maintain the feed concentration constant, and downstream pressure was kept below 10mmHg. The permeated vapor was trapped using liquid nitrogen. The total flux and selectivity for dioxin-water mixtures through the membrane were determined by the weight of permeant and by the Gas chromatography (GC: FID), respectively. The flux J was determined by measuring the amount of permeant Q passed through the membrane during the time interval t at steady state.

$$J = Q/At$$

where A is the permeation area. The separation factor α of dioxin over water is defined as follows;

$$\alpha = (Pd/Pw)/(Fd/Fw)$$

where P and F are weight fractions of permeate and feed, and the subscripts d and w stand for dioxin and water, respectively.

3. RESULTS AND DISCUSSION

The unusual manner by which the number of fluence affects the dynamic loss tangent is listed in Table 1. The tanδ of Xe ion-irradiated membrane is approximately 160% higher than that of pure PET membrane at the fluence of 3×10^8 ions/cm^2, suggesting that the decreasing of ratio at the fluence of 3×10^9 ions/cm depends strongly on the damage caused by the overlapping of the ion track at the higher fluence. Also, an increase in the dynamic loss tangent (tanδ) also meant an enhanced absorption capacity of impact. These characteristic changes depended on the ion fluence that was newly observed in this study.

Table 1 The characterization data by DMA and tensile test

Membrane	tan δ	Tensile Elongation [%]	Tensile Modulus [kgf/cm^2]
PET	0.098	280	1200
Xe-3	0.141	-	-
Xe-6	0.145	-	-
Xe-7	0.150	-	-
Xe-8	0.155	-	-
Xe-9	0.146	150	1580

The tensile elongation and modulus of the materials studied is also represented in Table 1. PET is equipped with both high tensile strength and elongation, a so-called toughness material. The PET used in this study is also a toughness material with elongation breaking at around 280%. Xe-ion irradiation of 3×10^9 ions/cm^2 enhanced the tensile strength but decreased the elongation at the break. The heavy-ion-irradiated PET changes to a high-strength material. However, elongation of the ion-irradiated membrane was reduced to one-half that of PET. It is suggested that a significant cross-linking is formed after the heavy ion irradiation. We consider that the decreasing elongation at the break contributes to the polymer chain scission by ion irradiation. We believe that the secondary electron induced by the collision between the irradiated ion and the constituent atoms of the

membrane material form the cross-linked penumbra region. The polymer chain scissions and structure degradations are expected to occur at higher ion fluence. It can be presumed that this damage is caused by the overlapping of the ion track at the higher fluence. This consideration can explain the slight increase in tanδ, which depends on the increase in the ion fluence.

PET and 6FDA-PI membranes were irradiated Xe ion and grafted Amino-styrene to produce a fabricated membrane, which was expected to have better affinity for dioxin than the pure polymer membrane. PET series membranes couldn't have high dioxin selectivity from the aqueous solution. On the other hand, the 6DA-PI membrane has a good stability and high gas permeability. As can be seen in Figure 2, dioxin doesn't also have a good affinity for the grafted amino-styrene. We found out that dioxin-separation-factor decrease in proportion to the increase of flux. It is assumed that grafted amino-styrene has not a chemical affinity for dioxin. But we believe that the separation membrane above the proportional line would be created as long as we select the affinity material for dioxin as graft molecule.

4. CONCLUSIONS

Various characterizations were used to study the effect of heavy ion irradiation on the poly(ethylene terephthalate) membrane. The analyses used in this study are mainly DMA, tensile measurement. The overall structure change in the PET polymer was investigated as a function of the Xe-ion fluence in the range from 3×10^3 ions/cm^2 to 3×10^9 ions/cm^2. Based on mechanical measurements such as the tensile test and DMA, the heavy-ion-irradiated PET membranes exhibited a significant change to their cross-linking. An increase in the dynamic loss tangent (tanδ) was also confirmed, and suggested an enhanced absorption capacity of impact. Moreover, the Xe-ion irradiation of 3×10^9 ions/cm^2 enhanced the tensile strength but decreased the elongation at the break. In this study with a view to separation of the dioxin from the aqueous solution, also, the 6DA-PI membrane which has a good stability and high gas permeability was used. It is proved that dioxin-separation-factor decrease in proportion to the increase of permeation flux.

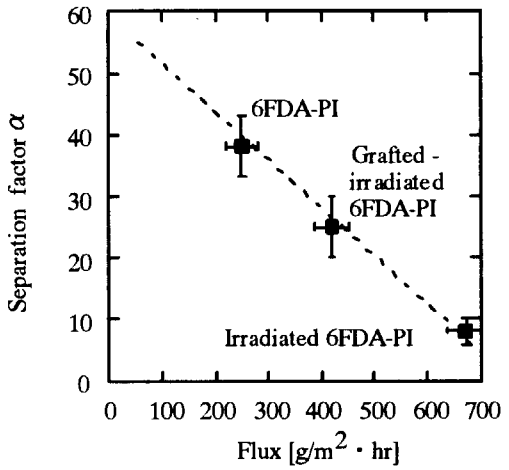

Figure 2. Dependence of separation factor on flux in the pervaporation (PV) at 75 °C.

REFERENCES

1) M. Yoshida, N. Nagaoka, M. Asano, H. Omichi, H. Kubota, K. Ogura, J. Vetter, R. Spohr, R. Katakai. Nucl. Instr. and Meth. Phys. Res. B 1997, **122**, 39.

2) H. Koizumi, T. Ichikawa, H. Yoshida, H. Shibata, S. Tagawa, Y. Yoshida. Nucl. Instr. and Meth. Phys. Res. B 1996, **117**, 269.

3) H. Koizumi, T. Ichikawa, H. Yoshida, H. Namba, M. Taguchi, T. Kojima. Nucl. Instr. and Meth. Phys. Res. B 1996, **117**, 431.

3.8 Suppression of charge build-up during ion bombardment into organic insulators using a cluster ion beam

K. Hirata*, Y. Saitoh**, A. Chiba**, K. Narumi***, Y. Kobayashi*, and K. Arakawa**

National Institute of Advanced Industrial Science and Technology (AIST), Tsukuba, Ibaraki 305-8565, Japan*

Advanced Radiation Technology Center, JAERI **

Advanced Science Research Center, JAERI ***

1. Introduction

Ion bombardment to insulators usually leads to charge accumulation on targets, which finally causes electric breakdown. The electric breakdown must be avoided because it causes serious damage to the target and makes surface analysis using ion beams difficult. Cluster ion bombardment provides a nonlinear irradiation effect on secondary emissions, which is expected to lead to a charge accumulation process for cluster ion bombardment different from that for a monoatomic ion. In this study, we have simultaneously measured the target and secondary emission currents as a function of an atomic dose and compared the charge accumulation process of organic insulators during monoatomic and cluster ion bombardments [1].

2. Experimental

Amorphous polycarbonate (PC) films with a thickness of 100 μm and a density of 1.2 g/cm^3 were irradiated with 0.5MeV/atom monoatomic carbon ion C_1^+ and carbon cluster ion C_8^+ by a 3 MV tandem accelerator of the Japan Atomic Energy Research Institute (JAERI)/Takasaki [2-6]. A schematic diagram of the experimental arrangement is shown in Fig. 1. The irradiations were performed in a pressure below 5×10^{-8} Torr, and the incident angle of the beam was normal to the sample surface. A current at the target *It* and an emission current by secondary charged particles *Is* were simultaneously measured by two high-sensitivity electrometers. A fresh sample was used for each measurement.

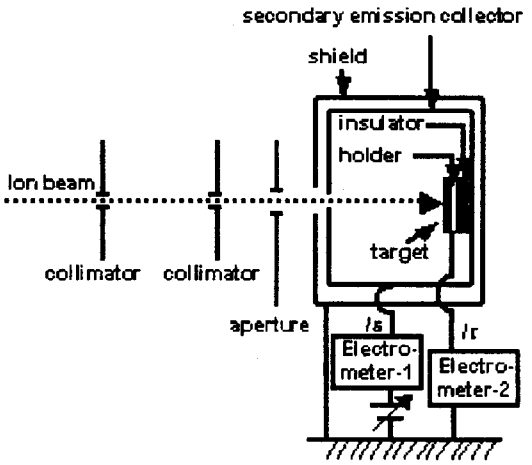

Fig. 1 Schematic illustration of the experiment set-up.

3. Results and discussion

Fig. 2 shows atomic dose dependence of *Is* and *It* normalized to the incident beam current I_0 (Is/I_0 and It/I_0) for C_1^+ and C_8^+ bombardments. Is/nI_0 and It/nI_0 (n:cluster number) of the right vertical axis represent the normalized secondary emission and target currents per atom, respectively. We can see a series of abrupt changes for C_1^+, which are attributed to the repeated charge accumulation and electric

breakdown (Fig. 2a), whereas no such changes are observed for C_8^+ (Fig. 2b). Therefore, use of C_8^+ instead of C_1^+ prevents the electric breakdown during ion bombardment.

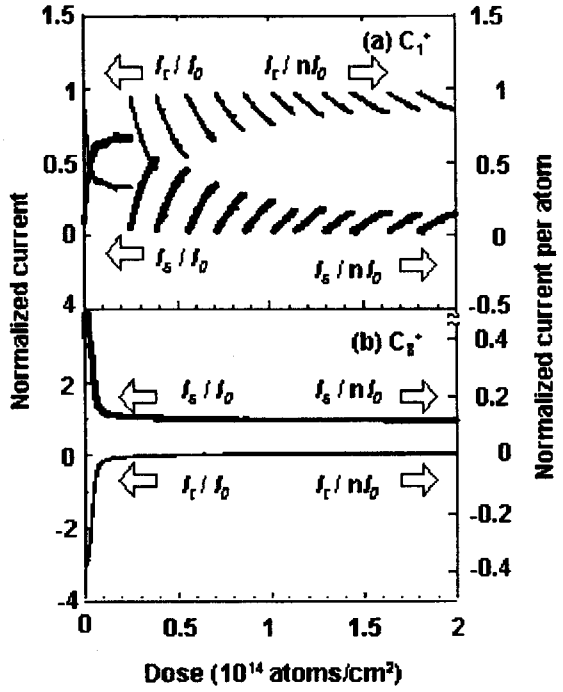

Fig.2 Variations of Is/I_0 and It/I_0 with atomic dose for (a) C_1^+ and (b) C_8^+. The data were obtained every 1s during continuous ion bombardment.

At the beginning of the C_8^+-irradiation, It exhibits a negative value although positive charges are injected into the target (Fig. 2b). This is ascribed to the higher emission current than the incident beam current ($Is/I_0>1$). Is/nI_0 at the beginning of the C_8^+-irradiation (~ 0.4) is ~ 4 times larger than that for C_1^+ (~ 0.1), showing that $Is/I_0>1$ for the C_8^+ irradiation is caused not only by a smaller amount of injected charge per atom but also by the higher emission current per atom (Is/nI_0) than that for the C_1^+ irradiation. This indicates that C_8^+ cluster impact produces more positive secondary emission per atom than C_1^+ impact.

Continuing ion bombardment to an insulator under an $Is/I_0>1$ condition causes negative-charge accumulation on the target, which causes a reduction of the target surface bias potential. This reduction makes positive secondary emissions having less energies to overcome the surface bias potential for reaching the secondary emission collector return to the target. The dose-dependent reduction of Is/I_0 for C_8^+ shown in Fig. 2b is due to the reduction of positive-charge contribution to Is by the negative-charge accumulation.

Meanwhile, for $Is/I_0<1$, positive charges are accumulated on the target because of the lower secondary emission current than the incident beam current. Analogously to C_8^+, the increase of Is/I_0 for C_1^+ with atomic dose until a first electric breakdown appears due to the positive charge build-up and a resultant reduction of negative-charge contribution to Is. However, the value of Is/I_0 at the beginning of the C_1^+-irradiation (~ 0.1) is not clearly changed by the external bias potential (from −100V to 100V) applied to the secondary emission collector [1], indicating that the charging potential of the target surface is already high enough to be insensitive to the variation of the external potential. Therefore, most of negative secondary emissions are probably returned to the target by the charging potential at the beginning of the irradiation. Since the surface charging potential increases with dose until the first electric breakdown, the dose-dependent reduction of the negative-charge contribution to Is can not explain the enhancement of Is/I_0. The charging potential build-up may enhance a positive-ionization probability at the target surface.

Is/I_0 for C_1^+ is almost saturated with a value below unity around 0.1×10^{14} atoms/cm^2. When the accumulated charge exceeds a certain capacitance of the target, the first electric breakdown occurs and the Is/I_0 is abruptly reduced. After the breakdown,

Is/I_0 gradually increases and the charge accumulation is followed by a second electric breakdown. The gradual increase of Is/I_0 with dose and the abrupt reduction of Is/I_0 by the electric breakdown continue to alternately occur afterward.

In contrast to Is/I_0 for C_1^+, Is/I_0 for C_8^+ shown in Fig. 2b maintains unity at higher doses. As part of positive secondary emissions is pulled back to the target by the surface potential produced by the negative-charge accumulation, Is/I_0 decreases. The reduction rate of Is/I_0 is gradually decreased and Is/I_0 reaches unity. Because an equilibrium between the injecting and emitting charges is attained under the Is/I_0=1 condition, the charge ceases to accumulate. In conclusion, the electric breakdown during the ion bombardment to PC was avoided using C_8^+ cluster ions instead of C_1^+ monoatomic ions.

References

1) K. Hirata, S. Saitoh, K. Narumi, and Y. Kobayashi, Appl. Phys. Lett., **81**, 3669 (2002).
2) Y. Saitoh, K. Mizuhashi and S. Tajima, JAERI-Review **97-015**, 240 (1997).
3) Y. Saitoh, S. Tajima, I. Takada, K. Mizuhashi, S. Uno, K. Ohkoshi, Y. Ishii, T. Kamiya, K. Yotsumoto, R. Tanaka, E. Iwamoto, Nucl. Instrum. Methods Phys. Res. B **89**, 23 (1994).
4) K. Narumi, K. Nakajima, K. Kimura, M. Mannami, Y. Saitoh, S. Yamamoto, Y. Aoki, and H, Naramoto, Nucl. Instrum. Methods Phys. Res. B **135**, 77 (1998).
5) K. Hirata, Y. Saitoh, K. Narumi, Y. Nakajima, and Y. Kobayashi, Nucl. Instrum. Methods. Phys. Res. B **193**, 816 (2002).
6) Y. Saitoh, K. Mizuhashi, and S. Tajima, Nucl. Instrum. Methods Phys. Res. A **245**, 61 (2000).

This is a blank page.

4. Inorganic Materials

4.1 Changes of Ductile-Brittle Transition Temperature due to Helium and Hydrogen Implantations in F82H Steel

E. Wakai*, K. Furuya**, M. Sato**, K. Oka***, T. Tanaka***, S. Ohnuki***, K. Kato****, F. Takada****, H. Tanigawa**, T. Sawai* and S. Jistukawa*

Department of Materials Science, Tokai Establishment*,
Department of Fusion Engineering Research, Naka Establishment, JAERI**, Faculty of Fusion Engineering, Hokkaido University***,
Department of JMTR Hot Laboratory, Oarai Establishment, JAERI****.

1. Introduction

Low-activation ferritic/martensitic steels are candidated materials for the first wall and blanket structure of fusion reactors and also prominent materials for the target vessel of spallation neutron source. In the systems, the high-energy neutrons or protons induce displacement damage and generate hydrogen and helium gas atoms in the materials. Helium and hydrogen accumulations due to transmutation and implantation in martensitic steels for first wall and blanket structure of fusion reactors have been considered as a potential factor to control. In this study, the effects of helium or hydrogen atoms on ductile-brittle transition temperature (DBTT) and on deformation behaviors of ferritic/martensitic steel has been examined by mechanical testing for small size specimens, small punch testing.

Small punch tests were developed to extract strength and ductility information for mechanical properties of small size in fusion reactor structural materials. The test is based on driving a cylindrical punch through a clamp specimen, and instrumenting the punch to obtain a load-displacement curve of the punching process.

2. Experimental procedure

The specimens used were F82H (Fe-8Cr-2W-0.2V-0.04Ta-0.1C) steel and Fe-9Cr binary alloys. The TEM disk specimens of 0.3 mm thickness were implanted at about 120°C with a beam of 50 MeV-He^{2+} or 20 MeV-H^{+} particles by AVF cyclotron at TIARA facility of JAERI. An energy degrader was used to implant helium or hydrogen into the specimens from top to bottom uniformly. The hydrogen concentration was estimated as about 20 appm H. Following the implantations, small punch (SP) tests were carried out at temperatures between -180°C and 25°C in a hot cell of the JMTR hot laboratory. The SP test machine consists of a load controller, turntable with twelve specimen holders, vacuum chamber and furnace. A cross-sectional view of specimen holder in the SP test machine is shown in Fig. 1.

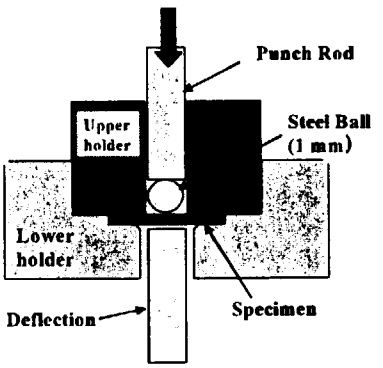

Fig. 1 Cross-section of specimen holder for SP test.

The specimen holder consists of the upper and lower holders, punch and steel ball of 1mm diameter. The steel ball and punch were pushed by punch rod. The maximum load and stroke of the punch rod is 5 kN and 8 mm, respectively. The punch speed was controlled at 0.5 mm/min. The microstructures after the implantation were observed by a transmission electron microscope (TEM) operated at 200 kV in the Tokai hot laboratory. After the SP tests, the fracture surface was observed by a scanning electron microscope (SEM) in the JMTR hot laboratory.

3. Results and discussion

The concentration of helium in the specimen was measured by a mass analyzer of magnetic reflection type. In this measurement, helium gas was released into the measurement system from the ion-implanted specimen after melting. In this technique, a known concentration of He gas is used for a standard relation between the gas intensity and concentration of He, as given in Fig. 2. The concentration of the He in the specimen implanted by cyclotron irradiation was evaluated as about 84 appm He.

In Fig. 3(a) and 3(b), SP-results showed that the shifts of DBTT in the helium or hydrogen implanted F82H steel were evaluated as about 50°C and 35°C, respectively, from the correlation between SP data and 1/3CVN (1/3 size Charpy specimen with V-notch) data[1]. Similar result of the shift of DBTT was also obtained in Fe-9Cr alloy implanted with He ions. The result for the shift of DBTT due to He implantation is coincidence with the previous data for the boron doped F82H irradiated in JMTR[2] as given in Fig. 4. In the microstructural observation, a low density of dislocation loops with a size of 4 nm was formed in the helium-implanted specimen. However, the effect of formation of dislocation loops on the shift of DBTT is thought to be ignorable because of low density and small size of dislocation loops.

In the brittle temperature regime, the cleavage fracture surface was observed in the specimens tested at low temperatures and the fracture was transgranular type as seen in Fig. 5. The size of transgranular areas was comparable to the package size of lath martensite in the specimen implanted with helium atoms. The cause of the shift of DBTT is though to be the degradation of fracture energy due to trapping helium atoms at the boundaries of the package of lath martensite. The other helium effects on mechanical properties are also found in fatigue testing [3), 4)].

4. Conclusion

The effects of helium or hydrogen atoms on ductile-brittle transition temperature and on deformation behaviors of ferritic/martensitic steel have been examined by small punch (SP) testing, SEM observation after SP testing and TEM observation. The cause of the shift of DBTT due to He implantation is though to be the degradation of fracture energy due to trapping helium atoms on the boundaries of the package of lath martensite.

Acknowledgement

The authors are grateful to the members of TIARA facility.

References

1) M. Eto, H. Takahashi, T. Misawa, M. Suzuki, Y. Nishiyama, K. Fukaya and S. Jitsukawa, Small specimen test techniques applied to nuclear reactor vessel thermal annealing and plant life extension, ASTM STP 1204, (1993)241.
2) E. Wakai, K. Furuya, M. Sato, K. Oka, T. Tanaka, S. Ohnuki, K. Kato, F. Takada, and S. Jituskawa, J. Nucl. Mater., in press.
3) H. Tanigawa, T. Hirose, M. Ando, S. Jitsukawa, Y. Katoh and A. Kohyama, J. Nucl.

Mater., 307-311(2002)293-298.
4) T. Hisrose, H. Tanigawa, M. Ando, A. Kohyama, Y. Katoh and M. Narui., J. Nucl. Mater., 307-311(2002)30.

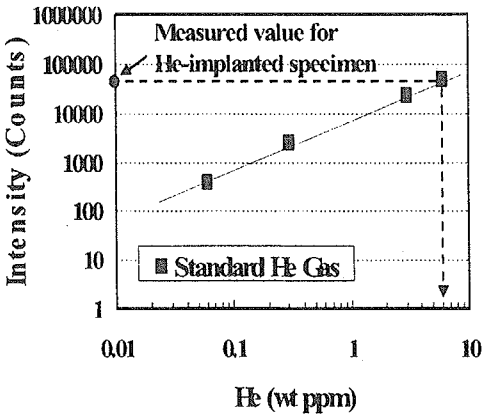

Fig. 2 Measurement of He concentration in the specimen implanted by cyclotron experiment.

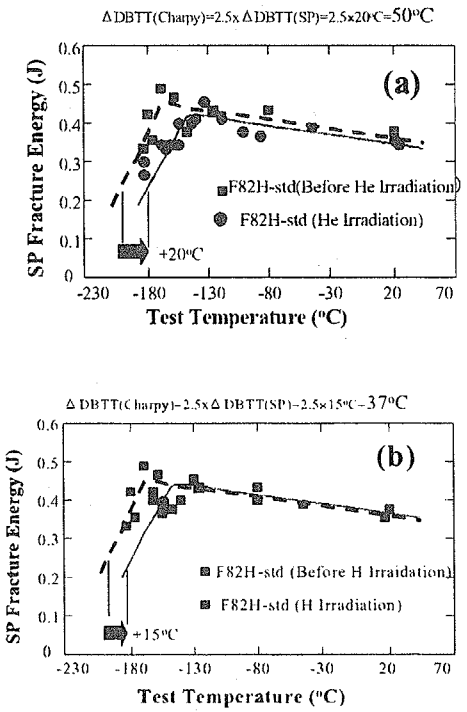

Fig. 3 SP testing behaviors of F82H steel implanted with (a) helium and (b) hydrogen..

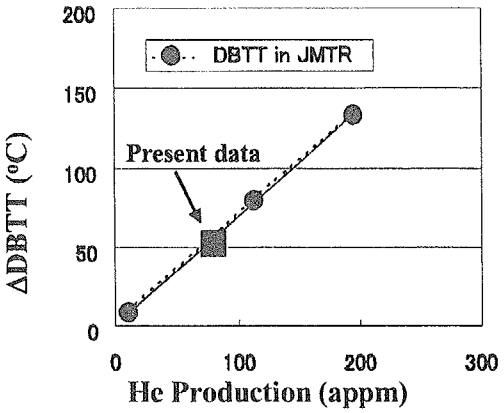

Fig. 4 SP testing result of F82H implanted by He irradiation and Fracture toughness result of boron doped F82H irradiated in JMTR.

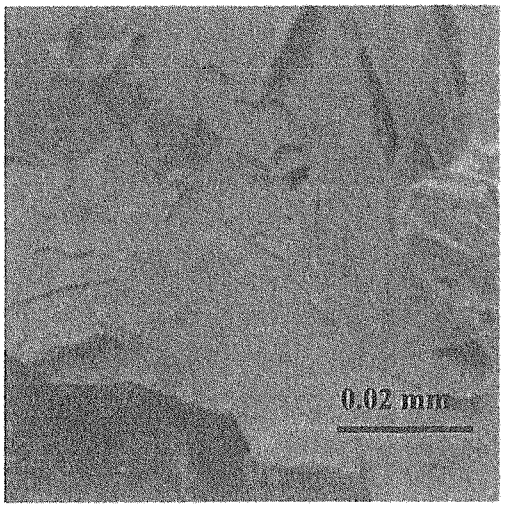

Fig. 5 Fracture surface in brittle temperature region in SP testing for F82H steel implanted with He ions.

4.2 FT-IR PAS spectra of Li_2TiO_3 irradiated with multi-ion beams

D. Yamaki, T. Nakazawa, T. Aruga, T. Tanifuji, S. Jitsukawa
Department of Materials Science, JAERI

1. Introduction

Li_2TiO_3 is regarded as one of the most suitable candidates for the solid tritium breeder material of D-T fusion reactors[1]. It is known that, in an operating fusion reactor, the radiation damage in Li_2TiO_3 will be caused by fast neutrons, energetic tritons and helium ions generated in $^6Li(n,\alpha)^3H$ reaction. The irradiation damage caused by such radiations may result in the microstructural changes, and the changes may affect the characteristics of Li_2TiO_3 such as tritium release behavior. Thus the study of irradiation defects and microstructural change caused by irradiation in Li_2TiO_3 is essential to evaluate its irradiation performance.

Simulation of the fusion reactor environment and hence the study of a synergistic effect of atomic displacement damage in Li_2TiO_3 are presumed to be approached by a simultaneous irradiation with "triple" ion beams which consist of O^{2+}, He^+ and H^+ ion beams. In the previous study, the formation of the anatase (TiO_2) layer on the surface of Li_2TiO_3 by irradiation with triple ions has been found. It is also clarified that the formation mainly caused by the effect of O^{2+} ion beam irradiation[2-4]. In the present study, the results of the FT-IR photoacoustic spectroscopy (PAS) with Li_2TiO_3 samples irradiated with the single and the triple ion beams were analyzed to study the relation between the irradiation effects and the microstructural change.

2. Experimental

The characteristics of the Li_2TiO_3 samples used in this experiment were described in ref.4. The Li_2TiO_3 samples were irradiated at 573K with the single and the triple ion beams of 0.25 MeV H^+, 0.6 MeV He^+ and 2.4 MeV O^{2+}. The fluence of the respective ions were about $1x10^{21}$ ions/m^2 The ion energies were so chosen that the projected ranges of the irradiated ions in Li_2TiO_3 were around 2 μm[3].

3. Results and discussion

The FT-IR PAS spectrum of a non-irradiated sample is shown in Fig.1. It should be noted that the photoacoustic signal is generated from the surface layers of sample with a thickness of some micrometers which is a function of the mirror velocity of the FT-IR interferometer and wavenumber. In this case, the thickness is about 5-15μm. As mentioned in section 2, the ion projection ranges are about 2 μm so that the obtained spectra of irradiated samples are a superposition of spectra of irradiated part and non-irradiated part.

As shown in Fig. 1, the characteristic peaks in FT-IR PAS spectra are observed in three regions; 500-900 cm^{-1}, 1300-1700 cm^{-1} and 2600-3600 cm^{-1}. These peaks are considered to be due to Ti-O bond in Li_2TiO_3, C=O bond in Li_2CO_3 as the impurity in the

samples and O-H bond in -OH adsorbed or absorbed near the surface, respectively. From the peak analysis, it is found that the spectrum in the Ti-O bond region has two peaks around 700cm^{-1} and 800cm^{-1} and that in the O-H bond region has also two peaks around 3200cm^{-1} and 3500cm^{-1}.

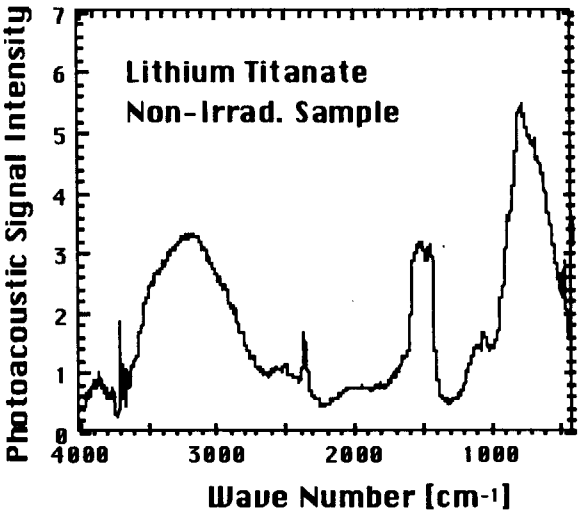

Fig.1 FT-IR PAS spectrum of non-irradiated Li_2TiO_3.

The peaks around 800cm^{-1} of the samples are compared in Fig.2. There is little difference in the peaks of the samples with non-irradiated, irradiated with He^+ and with H^+. The peaks of the samples irradiated with triple ion beams and O^{2+} beam are much larger than that of non-irradiated sample and the peak position of them shift to the higher from that of non-irradiated sample. These results show that the difference in the 800cm^{-1} peaks reflects the formation of the anatase (TiO_2) layer observed in the samples irradiated with triple ion beams and O^{2+} beam[2-4]. The ratio of the electron stopping power (Se) and displacements per atom (dpa) with triple, O^{2+}, He^+ and H^+ beam irradiation are about 10:7:2:1 and 10:9:1:0.1, respectively. The ratio of the area difference between the peaks of each irradiation and non-irradiation is about 10:6:1:0.5, that is, rather close to that of Se. It may depicts that the formation of anatase is effected by Se.

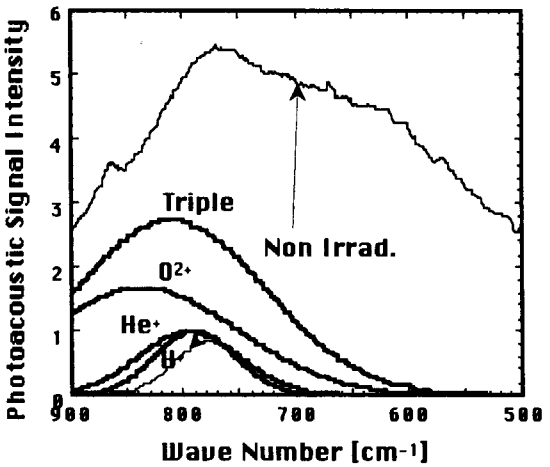

Fig.2 The comparison of the peaks around 800 cm^{-1} in the Ti-O bond region.

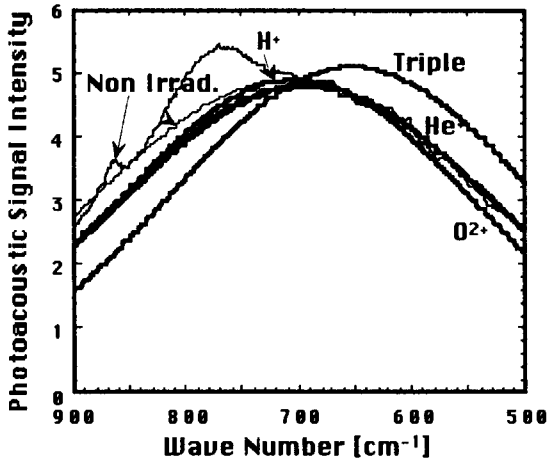

Fig.3 The comparison of the peaks around 700 cm^{-1} in the Ti-O bond region.

The peaks around 700 cm^{-1} of the samples are compared in Fig.3. There is little difference in the peaks of the samples with non-irradiated and irradiated with each single ion beam. The peak of the sample irradiated with triple ion beams is rather larger than that of non-irradiated sample and the peak

position shift to the lower from that of non-irradiated sample. It suggests that a certain kind of microstructure change related to the Ti-O bond occurs by simultaneous multi-ion beams irradiation.

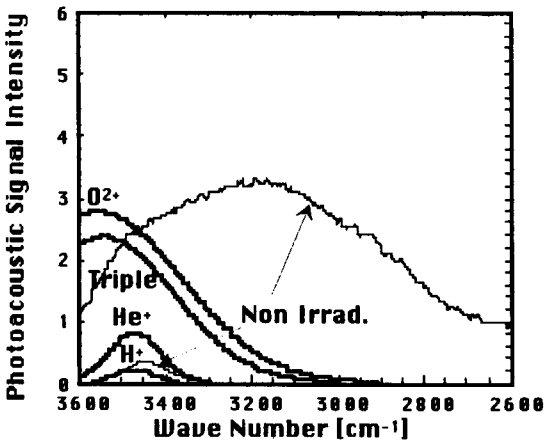

Fig.4 The comparison of the peaks around 3500 cm^{-1} in the O-H bond region.

The peaks around 3500cm^{-1} of the samples are compares in Fig.4. Because the peak position is close to that of O-H bond in the TiOH on TiO_2 surface (about 3650cm^{-1}), the 3500 cm^{-1} peaks are considered to be caused by TiOH near the surface of Li_2TiO_3. The 3200 cm^{-1} peak in the O-H bond region is considered to be due to the water vapor which inevitably exists in the measurement system. There is little difference in the peaks of the samples with non-irradiated and irradiated with H^+. The peak of the sample irradiated with He^+ beam is rather larger than that of non-irradiated sample. The peaks of the samplers irradiated with triple ion beams and O^{2+} beam are much larger than that of non-irradiated sample and the peak position of them approaches to that of TiOH on TiO_2 surface. It is considered that the peak position shift observed with the samples irradiated with triple ion beams and O^{2+} beam reflects the interaction between -OH and TiO_2 formed by irradiation. The ratio of the area difference between the peaks of each irradiation and non-irradiation is about 10:12:1:0, that is, rather close to that of dpa. It suggests that the irradiation defects become the trapping sites of hydrogen causing the O-H bond near the surface.

4. Conclusion

The microstructure changes in Li_2TiO_3 irradiated with the single and the triple ion beams of H^+, He^+ and O^{2+} were observed with FT-IR PAS. From the results in the Ti-O bond region, it is considered that the formation of anatase is affected by the electron stopping power of each irradiation, and a certain kind of microstructure change related to the Ti-O bond occurs by simultaneous multi-ion beams irradiation. From the results in the O-H bond region, the interaction between the irradiation defects and hydrogen are suggested.

Reference

1) P.Gierszewski, Report no CFFTP G-9561, 1995.

2) T.Nakazawa, V.Grishmanovs, D.Yamaki, Y.Katano, T.Aruga, A.Iwamoto, S.Jitsukawa, JAERI-Review 2001-039 (2001) 146.

3) T.Nakazawa, V.Grishmanovs, D.yamaki, Y.Katano, T.Aruga, A.Iwamoto, 2000 Int. Comf. on Ion Implantation Technology Proc.(2000)753.

4) D.Yamaki, T. Nakazawa, T. Aruga, T. Tanifuji, S. Jitsukawa, A. Iwase, JAERI-Review 2002-035 (2002)133.

4.3 Effect of triple ion irradiation on microstructural development and mechanical properties of SiC/SiC composites at high Temperature

T. Taguchi*, S. Miwa**, N. Igawa*, E. Wakai***, S. Jitsukawa*** and A. Hasegawa**
Neutron Science Research Center, JAERI *
Department of Quantum Science and Energy Engineering, Tohoku University**
Department of Materials Science, JAERI ***

1. Introduction

Ceramic matrix composites show excellent mechanical properties at high temperature and non-catastrophic failure behavior. These materials, therefore, are expected to be used for structural applications at high temperature. In particular, silicon carbide fiber reinforced silicon carbide matrix (SiC/SiC) composites are candidate materials for first wall and blanket components in a fusion reactor because of their low residual radioactivity after neutron irradiation. In the fusion environment, helium (He) and hydrogen (H) atoms are produced by 14-MeV neutron-induced transmutation reactions which are (n,α) and (n,p), respectively. These transmutation rates in SiC, which are 130 appm He / dpa and 40 appm H / dpa, are larger than those in the other candidate materials such as ferritic steels and vanadium alloys[1),2)]. The effect of He atoms with displacement damage on microstructural change and mechanical properties had been examined[3)]. However, the effect of H atoms with He atoms and displacement damage on their properties has not been investigated.

In this study, the effect of H atoms with He atoms and displacement damage on microstructural change and mechanical properties of SiC/SiC composites at higher temperature than 800 ' C.

2.Experimental procedure

2.1 Materials

The SiC/SiC composites were fabricated by Forced Chemical Vapor Infiltration process in Oak Ridge National Laboratory. Igawa et al. reported the details of fabrication procedure[4)]. The 2D plane weave of Hi-Nicalon Type S SiC fiber fabric, which has high crystallinity and stoichiometry, was used in these composites. These composites have approximately 150 nm carbon layer as an interphase layer between matrix and fiber. The surfaces of these specimens were polished by diamond blade (#100, 600 and 8000).

2.2 Irradiation

The simultaneous ion irradiation was carried out at TIARA facilities of JAERI. The specimen was irradiated with 6.00 MeV Si^{2+} ions from the surface with simultaneous implantation of He and H by 1.0 MeV He^{+} and 340 keV H^{+} ions at 800, 1000 and 1300 'C. He and H ions implantation was performed with using the Al foil energy degrader in order to widen the He and H distribution region in the specimen. Figure 1 shows the distribution of He, H concentration and displacement damage as a function of depth from surface in SiC calculated by TRIM code[5]. In this study, the average displacement threshold energies of Si and C were assumed to be 35 eV and 20 eV[6], respectively.

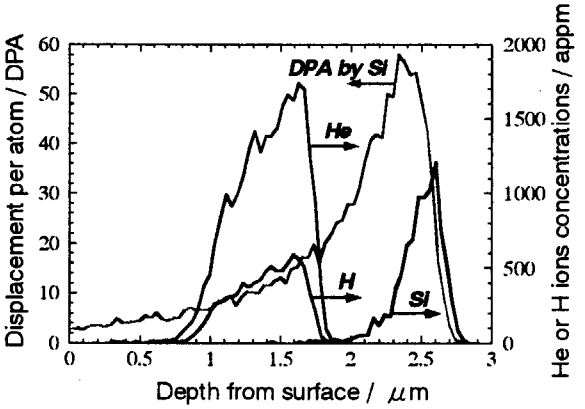

Fig.1 Distribution of He, H concentration and irradiation damage as a function of depth from surface in SiC calculated by TRIM code [5].

2.3 Microstructure observation

The Focused Ion Beam processing was performed in order that a single thin film for Transmission Electron Microscopy (TEM) observation can contain the fiber, matrix and interphase layer and each phase can contain the irradiation region and non-irradiation region. Microstructure observation was performed with Hitachi HF-2000 field emission TEM operating at 200 kV.

3. Results

The TEM microphotographs of irradiated matrices in the SiC/SiC composites are shown in Fig. 2. Helium bubbles were observed in the irradiated matrices at higher irradiation temperature than 800 'C. The average size of He bubbles increased with increasing the irradiation temperature. And the average size of He bubbles in the matrix irradiated by triple ion beams is larger than that in the matrix irradiated by dual ion beams. He bubbles were observed in the range of only He implanted depth by dual and triple ion irradiation at 800 'C. At 1000 'C, they were observed in the range only He implanted depth by dual ion irradiation while they were formed in the widened region from He implanted depth to the irradiation surface by triple ion irradiation. At 1300 'C, they were observed in the widened region from He implanted depth to the irradiation surface by dual and triple ion irradiation. They were mainly formed at the grain boundary of the matrix irradiated at 800 and 1000 'C while they were formed in the grain and at the grain boundary of the matrix irradiated at 1300 'C. These results revealed that H with He and displacement damage enhanced He bubbles

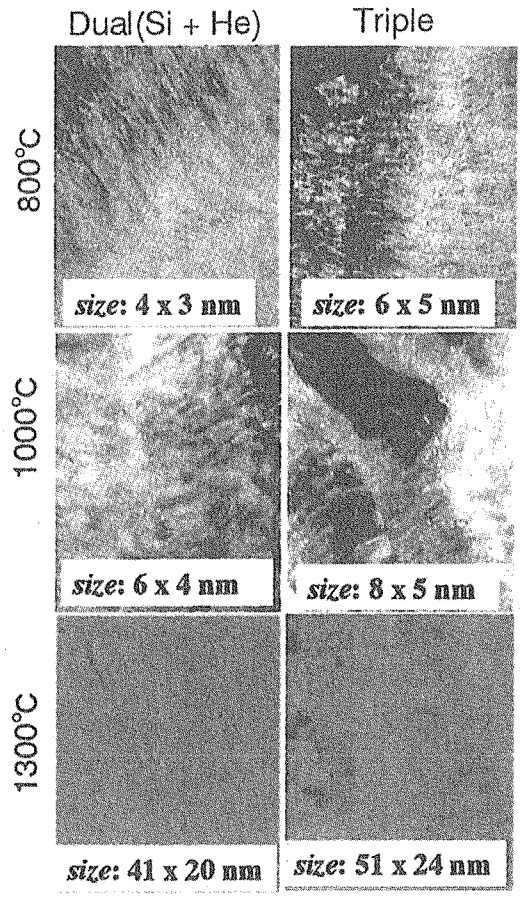

Fig. 2 TEM microphotographs of irradiated matrices in the SiC/SiC composites at higher temperature than 800 ' C.

formation; the average size was increased and the formation range of He bubbles was widened.

Figure 3 shows the hardness change of the matrix after the ion irradiation. The hardness of un-irradiated matrix was approximately 43 GPa. The effect of He and H implantation with displacement damage on the hardness change of the matrix after the ion irradiation was not significant.

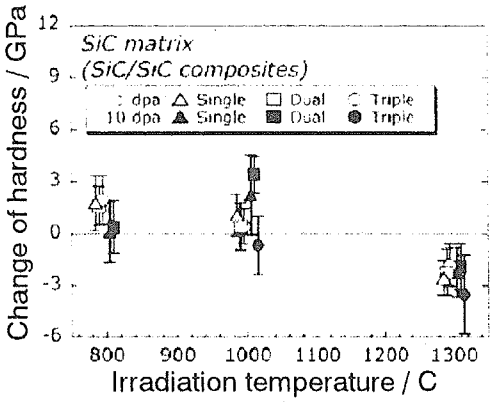

Fig.3 Hardness change of the matrix after ion irradiation.

References

1) L. L. Snead, R. H. Jones, A. Kohyama and P. Fenici, Journal of Nuclear Materials 233-237 (1996) 26-36

2) T. Noda and M. Fujita, Journal of Nuclear Materials 233-237 (1996) 1491-1495

3) S. Nogami, A. Hasegawa, K. Abe, T. Taguchi and R. Yamada, Journal of Nuclear Materials 283-287 (2000) 268-272

4) N. Igawa, T. Taguchi, L. L. Snead, Y. Katoh, S. Jitsukawa, A. Kohyama and J. C. McLaughlin, Journal of Nuclear Materials 307-311 (2002) 1205-1209

5) J. F. Ziegler, J. P. Biersack and U. Littmark, The Stopping and Ranges of Ions in Matter, vol.1, Pergamon Press, New York, 1985

6) R. Devanathan and W. J. Weber, Journal of Nuclear Materials 278 (2000) 258-265

4.4 Damage evolution in high energy multi ion-irradiated BCC metals and the interaction between gas atoms (H and He) and damage defects

I. Mukouda*, Y. Shimomura**, D. Yamaki***, T. Nakazawa***, T. Aruga*** and S. Jitsukawa***

Graduate School of Engineering, Hiroshima University*, Hiroshima Institute of Technology**, Department of Materials Science, JAERI***

1. Introduction

For fusion reactor applications, there is an interest in vanadium and its alloys. Hydrogen and helium atoms are generated by nuclear transmutation in the fusion environment. These gas atoms play an important role in the evolution of the damage microstructure. It is well known that helium is active in cavity nucleation. Sekimura et al.[1] have carried out on multiple beam ion irradiation to study the role of gases. In the present work, quantitative experiments were carried out study the role of helium and hydrogen in the evolution of damage microstructure in irradiated materials. It is possible to control the concentration of gas atoms in irradiated metals by ion irradiation at high energy. We examined void formation in high energy ion-irradiated pure vanadium by both single beam (5 MeV Ni) and dual-beam (5MeV Ni ion and 600 keV He or 260kV H ion) irradiation. The ion energy was selected so that the projected range of the gas ions in vanadium might coincide with depth of peak damage (1.3 μm) calculated by the TRIM 95 code. Specimens for TEM cross sectional observation were prepared by a FIB (Focused Ion Beam) device. The relation between gas atoms and damage structure was derived from experimental results.

2. Experimental procedure

The pure vanadium had a nominal purity of 99.8%. This material was called as-received vanadium (V(AR)). Some specimens were degassed by melting in vacuum at 10^{-5} Pa in a levitation furnace [2]. This specimen was called residual-gas-free V (V(RGF)). Annealed disks of 3mm in diameter and 0.05 mm thick were prepared from each material. The irradiation was carried out with the TIARA (Takasaki Ion Accelerators for Advanced Radiation Application) accelerators at the Takasaki-establishment of JAERI (Japan Atomic Energy Research Institute) at 500 and 600°C. The ion energy was selected so that the projected range of the gas ions in vanadium coincides with the depth of peak damage (1.3 μm) calculated by the TRIM 95 code [3]. The peak damage rate was 2 x 10^{-3} dpa/s and total dose at the damage peak was 22 dpa. The ions stop within the depth of two microns from the surface and damage was formed up to this depth. For quantitative investigation, the damage structure has to be observed as a function of depth. We utilized FIB microscopy. The FIB generates 30 keV Ga ions and illuminates specimen surface with glancing angle. To preserve the surface of the ion-irradiated metals from sputtering, we deposited tungsten on the irradiated surface. In our previous work, it was found that interstitial atoms form near surface clusters throughout FIB-thinned specimens. To overcome this difficulty, we developed a TEM specimen preparation method which is a combination of FIB thinning and electro-polishing [4-6]. To remove regions damaged by the Ga ions, the

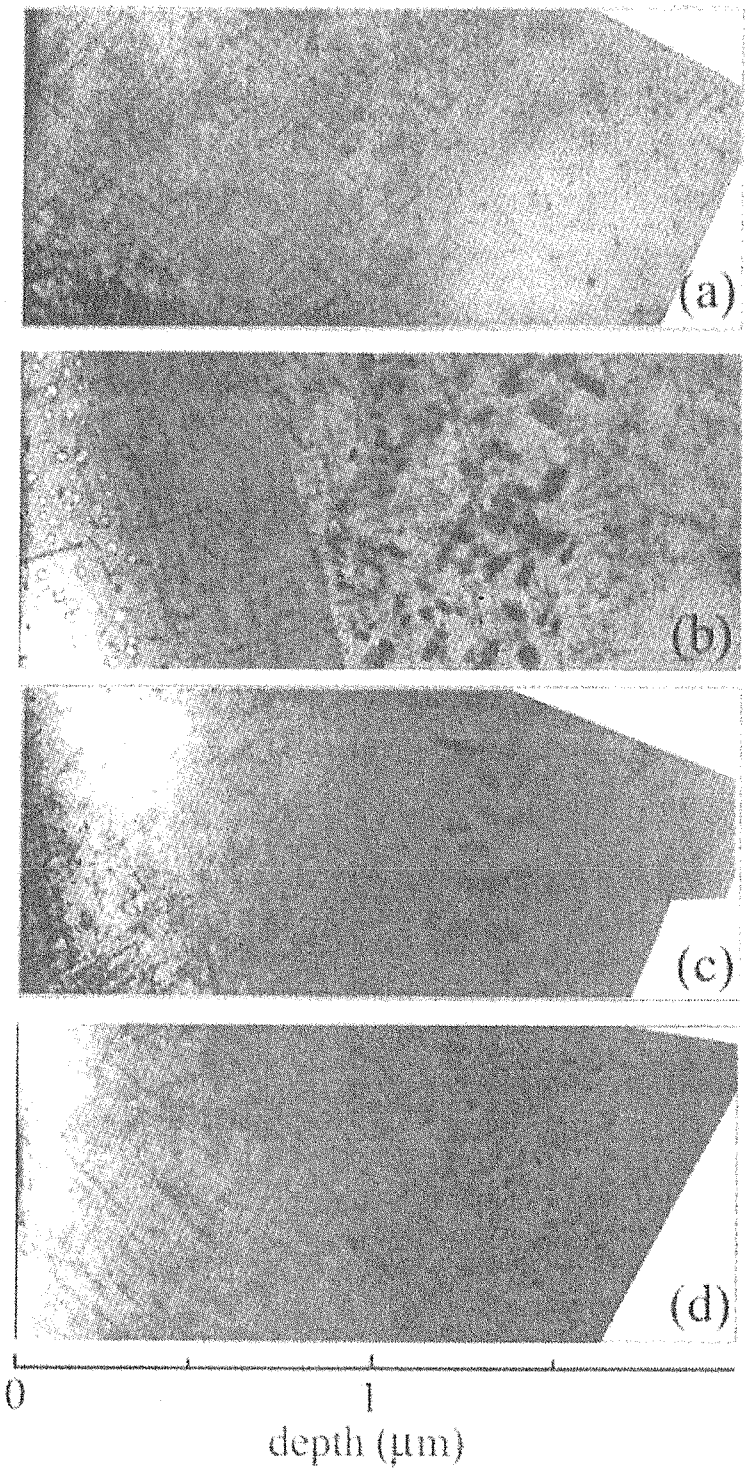

Fig. 1 Damage structure of ion-irradiated, as-received pure vanadium.(a) 5MeV Ni ion irradiation at 500°C, (b) 5MeV Ni ion irradiation at 600°C and (c) 5MeV Ni + 0.26MeV H ion irradiation at 600°C, (d) 5MeV Ni + 0.6MeV He ion irradiation at 600°C.

specimens were electro-polished in a solution of 20% H_2SO_4 and 80% methanol cooled to -30°C at an applied potential of 12V for 1 sec. The specimens were electro-polished to remove the

region damaged by FIB. After electro-polishing, no dot type defects were observed.

3. Results and discussion

When only nickel ions were used, voids formed in the region from the surface to a depth of about 0.5 μm when irradiated at 500 and 600°C, as shown in Fig. 1(a) and (b). However, in the region of the damage peak, voids were not observed. Needle-like precipitates of about 100nm in length were observed in all specimens covering the whole penetration depth of the ion. It is thought that the precipitate is some type of carbide, because there is oriented <100> direction[7] and the specimen includes a few hundred ppm carbon as a impurity. Moreover, in the specimen irradiated at 600°C, granular precipitates were observed in the region of 1.0 to 1.5 μm depth. In the case of Ni + H irradiation, the size of the voids was small and the number density was similar to that in the case when only nickel ions were used, as shown in Fig. 1(b) and 1(c). Void swelling was suppressed by simultaneous hydrogen irradiation. Void formation was observed within the whole ion penetration depth in the specimen irradiated with Ni + He ions simultaneously, as shown in Fig. 1(d). The needle-like precipitate was observed. Needle-like precipitation formed in any combination of Ni, Ni + H, Ni + He irradiation, but void formation depended on gas ion implantation. In pure vanadium, helium atoms promote void nucleation for irradiation at 500 and 600°C in the low dose region. In the case of Ni + H irradiation at 500°C, small voids were observed within the whole ion penetration depth, while hydrogen atoms suppressed void formation in the case of irradiation at 600°C. These results show that hydrogen atoms trap small vacancy clusters at 500°C, and vacancy clusters and H atoms or molecules dissolved with increasing temperature.

References

1) N. Sekimura, T. Iwai, Y. Arai, S. Yonamine, A. Naito, Y. Miwa and S. Hamada, J. Nucl. Mater., 283-287 (2000) 224-228.

2) K. Sugio, Y. Shimomura, I. Mukouda and M. Kiritani, Radiation Effects and Defects in Solids, 157 (2002) 43-51.

3) J. F Ziegler and J.P. Biersack, The Stopping and Range of Ions in Solids (Pergamon Press, New York, 1985)

4) I. Mukouda, Y. Shimomura, T. Iiyama Y. Katano, D. Yamaki, T. Nakazawa and K. Noda, Mat. Res. Soc. Symp. Proc. Vol. 540 (1999) 549-554.

5) I. Mukouda, Y. Shimomura, T. Iiyama, Y. Harada, Y. Katano, T. Nakazawa, D. Yamaki and K. Noda, J. Nucl. Mater. 283-287 (2000) 302-305.

6) I. Mukouda, Y. Shimomura, D. Yamaki, T. Nakazawa, T. Aruga and S. Jitsukawa, J. Nucl. Mater., 307-311 (2002) 412-415.

7) K. Ochiai, H. Watanabe, T. Muroga, N. Yoshida and H. Matsui, J. Nucl. Mater. 271-272 (1999) 376-380.

4.5 Influence of H and He on corrosion behavior of ion irradiated stainless steel

Y.Nemoto*, Y.Miwa*, H.Tsuji*, T.Tsukada*, H.Abe** and N.Sekimura**
Department of Nuclear Energy System, JAERI*
Department of Quantum Engineering and System Science, The University of Tokyo**

1. Introduction

Irradiation assisted stress corrosion cracking (IASCC) is one of the main concerns of aging problem on light water reactors (LWR),[1-5] and also on the design of international thermonuclear experimental fusion reactor (ITER).[2]

Degradation of corrosion resistance by irradiation is important to study IASCC. The corrosion resistance is influenced by formation of precipitations, defects and inhomogeneous regions due to redistribution of alloying elements by irradiation.[6] Moreover, under neutron irradiated condition, neutron transmutation produce hydrogen (H) and helium (He) atoms in materials. However, the effect of these atoms on corrosion behavior had not been studied yet.

The aim of this work is to develop an evaluation method for corrosion behavior of irradiated materials using atomic force microscope (AFM), and to study the influence of H and He atoms on corrosion behavior of ion irradiated materials.

2. Experimental procedure

The chemical composition of stainless steel used in this study is listed in table 1. The stainless steel was high purity Fe-18Cr-12Ni alloy that was solution annealed at 1323K for 30min. Specimens were fabricated to sheet of 6mm in length, 3mm in width and 0.3mm in thickness. The surface of specimens were mechanically polished with emery papers and diamond paste of 0.3μm diameter, then electrochemically polished in a solution with

Table 1 Chemical composition (wt.%)

C	N	Si	P	S	Ti
0.003	0.0014	0.01	0.001	0.0014	0.01

Mn	Cr	Ni	Al	Fe
1.36	18.17	12.27	0.16	Bal.

Table 2 Irradiation conditions

Radiation damage at examined area (dpa)	Irradiation temperature (K)	H or He concentration at 1.5μm (appm)
35	573	0
35	573	17500 (H)
35	573	1750 (He)
35	573	17500 (He)

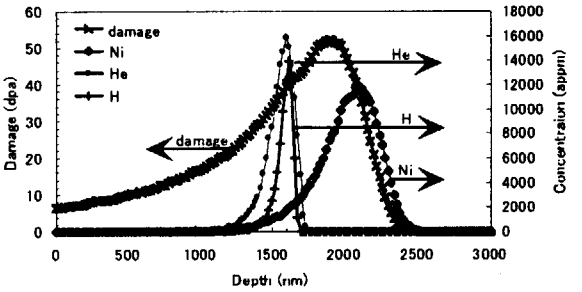

Fig.1 Typical distributions of radiation damage and ion contents along the depth in specimens.

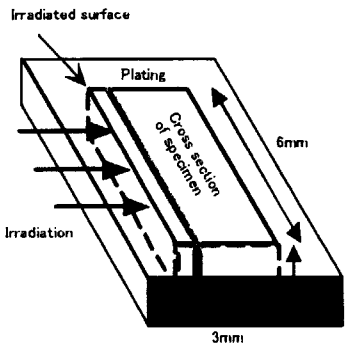

Fig.2 Illustration of the sheet shaped specimen.

H_3PO_4 54%, H_2SO_4 36%, CH_3OH 10% at about 278K with a potential of 18V for 5.0s.

Ion irradiation experiments of specimens were conducted at the Takasaki ion accelerators for advanced radiation application (TIARA) of the Japan atomic energy research institute

(JAERI).

Irradiation for the specimens was conducted at the side of sheet. 12MeV Ni^{3+} ion was irradiated to give radiation damages, and H^+ or He^{2+} ion was synergistically implanted to the specimens. Irradiation conditions are listed in Table 2.

Depth profile of radiation damage and implanted ion was calculated by TRIM85 code, and the typical result of the depth profile is shown in Fig.1. The depth profile was almost the same for every irradiation conditions. H^+ or He^{2+} ion was implanted at depth of about 1.5 μm where not peak-damage region. Near peak-damage region, implanted Ni ion may affect on radiation damage. Therefore, the peak-damage region was avoided for H^+ or He^{2+} ion implantation, although steep distribution profile for radiation damage exists at depth of 1.5 μm.

To protect the irradiated surface, copper (Cu) film was plated on the sheet type specimens before corrosion test. The aqueous solution used for Cu plating contains $CuSO_4$ 90g, H_2SO_4 15ml and pure water 475ml. Plating was processed with current density about 0.03A/cm^2, at ambient temperature with anode metal of pure Cu. After plating, side of specimens was mechanically polished as smooth as possible with alumina powder of 0.3μm in diameter. Corrosion behavior was evaluated at surface parallel to irradiation direction, as seen in Fig.2. As seen in Fig. 1, radiation-induced damage had a distribution along ion penetration depth. On the cross-sectional surface of sheet type specimens, effect of radiation damage profiles on corrosion behavior could be examined. In this work, a corrosion test at passivation potential (150mV vs. Ag/AgCl) for 500s in solution of 0.5mol/l H_2SO_4 and 0.01mol/l KCSN at 303K gave moderate surface condition for AFM (Thermo Microscope co. ltd., Explorer SPM system) evaluation.

3. Results and discussion

Influence of irradiation conditions on corrosion behavior was evaluated. Typical AFM topography on the cross-sectional surface of irradiated specimen after corrosion test is shown in Fig.3. In Fig.3, irradiated surface is indicated on left side of topography by dotted line, and peak area of radiation damage was at depth of about 1.0 to 2.0μm inside from the irradiated surface. Only peak area of radiation damage was etched uniformly. Height distribution was measured along the line drawn on topography; it is across peak area of radiation damage, as shown in Fig.3. In this study, corrosion rate was estimated by cross sectional area of corroded region. Fig.4 shows the effect of synergetic H or He implantation on corrosion rate. H implantation seems to increase corrosion rate. On the other hand, increasing He implantation content decreased corrosion rate.

To investigate the mechanism of these effects of implanted ions, detailed microscopic studies are required. The effect of H implantation would be more complicated, but the effect of He implantation can be drawn from some information on former studies.[4), 7-9)] He atoms are insoluble to stainless steels. They combine with vacancies preferentially, and form stable He-vacancy pairs and He atoms-vacancies clusters. Therefore, the diffusion of vacancies to sinks and the loss of vacancies due to mutual recombination between vacancies and interstitials may be suppressed in materials containing He atoms. This mechanism could result in the suppression of Cr depression at sinks such as grain boundaries. Dewi et al. reported that radiation induced Cr depression at grain boundaries was suppressed by He implantation.[9)] In this study, suppression of corrosion behavior by He implantation was

observed in matrix of grains. The mechanism might suppress redistribution of element by radiation damage at/near radiation-induced defects such as dislocation loops and cavities that also act as sink for both interstitials and vacancies. Cr depleted zones at/near such defects are considered to become initiation points of corrosion. Therefore, it could be inferred that He implantation suppressed corrosion on irradiated specimens.

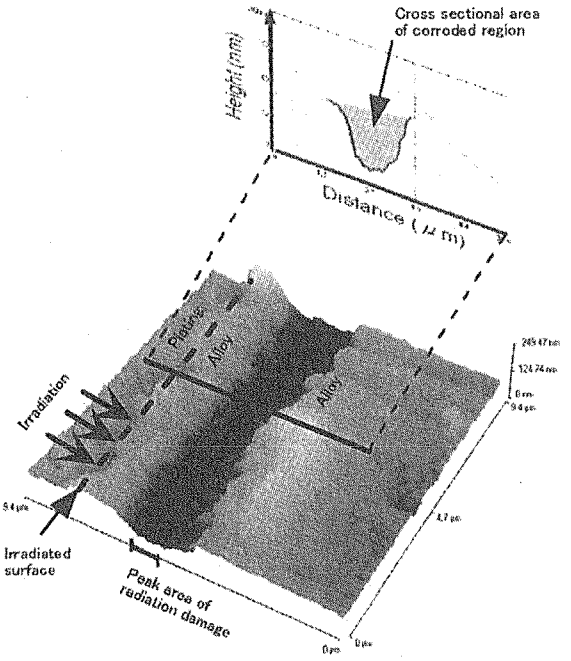

Fig.3 Typical AFM topography on cross section of the specimen ion irradiated.

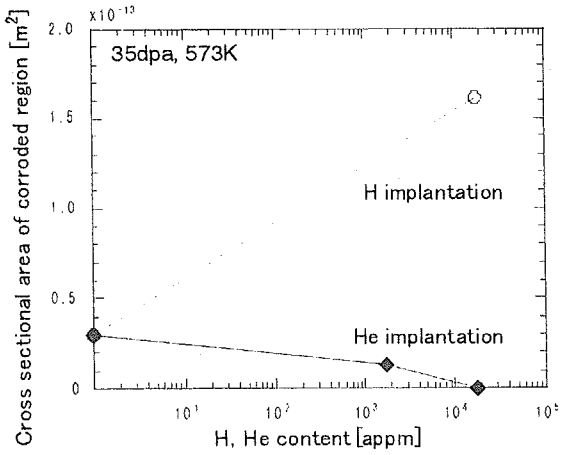

Fig.4 Effect of H and He implantation for corrosion behavior of ion irradiated stainless steel.

Acknowledgement

The authors are grateful to Mr. Tomio Suzuki, Drs. Chiaki Kato and Hiroyasu Tanigawa of Japan Atomic Energy Research Institute (JAERI) for many useful advises about plating, polishing, corrosion procedure and AFM evaluations.

Reference

1) M. Kodama, R. Katsura, J. Morisawa, S. Nishimura, S. Suzuki, K. Asano, K. Fukuya, K. Nakata, *Proc. 6th Int. Symp. on Environmental Degradation of Materials in Nuclear Power Systems - Water Reactors*, (1993) 583.
2) T. Tsukada, *JAERI-Research 98-007* (1998).
3) P.L. Andresen, *Stress - Corrosion Cracking*, Chapter 6, ASM, (1992) 181.
4) S.M. Bruemmer, *J. Nucl. Mater.*, 274 (1999) 299.
5) J. Robertson, *Corrosion Science*, Vol. 32, *No.4* (1991) 443.
6) V.V. Sagaradze, *J. Nucl. Mater.*, 280 (2000) 345.
7) H. Takahashi, *J. Atomic Energy Society of Japan*, Vol.27 (1985) 507.
8) T. Hashimoto, *Physical Review* B, 38 (1988) 868.
9) K. Dewi, A. Hasegawa, S. Otsuka, K. Abe, *Fusion Technology*, 39 (2001) 585.

4.6 Radiation Hardening of Low-Activation Ferritic/Martensitic Steel

E. Wakai*, T. Sawai*, S. Jitsukawa*, M. Ando**, H. Tanigawa**, K. Nakamura**, H. Takeuchi**, K. Oka***, T. Tanaka*** and S. Ohnuki***

Department of Materials Science, JAERI*,
Department of Fusion Engineering Research, JAERI**,
Faculty of Fusion Engineering, Hokkaido University***.

1.Introduction

Ferritic/martensitc (F/M) steels are first candidate materials for the structural materials of fusion nuclear reactor and also prominent materials for the target vessel of spallation neutron source because of their excellent mechanical properties and low-activation. The various properties of F/M steels irradiated by high-energy particles are intensively examining. In these irradiation environments, the incident of high-energy particle into materials produces not only displacement damage but also transmutation atoms such as helium and hydrogen, and the synergistic effects of displacement damage and transmutation atoms on mechanical properties and microstructures are required for the evaluation of F/M steels. The evaluations for the property changes of F/M steels up to high dose level about from 50 to 100 dpa are very important theme, and the simultaneous triple ion irradiation experiments using triple ion accelerators are extremely necessary. The combination of ultra micro-indentator and TEM microstructure analysis is a leading role for examining the dependence of displacement damage on change of radiation-hardening[1), 2)]. The synergistic effect of displacement damage and transmutation gas atoms on swelling behavior of F/M steels is recently found by our studies[3), 4)]. For the suppression of radiation-embrittlement, it is very important to reduce radiation-hardening. The main purpose of this study is to examine the method of reducing radiation-hardening and the effect of transmutation gas atoms on radiation hardening.

2. Experimental procedure

The specimens used for this study is low-activation ferritic/martenistic steel F82H (Fe-8Cr-2W-0.2V-0.04Ta-0.1C). The specimens were treated by several heat conditions to improve the radiation-resistance. The shape of the specimen is 6 mmL x 3 mmH x 0.8 mmt. A plane of 6 mm x 0.8 mm were polished by the SiC paper up to #4000 and 0.3 μm alumina powder and the final polishing was perfomed by electrolytic surface polishing. The area of 2 mmL x 0.8 mmt within 6 mmL x 0.8 mmt was irradiated. The irradiations were performed by several conditions of Fe^{3+} single irradiation, a simultaneous dual irradiation of Fe^{3+} and He^{+} ions, and a simultaneous triple irradiation of Fe^{3+}, He^{+} and H^{+} ions. The energies of the ions were 10.5 MeV-Fe^{3+} ions, 1.05 MeV-He^{+} ions and 0.38 MeV-H^{+} ions. Two energy degraders were used to spread the depth ranges of He and H ions during the irradiation. The irradiation temperature is from 270 to 600°C. The level of displacement damage is from 5 to 62 dpa (displacement per atom) at a depth of $1x10^{-6}$ m. The main component of displacement damage is caused by 10 MeV-Fe^{3+} ions, and the damage peak is 1.75×10^{-6} m in depth. After the

irradiations, the change of hardness was measured by an ultra micro-indentation testing system of UMIS-2000. The direction of indentation was chosen to be normal to the irradiated surface. The irradiated specimens were also machined to observe into thin films by a Hitachi FB-2000A focused ion beam (FIB) processing instrument with a micro-sampling system using Ga^+ ions at 30 kV. After the FIB machining, the surface was removed by electrical polishing. The microstructures were observed by transmission electron microscopes operated at 200 kV.

3. Results and discussion

Ultra micro-indentation tests were performed on each of F82H steels at loads to penetrate about 400 nm at 23°C. The dependence of hardening induced by Fe single beam and simultaneous dual beams of Fe and He ions at 350°C is shown in Fig.1. The ratio of He/dpa for the dual ion beams is corresponds to the value of about 10 appm He/dpa in a fusion reactor. The hardness of the specimens irradiated by single Fe beam rapidly increased with the irradiation to 20 dpa and it was tends to saturate around 50 dpa. The difference of hardness between the single and dual beams was negligible up to 20 dpa and a slightly increment of hardness was observed at 50 dpa. In the TEM observation, very small dislocation loops of interstitial-type and dotted clusters were formed by these irradiations.

The dependence of radiation-hardening on displacement damage in F82H irradiated at 270 and 350°C was also examined in the specimens tempered at temperatures from 700 to 800°C as given in Fig. 2. The saturation level of radiation-hardening was found to be about 50 dpa in all specimens. This result shows that the saturation behavior of radiation-hardening does not depend on the initial microstructures such as the densities of dislocations and carbides.

The hardness of the specimens irradiated at 270°C to 20 dpa is shown in Fig.3. The heat condition of standard specimen was tempered at 750°C for 1 h. The modified condition of 1 was heated at 860°C for 0.5 h and at 700°C for 1 h. The modified condition of 2 was at 800°C for 1 h and at 700°C for 1 h. This result shows that radiation-hardening can be successfully reduced by modified heat treatments. The cause of reduction of radiation-hardening is thought to be changes of the concentration of solution carbon in matrix and density of dislocations by the heat treatment.

Swelling behavior of F82H and Fe-9Cr alloy was examined by triple ion beams (Fe+He+H) and dual ion beams (Fe+He or Fe+H) to 50 dpa at temperatures from 300 to 600°C. The swelling was remarkably enhanced by the synergistic effect of displacement damage, helium and hydrogen at around 470°C.

4. Conclusion

The method of reducing radiation-hardening and the effect of transmutation gas atoms on radiation hardening was mainly examined by an ultra micro-indentation technique and a transmission electron microscope. The irradiations were performed under 10.5 MeV-Fe^{3+} single irradiation, a simultaneous dual irradiation of Fe^{3+} and 1.05 MeV-He^+ ions, and a simultaneous triple irradiation of Fe^{3+}, He^+ and 0.38 MeV-H^+ ions. We have found that radiation-hardening can be reduced by modified heat treatments. The hardness of the specimens irradiated by single Fe beam increased rapidly with the irradiation to 20 dpa and it was tends to saturate around 50 dpa. The difference of hardness between the single and dual beams was negligible up to 20 dpa and a slightly increment of hardness was observed at 50 dpa. The dependence of radiation-hardening on

displacement damage was also examined at 270 and 350°C in the specimens tempered at temperatures from 700 to 800°C. The saturation level of radiation-hardening was found to be about 50 dpa in all specimens. This result shows that the saturation behavior of radiation-hardening does not depend on the initial microstructures such as the densities of dislocations and carbides.

Acknowledgement

The authors are grateful to the members of TIARA facility.

References

1) M. Ando, H. Tanigawa, S. Jitsukawa, T. Sawai, Y. Katoh, A. Kohyama, K. Nakamura and H. Takeuchi, J. Nucl. Mater., 307-311(2002)260.

2) T. Sawai, E. Wakai, T. Tomita, A. Naito and S. Jitsukawa, J. Nucl. Mater., 307-311 (2002)312.

3) E. Wakai, T. Sawai, K. Furuya, A. Naito, T. Aruga, K. Kikuchi, S. Yamamoto, H. Naramoto and S.Jitsukawa, J. Nucl. Mater., 307-311(2002)278.

4) E. Wakai, K. Kikuchi, S. Yamamoto, T. Aruga, M. Ando, H. Tanigawa, T. Taguchi, T. Sawai, K. Oka and S. Ohnuki., J. Nucl. Mater., 318(2003)267.

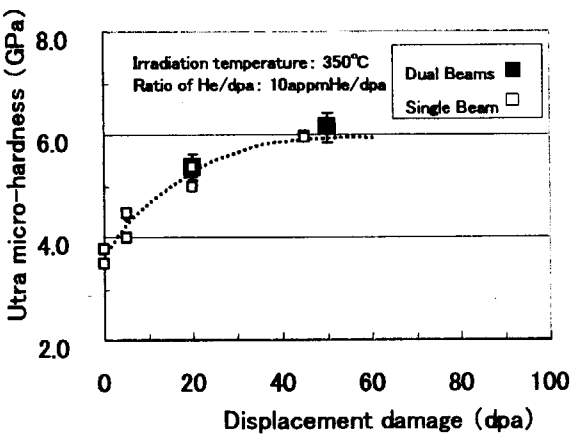

Fig. 1 Hardening induced by Fe single beam and simultaneous dual beams of Fe and He ions at 350°C

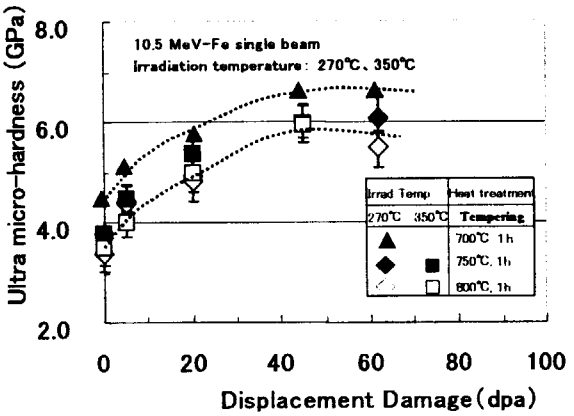

Fig. 2 The dependence of radiation-hardening on displacement damage in F82H irradiated at 270 and 350°C

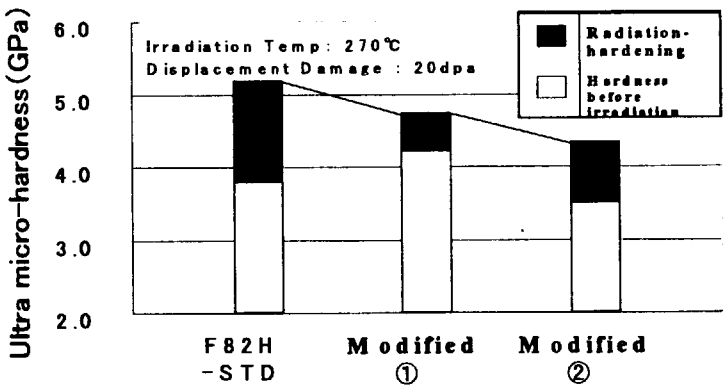

Fig.3 Reduction of radiation hardening in F82H steel by modified heat treatments.

4.7 Radiation Induced hardening under External Stress in Austenitic Stainless Steel

I.Ioka*, M.Futakawa*, Y.Nanjyo*, T.Suzuki*, K.Kiuchi* and T.Naoe**
Department of Nuclear Energy System, JAERI*
Graduate School of Ibaraki University**

1. Introduction

The ultra high burnup (>100GWD/t) of LWR(Light Water Reactor) is considered to be an important technology for establishing nuclear power plants as one of the most promising future energy system from a viewpoint of reducing radioactive waste and electrical cost. Cladding materials with the excellent long performance under heavy irradiation would be required to these developments. The high chromium austenitic stainless steel (25Cr-35Ni-0.2Ti UHP)[1,2] was selected as one of candidates that are possible to be made by the present engineering technologies.

The cladding tubes receive compressive stress under the irradiation environment by external pressure of primary coolant in the early burnup. In the latter burnup, they are subjected to tensile hoop stress by the swelling of fuel pellets (PCMI). Such stresses and neutron irradiation results in irradiation creep of the cladding tubes. It is important to evaluate mechanical properties and microstructural evolution including grain boundary segregation of the cladding in the development of cladding tube material for the ultra-high burn-up.

In this study, the change in hardness of the very shallow surface layer of the irradiated material under external stress was evaluated using the microindentation test.

2. Experimental procedure

The chemical compositions of the candidate material (25Cr-35Ni-0.2Ti UHP) and Type 304SS are shown in Table 1. 25Cr-35Ni-0.2Ti was machined from the plate produced by the thermo-mechanical treatment so-called SAR (strained, aged and recrystallized). Solution annealed Type 304SS was used in the test. The configuration of the specimen is shown in Fig. 1. The thickness of specimen is about 0.2mm. It has three different cross-sections (1.5mm, 1.75mm, 2.0mm in width) in order to irradiate in different stress at the same time. The surface of specimen was polished with #2400 paper and then was electro-polished. The schematic drawing of the ion irradiation holder for applying the required stress is shown in Fig. 2. The spring was used in order to apply the fixed stress in the specimen during irradiation. The strain gauge was attached at M division (1.75mm in width) of the specimen to measure the tensile strain before ion irradiation. The spring was adjusted so that the tensile strain of specimen may become about 0.2%. In this time, the strain of S division (1.5mm in width) and L division (2.0mm in width) were about 0.17% and 0.24%, respectively. The strain gauge was removed before irradiation.

The ion irradiation of specimen was carried out using TIARA facility. The irradiation condition was selected based on the condition calculated with computer simulation by assuming 100Gwd/t (MOX) on ABWRs. The dose rate, helium by (n, α) reaction and hydrogen by (n, p) reaction were simulated by the ion irradiation of 12MeV Ni^{3+}, 1.1MeV He^{+} and 380keV H^{+} at 573K corresponding to cladding surface temperature. The He^{+} and H^{+} ions were implanted in depth ranges from 1.0 to

1.5μm using energy degraders of aluminum foil. The concentration of He^+ and H^+ ions in the implanted range were 11 appmHe and 91 appmH, respectively. The dose was about 5dpa in the implanted range.

The microindentation test was carried out on the surface of specimens at room temperature. A testing machine, DUH-200 (Shimadzu Co.), was used for the microindentation test. A load was applied with a loading speed of 4.4mN/s, held 1 second and then removed. During loading, the load was continuously monitored along with the displacement with a resolution of 2mN and 0.01μm, respectively. The Berkovich indenter was used in the microindentation test. The obtained data was converted into the relationship between load/depth and depth (L/D-D curve), and the hardness was evaluated from the slope of these curves.

3. Results and discussion

The L/D-D curves of irradiated and unirradiated Type 30SS specimens are shown in Fig.3. The slope (straight solid and dotted lines in Fig.3) of L/D-D curve is in direct proportion to the hardness of the material. The slope of the irradiated specimen up to a depth of 0.4μm is higher than that of the curve over a depth of 0.4μm. The slope over a depth of 0.4μm is almost same as that of unirradiated. The slope of the irradiated specimen over a depth of 0.4μm corresponds to that of unirradiated specimen. From the slope of two lines before and after 0.4μm, the change in hardness of specimen by irradiation under the external stress was calculated. In the conversion of hardness, the average slope of 10 L/D-D curves was used.

Figure 4 shows the ratio of slope at irradiated region to that of the unirradiated region in the S, M and L divisions. In Type 304SS, the result of free load specimen added to Fig.4. The ion irradiated region hardened in comparison with the unirradiated division. The slope of unirradiated region at each division was almost same. The degree of the hardening decreased with increasing external stress. This tendency was recognized in 25Cr-35Ni-0.2Ti UHP specimens. It is considered that the tendency is attributed to the microstructural evolution by irradiation under external stress.

Although only the evaluation on hardness of irradiated specimen under external stress, these results are encouraging to continue the TEM observation.

4. Summary

The hardness of the ion-irradiated material under external stress was examined using the microindentation test.

(1) The degree of the hardening decreased with increasing external stress.

(2) The tendency of hardening under external stress was observed in Type 304SS and the candidate material (25Cr-35Ni-0.2Ti UHP) for ultra high burnup (>100GWD/t) of LWR.

References

1) K.Kiuchi, I.Ioka, M.Takizawa and Y.Wada, "Development of Advanced Cladding Material for Burnup Extension", IAEA Technical Meeting, Argentina, Nov. 25-298(1999).

2) K.Kiuchi, H.Ogawa, I.Ioka, Y.Kuroda and T.Anegawa, "Development of New Cladding Materials Applied for Advanced LWR Aiming at Ultra-high Burn-up and Fast Neutron Spectrum, International Congress on Advanced Nuclear Power Plants", June 9-13, 2002(Florida).

Table 1 Chemical Composition of the Material Tested in Weight Percent (%).

Materials	Fe	C	Si	Mn	P	S	Cr	Ni	Ti	N	O	Co
25Cr-35Ni-Ti UHP	bal.	0.0013	<0.005	0.001	0.001	0.0009	24.55	34.99	0.18	0.0014	0.0011	
Type 304SS	bal.	0.063	0.49	1.45	0.016	0.012	18.72	10.27				0.03

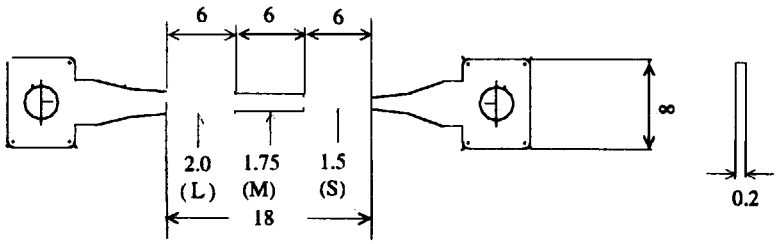

Fig. 1 Configuration of the specimen (mm)

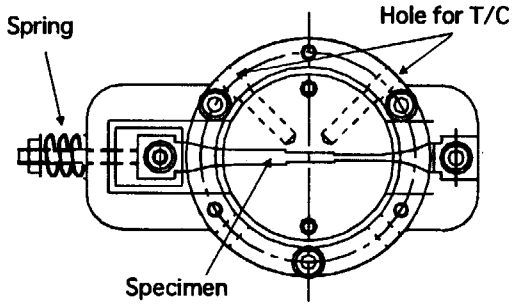

Fig. 2 Configuration of the ion irradiation holder

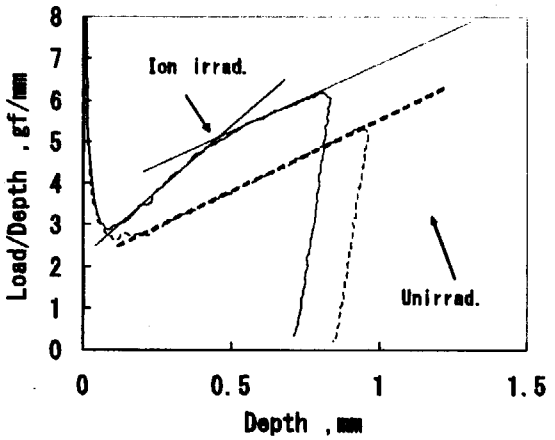

Fig. 3 L/D-D curves of irradiated and unirradiated specimens

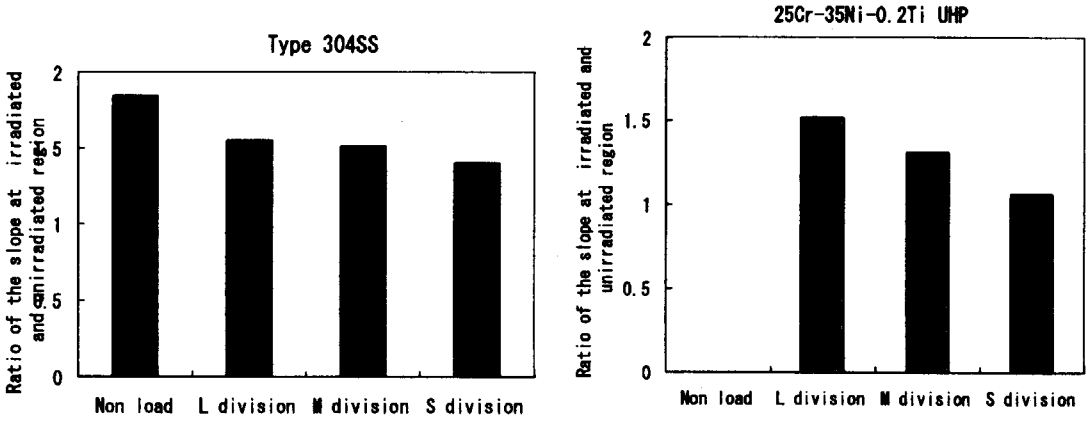

Fig. 4 Ratio of slope at ion irradiated region to that of the unirradiated region in the S, M and L divisions

4.8 Effect of ion irradiation on mechanical property of materials in contact with liquid metal

M.Futakawa*, Y. Kurata*, I. Ioka**, S. Saito*, A.Naito* and Y. Kogawa*
Center for proton accelerator facilities, JAERI *
Department of Nuclear Energy System, JAERI **

1. Introduction

The liquid metals are expected to use as neutron spallation targets, i.e. mercury for a high intensive neutron source [1] and lead-bismuth for accelerator-driven systems (ADSs) for transmutation of minor actinides and long-lived fission products [2]. The compatibility of the structural materials to the liquid metals is one of crucial issues from the viewpoint of the structural integrity and the determination of the lifetime of components under irradiation condition due to proton beam and spallation reaction. The material property on the interface between the liquid and solid metals under irradiation condition should be investigated to understand the feature of the compatibility to liquid metal. The schematic diagram on the investigation using TIARA facility to simulate irradiation condition is illustrated in Fig.1. In this paper, the mechanical properties change due to ion irradiation and mercury immersion against austenitic stainless steel, JPCA was examined by using the indentation technique that gives information on material properties of micro/nano-zones irradiated with ion beam and influenced by mercury immersion.

Additionally, in order to quantitatively evaluate the mechanical property, the inverse analysis was applied to the load and depth curves measured by using the instrumented indentation machine. In the inverse analysis, we have taken account of the irradiation damage distribution according to a distance from the specimen surface.

2. Experimental

Specimen is a disk of 3mm in diameter with 0.2mm thickness. The electrochemically polished specimens were irradiated at a temperature of 200°C with a triple ion beam; 12MeV Ni^{3+}, 750keV He^{+} and 290keV H^{+}, and a dual ion beam; Ni^{3+}, He^{+} and He^{+}, H^{+}. The SRIM97 code was used to compute the implanted ion concentration and the displacement dose as a function of depth beneath the specimen surface. The displacement damage in the specimen is mainly attributed to Ni^{3+} ion implantation. The peak dose position is around 2μm. The peak positions of implanted He^{+} and H^{+} ions are controlled so that the effect of implanted Ni^{3+} ions can be neglected. At the depth of approximately 1.3μm in the specimen, the dose is ca. 10 dpa and the He/dpa and H/dpa ratios are about 200 and 2000 appm/dpa respectively.

The irradiated specimens were immersed into the mercury of 300 cc covered by Ar gas. The temperature of the mercury was raised up to 150°C and kept to be constant up to certain periods, max. 2000 h. The indentation tests were carried out before and after the irradiation and immersion tests using the indenter with a hemispherical apex with radius of 1.2 μm and Berkovich indenter.

3. Inverse analysis

Mechanical property change on the interface between liquid and solid metals was evaluated by using indentation technique. The inverse analysis was applied to the indentation load and depth curves

in order to identify the material constants in the constitutive equation that defines the relationship between load and deformation. The inverse analysis was carried out using the FEM (Finite Element Method) model combined with Kalman filter, described in detail elsewhere[3]. The shape of the indenter is spherical because it was confirmed that the accuracy of identification of the constitutive equation using the spherical indenter is much better than that using the conventional Bervoovich or Vickers indenters [3]. The surface layer of the model is divided into 4 layers as taking account of the displacement dose distribution along to the depth from the surface, as illustrated in Fig.2. The formulation of the constitutive equation is assumed by the following Swift power low equation:

$$\sigma = E\varepsilon \qquad \sigma \le \sigma_y \qquad (1)$$

$$\sigma = A(\varepsilon_0 + \varepsilon)^n, \varepsilon_0 = (\sigma_y/A)^{1/n} - (\sigma_y/E) \qquad \sigma \ge \sigma_y \qquad (2)$$

where, σ is true stress, ε true strain, E Young's modulus, σ_y yield stress, A work hardening coefficient and n work hardening exponent.

4. Results

Figure 3 shows the load/depth and depth, L/D-D curves measured by using Berkovich indenter, in which the slopes of the L/D-D curves are correspondent to the hardness. The effects of irradiation and mercury immersion (after 100 hr immersion) on L/D-D curves are clearly recognized: the slopes of the surface layer contact with the mercury and the irradiated surface are larger than that of the substrate, and the slope of the as received specimen is almost constant independently of the depth. The slope change of the surface layer for each condition is shown in Fig. 4. The hardness change deduced by the slope becomes larger by mercury immersion after irradiation than by irradiation and by mercury immersion respectively. In spite of ion irradiation, the contact surface is hardened by mercury immersion. Figure 5 shows the depth distribution of yield stress evaluated by the inverse analysis. The evaluated yield stress is correspondent to the displacement damage distribution by Ni ion irradiation. The yield stress is increased homogeneously by mercury immersion throughout the evaluated surface layer. The nominal stress-strain curve, which is obtained from uniaxial tensile test simulation using material constants evaluated by the inverse analysis, is shown in Fig.6. Uniform elongation up to onset of necking deformation reduced to ca 1/5 of as-received one by mercury immersion after ion irradiation. This behavior seems to be associated with liquid metal embrittlement and the degraded fatigue life in mercury[4,5].

5. Summary

We are developing a novel technique to estimate the mechanical property of micro-zone by using indentation test with inverse analysis. The depth distributions of both ion irradiation and mercury immersion effects were taken into account by using the multilayer model in the inverse analysis. From the uniaxial tensile test simulation using evaluated material constants, it is deduced that the ductility loss by combined effects of irradiation and mercury immersion is much larger than by irradiation and than by mercury immersion respectively.

References

1) JAERI-Conf 99-003, 1999.

2) Sasa, T., Oigawa, H., Kikuchi, K. and Ikeda,Y., Proceedings of AccApp '01, Reno, USA.

3) Futakawa, M., Wakui, T., Tanabe, Y., and Ioka, I, 10th APCNDT Proceedings, Brisbane, Sept. 2001, CD-ROM.

4) Old C.F., J. Nucl. Mat., 92(1980)2-25.

5) Strizak, et al.,J. Nucl. Mat., 296(2001)225-230.

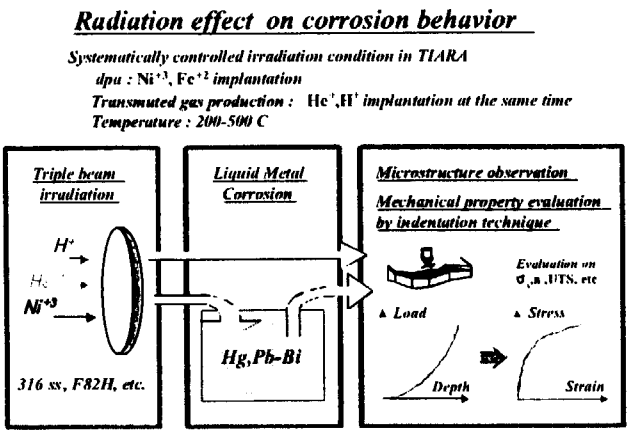

Fig.1 Schematic diagram on investigation

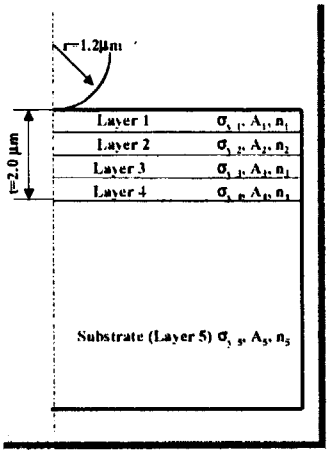

Fig.2 Multilayer model for inverse analysis

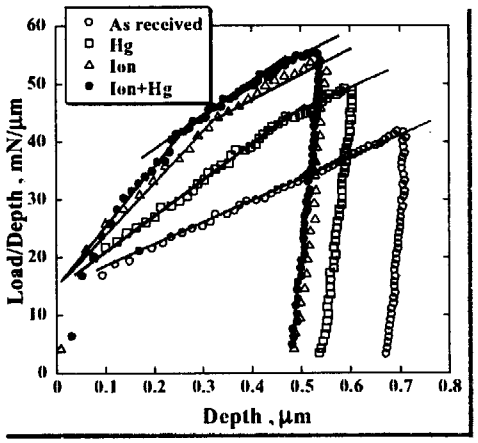

Fig.3 L/D-D curves for ion-irradiation and mercury immersion

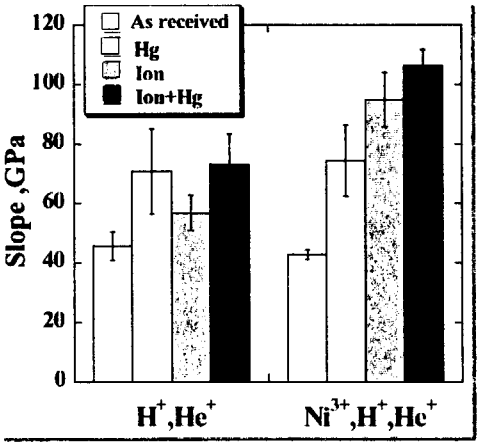

Fig.4 Slope change on L/D-D curves

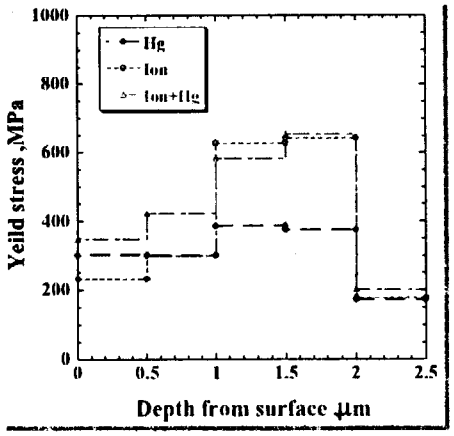

Fig.5 Depth distribution of yield stress evaluated by inverse analysis

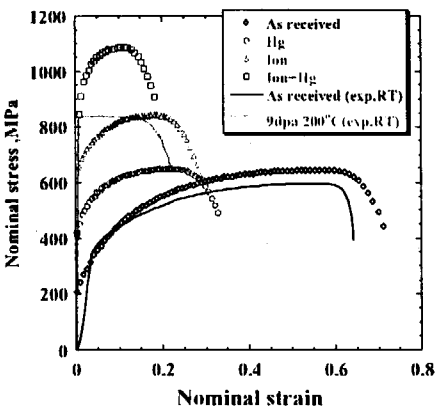

Fig.6 Nominal stress-strain curves using material constants evaluated by inverse analysis

4.9 Microstructure evolution of the advanced fuel cladding material by triple ion irradiation(Ⅱ)

Y.Nanjo*, I.Ioka*, A.Naito*, K.Kiuchi*
K.Yamamoto**
H.Kitamura***
Department of Nuclear Energy System, JAERI*
Japan Atomic Power Company**
Tokyo Electric Power Company***

1. Introduction

The advanced fuel cladding tube, adapted the burnup extension more than 100GWd/t with Mixed Oxide (MOX) fuel, is developed on the view points of the radioactive waste reduction, Pu effectual utilization and improvement economical efficiency. The candidate material for the advanced fuel cladding tube was adopted the stabilized austenitic stainless steel containing high Cr and high Ni for Cr depletion near grain boundary and gamma phase stabilization. Some others, impurities of C, N, etc, were reduced and the thermo-mechanical treatments were treated during the machining process to obtain the fine grain and uniformly dispersed precipitates, which are countermeasures against popular problems such as Intergranular Stress Corrosion Cracking (IGSCC) or ductility loss. Effects of those countermeasures are evaluated through the adaptability test under the simulated ultra high burn up condition.

In this study, effects of ion irradiation on the candidate tube, an equipment made on an experimental basis from the candidate material at 2000, were observed with TEM before neutron irradiation. The microstructural evolution was compared with that of the 304SS tube, the fuel cladding reserved for "Mutsu" atomic power ship.

2. Experiment

Chemical compositions of the candidate tube and 304SS tube are shown in Table 1. The disks, 3mm in diameter and 0.15~0.20mm in thickness, taken from the both tubes were irradiated with triple ion beams. For machining the candidate tube, the high purity ingots were machined to the radial thickness tubes, and then those were extruded and treated the thermo-mechanical treatments. The high purity ingots were made with the melting method mixed of VIM (vacuum induction melting) and CCIM (cold crucible induction melting). The radial thickness tubes were reduced the thickness to 40% with extruding. Those tubes were taken two heat treatments continuously, the first heat treatment is aging treatment at 873 K for 15 hours to uniformly stabilize impurities as precipitations, and the second one is recrystallized treatment at 1048 K for 10 hours to obtain fine grain. Finally, the tube was stretch formed corresponding to 7% cold work for obtaining sufficient strength and straightening. By above processes, the

Table 1 Chemical Composition of the candidate and 304SS

	Fe	Cr	Ni	Ti	C	N	O	S	Si	Mn	P
Candidate	bal.	24.55	34.99	0.18	0.0013	0.0014	0.0011	0.0009	<0.005	0.001	0.001
304SS	bal.	18.72	10.27	-	0.063	-	-	0.012	0.49	1.45	0.016

candidate tube, 11.3mm in outer diameter and 0.4mm in thickness, was prepared. The 304SS tube, 10.5mm in outer diameter and 0.4mm in thickness, was produced with the normal tube making process with 12~15 % cold work. The disks for irradiation were machined from those tubes. The flat surface was obtained on the outside of the tube with mechanically polishing, and the pre-disk was taken from the flat surface with slurry drill. The curved surface of the pre-disk, which the inside of the tube was turned to, was mechanically polished. The irradiation side was buff-polished, and that was electrochemically polished prior to irradiation.

For simulating the neutrons irradiation under 100GWd/t of ultra high burnup, both disks were irradiated with triple ion beams, 12MeV Ni^{3+}, 380KeV H^+ and 1.1MeV He^+, at TIARA in JAERI Takasaki. In irradiation, temperature of the disks were kept at 573 K. He^+ and H^+ were irradiated with energy degraders to be spread the implanting range. Distributions of displacement damage and each implanted ions in the disk were calculated with TRIM 98 code or TRIM 2000 code[1]. After irradiation, the bombarded surface of the disk was electrochemically removed to 1.2~1.3 μm in depth. Unbombarded surface was electrochemically removed to the bombarded surface to obtain the thin film at 1.2~1.3 μm from the bombarded surface for observing with TEM. Displacement damage was adjusted up to 50dpa at the depth because it was supposed that dose was about 50 dpa under 100GWd/t ultra high burn up for 10 years. Ni concentration was less than 1.0 at%, and H and He concentrations were 20-30 appm/dpa and 2-3 appm/dpa, respectively.

Microstructures were examined with the JEOL 2000FX electron microscope operated at 200KeV.

3. Result and discussion

Figure 1 shows the microstructures before irradiation, tangled dislocations formed at the machining process of the tube were observed in the candidate disk. In the 304SS disk, tangled dislocation as much density as the candidate disk was observed, and much twin crystals was observed. After irradiation, frank loops were formed over all in both disks, and those were not prejudiced near the grain boundary or precipitations such as Cr-rich alpha phase in the candidate disk or Cr-C composition in the 304SS disk. No voids and no babbles were observed in both disks.

For the measurement of the number densities and average loop diameters of flank loop formed in both disks, the weak-beam dark-field micrographs, shown in Figure 2, was taken on the beam direction B≈<110>, g=<111>, (g, 5g) diffraction condition. In this micrographs, white sharp lines was counted as the loops on {111} slip planes, and the number densities and average loop diameters were reckoned. Thickness of the observing sight was calculated with interpolating or extrapolating between the edge of the thin film and the crossing point, where the grain boundaries and twin boundary cross. The crossing point thickness was analyzed with that point micrographs taken different angle, or with the equal thickness fringe at that point.

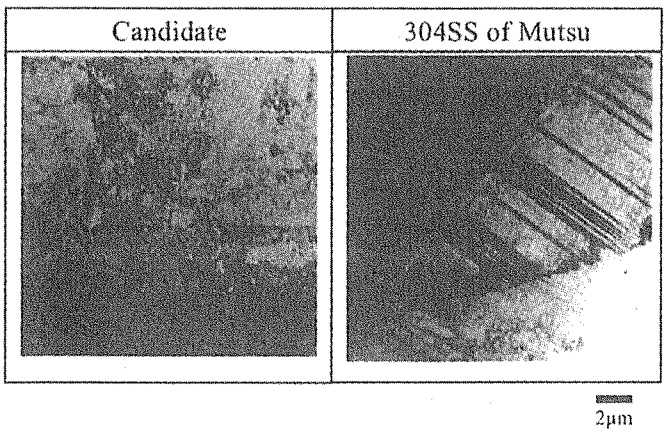

Fig.1 Microstructure evolution of the candidate and SUS304 of 'Mutsu' before irradiation.

Figure 3 shows the displacement damage dependence of the number densities of flank loop formed in both disks. The number densities are increased during some dose, and that are saturated at 10~20 dpa. At 51~53 dpa, the number density of the candidate disk and the 304SS are almost equal about 1.3×10^{22} m^{-3} and 1.4×10^{22} m^{-3}, respectively. Figure 4 shows the displacement damage dependence of the average loop diameters. Upto 10~13 dpa, the average loop diameters of both disks are equal, however that of 304SS disk increases to 17 nm upto 51 dpa depended on displacement damage. The average loop diameter of the candidate disk is about 13 nm upto 53 dpa. From the growth of secondary defect was almost not confirmed in the candidate, the candidate has higher irradiation resistance than the 304SS. That reason can not be expanded clearly because both disks differ in the purities, chemical composition, thermal history and cold working degree and the effect of the triple ion irradiation to the microstructure evolution in austenitic stainless steels is not clear. But, from the studies of the fast reactor, high Ni austenitic stainless steels are inhibits growth of the secondary defect such as flank loops[2),3)]. On the score, it is assumed that the candidate contained higher Ni than 304SS has higher irradiation resistance than 304SS

Reference

1)J.F.Ziegler, "The Stopping and Range of Ion in Solids", vol.1, Pergamon Oress, New York (1985)

2)N.Sekimura, F.A.Garner, R.D.Griffin,. J. Nucl.Mater.,vol.191-194(1992)P1234-P1238

3)T.Muroga, F.A.Garner, S.Ohnuki,. J.Nucl. Mater.,vol.179-181(1991)P546-P549

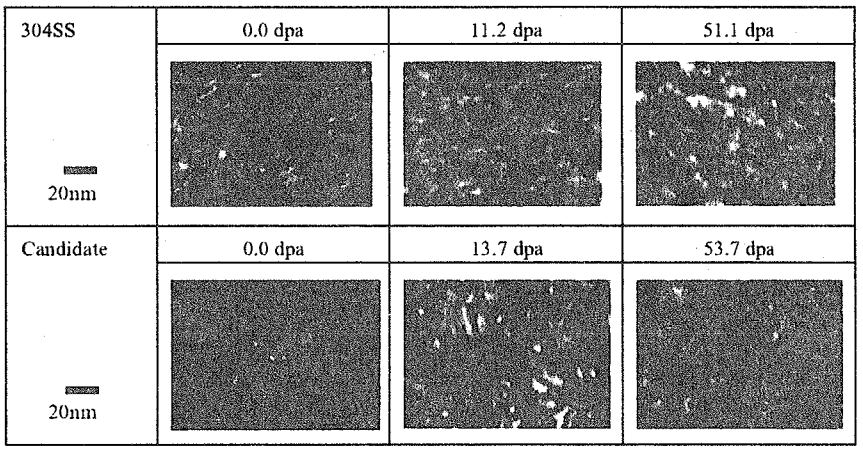

Fig.2 Weak-beam dark-field micrographs of the both disks B≈<110>, g=<111>, (g, 5g) diffraction condition

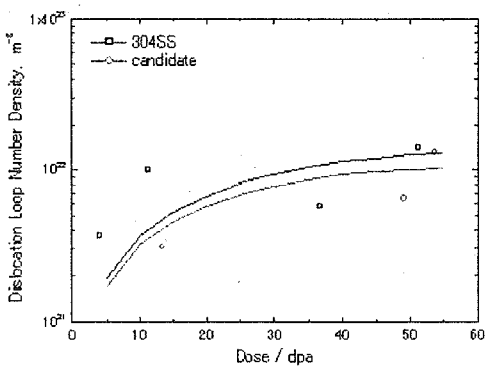

Fig.3 The number densities of the dislocation loops of the candidate and 304SS

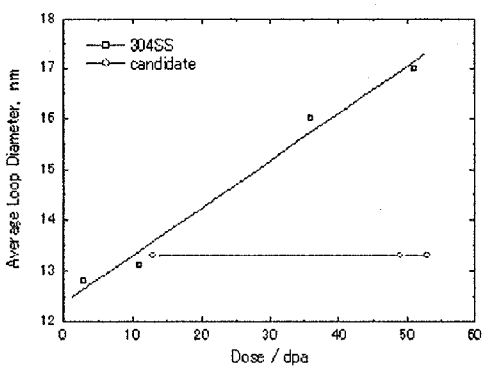

Fig.4 Average loop diameters of the candidate and 304SS

4.10 Simulation by accelerator for formation of lattice defects in Zircaloy-2 cladding irradiated in commercial reactor

Susumu Yamada*, Joji Ohta**, Takeshi Sonoda***, Motoyasu Kinoshita***, Tomotsugu Sawai**** and Siro Jitsukawa****

Materials Science Department, Central Research Institute of Electric Power Industry (CRIEPI)*, Energy Materials Department, CRIEPI**, Nuclear Energy Systems Department, CRIEPI***, Department of Materials Science, JAERI****

1. Introduction

In order to reduce costs of electric power generation by using boiling water reactors (BWRs), it is useful to develop fuel cladding tubes tolerant of high burnup. The fuel cladding tubes in the current BWRs are made from Zircaloy-2 which is the Zr base alloy with predominant addition of Sn (~1.5wt. %). The cladding shows excellent performance of corrosion resistance, however a problem has been recently reported that the cladding occurs an axial crack at the power rump test[1]. The principal cause of the axial crack is not revealed yet, an elucidation of the ductility loss is required. A characterization of microstructures is effective to overcome the problem because the ductility loss is thought to be influenced by lattice defects. It is known that <a> and <c> component dislocation loops are produced in Zircaloy-2 by neutron irradiation[2]. The former is formed on the prismatic plane $(11\bar{2}0)$ and the latter is on the basal plane (0001).

On a joint project between CRIEPI and KTH (Royal Institute of Technology, Sweden), we have examined transmission electron microscopy (TEM) structures of Zircaloy-2 cladding irradiated up to high burnup of 60 MWd/kgU in the commercial reactor (Ringhals-1, Sweden). We could characterize damage structures which show a dose-dependence. Furthermore it was confirmed that the damage structures of commercial reactors can well be reproduced experimentally by using neutron accelerators.

Compared to neutron experiments, to simulate damage structures under neutron irradiation by using ion irradiation is valuable from the viewpoint of saving cost and time. At present the reported data on microstructures of commercial reactors are scarce. In particular no information on the neutron irradiated structures at an atomic scale has been reported.

The purpose of this study is to simulate a microstructure of <c> component dislocation loops formed in the commercial reactor by using ion irradiation and to study the simulated structure at an atomic scale by TEM for clarifying the mechanism of the axial crack.

2. Experimental

The materials examined in this study were Zircaloy-2 fuel cladding tubes of 8×8 BWR fuel design. 12 MeV Zr^{4+} ions with 20 dpa were irradiated perpendicular to the cladding tube axis at 573 K by 3 MV tandem accelerator at TIARA facilities of JAERI. Thin foils for TEM experiments were prepared by the focused ion beam method and were examined in 300kV field emission TEM (Hitachi HF-3000).

3. Results and discussion

Figure 1 shows a bright-field TEM image of

Zircaloy-2 under neutron irradiation. The groups of <c> component dislocation loops form straight lines with a ~30 nm spacing parallel to the trace of the basal plane.

The loop structure very similar to the neutron irradiated materials could be formed by ion irradiation. Figure 2 shows a bright-field image of ion irradiated specimen extracted at the depth of 3 μm from the front surface. The direction and the inter-distance of the straight lines are same as the case of neutron irradiation. Monte-Carlo calculation predicts that a damage peak is at the depth of 2.5 μm. We need further study on the relation between the depth and the loop density.

The high resolution TEM (HRTEM) was carried out to investigate the loop structure on an atomic scale. Figure 3 shows a HRTEM image of ion irradiated specimen shown in Fig. 2, the <c> component dislocation loops are thought to be dark spots. It was found that (0001) lattice fringes are deformed with periodicity of several nanometers. Therefore lattice potential with new periodicity reflecting the distortion will be produced. We think that the lattice distortion influences a hydrogen mobility and finally introduces the axial crack.

The results are summarized as follows.

(1) The structure of <c> component dislocation loops formed by neutron irradiation can be simulated by ion irradiation.

(2) The lattice distortion with periodicity of several nanometers is produced in the region where the regular arrangement of <c> component dislocation loops is formed.

References

1) Report on High Burnup Fuel Safety Experiments, Nuclear Power Engineering Corporation, March 2002 (in Japanese).

2) M. Griffiths, R. W. Gilbert, V. Fidleris, R. P. Tucker and R. B. Adamson, J. Nucl. Mater. 150 (1987) 159.

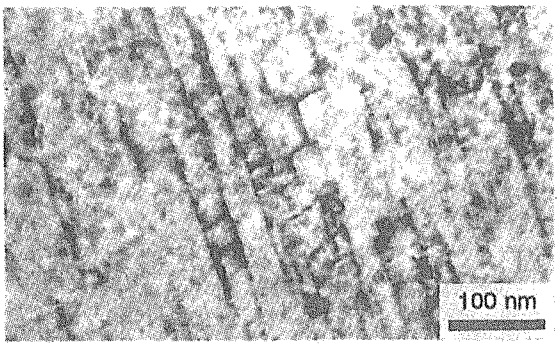

Fig. 1 Bright-field TEM image of Zircaloy-2 under neutron irradiation (60 MWd/kgU).

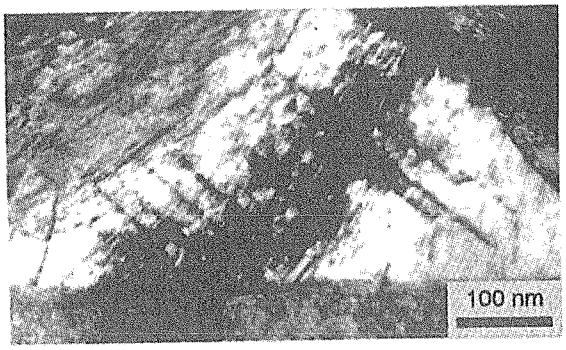

Fig. 2 Bright-field TEM image of Zircaloy-2 under ion irradiation (20 dpa).

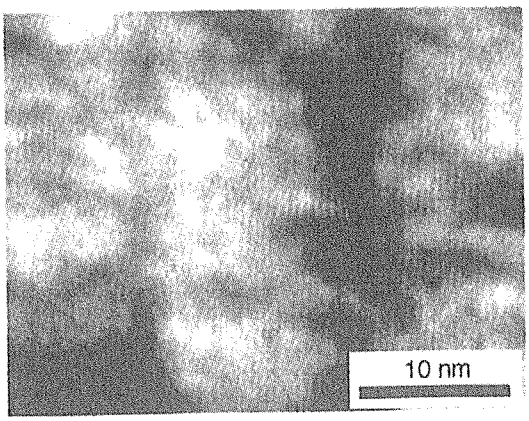

Fig. 3 HRTEM image of Zircaloy-2 under ion irradiation (20 dpa).